UNIVERSITY OF CAPE TOWN

OPTIMAL SIZING AND PLACEMENT OF INDEPENDENT POWER PRODUCERS ON MV, HV AND EHV NETWORKS FOR MINIMUM POWER LINE LOSSES USING NEURAL NETWORKS

PREPARED BY:
JAMES LOMBARD
LMBJAM003

THESIS SUBMITTED IN FULFILMENT OF THE REQUIREMENT FOR A MASTER OF SCIENCE DEGREE IN ELECTRICAL ENGINEERING

JULY 2023

SUPERVISOR
Associate Professor Sunetra Chowdhury
Department of Electrical Engineering
University of Cape Town

DECLARATION

I, James Lombard, hereby declare that this is my own work. All information obtained from reference material has been identified and acknowledged. This thesis has not been submitted before to this or any other institution for any degree or examination.

Signature: Signed by candidate **Date: 27 August 2023**

ACKNOWLEDGEMENTS

I would like to thank my mother Loraine, and my brother Mark, for giving me the strength and courage to persevere and carry out my thesis work. Without you this would not have been possible.

My sincere gratitude goes out to my supervisor Prof. S. Chowdhury for the supervision,

support and guidance throughout this research.

ABSTRACT

In June 2021, the South African president announced the adjustment of schedule 2 of the Electricity Regulation Act. The effect of this adjustment was to increase the National Energy Regulator of South Africa's (NERSA) licensing limit for renewable projects applying for direct connection to the national grid, having export capacities ranging from 1 MW to 100 MW. This increased the number of Independent Power Producers (IPPs) seeking connection to the South African electricity transmission system (TS) or distribution system (DS) – which, as a mandatory requirement, are to comply with the minimum technical and design grid connection regulations stipulated within the South African Grid Code (SAGC) covering renewable energy.

The contribution of this thesis is therefore the design and testing of an ANN model that locates and sizes IPPs of Category B (1 MW to 20 MW) and Category C (> 20 MW) of the SAGC seeking connection to MV/HV/EHV backbone feeders from geographical locations far from the Point of Connection (POC). In the ANN model developed using MATLAB, the user is prompted to enter specific network parameters applicable to the grid connection study. These parameters include backbone voltage (kV), backbone length (km), interconnecting feeder length (km), maximum load seen at the receiving end (MW), distance from the IPP at the POC to the sending end busbar as a percentage of the total backbone length (km) and the load power factor at the receiving end. Based on these inputs, the model determines the most suitable IPP location, IPP size, interconnecting conductor and IPP power factor in order to achieve the lowest overall power line losses for the network.

The algorithm consists of 7 ANN models, with each ANN model applied specifically to a unique nominal voltage network undergoing IPP interconnection. Seven cases are presented starting from the lowest voltage test case (11kV) to the highest voltage test case (400kV). Case 1 and Case 2 test the 11kV and 22kV ANN models on modified IEEE 13–bus systems, while Case 3 to Case 7 test 66kV, 132kV, 220kV, 275kV and 400kV ANN models on modified IEEE–14 bus systems.

For the 11kV test case, the user enters input parameters: backbone conductor length of 5km, receiving end power of 4.05MVA and receiving end power factor of 0.85 (lagging). The 11kV ANN model returns an IPP size of 1.5MW operating at 0.975 (lagging) power factor, located 4.5km from the sending end substation using an ACSR Chickadee conductor. The 11kV ANN model also returns a total line loss value of 0.05351MW, while the true loss value is shown to be 0.05343MW (when compared to DIgSILENT Powerfactory simulations). This translates to an error of 0.1684%. The 22kV case is presented using the same network parameters as the 11kV case but uprated to nominal voltage of 22kV. The same trend is seen for the 22kV case but with total losses significantly less than the 11kV case due to the increased network voltage.

For the 66kV test case, the backbone conductor considered is a 15.6 km ACSR Kingbird with receiving end power 30MW operating at 0.95 lagging power factor. The 66kV ANN model recommends an optimal IPP size of 12MW operating at 0.975 (lagging) power factor, located 14.04km from the sending end substation using an ACSR Kingbird conductor. The 66kV ANN model also returns a total line loss value of 0.0193MW, while the true loss value is shown to be 0.01868MW when compared to DIgSILENT Powerfactory. This translates to an error of 3.29%. The 132kV test case achieves a prediction error of 0.775% and returns an optimal IPP size of 67.5MW, located 31.5km from the sending ending busbar on the 35km backbone feeder, operating at 0.95 lagging power factor.

For the EHV cases (220kV – 400kV), the same trend is seen. For the 220kV network, the lowest losses are seen for an IPP connected furthest away from the sending end (120.9km) along the 134km backbone with receiving end power 201MW at 0.95 lagging power factor. This requires a 110MW IPP at operating at 0.95 lagging pf resulting in 3.7MW of line losses using a Single ACSR Zebra interconnecting conductor. It is shown that for an IPP operating at 0.95 leading power factor, the total system losses increase to 5MW, indicating that the algorithm predicted correctly. The 275kV case has lowest losses for a 110MW IPP size operating at a lagging power factor of 0.95. This generates 1.8MW of losses (approximately 500kW lower than the capacitive case), but also is significantly lower than the 220kW case since a twin conductor Zebra bundle is used for the interconnecting feeder.

Since the 400kV network is modelled using quad Zebra backbone conductors, losses are significantly smaller than the 220kV and 275kV cases, which only used a Twin bundle conductor geometry per phase. This increased the geometric mean radius which increased the maximum power transfer of 150MW required at the receiving end. Since the power factor at the 400kV receiving end load is unity, the required reactive VAR support, in addition to the high voltage level (400kV at 1.04pu), saw an optimal IPP power factor setpoint of 0.95 (leading) resulting in a surplus of VARs. For a 138km backbone feeder with receiving end load of 150MW at unity power factor, the 400kV ANN model returns a total loss value of 179kW.

The model developed can be used as a tool for providing additional support to network engineers and independent power producers (IPPs), especially for performing grid application studies. DIgSILENT PowerFactory power system simulation software is used to verify the accuracy of the algorithm. This tool is especially relevant for current needs and caters specifically to IPP units that fall under Category B and Category C of the SAGC, since these are rapidly growing in today's South African Energy Sector.

TABLE OF CONTENTS

LIST OF TABLES

LIST OF FIGURES

LIST OF SYMBOLS AND ABBREVIATIONS

AC	Alternating Current
ACRS	Aluminium Copper Reinforced Steel
ACOs	Ant Colony Optimisation
ANN	Artificial Neural Network
CSP	Concentrated Solar Plant
DC	Direct Current
DS	Distribution System
EG	Embedded Generation
GD	Gradient Decent
EHV	Extra High Voltage
GE	Genetic Algorithm
GUI	Graphical User Interface
IRP	Integrated Resource Plan
HV	High Voltage
LF	Load Factor
LSF	Loss Sensitivity Factor
LV	Low Voltage
MSE	Mean Square Error
MV	Medium Voltage
NSP	Network Service Provider
NIPS	National Integrated Power System
NERSA	National Energy Regulator of South Africa
PCC	Point of Common Coupling
POC	Point of Connection
PSO	Particle Swarm Optimisation
PUC	Point of Utility Connection
PV	Photovoltaic
REIPPP	Renewable Energy Independent Power Producer Procurement Program
RPPs	Renewable Power Plants
SAGC	South African Grid Code
SANS	South African National Standards
SCADA	Supervisory Control and Data Acquisition

SLD	Single Line Diagram
TS	Transmission system
VAr	Volt-Ampere reactive

CHAPTER 1

INTRODUCTION

Existing research on the integration of distributed generation on utility grids indicates there are two areas that require thorough investigation, especially from an independent power producer (IPP) optimisation perspective:

1. Optimal sizing and placement of IPPs connecting to MV/HV/EHV backbone feeders for minimising power line losses. These IPPs fall under Category B (1 MW – 20 MW) and Category C (> 20 MW) of the South African Grid Code (SAGC).
2. Optimal interconnecting conductor selection for IPPs connecting to MV/HV/EHV backbone feeders for minimising power line losses. These also fall under IPP Category B (1 MW – 20 MW) or Category C (> 20MW) of the South African Grid Code (SAGC). Many IPP units falling in Categories B and C are at great distances from the backbone feeder itself, thus requiring an Artificial Neural Network (ANN) based optimal interconnecting conductor selection feature.

This research focusses on developing an ANN model that incorporates point 1 and point 2 into the final solution. Given that conductor impedance significantly affects line losses and voltage characteristics in power lines, ANNs would be a suitable technique to address point 2 above. Most Category B and C applications at the MV/HV/EHV level need lengthy interconnecting conductors to transfer significant power, which as a result generate heat-related losses. Many of these power losses will go unaccounted for if a conductor selection function that supports point 1 is not included. This will result in a significant amount of mistake and inaccuracy, particularly while training the ANN.

1.1 Background

Prior to an IPP being successfully connected to the utility grid, the network engineer and IPP developer conduct network integration and connection studies to make sure the IPP unit not only operates within the parameters of the SAGC but also to ensure an optimal network solution that is both feasible and affordable to implement over the long term. Since these losses can account for up to 13% of technical system losses in the transmission and distribution system, active power loss minimization has long been a research issue of interest (particularly in relation to IPP connection studies) [1]. Inadequate placement of IPPs on power lines can worsen the impact of power line losses and jeopardize the technical performance of both the IPP and the utility by reversing the traditionally unidirectional power flow on lines, which in turn affects the effectiveness of current protection coordination settings on feeders [2,3]. Consequently, the network engineer needs additional tools to limit the impact of network power losses.

1.2 Objectives of the Research

The objectives of this thesis are therefore to:

1. Design and test an ANN model that locates and sizes IPPs of Category B and Category C of the SAGC, seeking connection to MV/HV/EHV backbone feeders, from geographical locations far from the Point of Connection (POC), while additionally determining the most suitable interconnecting conductor and IPP power factor setpoint applicable.

2. Test the accuracy of the model on modified IEEE 13-bus and IEEE 14-bus electrical networks.

1.3 Problem Statement

The majority of the existing literature has focused on IPP size and optimization primarily for low voltage networks falling under category A (0–1MW), which the grid code limits IPP sizes to 13.8 kVA [4], most studies are for small scale IPP power applications that are typically located close to huge rooftops. In these circumstances, the interconnecting

conductor losses are regarded as insignificant and are not necessary to be included in the ANN training process. The influence of line losses cannot be completely eliminated for interconnecting conductors longer than 5 km, hence they are (as demonstrated in this study) included to the ANN training process for increased accuracy.

ANNs are especially suited for this task since they can learn large and complex data sets even when provided with poorly defined or incomplete input data. ANNs do not require an extensive database to save historical and current data since it is automatically encapsulated within the ANN layer structure. This is especially useful since it minimises potential data loss concerns.

1.4 Scope of Investigation and Limitations

For this research, the scope of investigation includes:

1. A literature review of the SAGC. The SAGC defines the operating limits and constraints needed to develop an ANN model especially applicable to the South African electricity network.
2. The ANN model will specifically apply to 11kV, 22kV, 66kV, 132kV, 220kV, 275kV and 400kV networks.
3. Where applicable, assumptions are made since all input data could not be derived from the utility for security reasons. All assumptions are referenced and justified where needed.
4. The study only considers steady state conditions and is limited to the following: voltage profiles, power line losses, fault levels and thermal loading of the conductors under study. Frequency fluctuation, power system harmonics and voltage stability are not considered and not necessary since the tool developed is designed for the first phase of IPP grid connection.

1.5 Software Package used for Modelling and Simulation

DIgSILENT PowerFactory software version 14 [5] is used for load flow studies, while MATLAB is used to develop the ANN structure [6]. DIgSILENT PowerFactory is a widely verified and accepted software tool that accurately computes power system load flow simulations. MATLAB is supported across a number of computer platforms such as Windows and Linux with a large library that contains powerful built in and predefined functions specifically designed to handle complex problems with large data sets. MATLAB also contains a tool that allows for the programmer to interactively design a Graphical User Interface (GUI), which is especially useful for this research. For this research MATLAB and DIgSILENT PowerFactory will be run on a Windows 10, 64-bit operating system.

1.6 Outline of the Thesis

Chapter 1 provides the objectives and research outline. It addresses the process to be carried out for the remaining chapters.

Chapter 2 presents a literature review of existing methods used in current research relating to IPP sizing and placement. It discusses line losses and voltage from a mathematical perspective. The SAGC is also discussed briefly along with the growth and deployment of solar PV systems within South Africa.

Chapter 3 discusses research steps and methods followed. This includes an explanation of the nature and collection of data used. For every voltage technology, the process for input and target data collection is explained. The ANN structure and training is also discussed.

Chapter 4 presents the actual test networks used for validating the accuracy of the ANN model. The networks used are modified versions of the IEEE 13-bus and IEEE 14-bus systems. Seven case studies are presented for every voltage level and results cross-examined using DIgSILENT PowerFactory.

Chapter 5 A final conclusion is presented which summarises the research undertaken and further evaluates the model based on what was expected in the initial problem statement of this thesis. More detailed analysis of the ANN performance based on the seven cases studies done in Chapter 4 is also provided. The benefits of this work in the power and energy industry are also discussed, and recommendations for future research are advanced.

References All referenced information is contained in this section of the thesis.

Appendix Where needed, all additional supporting information and results are referred to in the Appendix.

CHAPTER 2

LITERATURE REVIEW

2.1 Introduction

The principles elaborated in this chapter serve as the platform for the concepts and methodology developed in this research. Section 2.2 provides background context to Independent Power Producers (IPPs) in industry and considers their operation. It discusses the development, growth and history of solar PV technology within a South African context. Section 2.3 discusses the fundamentals of solar power production and design. Section 2.4 discusses the impacts and effects of connecting IPPs to the grid in terms of line losses, voltage regulation, thermal loading and fault levels – all of which need to be taken into account when considering the most suitable size and location for IPP integration. Section 2.5 provides an overview of the South African Grid Code (SAGC) for renewable power plants connected to the electricity transmission system (TS) or distribution system (DS) in South Africa. The SAGC stipulates the limitations and technical requirements for IPP integration to Low Voltage (LV: Nominal voltage levels up to and including 1 000 V), Medium Voltage (MV: The set of nominal voltage levels greater than 1 000 V and up to and including 44 000 V), High Voltage (HV: The set of nominal voltage levels greater than 44 000 V and up to and including 220 000 V) and Extra High Voltage (EHV: The set of nominal voltage levels greater than 220 000 V and up to and including 400 000 V) networks [7]. Finally, Section 2.6 provides a critical review of existing research literature that is centred around the topic of optimising the size and location of an IPP unit on MV/HV/EHV networks for minimising real or active power losses. An analysis of the strengths and limitations of existing research is also discussed and gaps that require further investigation are highlighted. According to the findings and to the best of the researcher's knowledge, no research to date investigates the ability of an Artificial Neural Network (ANN) to be sufficiently trained to determine both the optimal IPP unit size and location on an MV/HV/EHV power line, while also considering the correct interconnecting conductor specification for minimising power line losses for cases in which the IPP unit is far from the Point of Connection (POC).

This chapter will set the stage for the next phase of this research involving the design of a test bed simulation model representing a realistic MV/HV/EHV grid tied power network. The test bed model will be used to generate input and target data for the training of the ANN. Once trained, the ANN will be capable of recognising the most optimal size, location and power factor set point of an IPP unit to be connected to the MV/HV/EHV power line for minimising power line losses while adhering to the SAGC. In addition, the ANN will be trained to select the most suitable interconnecting conductor between the IPP unit and utility.

For the test bed model to be technically valid – especially from a South African perspective – it will need to take into account the limits and requirements specified by the SAGC. For this reason, it is critical to highlight/understand the technical requirements that the grid code presents.

2.2 Background to Independent Power Producers

In this section the following topics will be covered:

- Development of solar PV plants
- Solar PV components
- Principles of solar power generation
- Types of solar PV technologies

2.2.1 Development of Solar PV

The rapid growth of industrialisation from the 1850s saw the increase of coal use worldwide. Internationally, coal remains the most used primary fossil fuel and accounts for 41% of global power produced [8,9]. In South Africa since the early 1880s, coal has also been the predominant force in the production of electrical energy. In view of rising

concerns over the past few decades around frequent load shedding, increasing electricity prices, negative environmental impacts (rising CO_2 levels) and increasing electricity demands, the South African government expressed interest in an alternative to coal-based production – namely renewable energy [10]. In 2010, the Integrated Resource Plan (IRP) highlighted targets of up to 18 000MW of new renewable generation capacity to be introduced onto the national grid by 2030 [11].

In 2011, the Renewable Energy Independent Power Producer Procurement Program (REIPPP) was initiated to procure energy from IPPs in the form of solar PV, CSP, wind, landfill gas and small hydro plants to the ESKOM network. The plan was designed to accelerate the IPP integration process to the national grid through a 5-year bidding process, resulting in the rapid influx of IPPs in the South African energy market. The grid connection code for renewable power plants connected to the electricity transmission system or distribution system in South Africa was then developed to guide and facilitate IPPs connecting to the grid [12].

South Africa has amongst the highest solar PV power potential in the world, with some areas averaging over 2,500 sunlight hours per year and experiencing average solar-radiation levels between 4.5 and 6.5kWh/m^2 per day. By 2030, South Africa plans to add an additional 8,400MW of photovoltaic plants. Currently in South Africa, concentrated solar power (CSP) has a total cumulative installed capacity of 500MW, while solar PV has 2,157MW. Combined, this accounts for approximately 51% of the total installed renewable capacity in South Africa [13,14]. For this reason, solar PV technologies will form the focus of this research. Figure 2-1 shows the grow of Solar PV in South Africa from 2013-2020 while Figure 2-2 shows the worldwide growth of Solar PV 2011-2020.

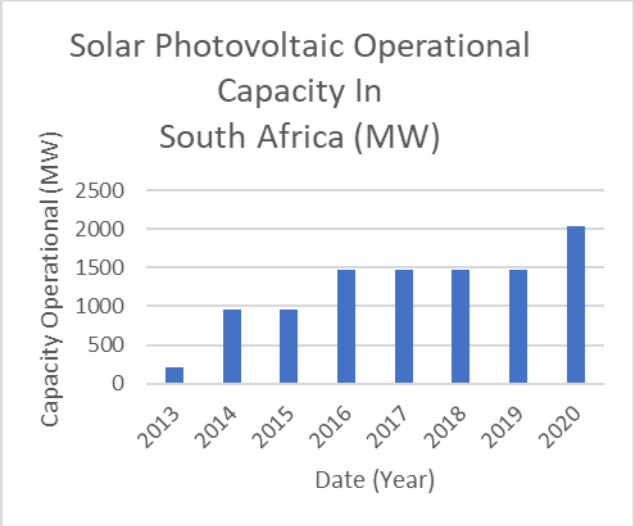

Figure 2-1: Growth of solar PV in RSA (2013-2020) [15].

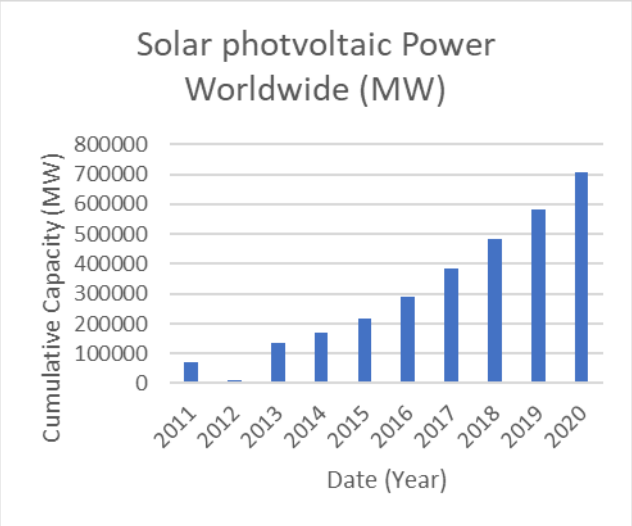

Figure 2-2: Growth of solar PV worldwide [16].

2.2.2 Solar PV Components

Solar PV systems generally exist in three topologies: off-grid, grid-tied and hybrid (as shown in Figure 2-3, Figure 2-4 and Figure 2 -5 respectively). Hybrid systems generally consist of a combination of solar PV/wind, diesel generator and battery integration. All comprise most of the following standard components[7]:

- **Solar PV array**: Absorbs sunlight and converts it into direct current (DC) current electricity
- **Charge controller**: Controls flow of DC current into battery to ensure it is optimally/safely charged
- **Battery bank**: Stores energy from solar arrays
- **Inverter**: Converts DC current from battery bank to AC current
- **Utility meter**: Monitors electricity flow between customer and utility
- **Electrical grid**: Network which the PV plant is connected to and exchanges energy with.

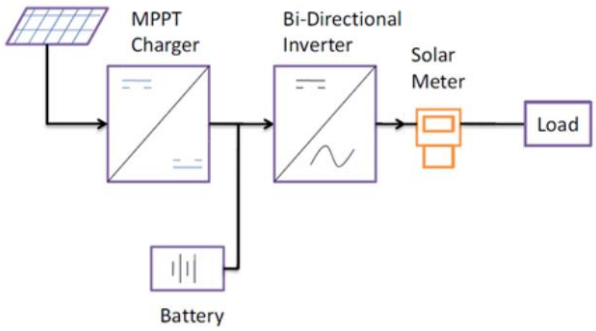

Figure 2-3: Basic off-Grid solar PV configuration [17].

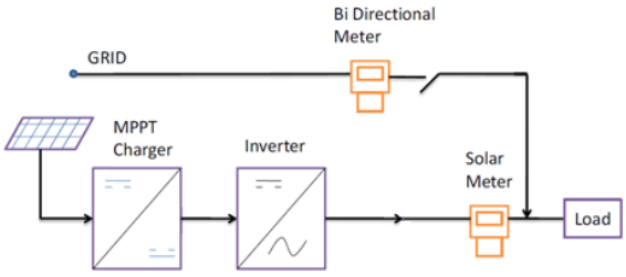

Figure 2-4: Basic grid-tied solar PV configuration [17].

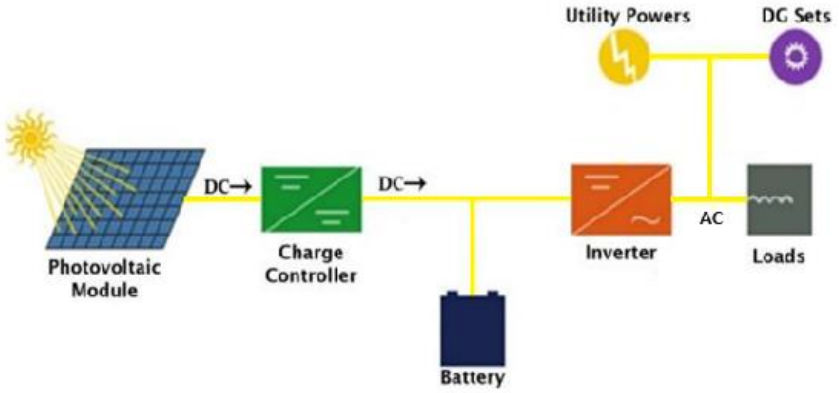

Figure 2-5: Hybrid solar PV configuration [18]

2.3 Basic principles of grid-tied solar energy production

In this section the energy conversion process in solar PV plants is discussed.

Solar PV systems use discrete cells connected to convert light energy to DC electricity. The output power produced by PV systems depends primarily on the size of cells on the panel, the overall system efficiency, and solar irradiation level penetrating the cells (which is dependent on the surrounding weather conditions). PV panels are constructed using silicon n-type and silicon p-type semiconductor material. The panel operates using the principle of the Photoelectric effect. When sunlight (photons) penetrates a PV panel, an energy transfer takes place, which displaces free electrons from the silicon material. This exchange occurs constantly under direct sunlight and eventually creates electron flow across the p-n junction resulting in a steady flow of DC current [19].

As aforementioned, solar PV systems are broadly categorised as off-grid, grid-tied, and hybrid. Off-grid or stand-alone systems are typically used with batteries and inverters for AC load requirements; these systems are completely disconnected from the main grid and suitable for remote locations. Hybrid systems use more than one source of energy. This could be in the form of wind, solar or diesel.

Since the focus of this research is utility grid-tied IPPs in the form of solar PV, the basic operating principle for a traditional grid-tied solar PV plant is presented here (illustrated in Figure 2-6) [20].

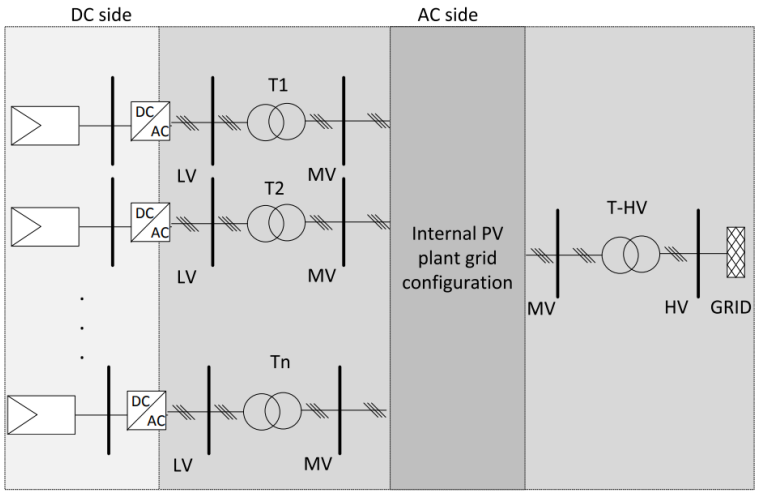

Figure 2-6: Traditional grid-tied solar PV plant configuration [20]

- Solar energy in the form of light is transferred to multiple PV modules which displaces free electrons resulting in current flow.
- PV modules are typically connected in series formation forming a 'string'. This is to achieve a higher voltage across each string. The strings of modules are then connected in parallel to increase the DC current and overall power output of the PV field.
- The multiple strings of PV modules are connected to an inverter unit. Traditionally the converter unit is centralised, but other topologies exist (such as string inverters).
- The inverter unit – among other functions – converts the DC current to a 50Hz sine wave which is connected to a step-up transformer.
- The step-up transformer increases the inverter output voltage from the LV level to an appropriate MV level. If the POC of the plant and the utility is at the HV or EHV level, an additional transformer is required to further increase the voltage requirement of the grid.

2.4 Integrating Solar PV Plants to the Grid

With increased solar penetration to the grid, the dynamic response of the existing external network will shift [21]. A number of electrical studies are hence required to ensure that the system voltage regulation, thermal loading, fault level, losses and overall security of the power system are within legal stipulated requirements and standards. In this section, the impact of solar PV units connecting to the grid are hence discussed in terms of:

- losses
- steady state voltage limits
- thermal rating
- fault level

2.4.1 Power Losses

Active or real power losses (I^2R) in an MV/HV/EHV network depend on the resistances of power delivery elements (power lines), core losses of transformers and motors, dielectric, and rotational losses. The magnitude of current (measured in amperes (A)) flowing through the line as shown in Figure 2-7 feeder schematic diagram, is given by equation (2.1),

$$[I] = \frac{|S_s|}{|V_s|} = \frac{|S_r|}{|V_r|} \qquad (2.1)$$

where $S_s = P_s + jQ_s$ and $S_r = P_r + jQ_r$ are the sending and receiving end complex power respectively. S, P and Q represent the complex, active and reactive power and measured in units of VA, W and Vars respectively. V_s and V_r are the voltages at the sending and receiving end respectively, measured in per-unit quantities (p.u.) [22].

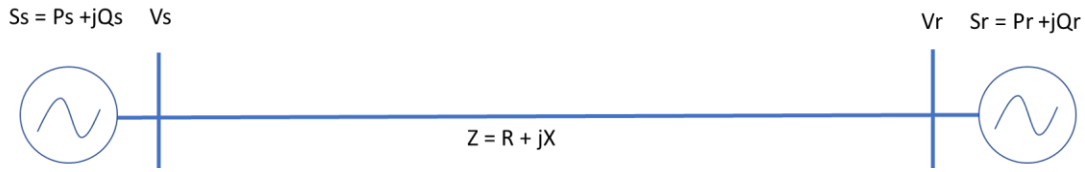

Figure 2-7: Circuit diagram of 3 phase MV/HV/ EHV feeder [22]

S_s is expressed in terms of power at the receiving end and the line losses [20] as per equation (2.2),

$$S_s = (P_r + I^2R) + j(Q_r + I^2X) \qquad (2.2)$$

In order to solve for the I^2 term, the square of the magnitude of S_s is performed as shown by equation (2.3) [20],

$$|S_s|^2 = ((P_r + I^2R)^2 + (Q_r + I^2X)^2)^2 \qquad (2.3)$$

Multiplying out equation (2.3) and rearranging in the form of a polynomial shown by equation (2.4) gives line losses in equation (2.5) ,

$$|S_s|^2 = (R^2 + X^2)(I^2)^2 + (2P_rR + 2Q_rX - V_s{}^2)I^2 + (P_r{}^2 + Q_r{}^2) \qquad (2.4)$$

$$I^2R = 3\frac{(V_s{}^2 - 2P_rR + 2Q_rX) \pm \sqrt{(2P_rR + 2Q_rX - V_s{}^2)^2 - 4(R^2 + X^2)(P_r{}^2 + Q_r{}^2)}}{2(R^2 + X^2)}R \qquad (2.5)$$

2.4.2. I²R Losses with IPP's Connected to Feeder Backbone

Figure 2-8 shows an IPP unit connected at some location on the backbone feeder. While the backbone feeder represents the main MV/HV/EHV conductor between the sending and receiving ends (as shown in Figure 2-7), the interconnecting feeder is the conductor connecting the IPP unit to the backbone feeder. These names are given to differentiate between the two conductors. Point x specifies the location of the IPP unit on the backbone conductor. Segments A and B represent the two sections that make up the backbone conductor. The backbone feeder losses change according to equation (2.6),

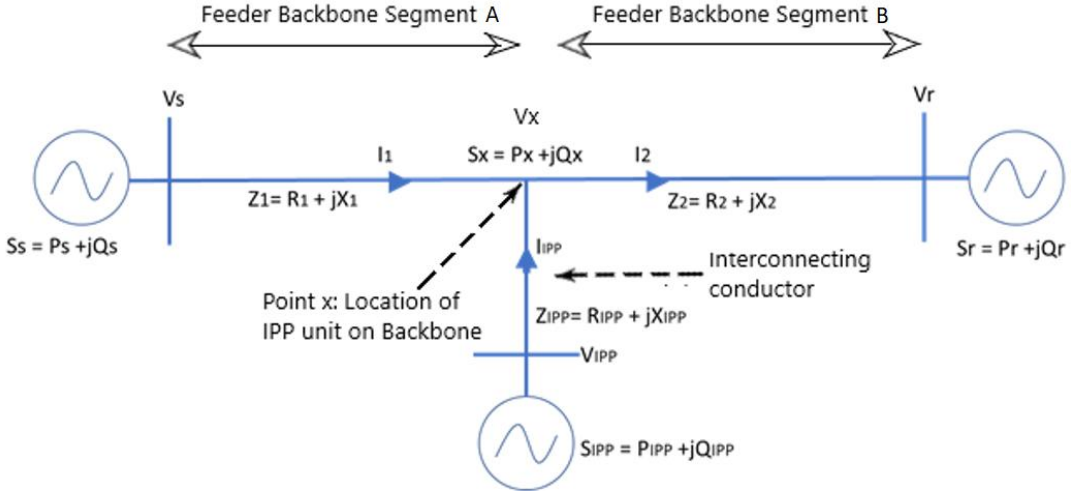

Figure 2-8: Diagram of the feeder as in Figure 2-7, but with IPP unit connected.

$$P_{loss} = 3I_1{}^2R_1 + 3(I_1 + I_{IPP})^2R_2 \qquad (2.6)$$

Where: I_1 is the current flowing through Segment A, measured in amperes (A), R_1 is the resistance of Segment A, measured in ohms (Ω), I_2 is the current flowing through Segment B, measured in amperes (A), R_2 is the resistance of Segment B, measured in ohms (Ω), I_{IPP} is the current flowing from the IPP, through the interconnecting conductor

measured in amperes (A). Since $I_2 = (I_1 + I_{IPP})$, the square of I_1 and I_2 can be determined as shown by equations (2.7) and (2.8) respectively,

$$I_1{}^2 = \frac{(V_s{}^2 - 2P_xR_1 + 2Q_xX_1) \pm \sqrt{(2P_xR_1 + 2Q_xX_1 - V_s{}^2)^2 - 4(R_1{}^2 + X_1{}^2)(P_x{}^2 + Q_x{}^2)}}{2(R_1{}^2 + X_1{}^2)} \quad (2.7)$$

$$I_2{}^2 = (I_1 + I_{IPP})^2 = \frac{(V_x{}^2 - 2P_xR_2 + 2Q_2X_2) \pm \sqrt{(2P_rR_2 + 2Q_rX_2 - V_x{}^2)^2 - 4(R_2{}^2 + X_2{}^2)(P_r{}^2 + Q_r{}^2)}}{2(R_2{}^2 + X_2{}^2)} \quad (2.8)$$

where $P_x = (P_s - I_1{}^2R_1) + (P_{IPP} - I_{IPP}{}^2R_{IPP})$ and $Q_x = (Q_s - I_1{}^2X_1) + (Q_{IPP} - I_{IPP}{}^2X_{IPP})$ [20].

The total feeder loss is calculated by substituting equations (2.7) and (2.8) to equation (2.6). For the case where the IPP unit is close to the backbone feeder, meaning the interconnecting feeder connecting the IPP to the backbone feeder is substantially short, the interconnecting feeder impedance can be neglected since line resistance (Ω/km << 1), then P_x and Q_x reduce to $P_x = P_s + P_{IPP}$ and $Q_x = Q_s$.

This can be extended to the cases where there are multiple IPP units connected to the feeder and the generalised form of equation (2.6) in that case will be,

$$P_{loss} = 3I_1{}^2R_1 + 3I_2{}^2R_2 + \cdots + 3I_n{}^2R_n = 3\sum_{n=1}^{m} I_n{}^2R_n \quad (2.9)$$

From equation (2.9) [20], it is clear that when connecting an IPP unit via a long interconnecting line to a backbone feeder, it can enhance line losses (for a larger I_{IPP} current value in equation (2.8)) or reduce the backbone line losses (for a smaller I_{IPP} current value).The value of I_{IPP} in equation (2.8) depends on the power factor setpoint of the IPP unit (leading, lagging or unity) [22].

2.4.3 Steady State Voltage Limits

For all integrated power producers there is a voltage constraint that needs to be adhered to, as the load profile varies daily and from season to season as stipulated in the NRS 048-2 [23]. This is to ensure equipment safety from both the utility and the end user. For MV, HV and EHV networks, the reference voltage is set to the nominal voltage as stated in SAGC [7], and voltages are restricted to within 5% of declared voltage.

2.4.4 Thermal Rating

Integration of PV systems onto the grid can result in an increase in the thermal loading level of the interconnecting feeder, backbone feeder and upstream components. The thermal rating of equipment can also be exceeded if the PV plant is too large and placed at a location on the feeder that already is experiencing high loading levels. The network planning engineer needs to ensure that the optimal location and sizing of PV plants is determined by checking the before and after thermal ratings when the network experiences high and low load levels [24].

2.4.5 Fault Levels

At the POC, the contribution of the PV unit to the fault level of the utility must be considered to ensure safe operation and protection of the service provider under fault conditions. The planning engineer will check the network fault level before and after the addition to the PV plant. This fault level check will apply to lines, transformers, and other components [7].

2.5 Technical Standards and Grid codes

2.5.1 Grid Connection Code for Renewable Power Plants in South Africa

The Grid Connection Code for Renewable Power Plants (RPPs) in South Africa was developed to establish the minimum technical requirements for RPPs seeking connection to the transmission or distribution network [7]. The grid code also applies to all electrical network service providers (NSPs) and systems operators facilitating in the connection process. For this thesis, only Category B and C RPPs are considered as shown in Table 2-1 below:

Table 2-1:Classification of RPP's [7]

Category	A1	A2	A3	B	C
Minimum Size (kW)	0	13.8	100	1000	>20000
Maximum Size (kW)	13.8	100	1000	20000	
Voltage level	LV	LV	LV	MV	MV/HV

2.5.2 Voltage and Frequency Tolerance Limits

2.5.2.1 Normal Operating Conditions

Under normal operating conditions RPP's in categories A1, A2 and A3 (see Table 2-1) are required to operate within 10%-15% of the nominal system voltage at the POC. Categories B and C are required to operate within the POC voltage range U_{min} and U_{max} shown in Table 2-2. The precise operating voltage between theses limits will depend on the geographical location of the RPP, determined by the network service provider and developer.

Table 2-2:Maximum and Minimum Voltage Limits for Different Nominal System Voltages[7]

Nominal System Voltage Un (kV)	Umin (pu)	Umax (pu)
132	0.9	1.0985
88	0.9	1.0985
66	0.9	1.0985
44	0.9	1.08
33	0.9	1.08
22	0.9	1.08
11	0.9	1.08

The nominal frequency of the National Integrated Power System (NIPS) is 50Hz and normally controlled within the specified limits of the Grid Code – which for continuous operation is between 49Hz and 51Hz [7].

2.5.3 Reactive Power Limits

RPPs of Category B and C are required to have voltage control and power factor or reactive power control modes. Category B IPPs producing between 20% and 100% of rated power are required to operate within a 0.975 lagging and 0.975 leading power factor range, while also operating within the specified -0.228MVAr (Qmin) and +0.228MVAr (Qmax) reactive power tolerance limit. Category C IPPs are allowed to generate between 20% and 100% of rated power and required to operate within a -0.95 and +0.95 power factor range, while also operating within the specified -0.330MVAr (Qmin) and +0.330MVAr (Qmax) reactive power tolerance limit [7].

RPPs of Category B and C have reactive power control functionality that allows the unit to operate under voltage control, power factor control or Q control – only one at a time. Q control is a control function controlling the reactive power supply and absorption at the POC independent of the active power and the voltage. Power factor control is a control function controlling the reactive power proportionally to the active power at the POC [7]. Voltage control is performed by controlling the voltage setpoint at the POC (Figure 2.9).

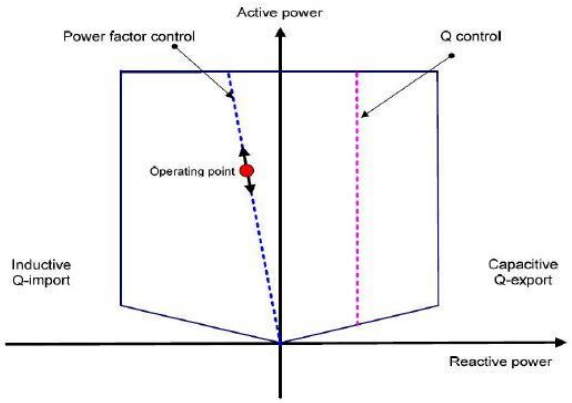

Figure 2-9: Voltage control limits for the RPP [7]

2.6 Existing Research: Critical review and appraisal

The network planner and the IPP developer perform network integration/connection studies that ensure the IPP unit operates within the limits of the grid code while also selecting the most optimal network solution that is both practical and cost effective. Network configuration studies focussing on minimisation of real power losses (i^2R) – which are considerably larger than other system losses [25] – have for several years been a popular topic of interest for many researchers [26, 27, 28].

Determining the most optimal IPP unit location and size for minimising network losses on an individual IPP application basis can be time consuming in nature and, depending on the complexity, may take anything from a few weeks to several months for individual cases to be processed and correctly validated. For this reason, several authors have explored innovative and creative techniques for a more automated and optimised application process – especially from an IPP location and sizing perspective that minimise real power losses. This will ultimately benefit the utility, especially when the network is under large financial and time constraints. Depending on the application, each approach explored in the literature has its own advantages and limitations both in terms of computational accuracy, computational time, and case complexity. The literature generally classifies each method approaches as either analytical [29-34], numerical [35-52] or heuristic in nature [52-67].

2.6.1 Analytical Methods for Optimal IPP Placement and Sizing

Analytical techniques typically simulate electrical networks using a mathematical viewpoint or methodology. These work effectively for calculations involving a limited number of system restrictions and objective functions. They can be computed very quickly and easily as a result, but they tend to struggle when system complexity and parameter sizes increase [28]. An analytical technique to lower active power losses for non-varying load scenarios that is applicable to IPP site and sizing is the Exact Loss formula [31]. The Exact Loss Formula for active power loss has been used in previous studies [29–34] together with appropriate IPP sizing and location. Although these papers show good results for evenly distributed load conditions, they do not consider IPP power factor variations, and do not cater for MV/HV/EHV scenarios according to the SAGC require power factor control functionality. Reference [30] improved on the method proposed by [29] by catering for four power factor scenarios, but the improved version is still unable to deal with numerous IPP connections for various locations. This limits the study to very specific cases only. Reference [34] also developed a modified Exact Loss Formula by simultaneously considering a costing function and loss function for improved accuracy and practicality. Although the economic component makes the overall solution more realistic, the formula also only considers single IPP unit locations on the line – also close to the POC.

According to [33], the Rule of Thumb technique assumes a fixed IPP unit position at 2/3rds of the line length and 2/3rds of the line's kVAR loading. This approach, although simple to implement, does not apply to varying load conditions/distributions along the line and applies strictly to uniformly distributed loads on the feeder. In addition, as the name suggests, the Rule of Thumb is also not as accurate as other more sophisticated methods, providing merely a guideline to IPP placement. The method suffers especially when accuracy cannot be compromised.

Other analytical methods used in the literature for the placement of IPPs for minimising overall losses are the Kalman Filter algorithm, the Loss Sensitivity Factor (LSF) and combinations of both [35,36]. To the best of the researcher's knowledge, the vast majority of analytical solutions in research only consider small IPP units (Category A in the SAGC) with low voltage applications close to the POC. There are also hardly any studies that simultaneously incorporate IPP location and sizing for minimising line losses with an added conductor selection feature. These are, for the vast majority of papers, separately implemented solutions.

2.6.2 Numerical Methods for Optimal IPP Placement and Sizing

Several authors have made use of numerical methods to identify research and application gaps in the IPP size and allocation problem [37-47]. By making fundamental theoretical assumptions, educated guesses, and approximations pertaining to convex, differential, and continuous applications, numerical methods like Linear Programming, Mixed Integer Nonlinear Programming, Gradient Search, Exhaustive Search, Tabu Search, and other probabilistic methods typically solve issues common to optimal power flow problems [48].

Previous research [37-38] used a Tabu search to examine the best IPP location and sizing for lowered line losses with a known number of IPP units and size. This study addresses a rather narrow issue because it only applies to residential

LV applications near the POC. Using a linear programming technique, Keane & O'Malley (2005) [39] identify a location where the maximum IPP dispatch power is practical given a variety of network parameter limitations, but they are unable to offer a workable financial solution to support the maximum power injection onto the grid. Reference [40] also uses Linear Programming for the IPP allocation and sizing problem, but the study applies strictly to high loading conditions and also does not take into account load variability. References [41] and [42] use mixed integer non-linear programming to place IPP units for minimal losses, but only take into account small to medium applications while experiencing multiple convergence issues.

Numerical methods, although useful in many optimisation problems, do suffer when the initial guess selection is incorrectly specified, especially from a convergence issue–- when searching for the global or most optimal solution as mentioned in a number of papers in literature [43,44,45,46,47]. For example, when trying to find the correct IPP unit size and location for a minimum loss, a large, more complex network may have multiple local minima (representing multiple optimal loss solution points) for a single power flow scenario. This makes it far more challenging when the goal is to identify the global minimum when numerous local minima exist – a common issue in a number of studies.

As with analytical studies reported in the majority of the literature, there are no numerical method solutions that simultaneously incorporate IPP location and sizing for minimising line losses with an added conductor selection feature.

2.6.3 Heuristic Methods for Optimal IPP Placement and Sizing

While methods shown in Sections 2.6.1 and 2.6.2 have proven to be helpful in specific application cases within the study of power system optimisation and planning– especially from an IPP location and sizing perspective, there is still huge interest in improving and building smarter, more robust systems that become computationally more intelligent, and that are practical and cost effective. Based on existing research [48-62], several publications specific to IPP allocation and sizing for minimum power losses make use of the following popular heuristic methods: Genetic Algorithm (GA), Simulated Annealing, Particle Swarm Optimisation (PSO) and Ant Colony Optimisation (ACO) tools. These are popular methods used for their simple implementation and ability to overcome global convergence issues [49,50].

The GA with a power flow approach is used in Reference [51] to determine the appropriate position and size of IPP units while taking network losses and voltage regulation limits into account for various loading scenarios. By choosing the ideal size and position with the fewest losses and taking into consideration realistic load variations throughout the day, the study is able to achieve its goal. Again, though, it only applies to low-voltage residential units and is insufficient for applications involving MV, HV, or EHV voltages. To reduce overall system losses, previous research [52,53] used the GA for IPP location and size, but they only applied to LV applications.

Authors of [54] use the PSO method for IPP sizing and location for improved voltage profile and loss minimisation. The study is performed using the IEEE 10 and 33 bus system with high accuracy of results, but only considers cases limited to less that 30MW capacity. References [55,56] use a combined PSO technique that considers IPP placement using a multi-objective combined approach on the IEEE 14,30 and 57 bus feeders with good results considering large power capacity cases. Reference [57] uses a PSO based technique that also considers automatic conductor selection for minimising network losses and overall system cost savings based on a 26 bus distribution system. The study also takes into account the IPP sizing and location. However, the network is tested for a fixed power factor of 0.85 for all loads with a maximum system voltage rating less than 20kV and power requirement of 1MVA. This would only cater for category A3 according to the SAGC [7].

ACOs are models used for combined optimisation problems that can escape local minimum issues and locate global optima points [58]. Authors of [59] and [60] use ACOs for optimal IPP sizing and location for minimising network losses and improving voltage stability. Reference [61] also applies the ACO to hybrid applications from both sizing and performance perspectives with high levels of accuracy. Study [62] proposes an improved ACO technique that selects design parameters over a range of values while also instilling maximum and minimum ranges within the objective functions. However, no indication of conductor selection is made.

2.6.4 Artificial Neural Networks

For various IPP applications, including the identification of power quality disturbances, the detection of faults on transmission and distribution lines, and the forecasting of load, Artificial Neural Networks (ANNs) have emerged as a popular and effective technique [63, 64, 65]. However, as [66] implies, ANN-based research for IPP placement and

sizing difficulties has a narrower scope than the intelligent approaches outlined above. In addition, the author [66] builds an ANN application tool that optimally sizes and places IPP units, however unlike the research previously mentioned, MV/HV/EHV networks located outside of the POC are not taken into account.

2.6.4.1 Advantages of Artificial Neural Networks

For various IPP applications, including the identification of power quality disturbances, the detection of faults on transmission and distribution lines, and the forecasting of load, Artificial Neural Networks (ANNs) have emerged as a popular and effective technique [63, 64, 65]. However, as [66] implies, ANN-based research for IPP placement and sizing difficulties have a narrower scope in terms of their use within the research - when compared to the intelligent approaches already outlined above. In addition, the author [66] builds an ANN application tool that optimally sizes and places IPP units, however, like the research previously mentioned, MV/HV/EHV networks located at distances far from the POC, are not taken into account.

2.6.4.2 Research gap

The reviewed literature indicates that there are two areas that still require further investigation, especially from an IPP optimisation perspective. More specifically:

1. Optimal sizing and placement of IPP's connecting to MV/HV/EHV backbone feeders for minimising power line losses. These fall under Category B (1MW to 20MW) and Category C (>20MW) of the SAGC [7].
2. Optimal interconnecting conductor selection (with suitable phase geometry configuration) for IPP's connecting to MV/HV/EHV backbone feeders for minimising power line losses. These also fall under Category B (1MW to 20MW) or Category C (>20MW) of the South African Grid Code [7]. Many IPP units falling in Category B and C are at great distances from the backbone feeder itself, thus requiring an ANN-based optimal interconnecting conductor selection feature.

Although point 1 also falls under the general 'IPP size and location' umbrella of research (around which numerous studies have been developed), it specifically deals with MV/HV/EHV networks of Category B (1MW to 20MW) and Category C (>20MW) only – something that has not been seen in the literature to date. The literature has for the most part addressed IPP sizing and optimisation specifically relating to low voltage networks falling under category A(0–-1MW) according to the SAGC, and to a large extent, the studies performed are small scale IPP power applications in most cases adjacent to large rooftops where the grid code restricts IPP sizes to 13.8 kVA.

Point 2 addresses IPP units that are located at great distance from the backbone feeder and which require optimal interconnecting conductor selection for minimising power line losses. As mentioned in Section 2.5.1.1 (*I^2R losses with IPP's Connected to Feeder Backbone*), conductor impedance plays a significant role in the line losses and voltage characteristic of a power line. At the MV/HV/EHV level, the vast majority of Category B and C applications require long interconnecting conductors to transfer large amounts of power that generate losses in the form of heat. By not incorporating a conductor selection feature that compliments point 1, a large portion of these power losses will not be accounted for. This will introduce a high level of inaccuracy and error especially when training the ANN. Therefore, existing LV, Category A ANN based solutions cannot be used for Category B and C applications because they do not cater for power losses that become significant especially for long interconnecting feeders.

2.6.4.3 Research to be Conducted

This research will investigate an ANN solution that can effectively incorporate points 1 and 2 to a single process that determines the correct IPP size, IPP location and optimal interconnecting conductor selection and phase geometry for minimising backbone power line losses. The performance of the ANN will be evaluated against existing IPPs that are already commissioned and currently in operation. This will be highly beneficial for both the network planner and IPP developer, since the number of IPP units that fall into these categories is growing, especially within the current South African Energy Sector [69].

2.7 Conclusion

This chapter has presented a background to IPPs in industry and their operation. Fundamental solar power production and design concepts have been discussed. The technical challenges that impact IPP connection to the national grid in terms of line losses, voltage regulation, thermal loading and fault level requirements have been shown. SAGC has also been summarised to further explain the requirements of IPP integration onto the South African electricity network. And a critical appraisal of existing research on a more automated IPP application process – especially from a placement and sizing perspective for minimising real power losses on MV/HV/EHV power lines – has been discussed.

The next chapter will describe how the theoretical concepts presented here have been applied in this study, and explain the research method undertaken to implement an ANN-based solution that can be used to develop a broader, more practical solution for the interconnection of IPP units to the South African Electricity Network. The design of a test bed simulation model representing a realistic MV/HV/EHV grid tied power network will be implemented. The test bed model will be used to generate input and target data for the training of the ANN. Once trained, the ANN will be capable enough to recognise the most optimal size and location of an IPP unit to be connected to the MV/HV/EHV power line for minimising power line losses while adhering to the SAGC. In addition, the ANN will be trained to select the most suitable interconnecting conductor and phase geometry between the IPP unit and utility.

CHAPTER 3

RESEARCH METHODOLOGY

3.1 Introduction

Chapter 2 provided the theoretical background and technical requirements for integration of solar PV plants to the grid. Chapter 3 will discuss the research method adopted for developing an ANN algorithm through simulation and modelling using DIgSILENT PowerFactory and MATLAB software [6]. Section 3.2.1 discusses the criteria used for the selection of input data and target data used for ANN training. Section 3.2.2 provides the modelling and simulation of the grid-tied network which consists of an IPP plant directly connecting (tying-in) to the backbone feeder (representing the grid) via a suitable interconnecting conductor. Section 3.2.3 discusses the generation of target data used for ANN training. The input and output data for every voltage level are then given in full in Section 3.2.4. Description of the ANN model is provided in Section 3.3. A case study is outlined in Section 3.4, which is used to implement the ANN model in chapter 4, for every voltage level at the receiving end, POC and IPP MV/HV/EHV sending end bus bar, with nominal values of 11kV, 22kV, 66kV, 132kV, 220kV, 275kV and 400kV. The results of Section 3.4 are further analysed in Chapter 4. All results are recorded and analysed in chapter 4, with a critical reflection on the findings provided in Chapter 5. Figure 3-1 describes this approach in the form of a flow diagram.

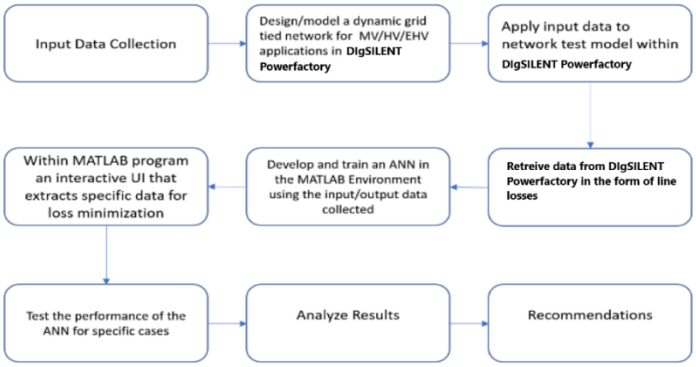

Figure 3-1: General process followed for the research method.

3.2 Nature and Collection of Research Data

Input and target data are necessary for the training, testing, and validation of ANNs [67, 68]. In order to ensure accurate ANN prediction, it is crucial to supply the ANN both pertinent input data and target data. The "correct data" with known values are the input data and target data. The output of the ANN is achieved using the input and target data that were previously utilized during the training of the ANN. This process is repeated once the ANN has been trained. Therefore, target data would be the appropriate output for the known input data and used for ANN training.

3.2.1 Third-Party and Open-Source Data Collection

Before presenting the criteria for input data selection, it is essential to point out that all the data used in this research is from open-source platforms only, generated taking into account the limits specified in the South African National Standards (SANS 182) [70, 71], SAGC [7], NRS048 (Compatibility levels, limits, and voltage characteristics for utilities, their customers, and the National Energy Regulator in managing power quality issues parts 2) [23], IEEE Guide for the Installation of Overhead Transmission Line Conductors (524-16) [72], and reference [73]. The parameters used to gauge the accuracy of the model during the testing phase (Chapter 4) are justified and referenced. For all cases involving modifications of existing networks in the literature, parameters are fully referenced and justified.

3.2.2 Nature of Data

The criteria for selecting the input data are based on fundamental system parameters that have the largest influence on backbone losses applicable to grid-tied solar PV networks. Input data is quantitative in nature and stored within 7 unique voltage specific input data matrices. Each of the 7 voltage matrices contain specific input data associated with the backbone nominal voltage level at which the IPP is to be connected (via a suitable interconnecting conductor). These voltages include: 11 kV, 22 kV, 66 kV, 132 kV, 220 kV, 275 kV, and 400 kV. Each voltage matrix consists of 8 columns – each column representing a unique parameter 'type', while the rows represent different 'values' of that same parameter type. It is decided that 8 parameter types are used for each voltage specific input data matrix. To illustrate this, the following example is used. For the 11kV input data matrix, the parameter type "IPP size (MW)" will consist of values 1MW, 1.5MW and 2MW. These values will form the rows of the parameter type "IPP size (MW)". The 8 parameter types used for all 7 input data matrix are therefore: (1) backbone length (km), (2) the interconnecting line length (km), (3) highest loading seen on the backbone feeder measured from the downstream (load) transformer (MW) , (4) IPP size (MW), (5) IPP location on the backbone from the sending end busbar (km), (6) IPP power factor, (7) interconnecting conductor selection, and (8) receiving end (load) power factor. The relationship between each unique voltage level and the associated parameter types (1) – (8), are explained below:

1. ***Backbone voltage*:** The backbone voltages chosen in this research are the standard nominal voltage levels currently in operation today. These are: 11 kV, 22 kV, 66 kV, 132 kV, 220 kV, 275 kV, 400 kV. These voltages cater for all MV, HV and EHV technologies as mentioned in the SAGC. The three-phase voltage limits are shown in Table 3-1, as specified in the SAGC, along with phase-to-earth and phase-to-phase clearance information in metres. All power lines in this study are assumed to be fully transposed wherever voltage balance is of concern. All forms of shunt compensation are not utilized on the backbone feeder or on the interconnecting feeder, for voltage support.

Table 3-1:Minimum Phase-to-Earth Safety Clearances and Operating Voltage Limits [7,71]

	Phase-to- Earth distance (m)	***Phase-to-Phase Distances(m)***	***Minimum Voltage at POC (pu)***	***Maximum Voltage at POC (pu)***
11kV	0.2	0.3	0.9	1.08
22kV	0.32	0.4	0.9	1.08
66kV	0.77	0.89	0.9	1.08
132kV	1.45	1.68	0.9	1.08
220kV	2.1	2.7	0.9	1.08
275kV	2.5	3.6	0.9	1.08
400kV	3.2	4.8	0.9	1.08

2. ***Backbone length and Loading:*** Balanced three-phase conductor lengths are determined based on their ability to transfer power under the limitations of thermal and voltage constraints [74]. In this research, the probabilistic approach is used [75]. Conductors are rated according to a Rate A (maximum operating current under normal conditions), for 50°C temperature template, to ensure that conductor sag will not encroach on the minimum safe phase to ground clearance distance. Considering the minimum phase-to-earth distance and maximum and minimum voltage limits from Table 3-1 above, the maximum active power transferred to the receiving end (load) via a distribution or transmission line is given by equation (3.1) below and as derived in textbooks [75–77]:

$$P_r = \frac{|V_s||V_r|}{Z}\cos(\theta_z - \delta) - \frac{A|V_r||V_r|}{Z}\cos(\theta_z - \theta_A) \qquad (3.1)$$

where Z is the series impedance given by equation (3.2) in ohm (Ω); R is the resistance in ohm (Ω), L is the inductance in Henry (H) and C, the capacitance in Farad (F); R, C and L are given by equations (3.3), (3.4) and (3.5) respectively:

$$Z = R + jwL - jwC \quad (3.2)$$

$$R = Ks\ \frac{pl}{A} \quad (3.3)$$

$$C = (Ks\ \frac{2\pi\varepsilon}{\ln\left(\frac{Dm}{r}\right)})(l) \quad (3.4)$$

$$L = (2)10^{-7} \ln\left(\frac{Dm}{Deq}\right)(l) \quad (3.5)$$

In the above equations, p is the resistivity constant, l is the line length (km), and A the conductor cross-sectional surface area (mm^2). Ks is the factor used when considering the skin effect, which applies to both resistance, inductance and capacitance having permittivity constant ε and radius r. Dm is the geometric mean distance (GMD) between all conductors for a single conductor bundle, given by equation (3.6), and Deq is the geometric mean radius (GMR) of the sub conductors within a conductor bundle and given by equation (3.7), both measured in meters (m),

$$Dm = \left(\sqrt[3]{(D_{ab})(D_{bc})(D_{ca})}\right) \quad (3.6)$$

$$Deq = \sqrt{(r)e^{-u}} \quad (3.7)$$

θ_z is the phase angle associated to Z, δ is the phase difference between sending and receiving end voltages, A and θ_A are the magnitude and phase angle respectively associated with parameter A from standard ABCD parameter model [75]. V_s, V_r are the sending and receiving end voltages respectively (measured in p.u). As seen from equation (1), maximum active power delivered to the receiving end of the line is inversely proportional to line length. Increasing the line length translates to an increase in Z value, which in turn reduces the maximum power flow between the sending and receiving ends of the power line. Equations (3.1)-(3.7) are used to determine the correct line and applicable load that can flow through both the backbone feeder and interconnecting conductor. To illustrate how this is done, a 22kV horizontal geometry feeder (Figure 3-2) consisting of a single Chickadee conductor [78], is shown below with the following parameters:

l = 30 km, Dm = 1889.9 mm (phase separation of 1.5 m), ACSR Chickadee single conductor having DC Resistance at 20˚C of 0.1426 Ω/km, overall conductor diameter of 18.87 mm (radius, r = 9.43 mm), current rating of 419A (at 50˚C template).

For a sending end voltage of 1.03pu, receiving end voltage of 0.95pu and receiving end (load) set to unity power factor, equations (3.1)-(3.7) result in the following line parameters: R = 4.28 Ω, C = 0.42 μF, L = 24 mH. This will allow for a maximum power transfer over 30 km to be 6.5 MW as shown by Figure 3-3. The corresponding voltage profile is shown in Figure 3-4.

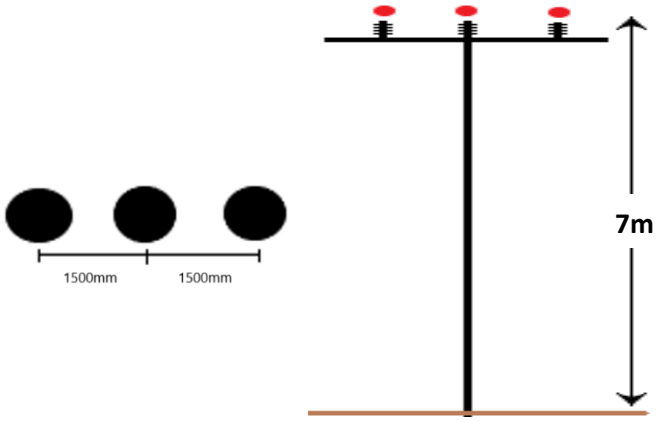

Figure 3-2: Horizontal geometry for 22 kV, 30 km feeder [77].

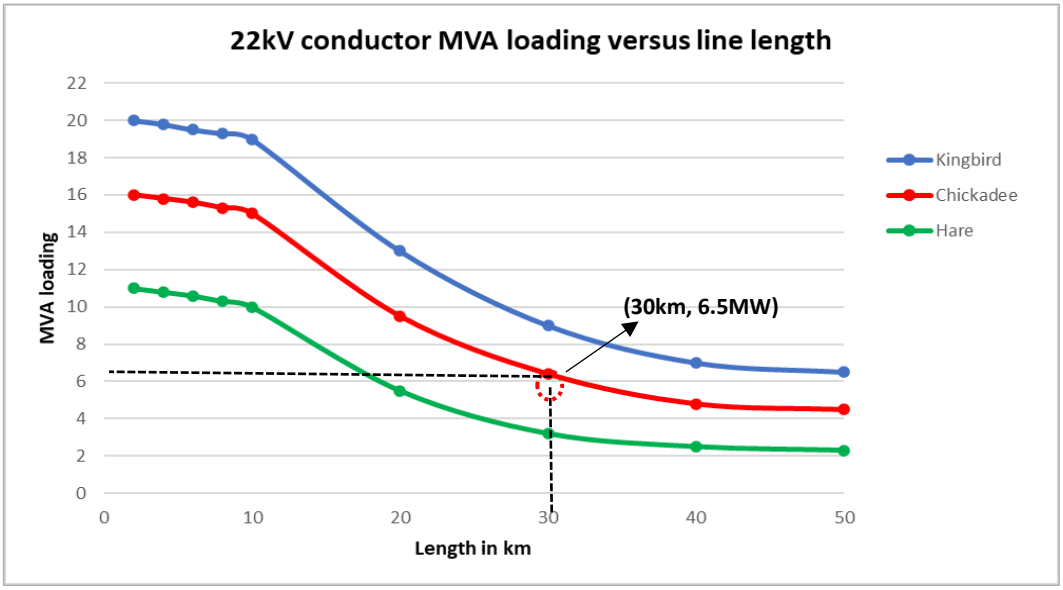

Figure 3-3: Maximum power transfer plots indicating a maximum power transfer of 6.5MW at 30km, using an ACSR single Chickadee conductor.

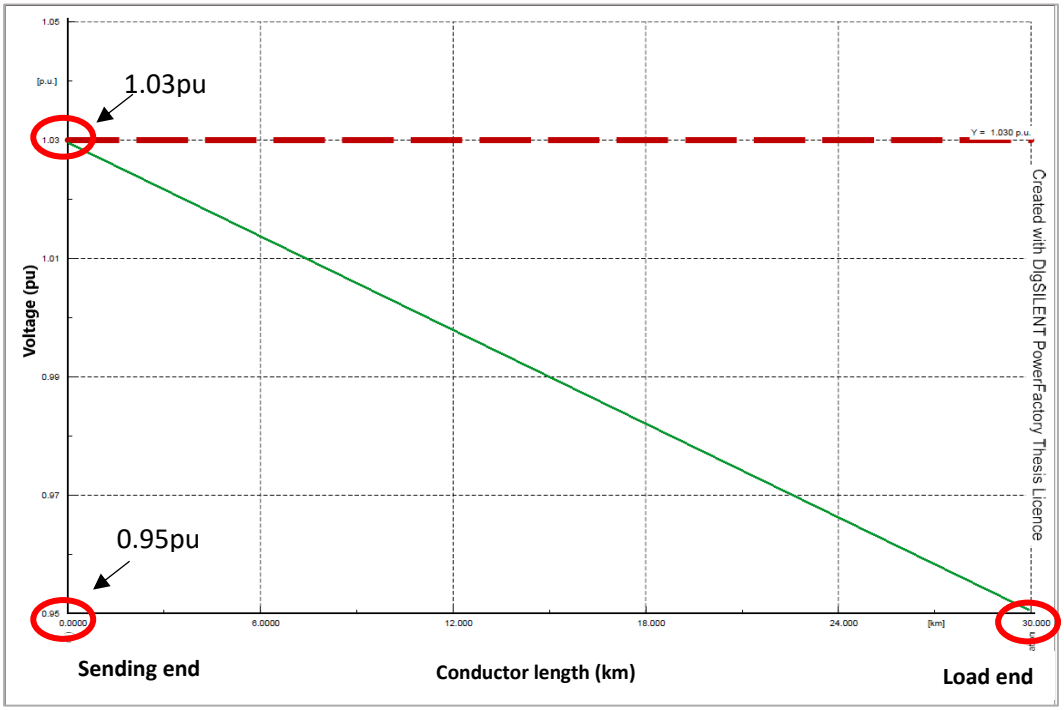

Figure 3-4: Voltage profile corresponding to Figure 3-3.

Extending this example by varying parameters R, C, L from equations (3.3), (3.4) and (3.5), equation (3.1) can be plotted for various line lengths as shown in Figure 3-3. This plot will be useful to determine the correct line length for specific conductors under varying load conditions. Based on the above information, the sending end, as well as receiving end voltages of the simulated test network used in this research (as shown in Figure 3-4), are chosen so as to ensure that before an IPP is connected to the backbone feeder, the network itself is assumed to be continuously operating well within the upper and lower voltage limits as defined by the SAGC and NRS048-2. However, cases involving interconnection to networks showing voltage operation closer to the outer limits defined by the SAGC and NRS048-2, will need to be tentatively considered on a per case basis, requiring more detailed analysis. For this reason, the maximum voltage at the sending end is chosen to be 1.03pu. This choice relates to voltage rise problems caused by low loading conditions (Ferranti effect [80]), that significantly limit the number of lower capacity load options that can be included in the ANN training phase discussed in sections to follow. Setting the sending end voltage to a value closer to the upper limit (1.05pu), would essentially mean that only large maximum load ranges can be considered as part of the training input data used at the

receiving end of the feeder (Segment B), so as to avoid excessively high voltages at the receiving end. This upper setpoint will also ensure that, after the interconnection of the IPP to the backbone, the POC and receiving end will have more freedom to 'see' higher increases in voltage, without exceeding the upper voltage boundaries. Taking the above into account, for the vast majority of cases, the upper setpoint of 1.03pu will suffice for this research, and only be adjusted on a per case basis where necessary.

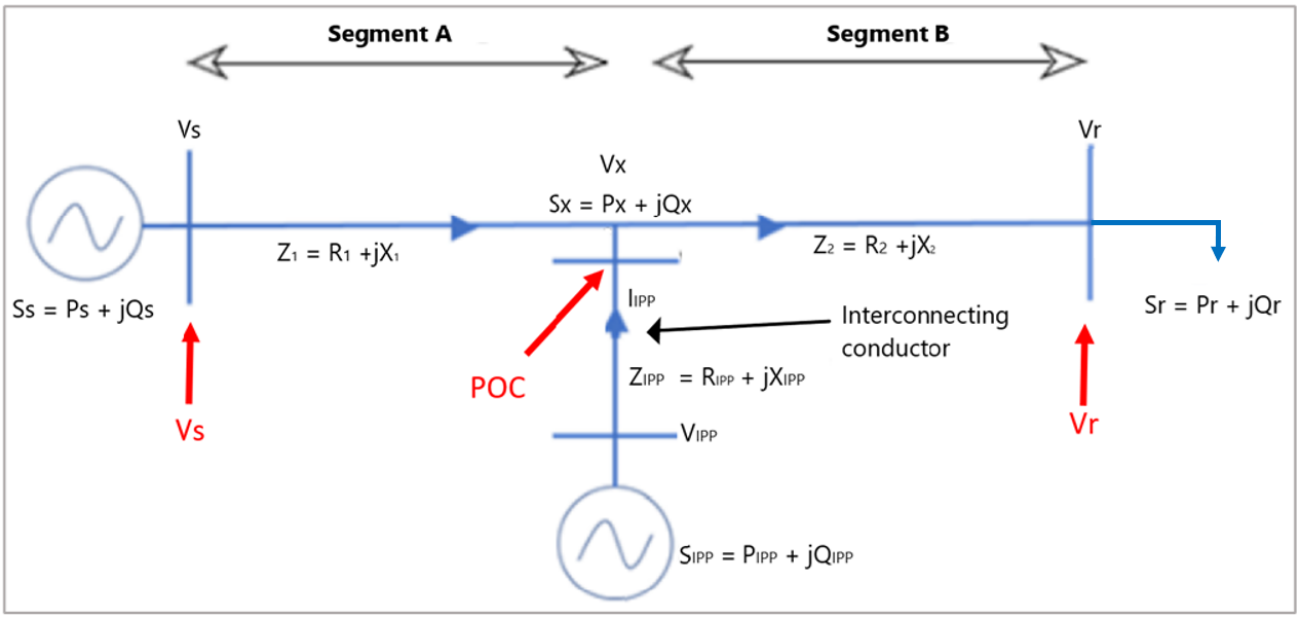

Figure 3-5: Network diagram indicating point of connection (POC).

3. ***Interconnecting feeder length and IPP Size:*** By changing typical unidirectional power flow on lines, improperly sized IPPs on power lines may worsen the impact of power line losses and further jeopardize the technical performance of both the IPP and the utility. The effectiveness of the current protective coordination settings on feeders may potentially be impacted by this. The situation of reverse power flow is illustrated using Figure 3-6 where the IPP supplies more than the load demand. For a load consuming 130 MW (at unity power factor), the excess power (10 MW) is consumed by the grid (sending end of the power line), as seen by the power flow arrows in red in Figure 3-6. An additional case may result from a fault condition at the receiving end, forcing the receiving end circuit breaker to operate. In this case the full 140MW of exported power from the IPP will also be transferred to the sending end, back into the grid, as indicated by the greed power flow arrow.

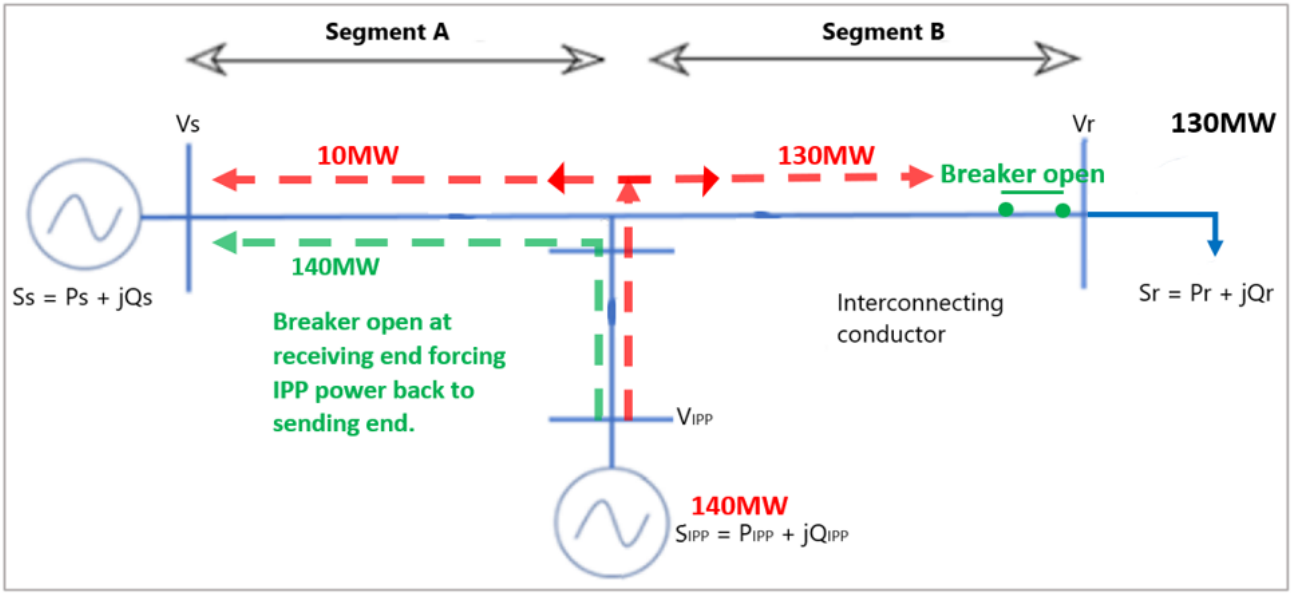

Figure 3-6: Reverse power flow condition due to IPP size exceeding load demand at the receiving end of the backbone.

In practice, there is no restriction to the IPP export capacity relative to the amount of load drawing power from the receiving end. For the purposes of this research though, this limit is set to 50% of the total load demand, while the other 50% contribution is supplied by the grid (sending end). This is to ensure reverse power flow is adequately prevented while also increasing network reliability and continuity of supply.

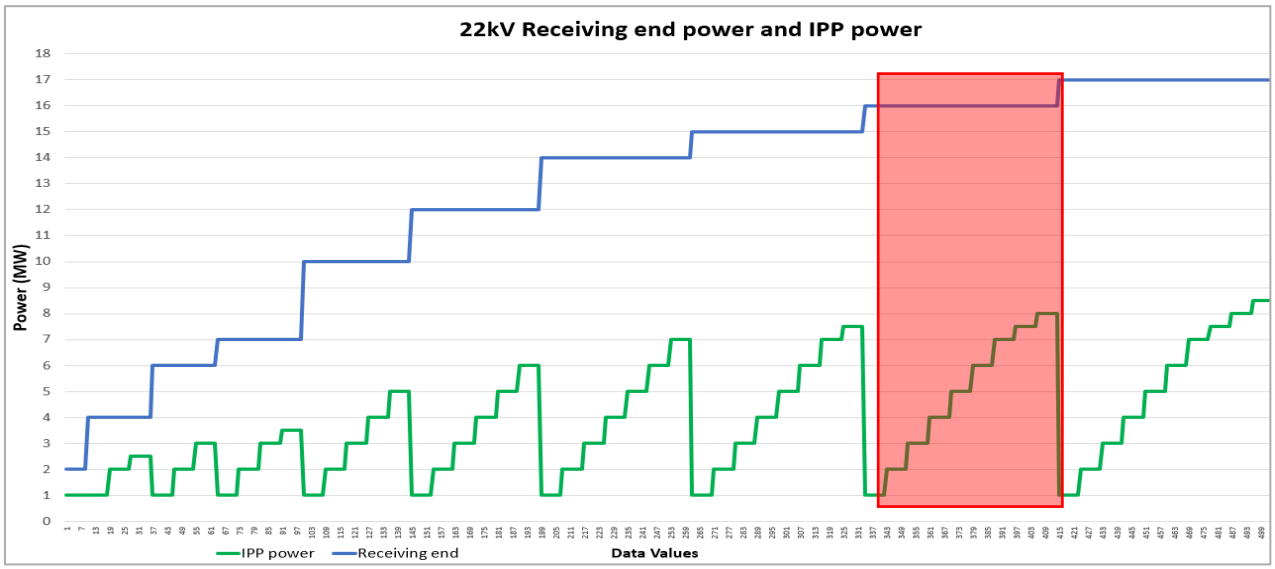

Figure 3-7: IPP export capacity per receiving end load demand

Figure 3-7 illustrates how this is done on a 22 kV backbone feeder. As seen, the load demand varies from 2MVA at unity power factor to a maximum of 17MVA at unity power factor (in agreement with equations 3.1-3.7). The upper limit of 17MVA allows for the receiving end to safely operate within the 1.05pu and 0.95pu voltage limits required for network planning studies [73]. This maximum value may be increased or decreased on a per case basis depending on the network nominal voltage, specific choice of conductor, tower geometry, network topology and receiving end power factor, but for the specific study conducted in this research, 17MVA is acceptable as will be illustrated in Section 3.2.3. The IPP export capacity graph shows multiple IPP size options available for a specified maximum load. Considering the red highlighted area, IPP's of sizes 1 MW to 8 MW will connect to a maximum load of 17MVA (pf = 1). The difference between any two power values, will be the required power supplied by grid (sending end). Since the aim of this research is to reduce power line losses, every IPP size, for a specific load value, will be used to determine if its contribution will result in a reduction or an increase in overall power line losses. Every case of the 9 IPP sizes, will have a different impact on the total line losses, generated on the network. The IPP size that results in the smallest total network loss, will be the most favourable size. Figure 3-7 also shows that for larger loads, more IPP combinations are available, while for smaller loads, there is limited variability in IPP sizes available for connection. This is because it was decided to make increments in IPP sizes discrete and constant for all cases in the data, which simplifies the data processing significantly. Allowing for equal IPP sizes for every load condition would also result in data storage concerns, especially when training the ANN.

4. ***IPP Location:*** In order to increase the accuracy of the ANN model, the largest possible IPP points of connection to the backbone feeder are considered. IPP interconnecting feeders connect to the POC at 10% increments of total backbone length from the sending end substation. Figure 3-8 illustrates varying points of interconnecting length to the backbone feeder. For 11kV-132 kV networks, interconnecting feeders are connected to the backbone at 10% interval multiples of the total backbone conductor lengths, while for 220kV and higher, interconnecting conductors are connected to the backbone at 10%, 30%, 50%,70% and 90% from the upstream sending end. This was done to reduce the data size required for longer lines while still ensuring adequate ANN learning and prediction ability.

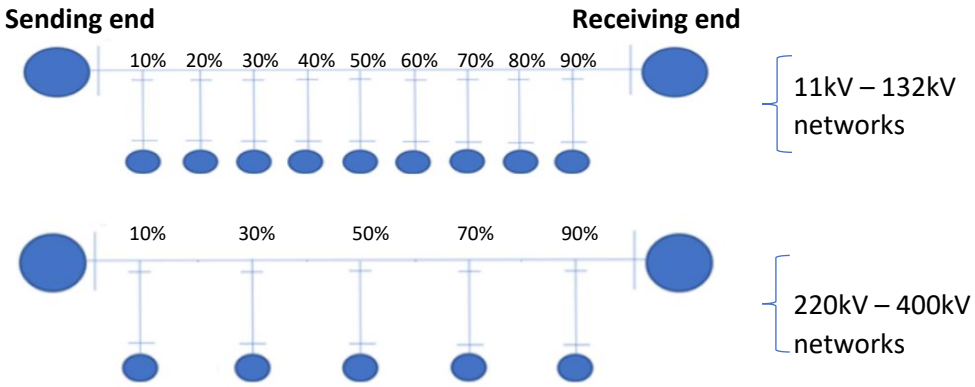

Figure 3-8: IPP connecting to the backbone for networks less than 132kV (top), and greater than 132kV (bottom).

5. ***IPP Power Factor:*** For Category B, power factor is varied from pf = 0.975 lagging to pf = 0.975 leading, including unity. For Category C, power factor is varied from pf = 0.95 lagging to pf = 0.95 leading, including unity as per SAGC [7].

6. ***Conductor Selection:*** All computations in this study are made using the probabilistic method [73,107]. To guarantee that conductor sag will not violate the minimal safe clearance distance, conductors are rated according to a Rate A (Maximum operating current under normal conditions), for 50°C temperature templates [7,73]. The nominal current, the DC-Resistance at 20°C, the DC-Resistance at 50°C, the geometric mean radius, and the outer conductor diameters are varied to adequately meet the required electrical requirements. All information can be found in a variety of open-source catalogs [78,107]. Table 3-3 lists the conductor parameters taken into account for this study.

Table 3-2:Maximum Loading per Nominal Voltage [79]

Ref	Conductor Name	Type	Overall Diameter	DC Resistance at 20˚C	DC Resistance at 50˚C	Current Rate A
1	Squirrel	ACSR	6,33	1,3677	1,533	104
2	Fox	ACSR	8,37	0,7822	0,8768	148
3	Mink	ACSR	10,98	0,4546	0,5106	206
4	Hare	ACSR	14,16	0,2733	0,3063	280
5	Chickadee	ACSR	18,87	0,1427	0,16	419
6	Kingbird	ACSR	23,9	0,0891	0,1	586
7	Tern	ACSR	27	0,0718	0,08	665
8	Zebra	ACSR	28.6	0,0674	0,0755	710
9	Bersfort	ACSR	35,56	0,0421	0,0472	965

3.2.3 Design and Model of Test Network

A single line diagram (SLD) representing the grid-tied "test network" used in this research is first built within the DIgSILENT Powerfactory GUI for every voltage technology mentioned in Section 3.2.1. Every test network per voltage level has the same configuration shown in Figure 3-9. The network is created by selecting and dragging the available network elements from the drawing tools pane (lines, busbars and transformers etc.) into the drawing pane. Lines representing conductors are drawn to interconnect the test network elements forming the SLD.

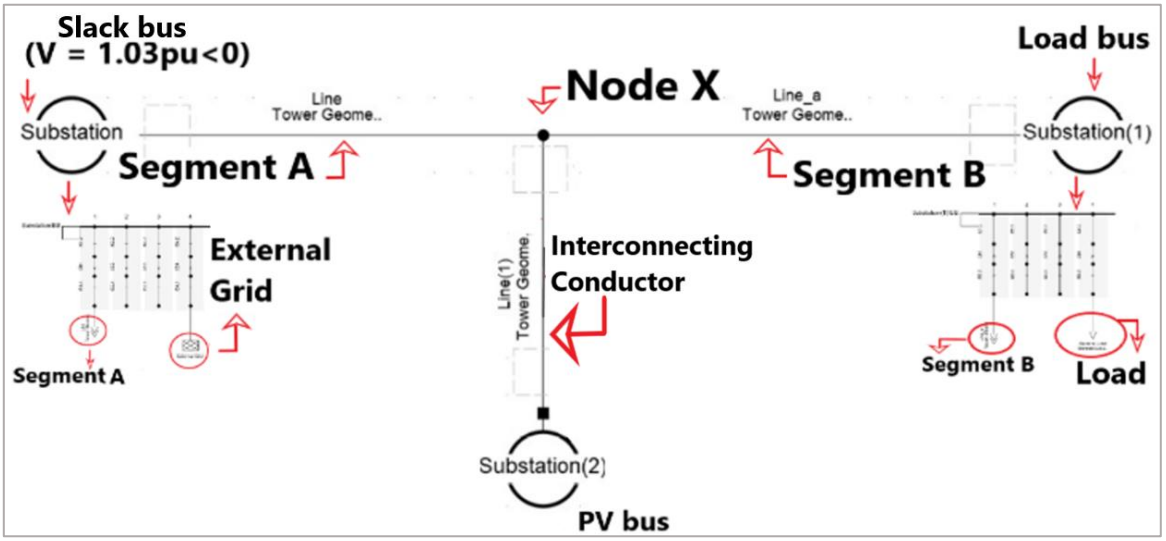

Figure 3-9: Test Network diagram representing the IPP grid-tied simulation model.

The test network elements are edited and assigned values. The values assigned to network elements are the "input data". DIgSILENT PowerFactory Quasi-Dynamic Simulation tool uses these test network element values to perform load flow studies spaced in user-defined time intervals, by manually adjusting the simulation period and the simulation step size, for a number of different input data samples [79]. The dynamic simulation feature allows for a maximum of 8 783 samples per network element, to be simultaneously computed for every load flow operation. Every simulation is SACG compliant according to conditions outlined in [7,107]. After every Quasi-Dynamic simulation load flow, a curve plot is created which displays the losses, thermal loads as well as maximum and minimum voltages of all terminals for every input data case. This way, it is easy to identify network parameters outside the stipulated limits of the SAGC.

As seen from Figure 3-9, the backbone of the test network consists of Segment A, Segment B, node X (representing the POC) and the interconnecting conductor. These are selected together along with the interconnecting conductor and allocated to a zone object. This is done by right-clicking and defining the selection as a "Zone". This ensures that the losses considered are only derived from these network components alone since it is the overall line losses that are of interest. "Zone" is set as the element and c:LossPlne parameter selected as the simulation variable. Additionally, the thermal loading as well as maximum and minimum voltages of all terminals (nodes) are set by using the "Grid" element and parameters c:umax, c:umin and c:Maxloading [107].

Figure 3-9 also shows a slack bus or swing bus, typically associated with a synchronous generator or external grid, which for this research will be the sending end power provided by the grid. This bus ensures that the power balance within the network is established. This value changes according to the amount of power supplied by the PV bus or consumed by the load end. The voltage sending end magnitude and angle are the only parameters required for the initialization of this bus since these values change depending on the PV and PQ bus setpoints. The PV bus model (Figure 3-10) represents the entire IPP plant, which in reality consists of strings of solar PV panels connected to a single inverter. Typically, two inverters feed into two separate LV windings of a step-up transformer (Star – Delta). The primary side (MV side) of each transformer is connected to a collector bus bar that feeds into a larger transformer, further stepping up the voltage to the transmission or distribution system, via a dedicated feeder.

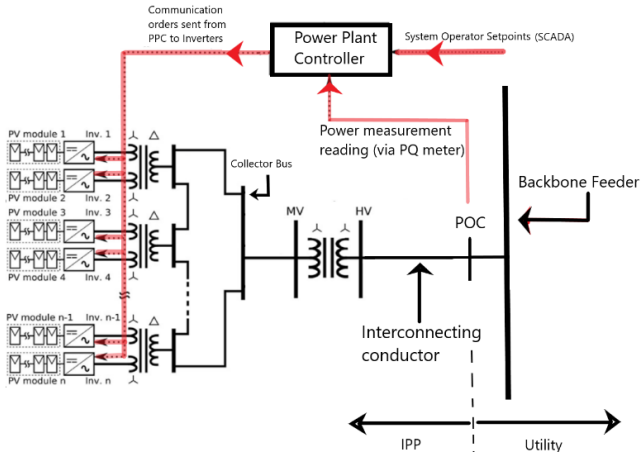

Figure 3-10:Generic IPP plant station electrical schematic diagram

A power quality meter measures IPP parameters such as active power, reactive power, voltage and frequency at the POC. These measurements are fed into a Power Plant Controller (PPC) which compares the system operator setpoints to the IPP operating setpoint and adjusts specific inverter operating parameters, by sending communication orders to the inverters. This way the overall plant, as measured at the POC, can be controlled and remain SAGC compliant. Site operators communicate these setpoints and parameters to the PPC either directly, or more commonly through a SCADA system. The PPC operation is therefore fully controlled by the IPP itself. For the above setup, the IPP plant is modelled in DIgSILENT Powerfactory using the PV System element (representing the actual PV plant) as shown in Figure 3-11. The PV system element has built in functionality that can simulate advanced dynamic PPC operation (in order for immediate IPP response to change in network voltage, frequency and power). For this research, however, the PV system element is set to adjust the maximum active power and power factor set points of the IPP unit itself (with values defined in Section 3.2.1), with local controller functionality set to "constant power factor" mode, as recommended by [79]. Constant power factor control means that the reactive power output of the IPP unit is maintained in proportion to the active power output such that the power factor remains constant regardless of the terminal voltage.

The IPP active power values are imported into the PV system element (which represents the actual PV plant) by first adding a project characteristic and selecting the time characteristic option as shown in Figure 3-11. The time characteristic allows for the IPP to export different active power values at different moments in time, using the Quasi–Dynamic Simulation feature. A single column of data allows for a maximum of 8783 power values to be imported as a set, with units defined in kW. From a MS Excel table containing the entire input data set of values as defined in section 3.2.1 above, the column containing the IPP Size in MW (which is the rated export capacity of the solar PV plant) is copied and pasted into the time characteristic table as shown in Figure 3-11 below. In a similar fashion, the corresponding IPP power factor setpoint data defined in section 3.2.1 are also inserted and stored, by creating a power factor defined time characteristic.

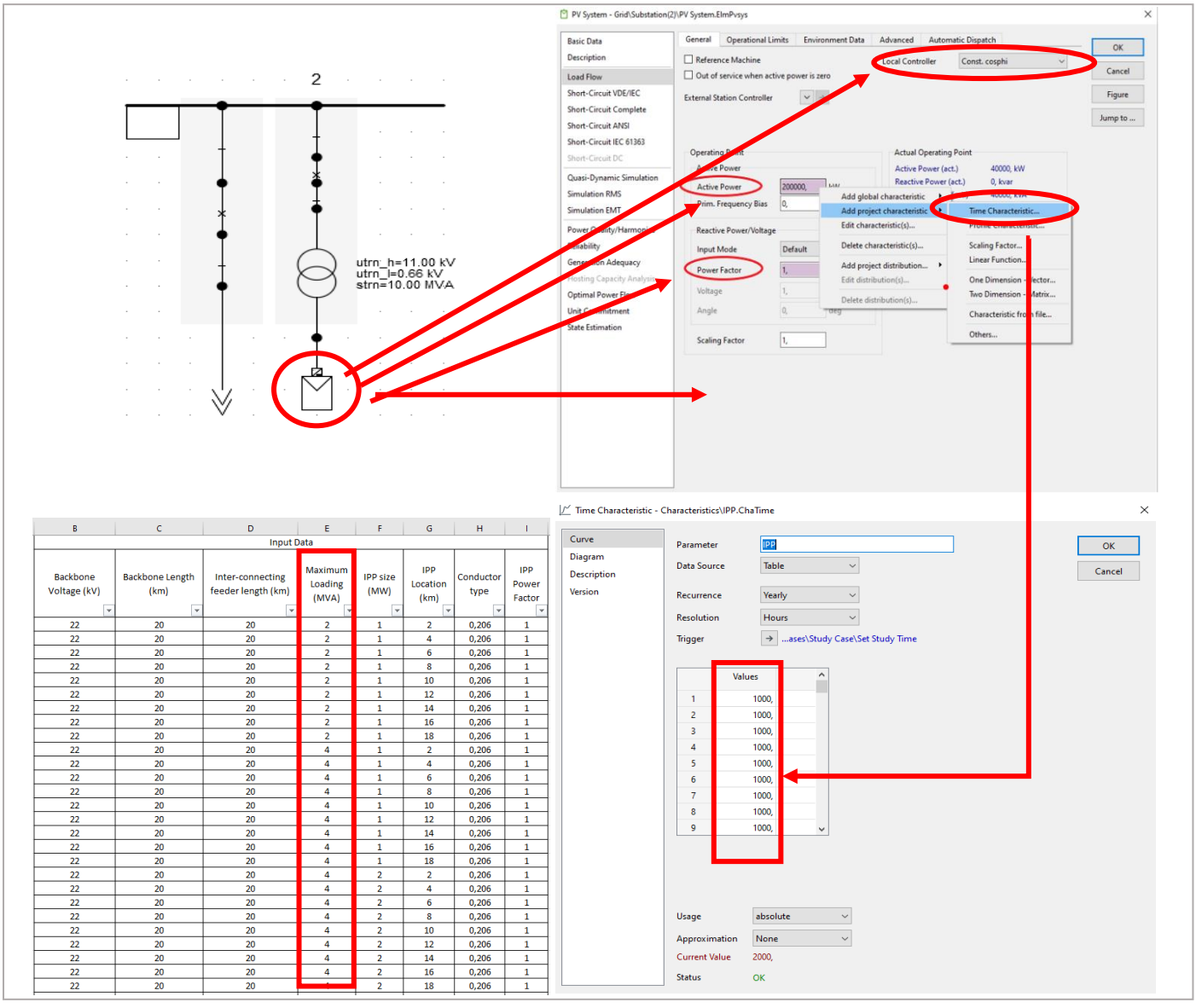

	B	C	D	E	F	G	H	I
	Input Data							
	Backbone Voltage (kV)	Backbone Length (km)	Inter-connecting feeder length (km)	Maximum Loading (MVA)	IPP size (MW)	IPP Location (km)	Conductor type	IPP Power Factor
	22	20	20	2	1	2	0,206	1
	22	20	20	2	1	4	0,206	1
	22	20	20	2	1	6	0,206	1
	22	20	20	2	1	8	0,206	1
	22	20	20	2	1	10	0,206	1
	22	20	20	2	1	12	0,206	1
	22	20	20	2	1	14	0,206	1
	22	20	20	2	1	16	0,206	1
	22	20	20	2	1	18	0,206	1
	22	20	20	4	1	2	0,206	1
	22	20	20	4	1	4	0,206	1
	22	20	20	4	1	6	0,206	1
	22	20	20	4	1	8	0,206	1
	22	20	20	4	1	10	0,206	1
	22	20	20	4	1	12	0,206	1
	22	20	20	4	1	14	0,206	1
	22	20	20	4	1	16	0,206	1
	22	20	20	4	1	18	0,206	1
	22	20	20	4	2	2	0,206	1
	22	20	20	4	2	4	0,206	1
	22	20	20	4	2	6	0,206	1
	22	20	20	4	2	8	0,206	1
	22	20	20	4	2	10	0,206	1
	22	20	20	4	2	12	0,206	1
	22	20	20	4	2	14	0,206	1
	22	20	20	4	2	16	0,206	1
	22	20	20	4	2	18	0,206	1

Figure 3-11:IPP sizes are imported and stored into the IPP size and power factor characteristic portal.

The PV system element (which represents the actual PV plant) is connected to the LV windings of a two winding, Star-Delta step-up transformer of vector group Dyn11. This means that the MV side has a Delta connection, with a Star – Neutral connection on the LV core of the transformer. This vector group is commonly used within industry for MV connections due to its harmonic suppression ability (especially for eliminating the 3rd harmonic produced by the PV inverter [81]) and will suffice since it complies with the IEC 60076-1 [82]. For IPPs requiring connection to network voltages greater than this, an additional YNd11 step up transformer is required, for instance - an IPP connecting to the 132kV network requires for the 660V inverter system to be stepped up to 22kV via a 22/0.66kV, Dyn11, transformer and fed into a 22/132kV, YNd11, transformer which then connects to the POC. Therefore, for this thesis the connection topology will be specific to the voltage at which the IPP is connected and justified accordingly. The rated power of every transformer is chosen to handle the maximum export capacity of the PV system element to prevent overloading and minimize thermal losses. The PV system element (representing the actual solar PV plant) is set to have an output voltage of 660V feeding into the LV terminal of the step-up transformer, with the MV/HV terminal being chosen depending on the network nominal voltage. This LV value is within range of typical inverter topologies within industry [82]. Figure 3-12 shows the transformer parameter page within DIgSILENT Powerfactory, It will be noticed that these parameters are entered manually.

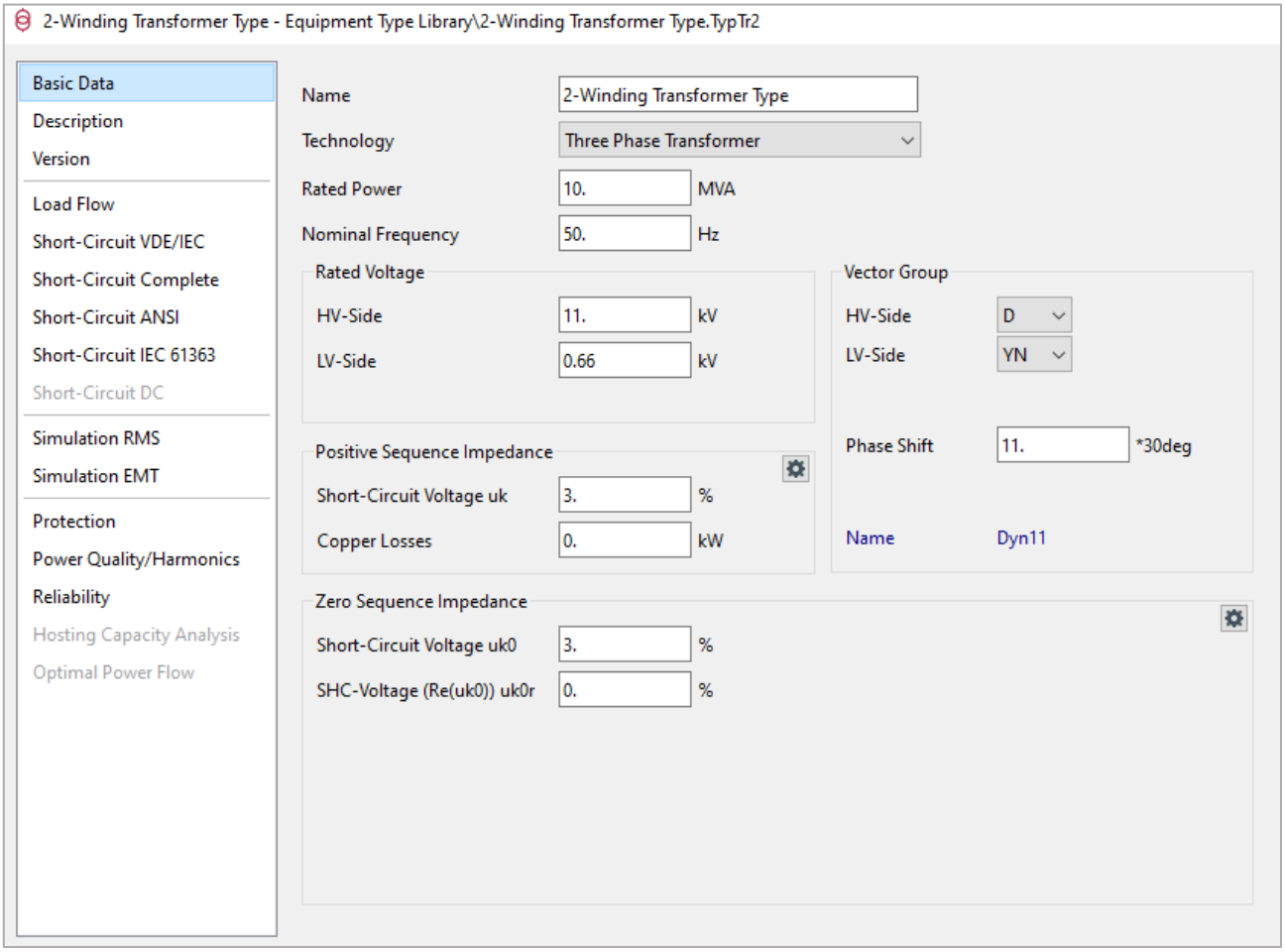

Figure 3-12:Transformer parameter input portal, showing the 11kV/660V 10MVA transformer parameters.

The PQ Bus (or load bus) is used to define fixed load values also at a specific power factor. The general load element is used to account for varying load power values (with maximum limits determined from equations 3.1-3.7). In the same fashion as was done for importing IPP Sizes into the PV system element (representing the actual solar PV plant) and using the same MS Excel table containing the entire input data set of values defined in Section 3.2.1, the column containing Maximum Loading (MW) is copied and pasted into the load time characteristic table as shown in Figure 3–13.The load time characteristic table is required in order for the user to predefine accurate load values (power consumed by the load, at the receiving end of the backbone feeder), in order for the simulation to be as accurate as possible. The Quasi-Dynamic feature of DIgSILENT Powerfactory will simulate each load condition (value) by iterating from the first value to the last value entered into this table. A step-down transformer is connected before the general load element, ensuring the correct voltage is applied to the load.

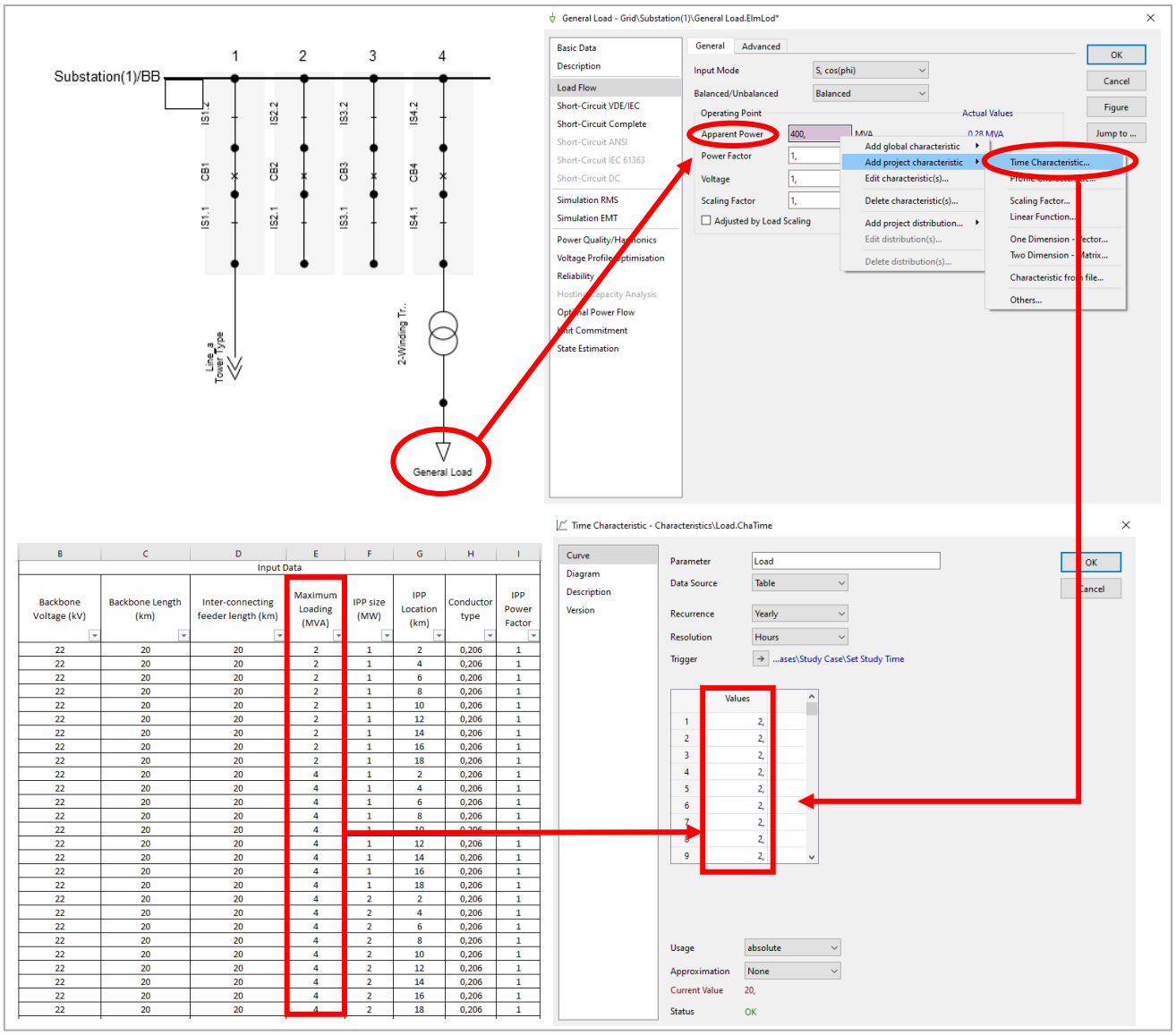

Figure 3-13:PQ bus consisting of a general load element with varying active power consumed by the load.

In order to account for changes in the position of the interconnecting conductor on the backbone feeder, Segment A and Segment B lengths are adjusted using the same time characteristic approach described earlier for IPP active power variation. As an example, for a backbone feeder of length 100km, the following scenarios are possible:

Segment A = 10km, while Segment B = 90km (IPP located closest to sending end)

Segment A = 20km, while Segment B = 80km

Segment A = 30km, while Segment B = 70km

Segment A = 40km, while Segment B = 60km

Segment A = 50km, while Segment B = 50km (IPP located in halfway between the sending and receiving end)

Segment A = 60km, while Segment B = 40km

Segment A = 70km, while Segment B = 30km

Segment A = 80km, while Segment B = 20km

Segment A = 90km, while Segment B = 10km (IPP located closest to receiving end)

It is required that two sets of varying data be imported using the time characteristic, while also ensuring that all combinations add to 100km of the total backbone length. This is also done by importing the line variations into the time characteristic table, as seen below in Figure 3-14. Figure 3–15 shows how, for a backbone of 100km, segment A and segment B always add up to 100km, for every IPP change in location. Location on backbone is also taken with reference

to the sending end, upstream busbar. When the IPP is at location 10%, it is thus located 10km from the upstream end and 90km from the load or downstream end. Blue and Orange dots representing segment A and segment B lengths respectively, always add to the total backbone length, as shown in Figure 3-15.

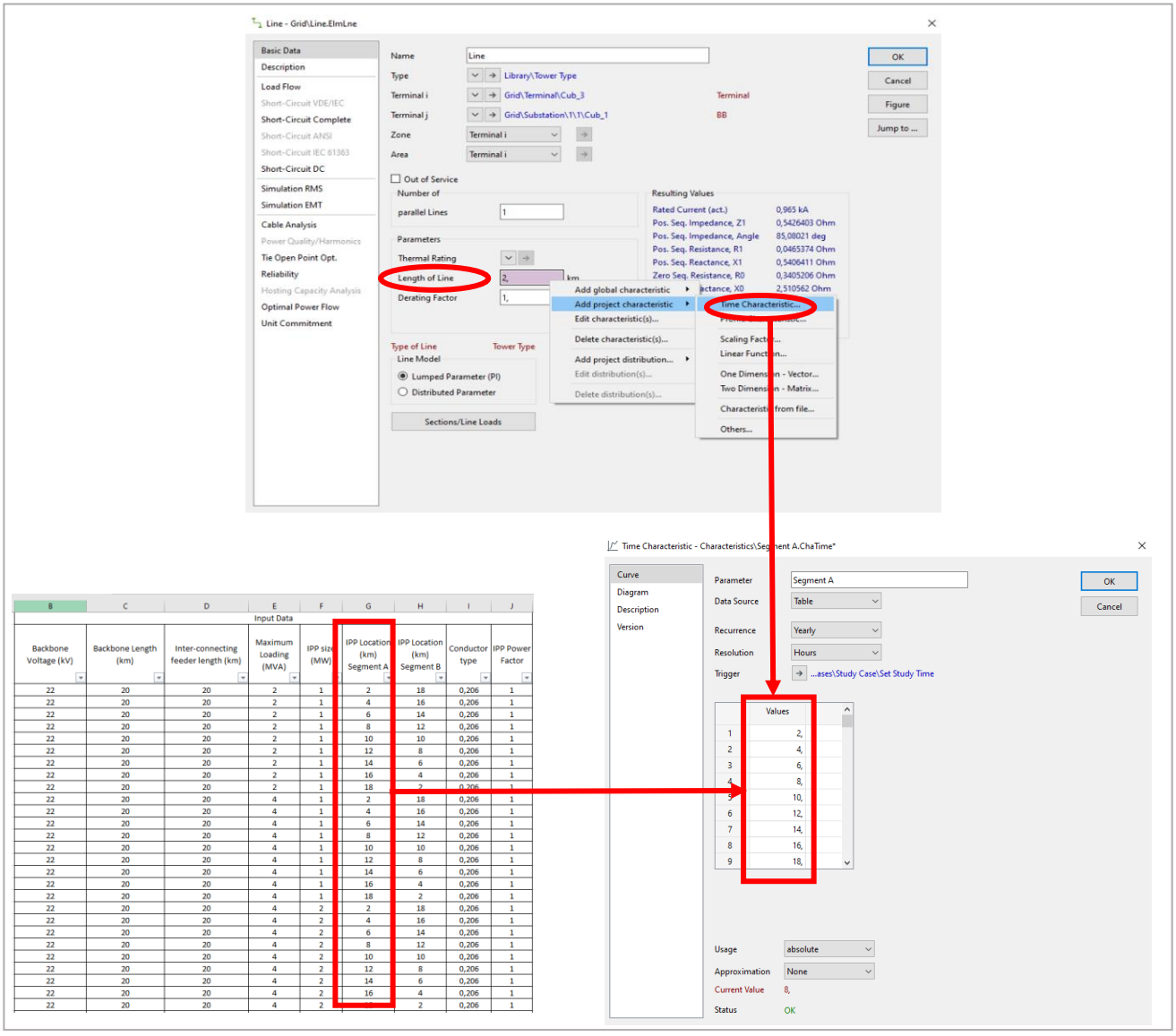

Figure 3-14:Line length variation input data portal.

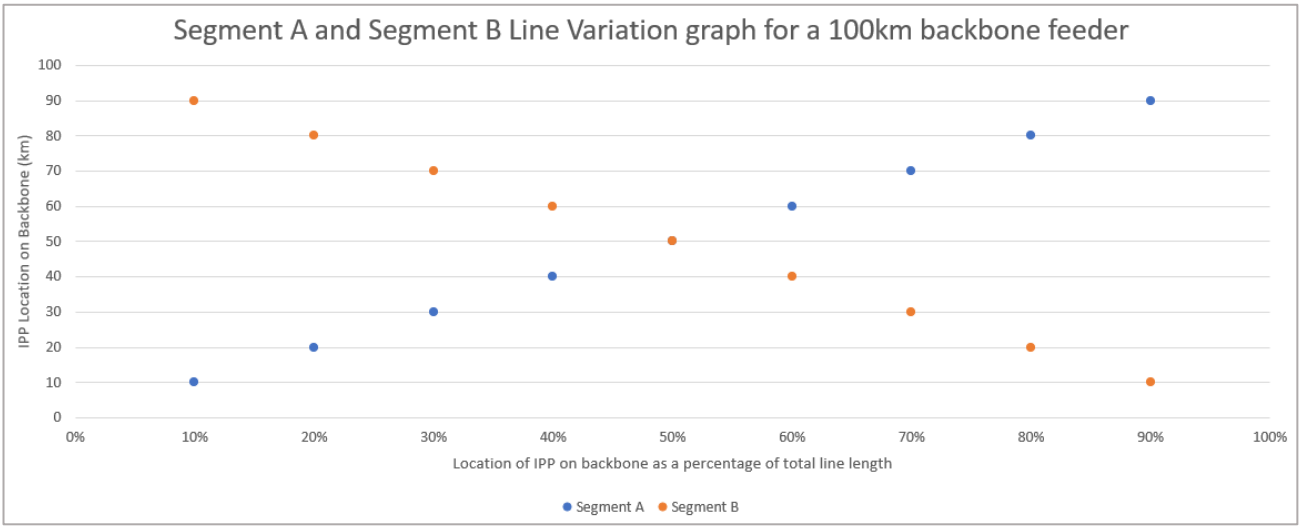

Figure 3-15:Segment A and Segment B length variation while maintaining 100km backbone length.

The interconnecting conductor length, as well as the conductor parameter specifications are also varied in the same fashion, shown in Figure 3-16.

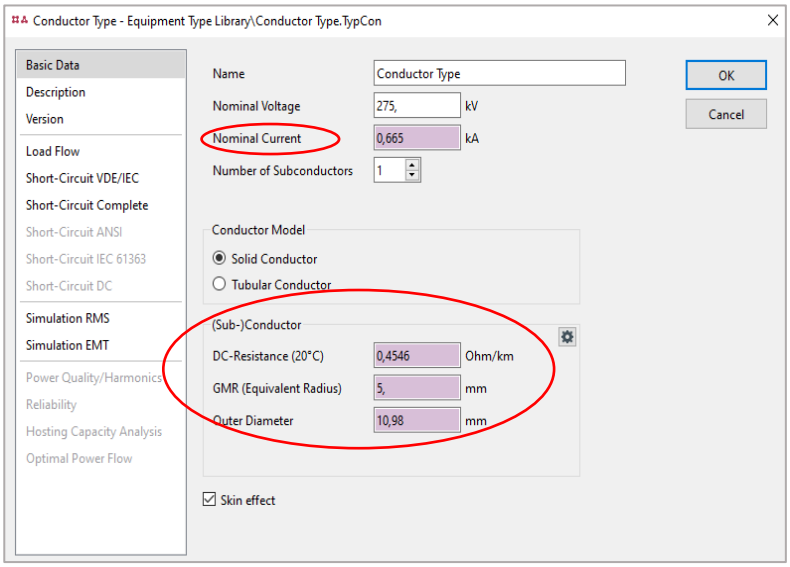

Figure 3-16:Variation of nominal current, DC resistance, GMR and outer diameter of the interconnecting conductor.

In order to account for phase - phase separation of conductors, as well as phase to earth clearances, the tower type model (TypGeo) is used. The three x and y coordinates per phase are entered, as seen on the 2D plane in Figure 3-17.

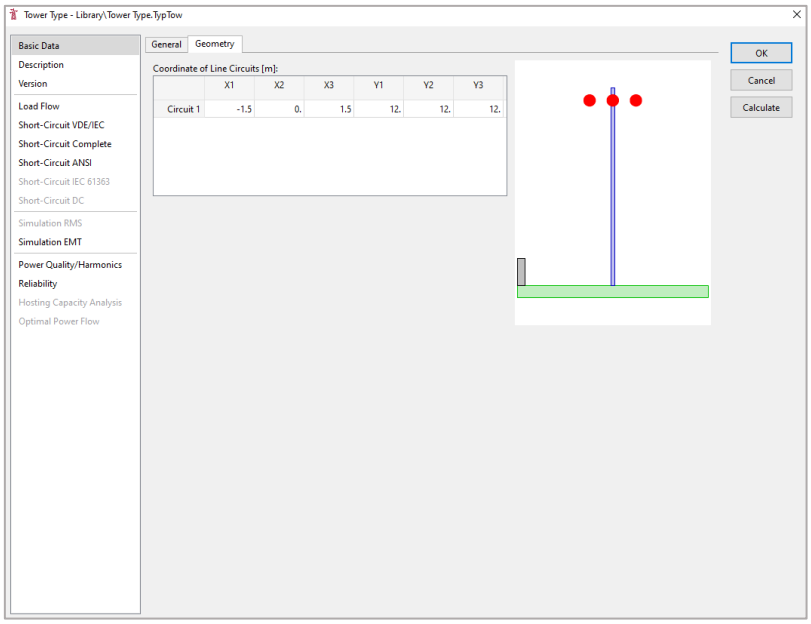

Figure 3-17:The tower type model (TypGeo) is used to enter relevant conductor phase-phase and phase-earth spacing.

3.2.4 Generation of Target Data

This section details the generation of target data. Target data is essential for the ANN training process since it represents the known output of the input data. The ANN training process requires target data to enhance its predictive ability, so that after the training phase, the ANN can predict its own output value as closely as possible to the target data. For this research, the target data represents the combined sum of line losses from Segment A, Segment B and the interconnecting conductor for every unique input data case. Target data consists of seven, (Nx1) line loss matrices for the following voltages: 11kV, 22kV, 66kV, 132kV, 220kV, 275kV and 400kV. Total line losses (combined sum of Segment A, Segment B and the interconnecting conductor) resulting from input data will be retrieved from DIgSILENT PowerFactory after every simulation run and stored in a single column matrix for every voltage type, each with the same number of rows as the input data set. Figure 3-18 shows the relationship between input and target data.

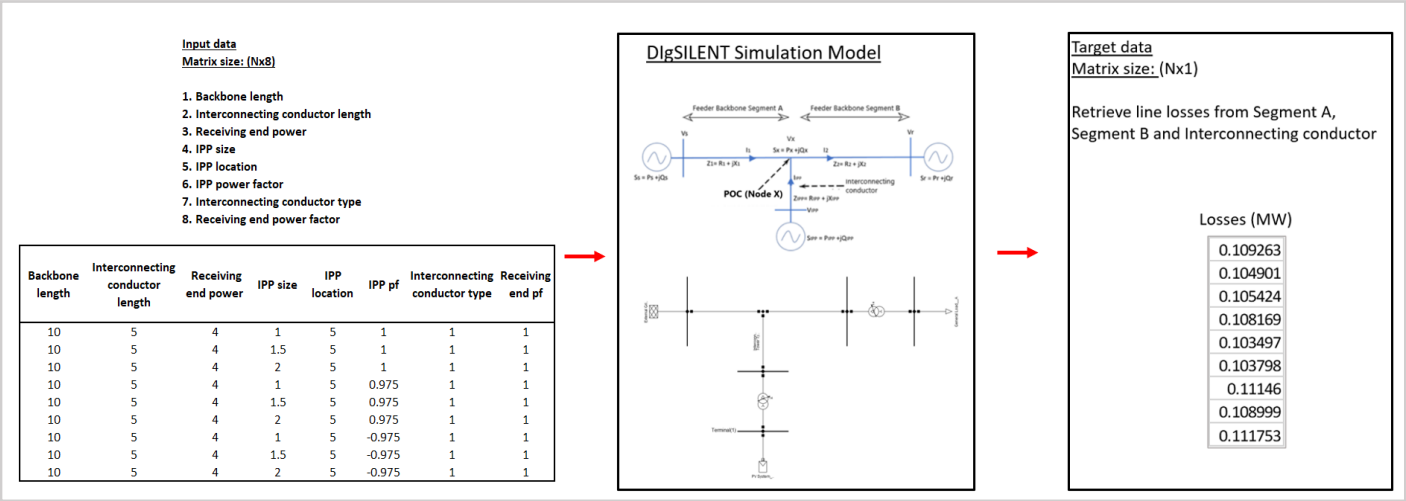

Backbone length	Interconnecting conductor length	Receiving end power	IPP size	IPP location	IPP pf	Interconnecting conductor type	Receiving end pf
10	5	4	1	5	1	1	1
10	5	4	1.5	5	1	1	1
10	5	4	2	5	1	1	1
10	5	4	1	5	0.975	1	1
10	5	4	1.5	5	0.975	1	1
10	5	4	2	5	0.975	1	1
10	5	4	1	5	-0.975	1	1
10	5	4	1.5	5	-0.975	1	1
10	5	4	2	5	-0.975	1	1

Figure 3-18:Relationship between ANN input data and target data.

An AC load flow calculation is conducted for each quasi-dynamic simulation with different 8xN input data combinations, which first converts the electrical network SLD values into non-linear nodal equations that are solved iteratively. The active and reactive power flow injections at each busbar or node in the power network under consideration are how the general form is expressed and how it was obtained according to [79].

The secondary parameters are established by DIgSILENT Powerfactory based on the solutions to the nodal equations once the basic parameters—the voltage magnitude (V), the voltage angle delta (δ) of the buses, and the active (P) and reactive (Q) power flow on all network branches—have been established. The user can get secondary data such as total line losses, system thermal loading (%), voltage profiles (line voltage vs. line length), voltage imbalance (for unbalanced loads), power factor, etc. [79]. The target data values are the total line losses that apply to Segment A, Segment B, and the connecting conductor in the grid-tied network depicted in Fig. 3-18.

3.2.5 Results Per Voltage Level Used as Input Data for the ANN

This section provides the actual input and target data used for ANN training for the 11kV case only, the remaining cases (22kV, 66kV, 132kV, 220kV, 275kV and 400kV) are presented in Appendix A for reference. This section will show that all input and target data are within the maximum and minimum limits of the SAGC. Every part will contain the following information:

A. Interconnecting conductor location on backbone graph (POC).

B. Maximum MVA loading graph for the interconnecting conductor and segments A and B of the backbone for loads operating at unity power factor. Inductive and Capacitive loads are not shown but included in the ANN training process.

C. Maximum and minimum voltage graphs at the receiving end of the network, as well as at the POC.

D. Thermal loading graphs for interconnecting conductor, and backbone conductors (Segments A and B).

E. Interconnecting conductor DC resistance at 20℃.

F. Interconnecting conductor diameter and geometric mean radius graph.

G. Interconnecting conductor nominal current graph.

H. Interconnecting conductor rated power versus IPP power graph.

I. IPP power factor variation graphs for unity, leading and lagging setpoints applicable to Category B (±0.975) and Category C (±0.95).

J. Total power line loss graphs, corresponding to different IPP power factor setpoints mentioned in I above.

3.2.6 Voltage Level

The data in this section consists only of 11kV data, the remaining 22kV, 66kV, 132kV , 220kV, 275kV and 400kV data are given in Appendix A.

3.2.6.1 11kV Data: Remaining data to be found in Appendix A

A. Interconnecting conductor location on backbone graph

Figure 3-19 superimposes two graphs onto one another, for a total of 126 data values. The first graph (in blue) shows 14 repeated sets of data, indicating the change in length of Segment A on the backbone feeder. For all 14 sets of data values, Segment A starts off at a length of 1km from the sending end, corresponding to data value 1 on the x - axis. It is increased to 2km for data point 2, 3km for data point 3 and so on, until Segment A is eventually 9 km long at the 9th data point. As Segment A is increased in length, Segment B is, at the same time, decreased in length, by the same value. This is to ensure that the total backbone length remains constant, which for the 11kV network is 10km. Segment B is not included in Figure 3–19, to simplify the interpretation of the graph, but for all simulations, Segment B is always adjusted as Segment A increases, to maintain the required backbone line length. The point connecting Segment A and Segment B is called Node X (as shown in Figure 3-18 above). For all simulations conducted in this research, the interconnecting feeder will always be connected to Node X. This way, the location of the POC of the interconnecting feeder on the backbone can be "virtually" changed with respect to its distance from the sending end, by adjusting the respective lengths of Segment A and Segment B on the backbone feeder. Therefore, every "point" on the blue curve in Figure 3–19, represents the POC of the interconnecting feeder on the backbone, as measured from the upstream, sending end, and every "set" of the 14 sets corresponds to a unique 11kV "network state" as the POC moves from the sending end location to the receiving end location in 1km increments of backbone length.

The second graph (in green on Figure 3-19) shows two corresponding interconnecting feeder lengths of 5km and 7.5km respectively. The 5km interconnecting feeder length corresponds to the first 7 sets of data, while the 7.5km interconnecting feeder length corresponds to the second 7 sets of data values, together making up a total of 14 sets of data values. For example, referring to Figure 3–19 and Figure 3-20, step 5 would correspond to a unique "network state" having an IPP size of 1MW, a receiving end power consumption of 4.5MW, an interconnecting conductor length of 5km on a 10km long backbone feeder, while step 10 corresponds to a network state having IPP size of 1.5MW, a receiving end power of 3.5MW, an interconnecting conductor length of 7.5km on a 10km long backbone feeder. The 11kV network is limited to 14 steps because at this voltage, the backbone and interconnecting feeder length cannot exceed 10km, due to low receiving end voltages (for a unity pf at the load).

The receiving end power values and IPP sizes shown in Figure 3-20 are determined using equation (3.1) and summarized in Table 3-2 (line lengths and loading levels suitable for the backbone feeder per voltage level), for 11kV lines, the maximum power transfer over 10km is limited to 5MW. It was therefore decided that for a load of 4.5MW, 3 corresponding IPP sizes will be used: namely 1MW, 1.5MW and 2MW. This is because every case of the 3 IPP sizes will have a different impact on the total line losses generated on the network. The IPP size that results in the smallest total network loss, will be the most favorable size. Hence, for data points 37 – 45 of Figure 3-20, the IPP will contribute 1MW towards the 4.5MW load demand, for data points 46 – 54, the IPP will contribute 1.5MW towards the 4.5MW load demand and for the 55 - 63 data points, the IPP will contribute 2MW towards the 4.5MW load demand. The same process is followed for data values 9 – 37, but for a 4MW load demand. Lastly, for the first 9 data points, the load demand is set to 2.5MW, for this case, a single IPP size of 1MW is used, since any value smaller than 1MW would fall outside category B of the SAGC (1MW – 20MW), and thus outside the scope of work of this research. Therefore, every set of 9 data values shown by the blue curve in Figure 3–19 corresponds to a specific IPP size that contribute to a specific load demand at the receiving end.

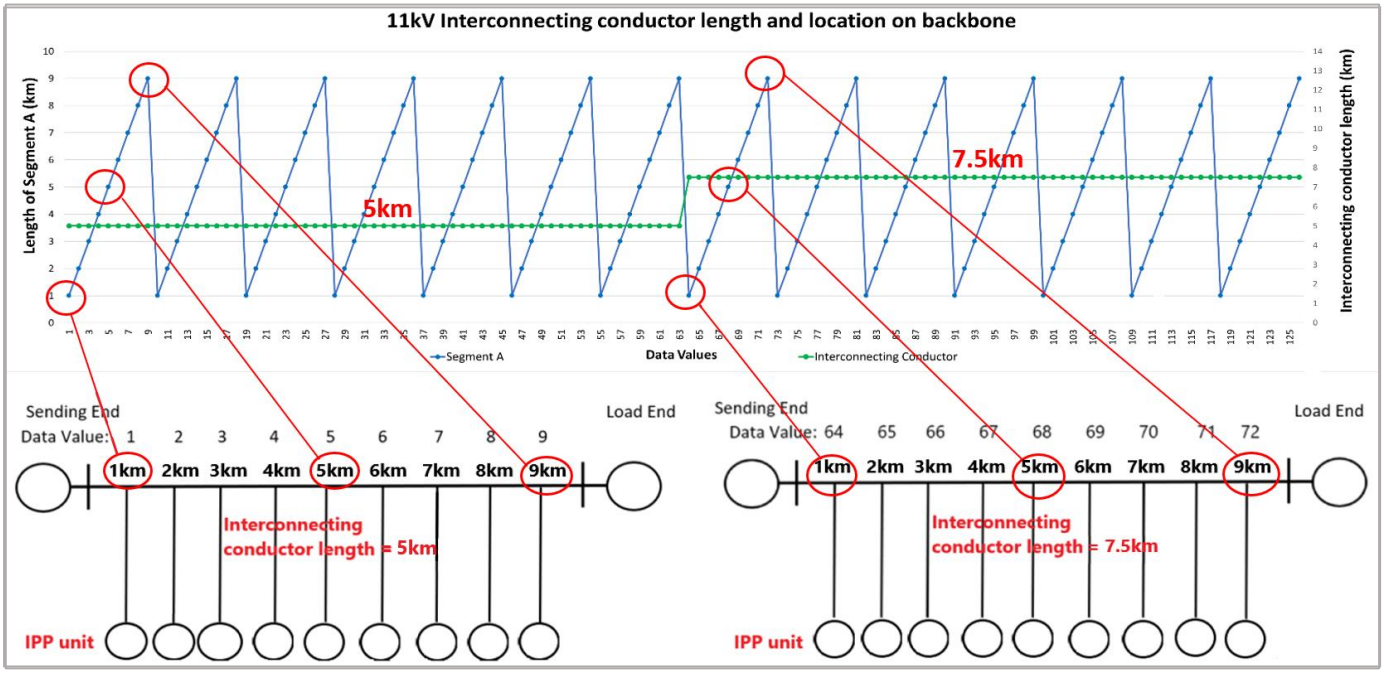

Figure 3-19:Interconnecting conductor length and location on backbone graph (Every point on the blue curve represents the length of segment A as part of the backbone feeder, with the length being measured from the sending end.)

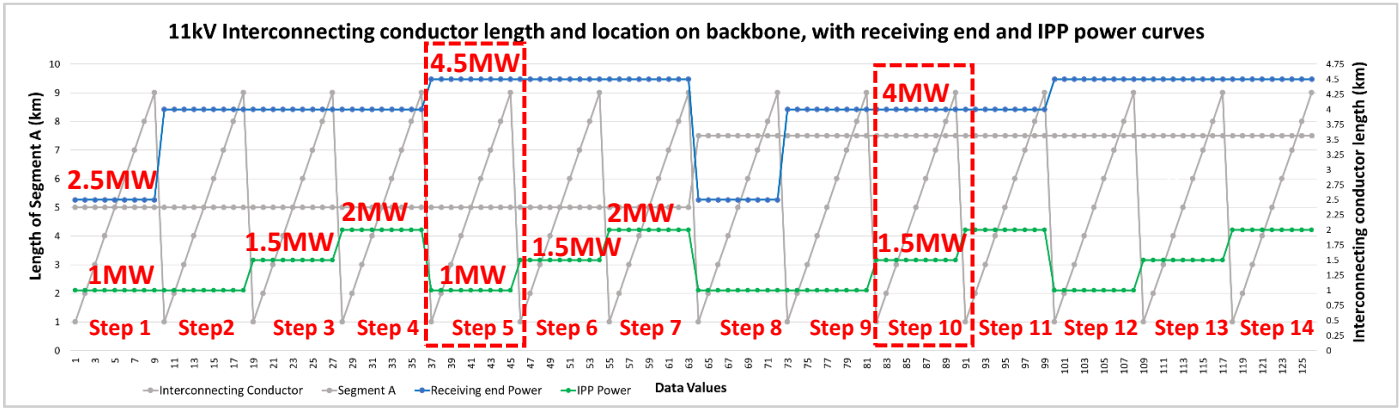

Figure 3-20:11 kV Interconnecting conductor length and its location on backbone graph, with receiving end power and IPP power curves

For all cases, both segment A and B use ACSR Single-Kingbird conductors per phase, having individual current ratings of 586A, with a maximum phase-to-phase separation of 1.5m. A horizontal intermediate structure geometry is used in the DIgSILENT PowerFactory simulation model, included with transposition, shown in Figure 3-20. Interconnecting conductors are ACSR type Chickadee, having individual current ratings of 419A. For both receiving end and IPP substations, a single transformer substation topology is used. The IPP model transfers its power via a single 10MVA 11/0.66kV step up transformer in order to transfer the maximum export power of 2MW. This is used to ensure that the IPP sending end voltage is controlled within the required per unit (pu) limit. The receiving end makes use of a single 20MVA transformer (see Figure 3-21 and Figure 3-22).

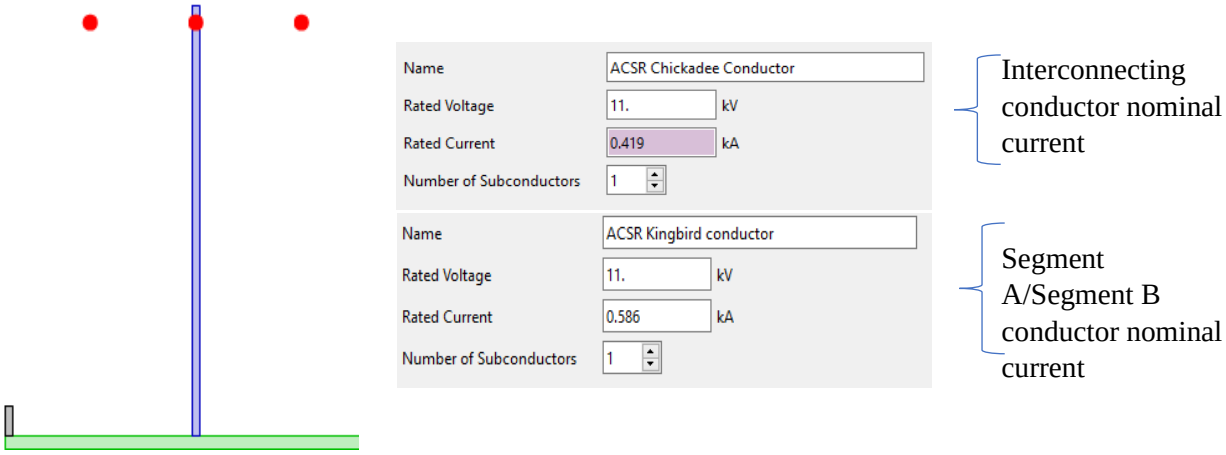

Figure 3-21: 11 kV Interconnecting conductor current rating and Segment A, Segment B current rating, with horizontal intermediate structure used for the 11kV network simulation.

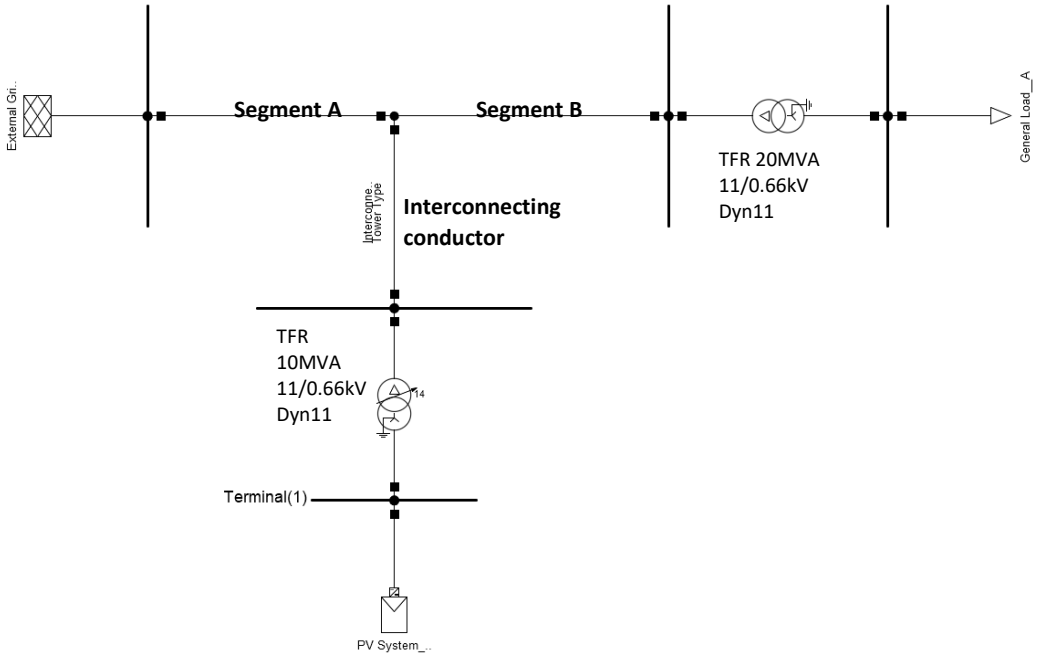

Figure 3-22: 11 kV network DIgSILENT Powerfactory model.

B. Maximum MVA loading graph for the interconnecting conductor, Segment A and Segment B of the backbone, for loads operating at unity power factor.

For completeness, Figure 3-23 shows same corresponding power curves over the same distances and interconnecting conductor locations as in Figure 3-19 and Figure 3-20, on the 11kV backbone, but also include the sending end power contribution. Since the maximum load power available at the load end, at unity power factor is compared with the IPP power contribution, the sending end power represents the power difference supplied by the sending end substation (difference between load demand and IPP power supplied). As can be seen, the load is varied from 2.5MW at unity power factor, to 4.5MW at unity power factor.

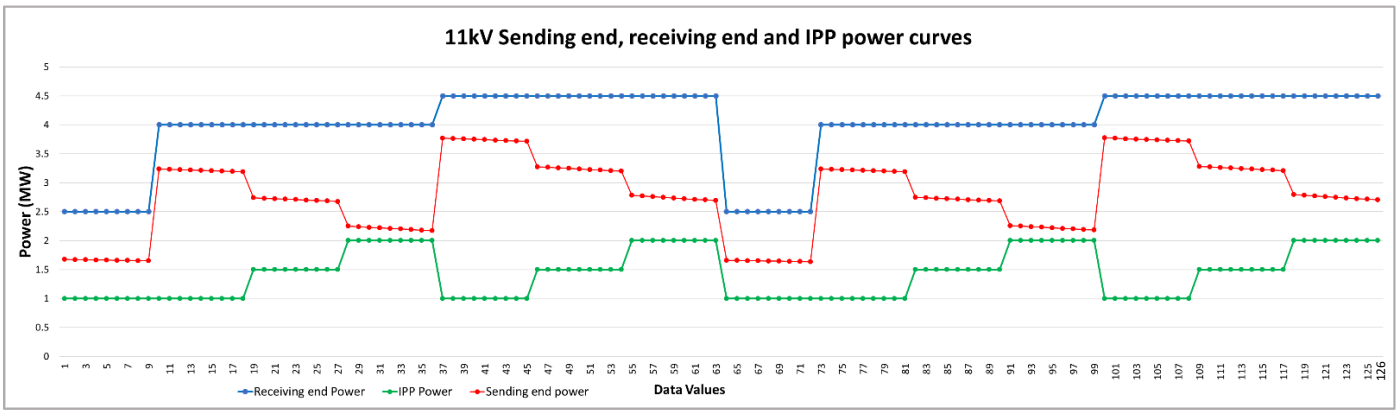

Figure 3-23:11 kV Receiving end, sending end and IPP power curves

C. Maximum and minimum voltage graphs at the load end of the network as well as POC.

The maximum and minimum voltages at the receiving end, POC and IPP 11kV busbar corresponding to Figure 3 -23 above are shown in Figures 3–24 to 3-26, below. Figure 3–24 shows the receiving end voltage, with respect to changes in IPP location on the backbone feeder. As can be seen, for all 14 sets of data values, as the POC moves closer to the receiving end (by increasing Segment A, and decreasing Segment B line lengths), regardless of the IPP size and power factor setpoint, it is observed that there is a voltage rise at the receiving end which is more pronounced for an IPP power factor of 0.975 (inductive) and less pronounced for a capacitive setpoint.

Figure 3–25 shows a decreasing trend of voltage at the POC, as the IPP moves from a location close to the sending end, towards the receiving end of the backbone. This is as expected, because as the POC moves further away from the source, the voltage drop created due to the increased resistance of Segment A, as it becomes longer in length, will in effect reduce the voltage at the POC. The IPP sending end voltage is shown in Figure 3 – 32. Figure 3 – 33 shows how the receiving end voltage responds to IPP size changes, and the corresponding load change. For data values 37 – 63, with IPP sizes of 1MW, 1.5MW and 2MW corresponding to the 4.5MW load demand, the 2MW IPP size has the greatest effect on voltage increase at the receiving end, for all IPP power factor setpoints. Figure 3 – 32 indicates that, as the load demand is increased, there is also a significant voltage drop at the receiving end of the feeder. Therefore, the maximum load used for the 11kV network is set to 4.5MW, so that the receiving end voltage of the backbone does not drop lower than the 0.95pu limit of the SAGC.

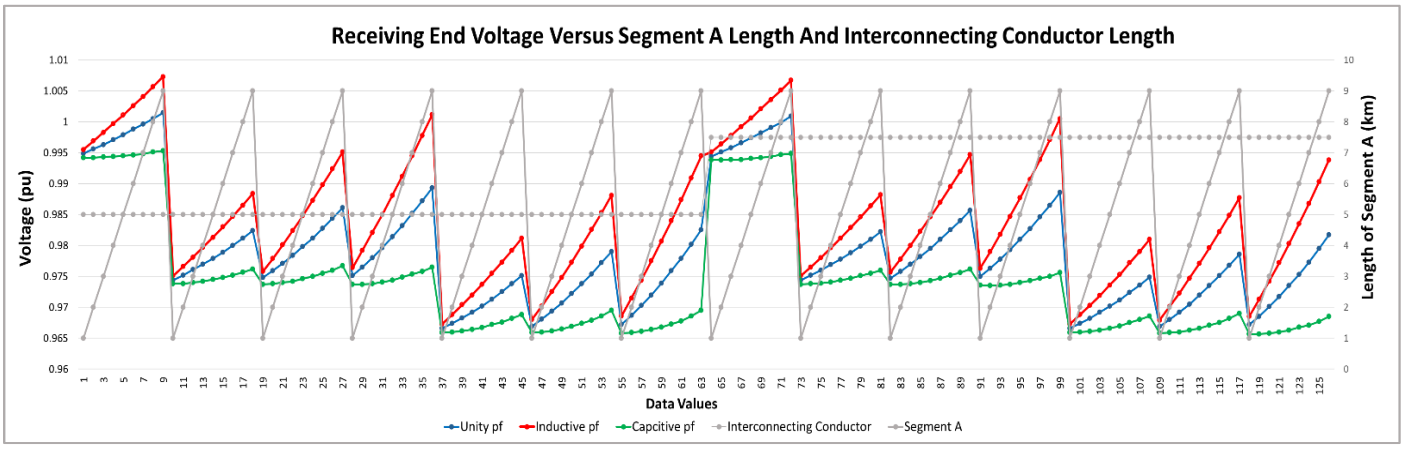

Figure 3-24:11 kV Receiving end voltage shown against Segment A and interconnecting conductor lengths

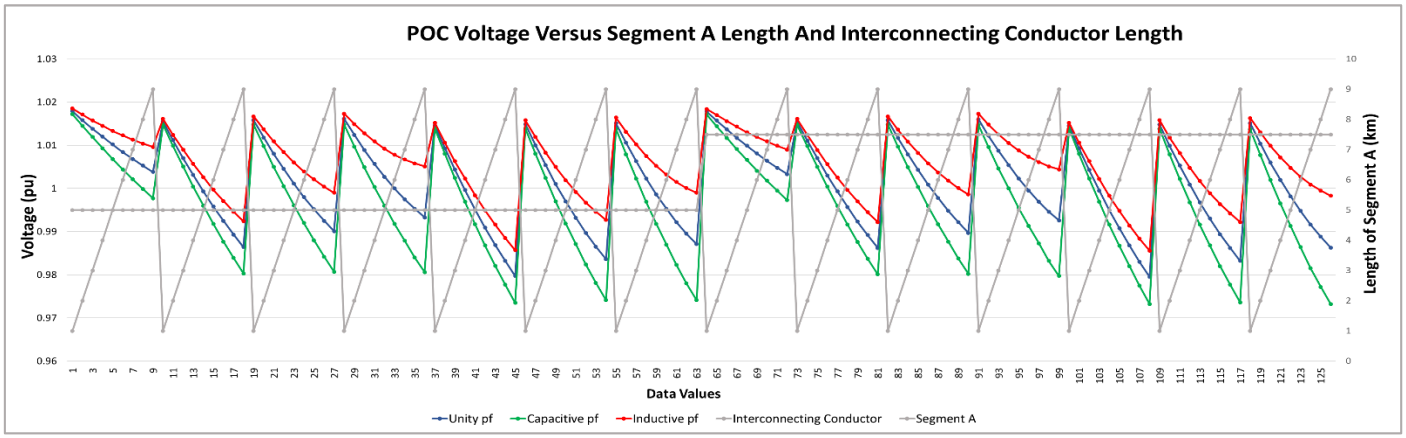

Figure 3-25:11 kV POC voltage shown against Segment A and interconnecting conductor lengths

Figure 3 -26 below shows the voltage at the 11kV side of the transformer that steps up the IPP inverter voltage. As seen the voltage is within the 10% voltage limit specified within the NRS048-2 [4].Figure 3-27 and Figure 3-28 also indicate the receiving end voltages and POC voltages respectively with values within the 10% voltage limit [4].

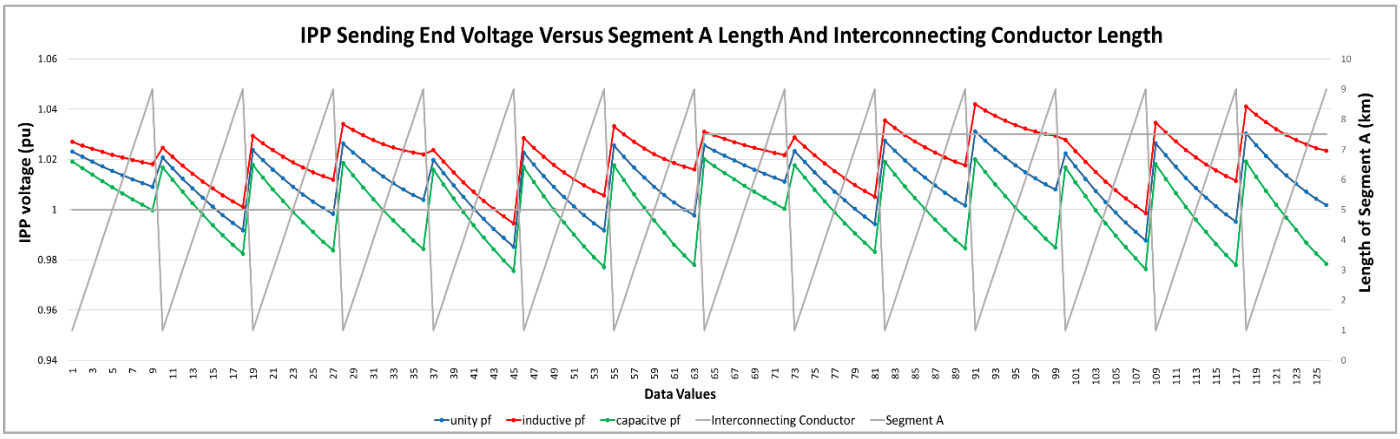

Figure 10-26:11 kV IPP sending end voltage shown against Segment A and interconnecting conductor lengths

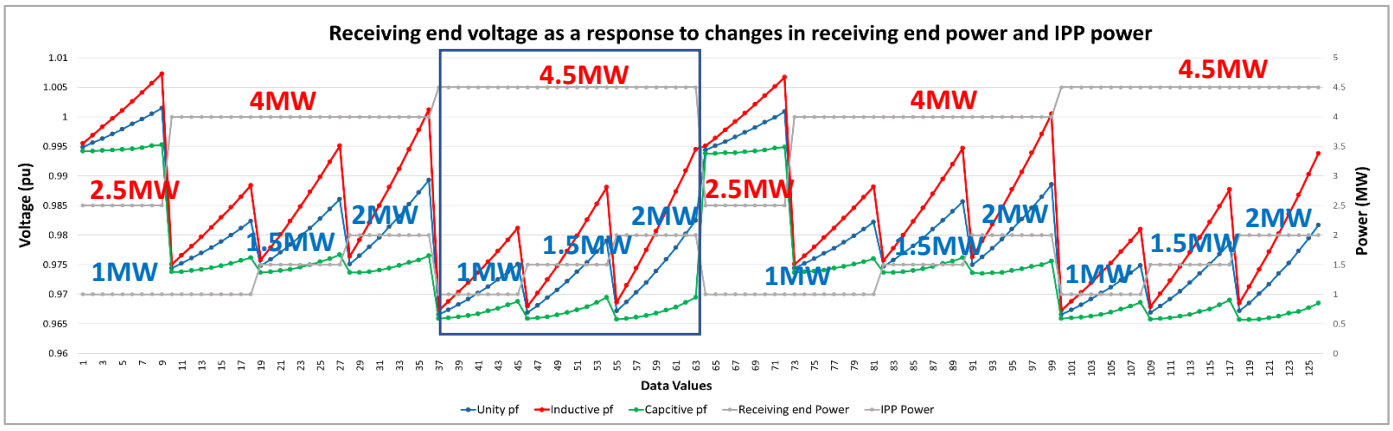

Figure 3-27:11 kV Receiving end voltage response to changes in IPP size and load.

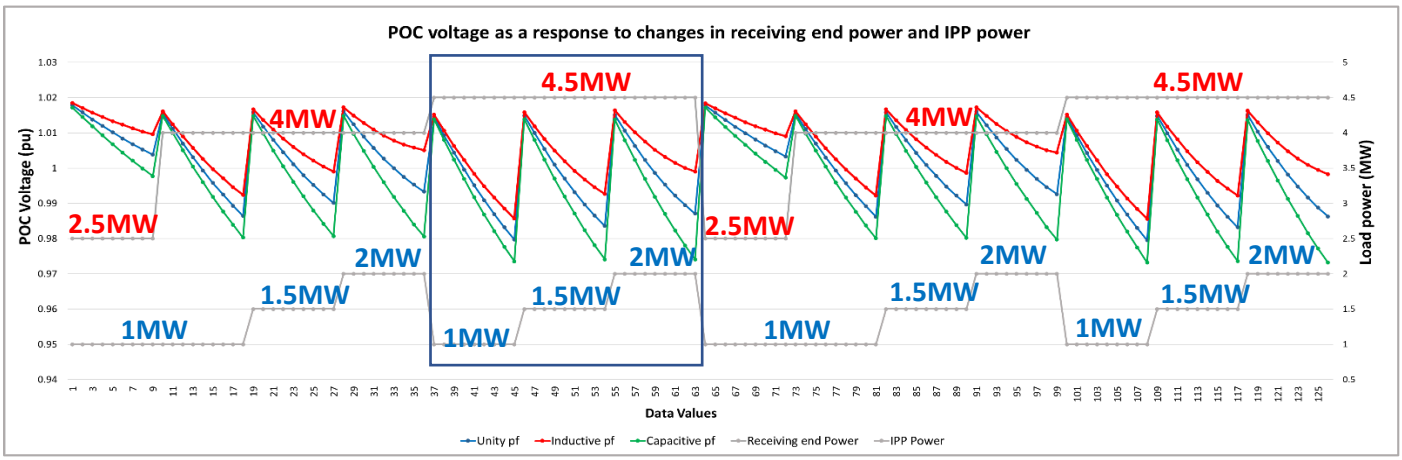

Figure 3-28:11 kV POC voltage response to changes in changes in IPP size and load

D. Thermal loading graphs for interconnecting conductor, and backbone conductors (Segment A and B).

Thermal loading is a measure of the amount of current flowing through a conductor, with respect to the rated current, expressed as a percentage. DIgSILENT Powerfactory calculates the loading value at both ends of a conductor and uses the maximum value of the two. The thermal loading of the backbone (Segment A and Segment B), and the interconnecting conductor are shown in Figures 3-29 to 3-31. As can be observed, in all simulations, there is no excessive thermal stress on all conductors in the network, with the maximum loading value not exceeding 70%. Thermal loading graphs are produced for IPP setpoints of unity, 0.975 capacitive and 0.975 inductive power factors. It is visible from all of the thermal loading curves, that for the second half of the data (from values greater than 63 on the x-axis), the interconnecting conductor maximum thermal loading is reduced. This phenomenon, as explained in [76], occurs as the power transfer in the interconnecting feeder changes from a thermal constraint to a voltage constraint.

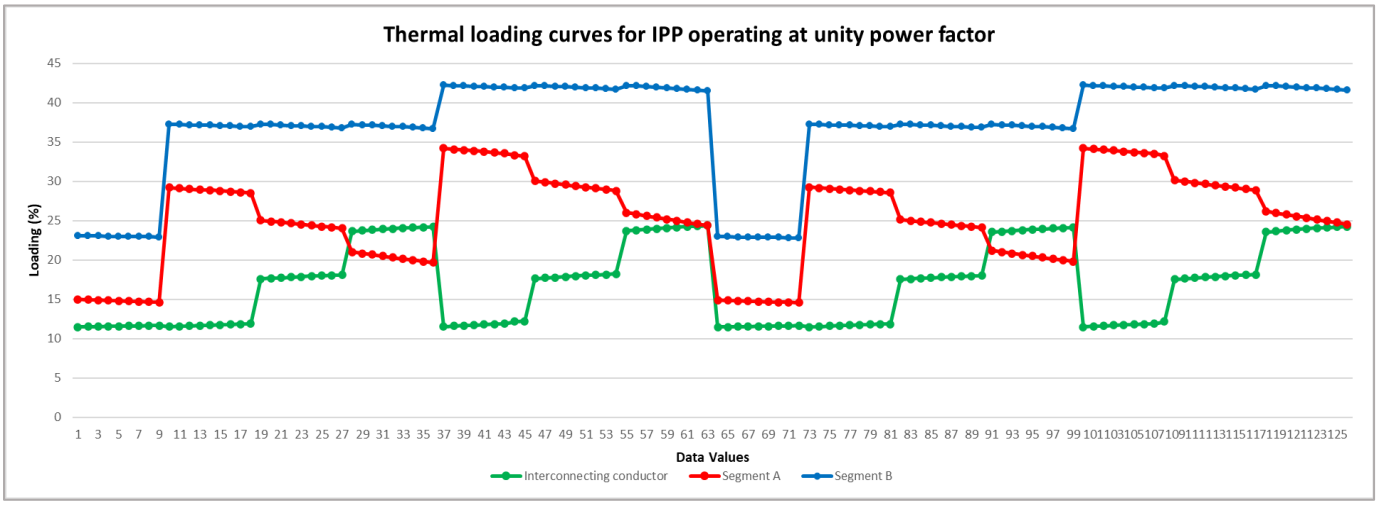

Figure 3-29:11 kV thermal loading for segment A, segment B and interconnecting conductor while IPP operates at unity pf

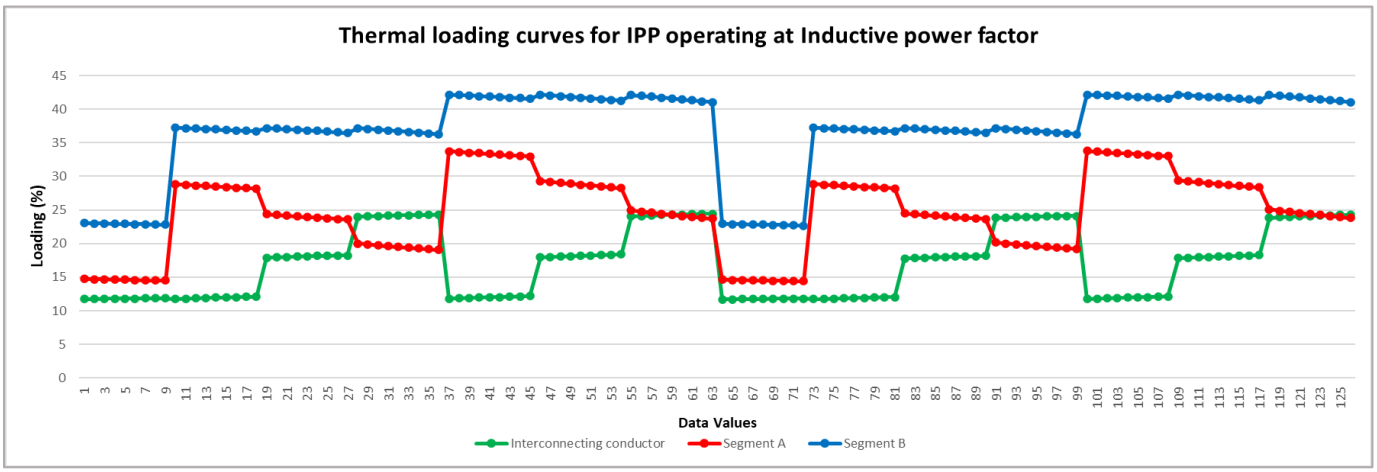

Figure 3-30: 11 kV thermal loading for segment A, segment B and interconnecting conductor while IPP operates at 0.975 inductive pf

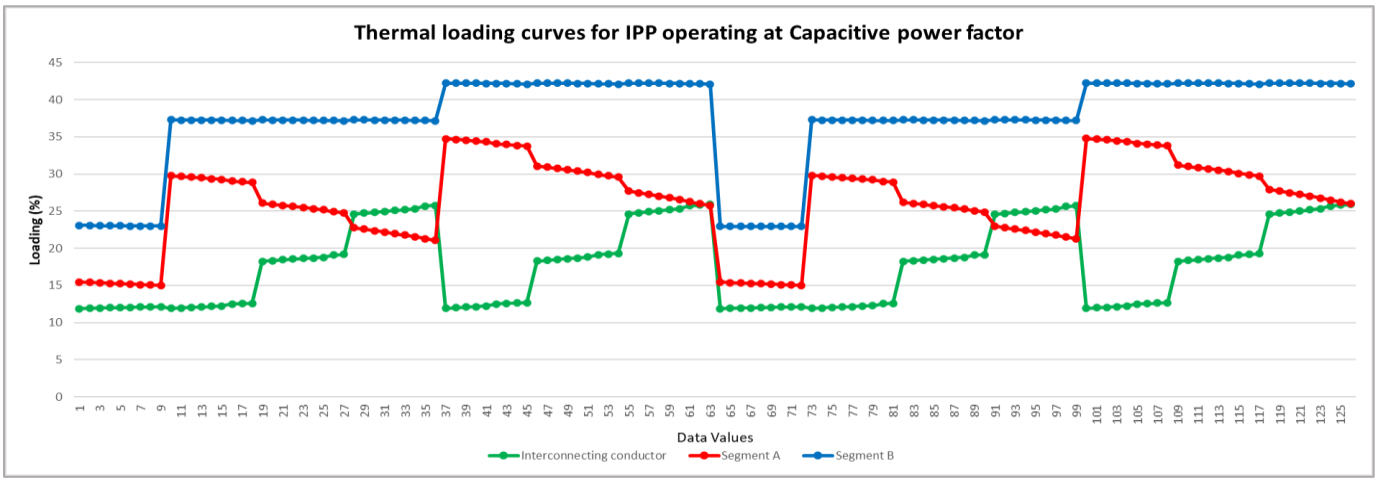

Figure 3-31: 11 kV thermal loading for segment A, segment B and interconnecting conductor while IPP operates at 0.975 capacitive pf

E. Interconnecting conductor DC resistance at 20 ℃.

Figure 3-32 illustrates changes in DC resistance of the interconnecting conductor, in order to accommodate for changes in IPP export power.

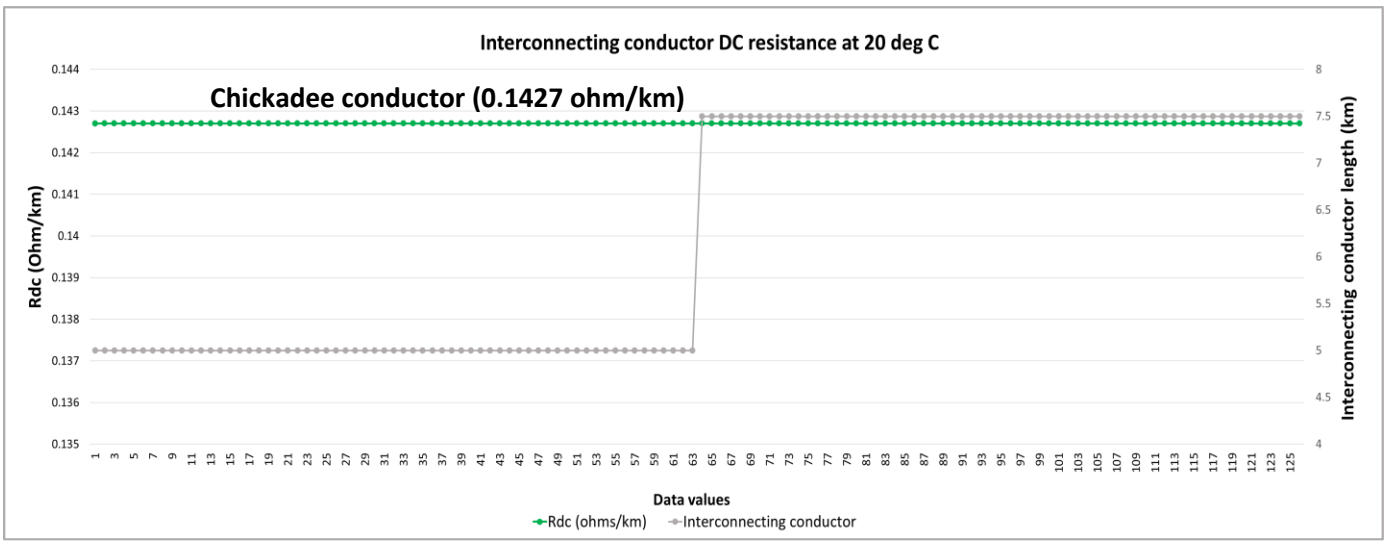

Figure 3-32:11 kV Interconnecting conductor DC resistance at 20 deg C

F. Interconnecting conductor diameter and Geometric mean radius graph.

Figure 3-33 illustrates changes in diameter and GMR of the interconnecting conductor, to accommodate for changes in IPP export power.

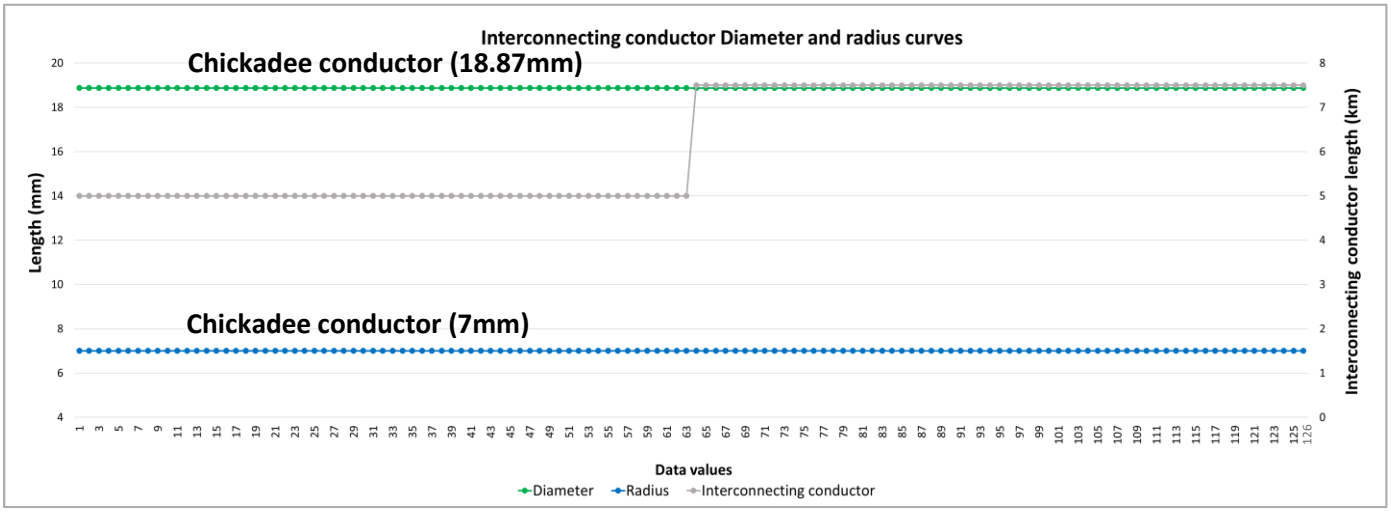

Figure 3-33: 11 kV Interconnecting Conductor diameter versus GMR values

G. Interconnecting conductor nominal current graph.

As seen in Figure 3-34, the nominal current for the interconnecting feeder is set to 0.419kA (i.e. 419A).

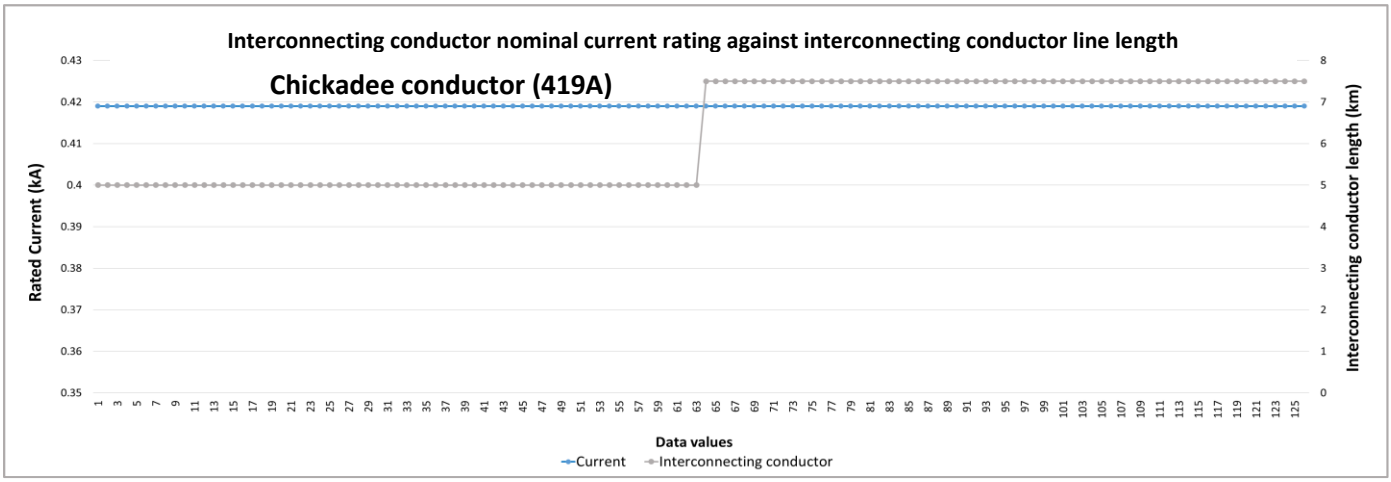

Figure 3-34: 11 kV interconnecting conductor nominal current

H. Interconnecting conductor rated power versus IPP power graph.

Figure 3-35 shows that for all 11kV IPP sizes, the interconnecting conductor is adequately rated. This is observed from the fact that the Green curve is always above the Blue curve for all points in time.

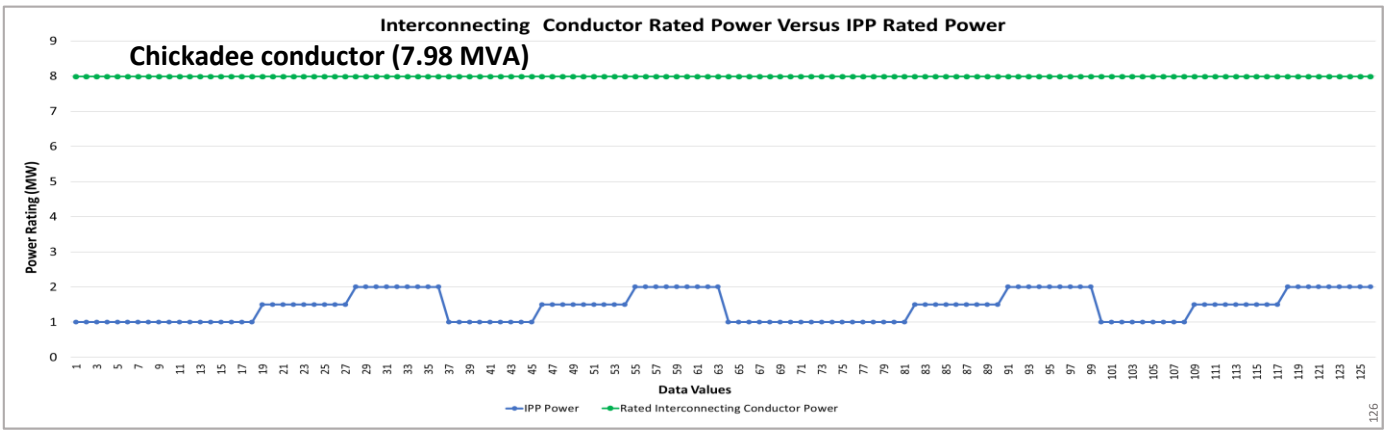

Figure 3-35:11 kV interconnecting conductor is adequately rated to handle IPP export power

I. IPP power factor variation graphs for unity, leading and lagging setpoints applicable to Category B (0.975) and Category C (0.95).

Since at 11kV, all IPP sizes are limited to 2.5MW (Category B of the SAGC), in the case the power factor setpoints used are as per Table 3.4 above and shown in Figure 3–36.

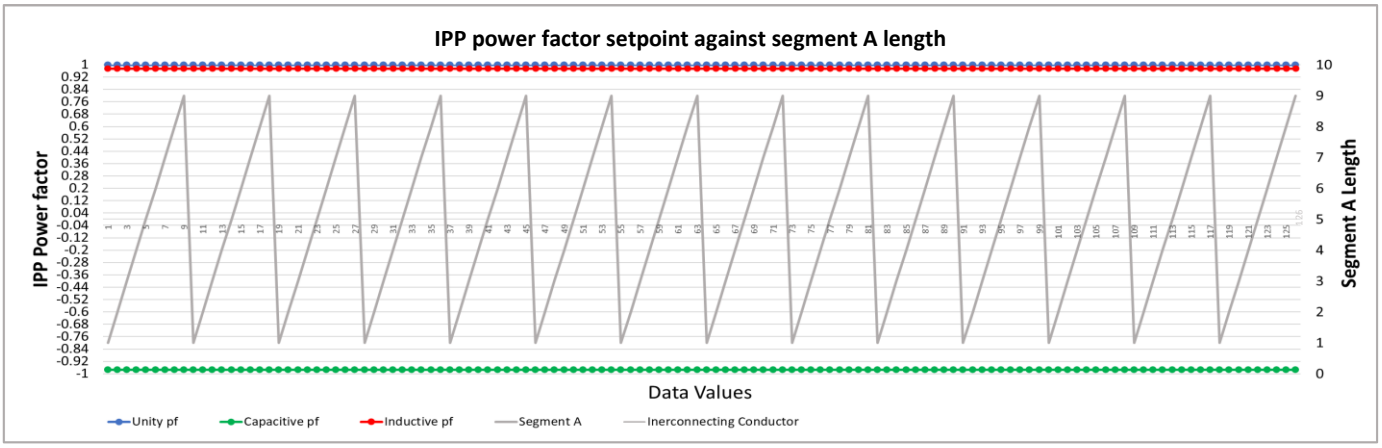

Figure 3-36:11 kV IPP variations in power factor

J. Power line loss graphs corresponding to IPP power factor variation graphs.

For IPP power factor setpoints of unity, 0.975 (inductive) and 0.975 (capacitive), Figure 3–37 shows the corresponding line losses that are generated from Segment A, Segment B and the interconnecting conductor. These curves represent the target data to be used in the ANN training process. It is noticeable that for the second half of the graph, losses increase considerably. This is because the interconnecting conductor length is also increased, which in effect increases the resistance of the interconnecting conductor, resulting in increased total line losses. This is seen from data values 64 – 126.

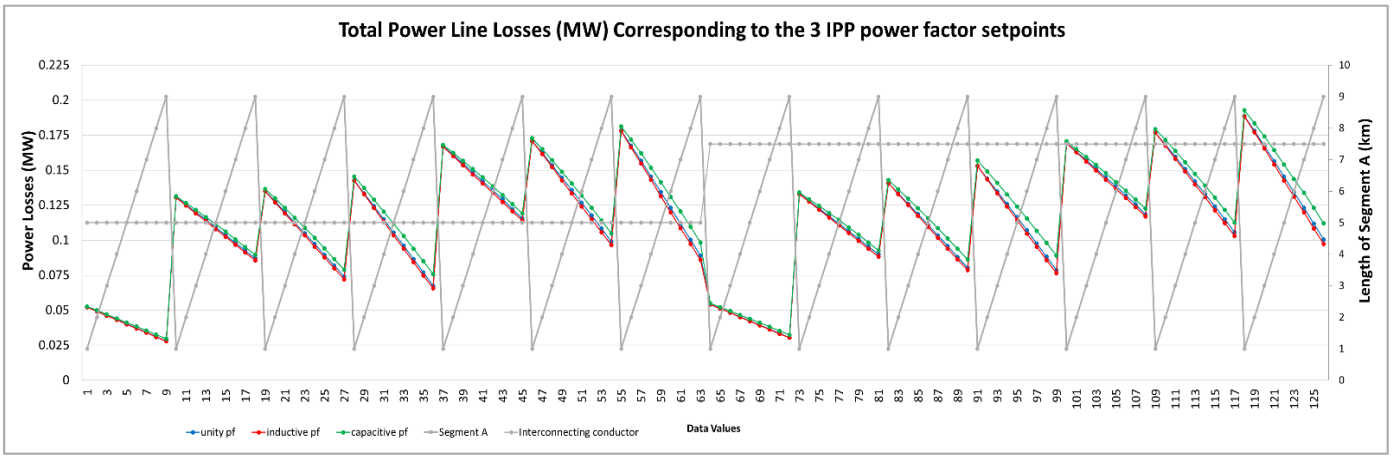

Figure 3-37: 11kV total power line losses for all 3 IPP power factor setpoints for a unity power factor load.

For the 11kV technology, data shown from Sections (A) – (J) above, are saved into three 126x8 input data matrices, one representing the unity power factor IPP setpoint, one representing the 0.975 lagging IPP setpoint, one representing the 0.975 leading power factor setpoint. When combined, a 378 x 8 input data matrix (126x3) is saved, as well as a 378x1 target data matrix is saved, representing results for a load receiving end power factor of unity.

In order to capture losses for the scenarios in which the load is non-unity, the above simulations are redone in the same fashion as before, but for a receiving end (load) power factor setpoint of 0.975 (inductive) as well as 0.975 (capacitive). This means that the combined input data matrix to be used in the ANN design and modelling section expands in size from 378x8 to 1134x8 and a target data size of 1134x1. This is also shown in Figure 3-38.

The remaining 22kV, 66kV, 132kV , 220kV, 275kV and 400kV data is given in Appendix A.

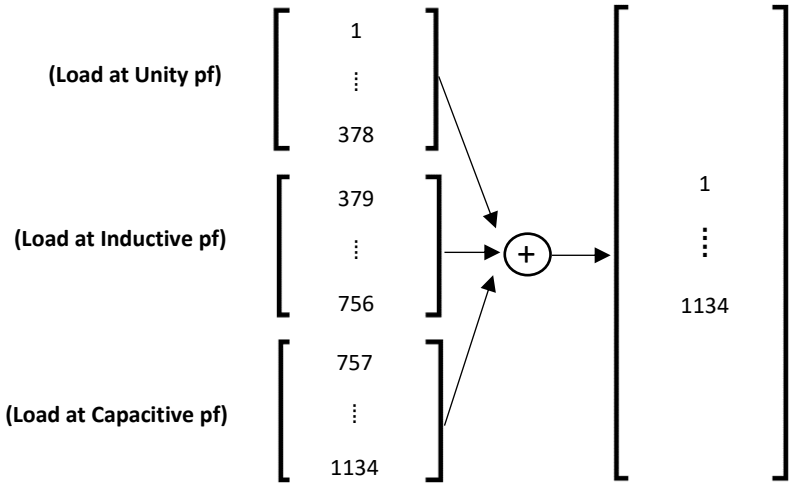

Figure 3-38:Combination of unity, inductive and capacitive receiving end power factor data, resulting in a 1134x7 input data matrix.

3.3 ANN Theory Development and Modelling

3.3.1 ANN Fundamentals

The objective of this research is to create an ANN-based tool that can accurately predict the optimal location, size and operating setpoint for IPP interconnection. Since the overall line losses (the target data), corresponding to input data are known, the ANN training process for optimal prediction requires a learning algorithm that is "supervised" so that incorrect predictions which do not adequately match the target data are removed from the ANN model. For this reason, the ANN learning process will fall under the category of "supervised learning", a popular and very well documented ANN learning algorithm [83]. This concept is explained using the ANN model shown in Fig 3-39.

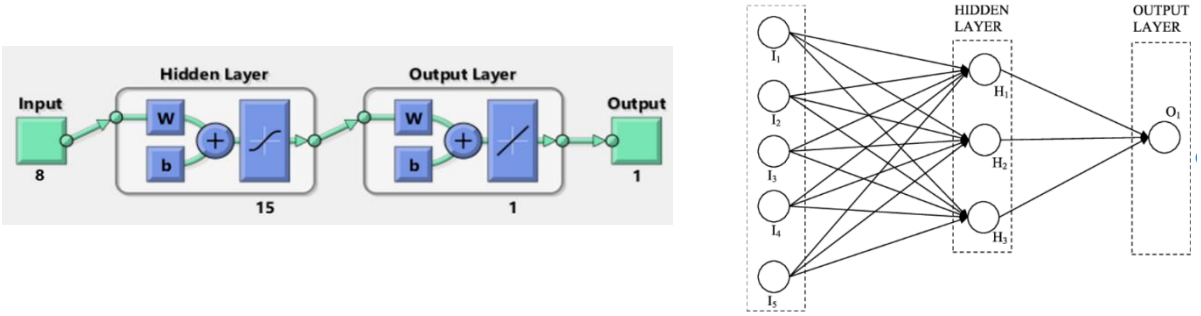

Figure 3-39:ANN Layers [17]

Supervised learning of ANNs requires input data and target data to ensure correct ANN prediction. Input data and target data are defined as the "correct data" that have been previously determined. This data is captured using the process shown in Section 3.2. Figure 3-39 shows the ANN model, where input data is passed through a "hidden layer". Within the hidden layer are nodes each containing a weight, bias and activation function. The "weights" and "biases" and "activation function" indicate how the inputs relate to the target data. If the weights, biases and activation function result in outputs deviating significantly from the target data, the training process is repeated, and weights and bias parameters are adjusted, until the outputs are close to desired target values. A weight represents the strength of the connection between nodes or neurons, and can be initialized with a unique value, or default value. A bias is an extra input to neurons and has its own connection weight [84].

There is a nonlinear function at the output of every neuron within the hidden layer (Figure 3–39). This function accepts the weighted sum of each connection to the neuron and performs an operation on the combined sum that translates into a value between an upper and lower limit. Different types of activation functions are available, that essentially transform the combined sum differently. For example, the sigmoid function shown in Figure 3–39, transforms any negative sum to a very small value close to 0, while enlarging positive sum combinations close to 1. For zero sum combinations, the sigmoid function will return a value of 0.5. A value close to 1 indicates that the neuron is highly activated, while a value close to 0 indicates a low activation of the state of the neuron. The nonlinear function therefore ensures that the ANN is trained for more complex input data through an iterative process. Supervised learning would not be able to take place without this function [85]. The sigmoid function passes the data onto the output layer which further manipulates the data by multiplying the data with an additional weighted value and adding another bias value to this. These are added together again and passed through another linear activation function at the output layer.

Output layer functions are usually linear or Softmax functions. Since the data being processed is regressive in nature i.e. the target data is non-binary and continuous, a linear output activation function is best suited [86]. Therefore, every connection between neurons contain a weight and bias that are tweaked over and over by returning back the difference between output and target data (the error), during ANN training. The process of returning the error back into the ANN to further adjust weights and biases is done until the error is as small as possible. The smaller the error, the more accurate the ANN prediction ability.

A sufficient "fit" between the target and output data determines the hidden layer's actual size. When a model is unable to produce the accurate output of the data it was trained by, it is said to be underfitting. The underfitting problem can be resolved by expanding the model's number of layers and neurons in each layer [87]. Overfitting is the term for a model

that too closely matches the training set of data. Overfitting is the process of a model learning the information and noise in the training data to the point where it negatively impacts the model's performance. If the validation results are worse than the training results, the model is said to be overfitting. It is to be noted here that developing a supervised regression ANN model within the MATLAB GUI encountered several limitations. For instance, an ablation study is not carried out, neither has hyperparameter tuning and testing with different structures, optimizers, and connections. It is recommended as a future exercise to conduct these tests to verify this preliminary study and possibly build on it. This in reality would require a more in depth understanding of ANNs and machine learning model testing and evaluation, which falls outside of the scope of this research. For this study, the Levenberg-Marquardt back propagation method, which is covered in more detail in the next section, is best suited for the supervised learning process.

3.3.2 Levenberg-Marquardt Backpropagation Algorithm

Backpropagation is based on the Gradient Descent (GD) method, which aims to lessen network error by reducing the gradient of the error curve [88]. This gives the ANN the ability to train over a number of iterations (or epochs), allowing it to increase its "knowledge" of what the intended target value is. GD minimizes the squared error between the intended and output, whereas Newton's method reduces the quadratic error by moving in the direction of the steepest descent (as previously noted). When the error is small, the Levenberg-Marquardt algorithm employs the Gauss-Newton method, and when the error is large, it employs the gradient-descent approach. Equation (3.8) illustrates how Newton's technique adjusts neural network training weights according to the following rule:

$$w_{n+1} = w_n - [J(n)^T J(n)]^{-1} J(n)^T e(n) \quad (3.8)$$

where J(w) is the Jacobian matrix (Vector of 1st order partial derivatives shown by equation 3.9 below), $J(n)^T J(n)$ is referred as the "Hessian" matrix.

$$J = \begin{bmatrix} \frac{\partial e_1}{w} & \cdots & \frac{\partial e_1}{\partial w_N} \\ \vdots & \ddots & \vdots \\ \frac{\partial e_N}{\partial w_1} & \cdots & \frac{\partial e_N}{\partial w_N} \end{bmatrix} \quad (3.9)$$

The Levenberg-Marquardt equation (3.10) is shown below,

$$w_{n+1} = w_n - [J(n)^T J(n) + \eta I]^{-1} J(n)^T e(n) \quad (3.10)$$

J(n) is the Jacobian matrix, $J(n)^T J(n)$ is referred as the Hessian matrix, I is the identity matrix, η is the learning rate which is updated depending on the output. η is multiplied by the decay rate β ($0< \beta <1$) whenever the error decreases, and is divided by β whenever the error increases in a new step. The ANN weights are first initialized, along with the learning rate. Inputs are passed through the ANN and the sum of square errors calculated. Equation (3.10) is updated based on the error calculated and sent back through the ANN. The new error is then compared with the old error value. If the error is decreased, u is multiplied by β, and weight is adjusted according to equation (3.10). If the error does not improve, u is divided by β and equation (3.9) is implemented again until an error value has been reached [87].

3.3.3 Development of ANN algorithm for 11 kV,22 kV,66 kV,132 kV,220 kV, 275 kV and 400 kV Networks

Sections 3.3.3.1 – 3.3.3.5 discuss the collection and quality control of input data, collection of target data, training, validation and testing of the ANN, and the ANN structure developed.

3.3.3.1 Collection and Quality Control of Input Data

To ensure adequate capturing of data is undertaken, outliers from the input data sets are searched for visually and replaced with input values that are SAGC compliant. Using the process shown in Section 3.2, it was concluded that all input features applied to DIgSILENT Powerfactory were of good quality.

3.3.3.2 Normalization of Data

Activation functions are used by ANNs to map the relationship between input data and output targets. Since the logistical sigmoid activation function given is a non-linear with an output value between 0 and 1, the input data needs to be normalized to be within this range. Equation (3.11) below shows the formula used to achieve this.

$$\text{Xnorm} = \frac{x}{\max(x)} \qquad (3.11)$$

As seen, every input data value within each column is divided by the absolute value of the largest value within each individual column of X. The first column (representing backbone length) of the 11kV input data matrix for example, is 10km. This value is chosen by virtue of it being the largest value within the entire column containing 1134 rows. For the second column (the maximum load), 4.5MW is the largest value and is therefore used as the maximum value. This process is followed for all 8 columns within the input dataset. This ensures that all values of every column within the 11kV matrix are adequately scaled between 0 – 1. For the training of the 22kV – 400kV networks, each network will have different values within their respective input data matrices and therefore maximum values within each individual column are divided accordingly.

3.3.3.3 Collection of Target Data

Target data consists of seven, Nx1 line loss matrices (N represents a single column of loss data) for the following voltages: 11kV, 22kV, 66kV, 132kV,220kV, 275kV and 400kV. Line losses resulting from input data will be retrieved from DIgSILENT Powerfactory after every simulation run and stored in a single column matrix for every voltage type, each with the same number of rows as the input data set and saved into .csv files as in Table 3-3 below. This data is pre-requisite for training, testing and validation of the 7 ANNs to be used. This is how all input and target data information is captured.

Table 3-3:Input and target data

Voltage	**11kV**	**22kV**	**66kV**	**132kV**	**220kV**	**275kV**	**400kV**
Input matrix size	1134x8	20169x8	144342x8	139968x8	159120x8	182160x8	198738x8
Target matrix size	1134x1	20169x1	144342x1	139968x1	159120x1	182160x1	198738x1

3.3.3.4 Training data, Validation data, and Testing data

All input and target data as specified in Table 3-3 are partitioned into a training set and a testing set. This allows for the ANN to be trained using a part of the total data, while the other part of remaining data is used for the validation and testing. Since the size of training data (both input and target) will have a direct influence on the training time and accuracy of the ANN – larger training sizes will lead to longer training times and require additional computational processing power. Therefore, the training data sizes were carefully selected to encapsulate the most relevant input data set applicable to line length/thermal loading and voltage limits. This is how the limitation due to large input data sets was overcome – by eliminating unnecessary data and only focusing and therefore storing the most relevant input data values. For instance, discrete line length values differing by 10 km was used instead of including all values between 10 km and 20 km. Within the literature there is no hard rule specifying the most optimal data split ratio to use, since the ratio is dependent on the type of data in question [20]. A number of splits were tested in MATLAB. These were 90:5:5, 80:10:10 and 70:15:15. The latter split (70:15:15) showed highest accuracy in prediction with the associated performance curves provided in Appendix B (Figure B-1 to Figure B-6). This value is also commonly used and documented in the literature for a similar study [88-89].

3.3.3.5 ANN Structure

The hidden layer number is determined through trial and error. Different layer sizes are implemented and tested and the most favorable configuration to achieve the best result is selected. This method is commonly observed in the literature for identifying the most optimal number of hidden layers (as seen in [90 - 92]). Figure 3 – 40 indicates the effect of hidden layer size and ANN performance using the popular Levenberg-Marquardt backpropagation algorithm and the Mean Square Error as the fitness function for the 11kV network (refer to Appendix B for the remaining cases). This figure shows the relationship between the outputs of the network and the targets. The four plots indicate the ANN

performance for the training, validation, and testing data. Each plot's dashed line depicts the ideal outcome, which is when outputs equal targets. The best-fitting linear regression line between the outputs and the targets is represented by the solid line. The link between the outputs and the targets is shown by the R value. There is a precise linear relationship between outputs and targets if R equals unity. There is no linear relationship between outputs and targets if R is close to zero. As seen from Figure 3 - 40, the value of R tends to approach unity as the number of hidden layers progressively increases, but as suggested in [90], the downside of having too many hidden layers is overfitting of data. Based on the results of these curves a hidden layer size per voltage ANN is tentatively chosen and shown in Table 3-4 below:

Table 3-4:Hidden layer size per voltage ANN

Voltage	11kV	22kV	66kV	132kV	220kV	275kV	400kV
Hidden layer size	3	4	4	4	4	4	4

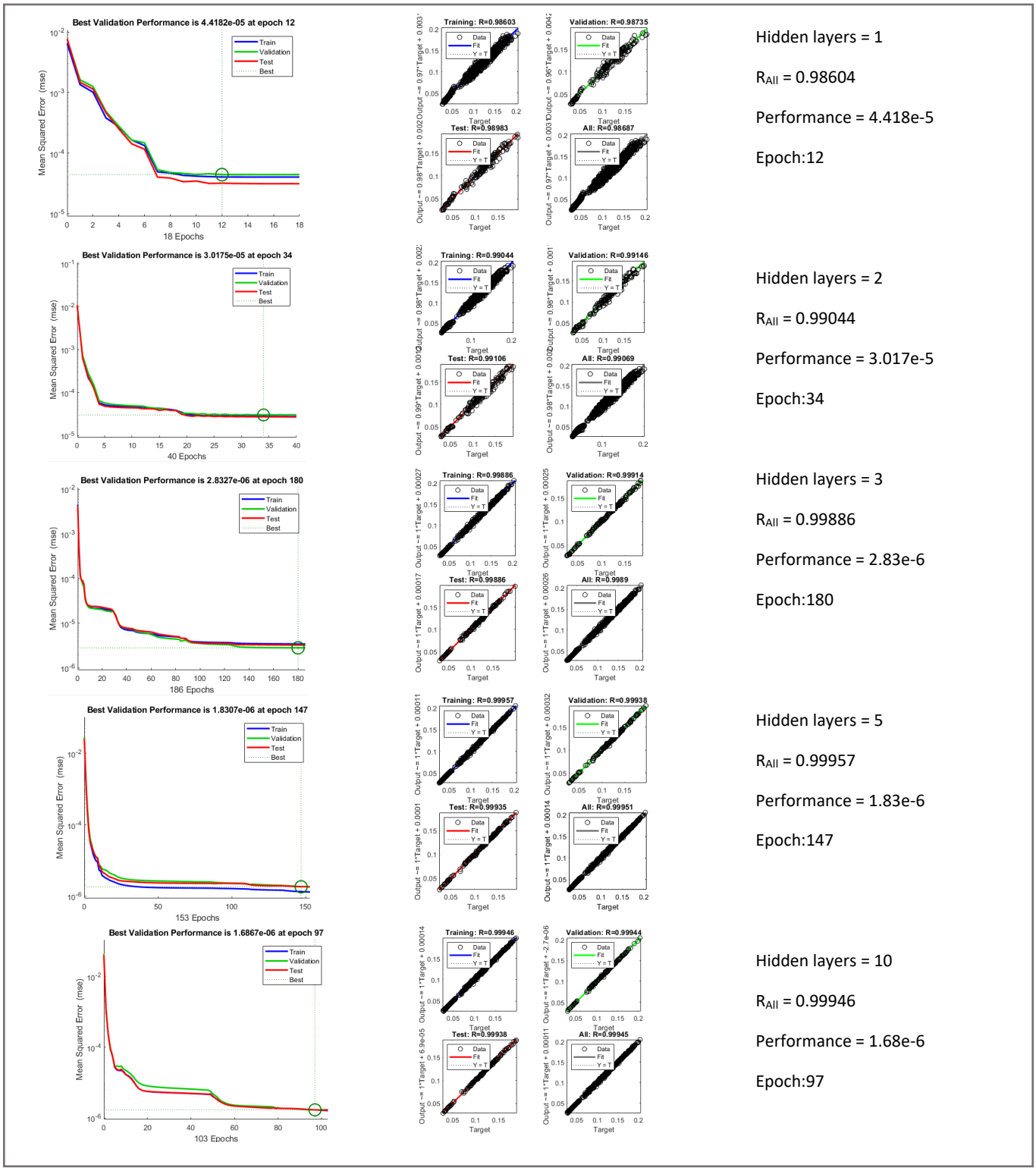

Figure 3-40: Performance curves representing the 11kV ANN for varying hidden layer sizes

3.3.3.6 trainlm Parameters

Within MATLAB, the training process applied to a single voltage level ANN is conducted using the 'trainlm' function which updates the weight and bias for a minimized error value. Table 3-5 shows standard parameters with default sizes. As seen, parameters are called using the dot operator within the MATLAB workspace. For example **net.trainParam.epochs = 1000** will assign 1000 to the maximum number of iterations during the training process. Variable assignment and other coding operations within the MATLAB Graphical User Interface (GUI) are discussed in the next section.

Table 3-5:Summary of MATLAB trainlm assignment operators [93]

net.trainParam.epochs	1000	Maximum number of epochs to train
net.trainParam.goal	0	Performance goal
net.trainParam.max_fail	6	Maximum validation failures
net.trainParam.min_grad	1,00E-07	Minimum performance gradient
net.trainParam.mu	0.001	Initial mu
net.trainParam.mu_dec	0.1	mu decrease factor
net.trainParam.mu_inc	10	mu increase factor
net.trainParam.mu_max	1,00E+10	Maximum mu
net.trainParam.show	25	Epochs between displays (NaN for no displays)
net.trainParam.time	inf	Maximum time to train in seconds

3.3.4 Simulation Software – MATLAB

MATLAB software is chosen as the primary tool for ANN training and user interface development. It is supported across a number of computer platforms such as Windows and Linux with a large library that contains powerful built in and predefined functions specifically designed to handle complex problems with large data sets. MATLAB also contains a tool that allows for the programmer to interactively design a GUI (Figure 3–41), which is especially useful for this research. For this research MATLAB will be run on a Windows 10, 64 bit operating system.

3.3.4.1 MATLAB GUI

This section will describe how the ANNs are implemented and trained using MATLAB code. This step is provided in Section A. Section B will then provide the logic and further code that will enable the ANNs to be integrated into a separate GUI, for the sorting, and identification of the most suitable IPP location, size and power factor. The mathematical equations on which the code logic is based is first given below with explanation. Equations and codes put together provide better clarity on the working of the ANN model.

Mathematically, the process of backpropagation can be expressed as follows: Inputs x are connected to all the neurons in the hidden layer through a weighted value (indicated by w), and bias value (indicated by b).The input matrix x (given by X = [x_1, x_2,.. x_n]), is multiplied by weight 'w' and bias 'b' added to form equation (3.12). Equation (3.12) is fed into the logsig function shown by equation (3.13). The combined sum is assigned to 'h' given by equation (3.14) which represents the hidden layer (H = [h_1, $h_{2..}$, h_n]). Parameter 'h' is multiplied by a second weight value 'v' given by v = [v_1,v_2, , v_n] and another bias parameter 'b_0' added. The combined sum is passed through a linear activation function 'r' giving output value (y) as shown by equation (3.15).

$$a = x_a w_{ai} + b \quad (3.12)$$

$$z(a) = \log sig\,(a) = \frac{1}{1 + e^{-a}} \quad (3.13)$$

$$h_a = z\sum_{a=1}^{n}(x_a w_{ai} + b)\ , \text{i} = 1,2,3\ \ldots..,\text{m} \quad (3.14)$$

$$y_p = r\sum_{i=1}^{m}(h_i v_p + b_0)\ , \text{p} = 1,2,3\ \ldots..,\text{l} \quad (3.15)$$

The update process adjusts weights and bias values shown by equation (3.16), so that the mean squared error function E, given by (3.17) is eventually as small as possible.

$$w_{n+1} = w_n - \eta \frac{1}{2} \frac{\partial E}{\partial w} \quad (3.16)$$

$$E = \frac{1}{Q} \sum_{k=1}^{Q} (G_{target} - G_{actual})2 \quad (3.17)$$

η is the learning rate, usually initialised in magnitudes of 0.001. E is differentiated with repect to the weights and biases, resulting in a "gradient" value. The negative term containing the product of learning rate and gradient called the step size, that is added to the previous weight value (w_n), and passed back into equation (3.12).This process continues until the error is acceptaby small. The variable 'net' given by equation (3.18) below, is a function fitting ANN, which is assisgned values from function "fitnet". Fitnet is a funtion of two variables:" hidden layer size" and the Levenberg-Marquardt backpropagation training function. HiddenLayerSize and trainingFunction are preassigned using equations (3.19) and (3.20) respectively. Equation (3.20) shows the numerical assignment of value a to variable hiddenLayerSize.

$$net = fitnet(hiddenLayerSize, trainingFunction) \quad (3.18)$$

$$trainFcn = trainlm \quad (3.19)$$

$$hiddenLayerSize = a \quad (3.20)$$

Equation (3.21) below is used to determine total line losses which are stored within matrix "Losses_Overall". Matrix best_parameters_overall is inverted and used as an argument to the net function which is assisnged to Losses_Overall:

$$Losses\_Overall = net(best\_parameters\_overall') \quad (3.21)$$

The matrix 'Losses_overall' given by equation 3.21 is passed through a minimisation function which returns the index (location) and the minimum loss value within matrix 'Losses_Overall' as shown by equation (3.22):

$$[min\_valueA, indexA] = min(Losses\_Overall') \quad (3.22)$$

The 'min' function is a search function which seeks the smallest value in a single column of values by first assuming that the first element in the column is the smallest value within the column matrix, and then compares it to the element in the second position, if the second value is smaller, the second value replaces the first value and variable min_valueA is re-assigned as the smallest value. This is performed using a simple for loop which iterates until all values are compared with each other. The row number is then also known since it is the location of the smallest element, this is given by variable indexA as shown in equation (3.22). Equations (3.23) to (3.26) below determine the most suitable IPP location, the most suitable IPP size, the suggested IPP power factor and the most suitable interconnecting conductor (cond – equation 3.26). Equations (3.23) – (3.26) all make use of matrix "best_parameters_overall" which contains the most favourable operating parameters resulting in the smallest line losses overall – the exact code and logic for this shown in detail later in this section for the 11kV ANN model.

$$Best\_Location\_overall = best\_parameters\_overall(indexA, 6) \quad (3.23)$$

$$Best\_Size\_Overall = best\_parameters\_overall(indexA, 4) \quad (3.24)$$

$$pf = best\_parameters\_overall(indexA, 7) \quad (3.25)$$

$$cond = best\_parameters\_overall(indexA, 5) \quad (3.26)$$

A. Creating the ANN

The following steps show the procedure used to create individual ANNs in the MATLAB workspace (see Figure 3-41).

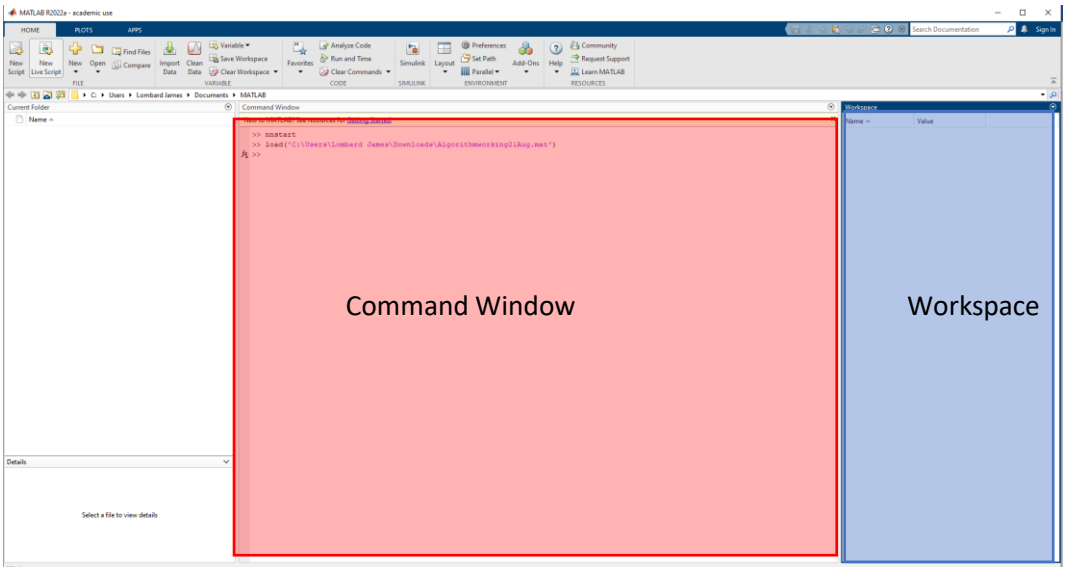

Figure 3-41:MATLAB GUI [93]

1. Input (normalized) and Target data are first imported into the MATLAB workspace. Input (normalized) and target data variables are named according to Table 3-6 and shown in the workspace in Figure 3–42.

Table 3-6:Input and target data per variable assignment names

Input data variable name	Size (Nx8)	Target data variable name	Size (Nx1)
inputdata_11kV	1134x8	targetdata_11kV	1134x1
inputdata_22kV	20169x8	targetdata_22kV	20169x1
inputdata_66kV	144342x8	targetdata_66kV	144342x1
inputdata_132kV	139968x8	targetdata_132kV	139968x1
inputdata_220kV	159120x8	targetdata_220kV	159120x1
inputdata_275kV	182160x8	targetdata_275kV	182160x1
inputdata_400kV	198738x8	targetdata_400kV	198738x1

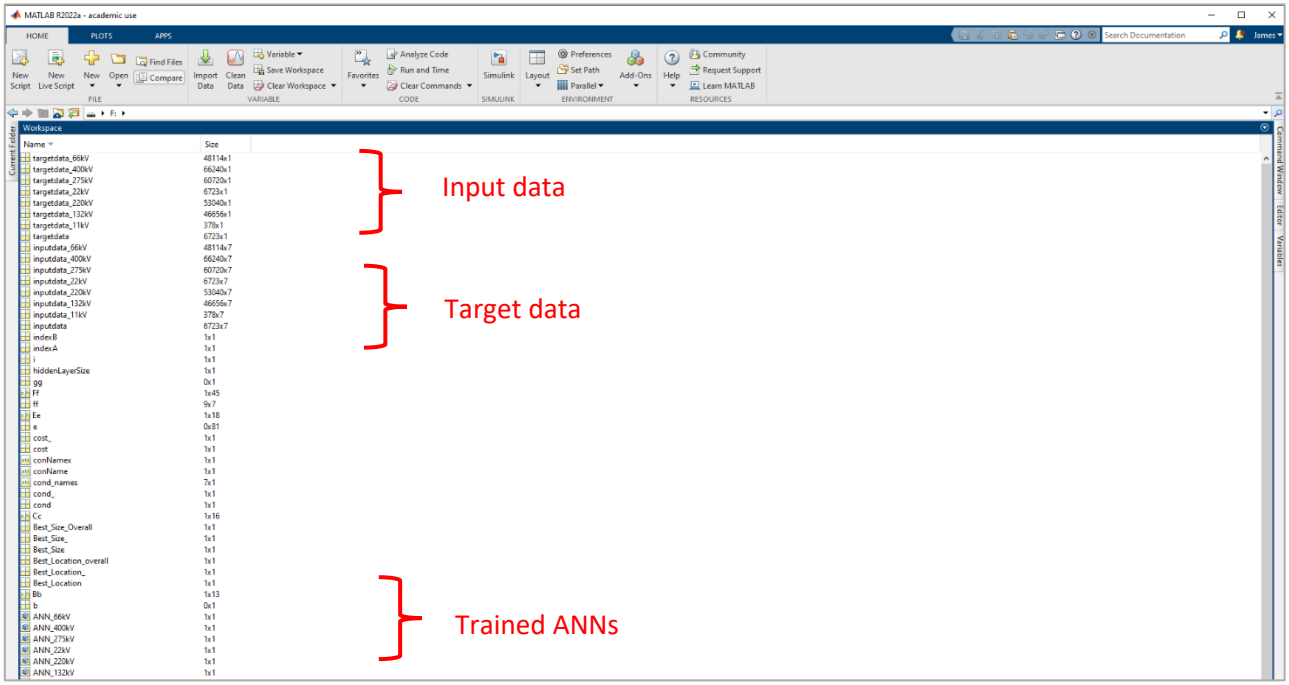

Figure 3-42:Importing input and target data into the workspace.

2. 7 ANNs are created and trained using the below assignment operations in the command window. Equations (3.13) – (3.17) are conducted within the 'train' function below until the MSE is acceptably low.

```
ANN_11kV = train(net,inputdata_11kV',targetdata_11kV')
ANN_22kV = train(net,inputdata_22kV',targetdata_22kV')
ANN_66kV = train(net,inputdata_66kV',targetdata_66kV')
ANN_132kV = train(net,inputdata_132kV',targetdata_132kV')
ANN_220kV = train(net,inputdata_220kV',targetdata_220kV')
ANN_275kV = train(net,inputdata_275kV',targetdata_275kV')
ANN_400kV = train(net,inputdata_400kV',targetdata_400kV')
```

   The variable 'net' is the function fitting ANN, which is pre-assigned with a hidden layer size and specific training function, as shown below, with arguments to the **fitnet** network function which returns a function fitting neural network, assigned to '**net**'.

```
net = fitnet(hiddenLayerSize,trainFcn);
```

   Since Levenberg-Marquardt backpropagation is used, '**trainFcn**' is initialized using '**trainlm**', while the **hiddenLayerSize** is set to a value of 3 for 11kV, 4 for the remaining cases):

```
trainFcn = 'trainlm';  % Levenberg-Marquardt backpropagation.
hiddenLayerSize = 3;
```

3. The Division of Data for Training, Validation, Testing is set to a ratio of 70:15:15 and instantiated as below. As seen the object net is assigned the split values 75:15:15 and mean square error function through the dot operator:

```
net.divideFcn = 'dividerand';  % Divide data randomly
net.divideMode = 'sample';  % Divide up every sample
net.divideParam.trainRatio = 75/100;
net.divideParam.valRatio = 15/100;
net.divideParam.testRatio = 15/100;
```

4. The error function is assigned and set to the mean square error:

```
net.performFcn = 'mse';  % Mean Squared Error
```

5. The functions used to plot the performance of the ANN are assigned as below:

```
net.plotFcns = {'plotperform','plottrainstate','ploterrhist','plotregression','plotfit'};
```

Steps 1 – 5 ensure all 7 ANNs are created and trained accordingly, and stored in the MATLAB workspace, ready to be access when needed.

B. Creating an Interactive User Interface

Once all input and target data are saved into the workspace, they are ready to be incorporated into the user interface. An m-file, or script file, is used to contain all MATLAB commands. When the file is run, MATLAB reads the commands and executes them accordingly.

The first step requires the user to enter specific network parameters via the MATLAB user interface. These are:

- The backbone voltage (kV) (prompt 1)
- Backbone length (km) (prompt 2)
- Interconnecting feeder length (km) (prompt 3)
- Maximum load seen at the receiving end (MW) (prompt 4)
- Distance from IPP at the POC to the sending end busbar (Segment A length) as a percentage of the total backbone length (km) (prompt 5)
- Load power factor at the receiving end (prompt 6)

The ANN algorithm returns two sets of information. This will give the user a comparison between the losses generated from the proposed IPP location as well as the losses generated from the overall best IPP location – offering a means to

compare the users proposed connection point, to the best connection point. For example, if the user proposes to connect in the middle of the line, a loss value based on this location will be given to the user which can be compared to a location having smaller losses (closer to the receiving end for example):

(a) The most favourable operating parameters resulting in the smallest line losses ***overall***

1. The best location of connection **overall** (km)
2. The best IPP size (MW) based on (1).
3. The applicable IPP SAGC category (Category A,B or C) based on (1).
4. Overall losses (MW) based on (1).
5. The conductor type based on (1).
6. The most suitable IPP power factor based on (1).

(b) The most favourable operating parameters resulting in the smallest line losses based ***on the proposed IPP location at the POC:***

1. The proposed location of connection (km)
2. The best IPP size based on proposed location (MW)
3. The applicable IPP SAGC category based on proposed location (Category A,B or C)
4. Overall losses (MW)
5. The conductor type
6. The most suitable IPP power factor

This is implemented in MATLAB by creating a script (m-file) containing the code shown below in Figure 3-43. The working principle of the algorithm is explained using the 11kV voltage level as an example, but the same principle is applied to all voltage levels.

```
disp('Enter the following network parameters:');
prompt1 = 'Backbone Voltage Level (kV): ';
prompt1_answer = input(prompt1);
prompt2 = 'Backbone length(km): ';
prompt2_answer = input((prompt2));
prompt3 = 'Length of interconnecting feeder (km): ';
prompt3_answer = input((prompt3));
prompt4 = 'Backbone maximum loading(MW): ';
prompt4_answer = input((prompt4));
prompt5 = 'Enter IPP distance as a percentage of total backbone length from sending end substation to POC(%): ';
prompt5_answer = input((prompt5));
prompt6 = 'Enter load power factor:';
prompt6_answer = input((prompt6));
```

Figure 3-43:Step 1 of user interface prompt code required to capture user specific network parameters.

As seen from Figure 3 – 43, after running the script the user enters all six sets of information which initializes all six prompts from **prompt1_answer** to **prompt6_answer** into individual 'double' data type variables. For a user entering the following parameters: Backbone voltage level of 11kV, backbone length 5km, interconnecting feeder length 5km, maximum loading of 2MW, IPP distance from sending ending end 10% and load power factor 1.0 (unity), variables **prompt1_answer** to **prompt6_answer** are initialised and values saved into the workspace. The nested if else statement is executed and variables '**row**', '**inputdata**' and '**targetdata**' are assigned values **1134**, **inputdata_11kV** and **targetdata_11kV** (Figure 3 – 44).

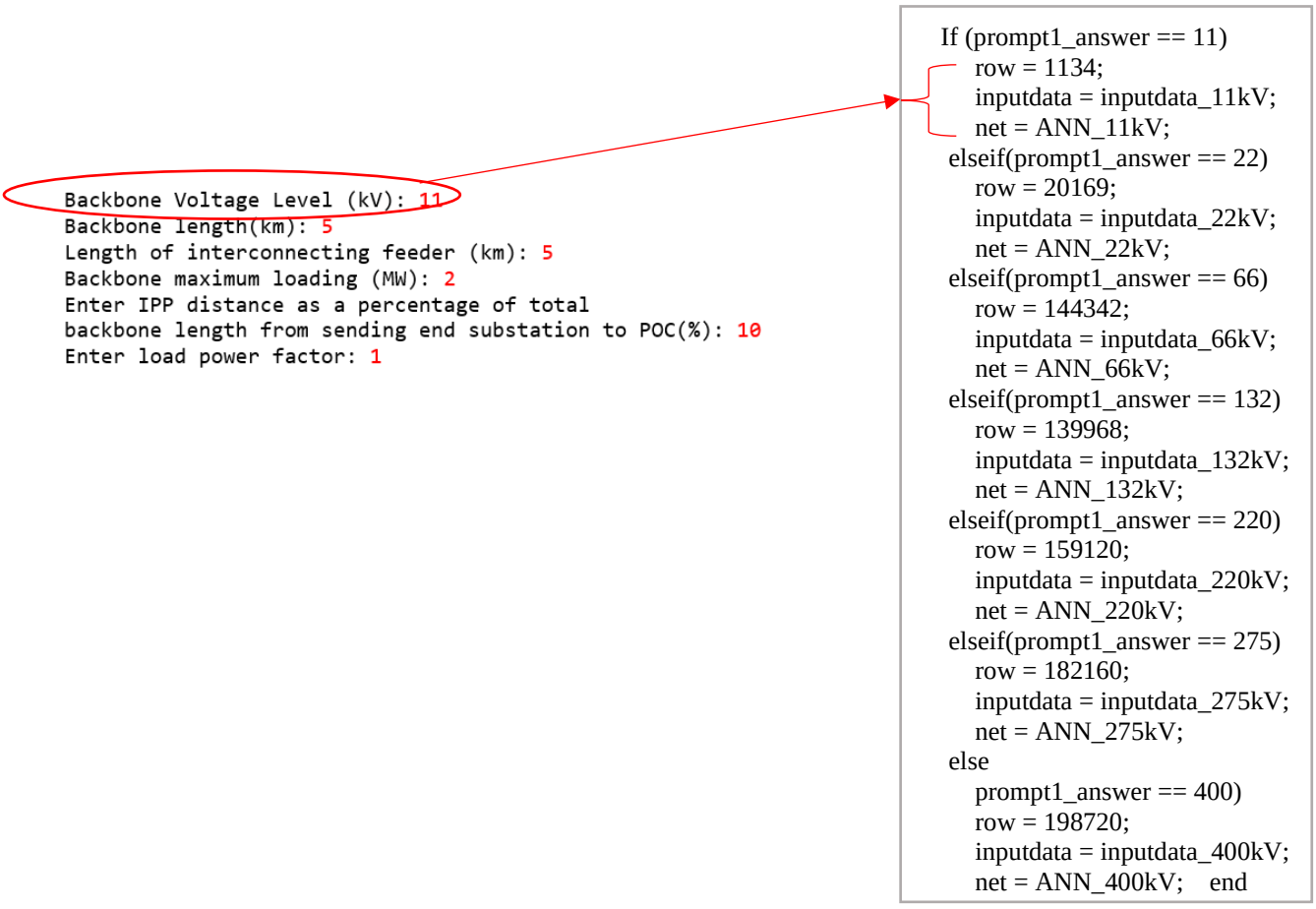

Figure 3-44: Step 2 of user interface prompt1_answer is set to '11' and variables 'row', 'inputdata' and 'net' are assigned.

The algorithm needs to process and generate results indicated by subsections (a) and (b) previously. Two data storage variables are used to store this data per subsection:

a) *The most favourable operating parameters resulting in the smallest line losses* ***overall:***
Data variable: **best_parameters_overall**
b) *The most favourable operating parameters resulting in the smallest line losses based on the proposed IPP location at the POC.*
Data variable: **best_paramaters_based_on_IPP_location**

The objective is to collect and save the required data into these two variables and use them as inputs to the voltage-specific ANN. This is how the losses per variable are retrieved and specifically related to the user inputs from Figure 3 – 43. Lines 1 and 2 of Figure 3 – 45 below, initialise the two variables with zero entries. This means that all values within these two variables are set to have a numerical value of zero. Since for illustrative purposes, it is known that the user enters values shown in Figure 3–44, the code presented in Figure 3–45 applies only to these specific inputs. For other inputs, the same code will not apply, but the structure of the sorting process will be identical. Figure 3–45 only provides a subset of the overall algorithm relating to the user inputs shown in Figure 3–44.

Three conditions are required to be true in order for the next step of the code to run as shown in Figure 3–45: If prompt1_answer is equal to 11kV; and if prompt2_answer is less than or equal to 7.5km; and if prompt4_answer is less than 2.5MW. Since prompt1_answer = 11, prompt2_answer = 5 and prompt4_answer = 2, all of these conditions are true (Line 3, Line 4, Line 5) and the next set of code is executed. Line 5 to line 20 shows a standard for loop setup which is responsible for saving data into data variables **best_parameters_overall** and **best_paramaters_based_on_IPP_location**. Line 6 to Line 15 saves data for variable **best_parameters_overall**, while line 16 to line 18 collect data for **best_paramaters based_on_the IPP_location** specified by prompt5_answer.

```
Line 1    best_parameters_overall  = zeros(row,8);
Line 2    best_paramaters_based_on_IPP_location = zeros(row,8);

Line 3    if prompt1_answer == 11 % if user enters 11kV: prompt1 of Figure 3 - 43
Line 4      &&prompt2_answer <= (7.5))... % for backbone length <= 10km: prompt2 of Figure 3 – 43
Line 5      &&prompt4_answer < (2.5) % and for maximum load less than 2.5MVA:prompt4(Figure 3 –43)

Line 6        m = 27;
Line 7        for i=1:m
                        % Part A start: The most favourable operating parameters resulting in the smallest line losses overall

Line 8          best_parameters_overall(i,1) = round((prompt2_answer/max(inputdata_11kV_unnormalized(:,1)),5);
Line 9          best_parameters_overall(i,2) = round((prompt3_answer/ max(inputdata_11kV_unnormalized(:,2)),5);
Line 10         best_parameters_overall(i,3) = round((prompt4_answer/ max(inputdata_11kV_unnormalized(:,3)),5);
Line 11         best_parameters_overall(i,4) = round(inputdata_11kV_2point5load(i,1),5);
Line 12         best_parameters_overall(i,5) = round(inputdata_11kV_2point5load(i,2),5);
Line 13         best_parameters_overall(i,6) = round(inputdata_11kV_2point5load(i,3),5);
Line 14         best_parameters_overall(i,7) = round(inputdata_11kV_2point5load(i,4),5);
Line 15         best_parameters_overall(i,8) = round(prompt6_answer/ max(inputdata_11kV_unnormalized(:,8)),5);

                    % Part A end

                        % Part B start: The most favourable operating parameters resulting in the smallest line losses based on
                                                the proposed     IPP location at the POC
Line 16         if (round(prompt5_answer/(9,5)== best_parameters_overall(i,6))
Line 17             best_paramaters_based_on_IPP_location (i,:) = best_parameters_overall (i, :);
Line 18         end

                        % Part B end


Line 19         end
Line 20   end
```

Figure 3-45:11kV code used to capture data for matrix '**best_parameters_overall**' – overall line losses, and matrix '**best_paramaters_based_on_IPP_location** ' – losses based on a specified IPP location on the backbone.

It can be observed from Figure 3-45 that lines 8,9,10 and Line 15 divide the users input by the respective maximum column value of the un-normalised input dataset, this is to scale the inputs between the range [0,1]. Figure 3 - 45 shows variable 'm' set to 27. This represents the size of **best_parameters_overall**. The reason for this size is explained using Figure 3 – 46 below. As seen, column 1, column 2, column 3, and column 8 are set based on the users answers from prompt2_answer = 5, prompt3_answer = 5, prompt4_answer = 2 and prompt6_answer = 1. This is required because the ***logsig*** function of the ANN only outputs values between 0 and 1, which requires the **inputdata** values to be within the same scale range. If the input data is outside this range, the activation function will automatically clip/cut off values outside of this range. As seen, column 1 values are obtained by dividing 5km (prompt2_answer) by 10km (the maximum backbone length in input data set), column 2: 5km (prompt3_answer) /7.5km (maximum interconnecting conductor length); column 3:2MW (prompt4_answer)/4.5MW (maximum load); column 4: 1MW(prompt5_answer) /2MW (maximum IPP size).

The only combinations of data allowed for these values are given by columns 4, 5, 6 and 7. This indicates that a total of 27 rows of input features are needed to feed into the 11kV ANN, to output 27 different loss values. Line 8, line 9, line 10 and 15 assign the user prompts to the columns highlighted in yellow (which are the normalized values), while lines 11- through 14 assign the outstanding four columns unhighlighted in Figure 3 – 46 which are already pre-saved (and norminalised) into the MATLAB workspace in data variable '**inputdata_11kV_2point5load**'. Lines 16 through 18 reduce **best_parameters_overall** to **best_paramaters_based_on_IPP_location** by checking if the IPP location (10%) – given by prompt5_answer (Figure 3 – 43) – matches the same IPP location of Figure 3 – 45. Since prompt5_answer only appears 3 times in Figure 3 – 46 (column 6), **best_paramaters_based_on_IPP_location** only contains 3 rows of data since there are only 3 positive matches within the second if statement of Figure 3 - 45.

best_parameters_overall								
Row	Column 1	Column 2	Column 3	Column 4	Column 5	Column 6	Column 7	Column 8
	prompt2_answer	prompt3_answer	prompt4_answer	IPP Size	Interconnecting conductor	IPP location	IPP pf	prompt6_answer
1	0,5	0,66667	0,44444	0,4	1	0,01111	1	1
2	0,5	0,66667	0,44444	0,4	1	0,02222	1	1
3	0,5	0,66667	0,44444	0,4	1	0,03333	1	1
4	0,5	0,66667	0,44444	0,4	1	0,04444	1	1
5	0,5	0,66667	0,44444	0,4	1	0,05556	1	1
6	0,5	0,66667	0,44444	0,4	1	0,06667	1	1
7	0,5	0,66667	0,44444	0,4	1	0,07778	1	1
8	0,5	0,66667	0,44444	0,4	1	0,08889	1	1
9	0,5	0,66667	0,44444	0,4	1	0,1	1	1
10	0,5	0,66667	0,44444	0,4	1	0,01111	0,975	1
11	0,5	0,66667	0,44444	0,4	1	0,02222	0,975	1
12	0,5	0,66667	0,44444	0,4	1	0,03333	0,975	1
13	0,5	0,66667	0,44444	0,4	1	0,04444	0,975	1
14	0,5	0,66667	0,44444	0,4	1	0,05556	0,975	1
15	0,5	0,66667	0,44444	0,4	1	0,06667	0,975	1
16	0,5	0,66667	0,44444	0,4	1	0,07778	0,975	1
17	0,5	0,66667	0,44444	0,4	1	0,08889	0,975	1
18	0,5	0,66667	0,44444	0,4	1	0,1	0,975	1
19	0,5	0,66667	0,44444	0,4	1	0,01111	0,4875	1
20	0,5	0,66667	0,44444	0,4	1	0,02222	0,4875	1
21	0,5	0,66667	0,44444	0,4	1	0,03333	0,4875	1
22	0,5	0,66667	0,44444	0,4	1	0,04444	0,4875	1
23	0,5	0,66667	0,44444	0,4	1	0,05556	0,4875	1
24	0,5	0,66667	0,44444	0,4	1	0,06667	0,4875	1
25	0,5	0,66667	0,44444	0,4	1	0,07778	0,4875	1
26	0,5	0,66667	0,44444	0,4	1	0,08889	0,4875	1
27	0,5	0,66667	0,44444	0,4	1	0,1	0,4875	1

Figure 3-46:**best_parameters_overall** data set (Columns highlighted in yellow are the known values retrieved from user prompts. Values indicated in this figure are the normalised values).

best_paramaters_based_on_IPP_location								
Row	Column 1	Column 2	Column 3	Column 4	Column 5	Column 6	Column 7	Column 8
	prompt2_answer	prompt3_answer	prompt4_answer	IPP Size	Interconnecting conductor	IPP location	IPP pf	prompt6_answer
1	0,5	0,66667	0,44444	0,4	1	0,01111	1	1
10	0,5	0,66667	0,44444	0,4	1	0,01111	0,975	1
19	0,5	0,66667	0,44444	0,4	1	0,01111	0,4875	1

Figure 3-47:**best_paramaters_based_on_IPP_location** data set (Columns highlighted in yellow are the known values retrieved from user prompts.)

Data saved in variable '**best_parameters_overall** ' and '**best_paramaters_based_on_IPP_location** ' are passed through the 11kV ANN previously assigned to '**net**', and the predicted losses are saved in variable '**Losses_Overall**' and '**Losses_based_on_userprompt5**':

```
Losses_Overall = net(best_parameters_overall ');
Losses_based_on_userprompt5  = net(best_paramaters_based_on_IPP_location ');
```

'**Losses_overall**' and '**Losses_based_on_userprompt5**' are then used as arguments to a minimisation function which returns the index (location) and the minimum loss value within **Losses_Overall** (min_valueA) and **Losses_based_on_userprompt5** (min_valueB):

```
[min_valueA,indexA] = min(Losses_Overall);
[min_valueB,indexB] = min(Losses_based_on_userprompt5);
```

As stated above, the min function given by equation 3.22 returns the index corresponding to the first occurrence of the minimum value of matrices: Losses_Overall and Losses_based_on_userprompt5. The 'min' function is a search function which seeks the smallest value in a column of values by first assuming that the first element in the column is the smallest

value, and then compares it to the element in the second position, if the second value is smaller, the second value replaces the first value as the smallest value. This is performed using a simple for loop which iterates until all values are compared with each other. The row number is then also known since it is the location of the smallest element. Since the location (given by indexA and indexB) of the smallest loss values corresponding to'**best_parameters_overall**' and '**best_paramaters_based_on_IPP_location** ' are now known, they are substituted in place of the row argument (x coordinate) of the variables below in order to find the corresponding best overall location, most optimal IPP size, most optimal IPP power factor setpoint and interconnecting conductor using the below lines of code:
For data matrix '**best_parameters_overall** ':

Best_Location_overall = best_parameters_overall (indexA,6)***max(inputdata_11kV_unnormalized(:,6)),5);**
Best_Size_Overall = best_parameters_overall (indexA,4)* **max(inputdata_11kV_unnormalized(:,4)),5);**
pf = best_parameters_overall (indexA,7)* **max(inputdata_11kV_unnormalized(:,7)),5);**
cond = best_parameters_overall (indexA,5)* **max(inputdata_11kV_unnormalized(:,5)),5);**

For data matrix '**best_paramaters_based_on_IPP_location** ':

Best_Location_ = best_paramaters_based_on_IPP_location (indexB,6)* **max(inputdata_11kV_unnormalized(:,6)),5);**
Best_Size_ = best_paramaters_based_on_IPP_location (indexB,4)* **max(inputdata_11kV_unnormalized(:,4)),5);**
pf_ = best_paramaters_based_on_IPP_location (indexB,7)* **max(inputdata_11kV_unnormalized(:,7)),5);**
cond_ = best_paramaters_based_on_IPP_location (indexB,5)* **max(inputdata_11kV_unnormalized(:,5)),5);**

It is observed that variables are de-normalized by multiplying the maximum column value within input data set. Since the input data is first normalized to contain values between [0,1] as required for the activation to operate correctly within its output range, the normalized data needs to be rescaled to obtain meaningful data. This is done by multiplying the output values of the ANN by the same individual maximum values per column that the input matrix was normalized by before training took place.

For the remaining voltage cases, the following maximum values (also called "features") are used per column:

22kV: {30 (30km backbone length – Figure A – 3, Appendix A); 10 (10km interconnecting conductor length– Figure A – 3, Appendix A); 17 (17MW maximum receiving end load – Figure A – 4, Appendix A); 8.5 (8.5MW maximum export IPP power – Figure A – 4, Appendix A); 1 (Chickadee interconnecting conductor indexed as '1' – Table 3 – 7); 27 (27km Segment A length, 90% of maximum backbone length – Figure A – 3, Appendix A), 1 (unity power factor of IPP – Figure A – 18, Appendix A) , 1 (unity power factor of receiving end).

66kV: {120 (120km backbone length – Figure A – 24, Appendix A); 40 (40km interconnecting conductor length– Figure A – 24, Appendix A); 45 (45MW maximum receiving end load – Figure A – 25, Appendix A); 28 (28 MW maximum export IPP power – Figure A – 25, Appendix A); 2 (Kingbird interconnecting conductor indexed as '2' – Table 3 – 7); 108 (108 km Segment A length, 90% of maximum backbone length – Figure A – 37, Appendix A), 1 (unity power factor of IPP – Figure A – 39, Appendix A) , 1 (unity power factor of receiving end).

132kV: {140 (140km backbone length – Figure A – 45, Appendix A); 50 (50km interconnecting conductor length– Figure A – 24, Appendix A); 176 (176 MW maximum receiving end load – Figure A – 47, Appendix A); 82.5 (82.5 MW maximum export IPP power – Figure A – 47, Appendix A); 4 (Zebra interconnecting conductor indexed as '4' – Table 3 – 7); 126 (126 km Segment A length, 90% of maximum backbone length – Figure A – 45, Appendix A), 1 (unity power factor of IPP – Figure A – 132, Appendix A) , 1 (unity power factor of receiving end).

220kV: {240 (240km backbone length – Figure A – 66, Appendix A); 80 (80km interconnecting conductor length– Figure A – 66, Appendix A); 300 (300 MW maximum receiving end load – Figure A – 67, Appendix A); 110 (110 MW maximum export IPP power – Figure A – 67, Appendix A); 5 (Twin - Zebra interconnecting conductor indexed as '5' – Table 3 – 7); 216 (216 km Segment A length, 90% of maximum backbone length – Figure A – 66, Appendix A), 1 (unity power factor of IPP – Figure A – 81, Appendix A) , 1 (unity power factor of receiving end).

275kV: {220 (220km backbone length – Figure A – 87, Appendix A); 90 (90km interconnecting conductor length– Figure A – 87, Appendix A); 300 (300 MW maximum receiving end load – Figure A – 88, Appendix A); 110 (110 MW maximum export IPP power – Figure A – 88, Appendix A); 5 (Twin - Zebra interconnecting conductor indexed as '5'

– Table 3 – 7); 198 (198 km Segment A length, 90% of maximum backbone length – Figure A – 87, Appendix A), 1 (unity power factor of IPP – Figure A – 102, Appendix A) , 1 (unity power factor of receiving end).

400kV: {260 (260km backbone length – Figure A – 108, Appendix A); 100 (100km interconnecting conductor length– Figure A – 108, Appendix A); 560 (560 MW maximum receiving end load – Figure A – 109, Appendix A); 110 (110 MW maximum export IPP power – Figure A – 109, Appendix A); 7 (Twin - Tern interconnecting conductor indexed as '7' – Table 3 – 7); 234 (234 km Segment A length, 90% of maximum backbone length – Figure A – 108, Appendix A), 1 (unity power factor of IPP – Figure A – 123, Appendix A) , 1 (unity power factor of receiving end).

It can be observed that when the 22kV – 400kV networks are trained, each network will have different maximum values per column. For example, the 11kV input data matrix consists of 8 columns. The first column (representing backbone length) of the 11kV input data matrix for example, is 10km. This value is chosen by virtue of it being the largest value within the entire column containing 1134 rows. For the second column (the maximum load), 4.5MW is the largest value and is therefore used as the maximum value. This process is followed for all 8 columns within the input dataset for all sets of input data per voltage level. This ensures that all values of every column are adequately scaled between 0 – 1.To summarise: For normalisation, these maximum values are used to divide every element per column of input data while for de-normalisation, these values are used to multiply every element per column of input data.

The assignments '**cond = best_parameters_overall (indexA,5);**' and '**cond_ = best_paramaters_based_on_IPP_location (indexB,5);**' refer to the type of interconnecting conductor used. A lookup table assigns a specific name of the conductor used to the number returned and stored in '**cond**' and '**cond_**'. Table 3-7 below shows the possible conductors and naming assignment:

Table 3-7: Input and target data per variable assignment names

Conductor name	Lookup table value
Chickadee	1
Kingbird	2
Twin Kingbird	3
Zebra	4
Twin Zebra	5
Tern	6
Twin Tern	7

Since '1' refers to the Chickadee conductor type, '**conName**' is assigned by the string variable "**Chickadee**" using the nested if statement below (Figure 3 – 48), where 'cond' is used for matrix 'best_parameters_overall ' and 'cond_' used for matrix '**best_paramaters_based_on_IPP_location** ':

'best_parameters_overall '

```
if(cond == 1)
   conName = cond_names(1);
elseif(cond == 2)
   conName = cond_names(2);
elseif(cond == 3)
   conName = cond_names(3);
elseif(cond == 4)
   conName = cond_names(4);
elseif(cond == 5)
   conName = cond_names(5);
elseif(cond == 6)
   conName = cond_names(6);
else
   conName = cond_names(7);
end
```

'best_paramaters_based_on_IPP_location '

```
if(cond_ == 1)
   conName = cond_names(1);
elseif(cond_ == 2)
   conName_ = cond_names(2);
elseif(cond_ == 3)
   conName = cond_names(3);
elseif(cond_ == 4)
   conName = cond_names(4);
elseif(cond_ == 5)
   conName = cond_names(5);
elseif(cond_ == 6)
   conName = cond_names(6);
else
   conName = cond_names(7);
end
```

Figure 3-48:Code used to assign conductor naming.

The category of the IPP size is assigned for '**best_parameters_overall**' and '**best_parameters_based_on_IPP_location**' using the code below:

```
if(Best_Size_Overall < 20)
   category = 'B';
else
   category = 'C';
end
if(Best_Size < 20)
   category_ = 'B';
else
   category_ = 'C';
end
```

The output of the algorithm is displayed using the lines of code in the GUI as seen in Figure 3-49:

```
disp('The most optimal parameters are displayed below:');
if prompt1_answer == 11
 Aa = ['Best Location:',num2str(round(Best_Location_overall*prompt2_answer/10,1)),'km'];
       disp(Aa);
Bb = ['Best Size:',num2str(Best_Size_Overall),'MW'];
      disp(Bb);

disp('Applicable South African Grid Code Category: ');
disp(category);
Cc = ['Losses:',num2str(min_valueA),'MW'];
      disp(Cc);
disp('Conductor         Type');
disp(conName);
Ee = ['Power Factor:',num2str(pf,3)];
      disp(Ee);

disp('*****************************************************');
disp('*****************************************************');
disp('The most optimal parameters based on IPP distance from sending end:');

Aa = ['IPP Location:',num2str(round(Best_Location_*prompt2_answer/100,1)),'km'];
      disp(Aa);
Bb = ['Best Size:',num2str(round(Best_Size_,2)),'MW'];
      disp(Bb);
disp('Applicable South African Grid Code Category:');
disp(category_);
Cc = ['Losses:',num2str(min_valueB),'MW'];
      disp(Cc);
disp('Conductor         Type');
disp(conName);
Ee = ['Power Factor:',num2str(pf_)];
      disp(Ee);
```

Figure 3-49: Code used to display final results.

The above algorithm is shown in its entirety using Figure 3 – 50 while Figure 3 – 51 shows the overall process followed. The user enters backbone voltage of 11kV (**prompt1**), backbone length of 5km (**prompt2**), interconnecting feeder length of 5km (**prompt3**), a maximum loading of 2MW (**prompt4**) and the IPP distance as a percentage of the total backbone length of 10% from the sending end (**prompt5**).

The best overall location is calculated to be at 4.5km from the sending end, with an IPP size of 1MW, operating at unity power factor using a Chickadee interconnecting conductor. This results in a total network loss of 0.017642MW and

classifies the IPP as Category B. The most optimal parameters based on the proposed IPP distance from the sending end substation (10% of 5km = 0.5 km) are IPP size of 1MW also operating at unity power factor, using a Chickadee conductor. But as observed, this location generates more losses (0.020667MW). For this case, it would be more favourable to connect closer to the receiving end of the feeder to improve on loss savings.

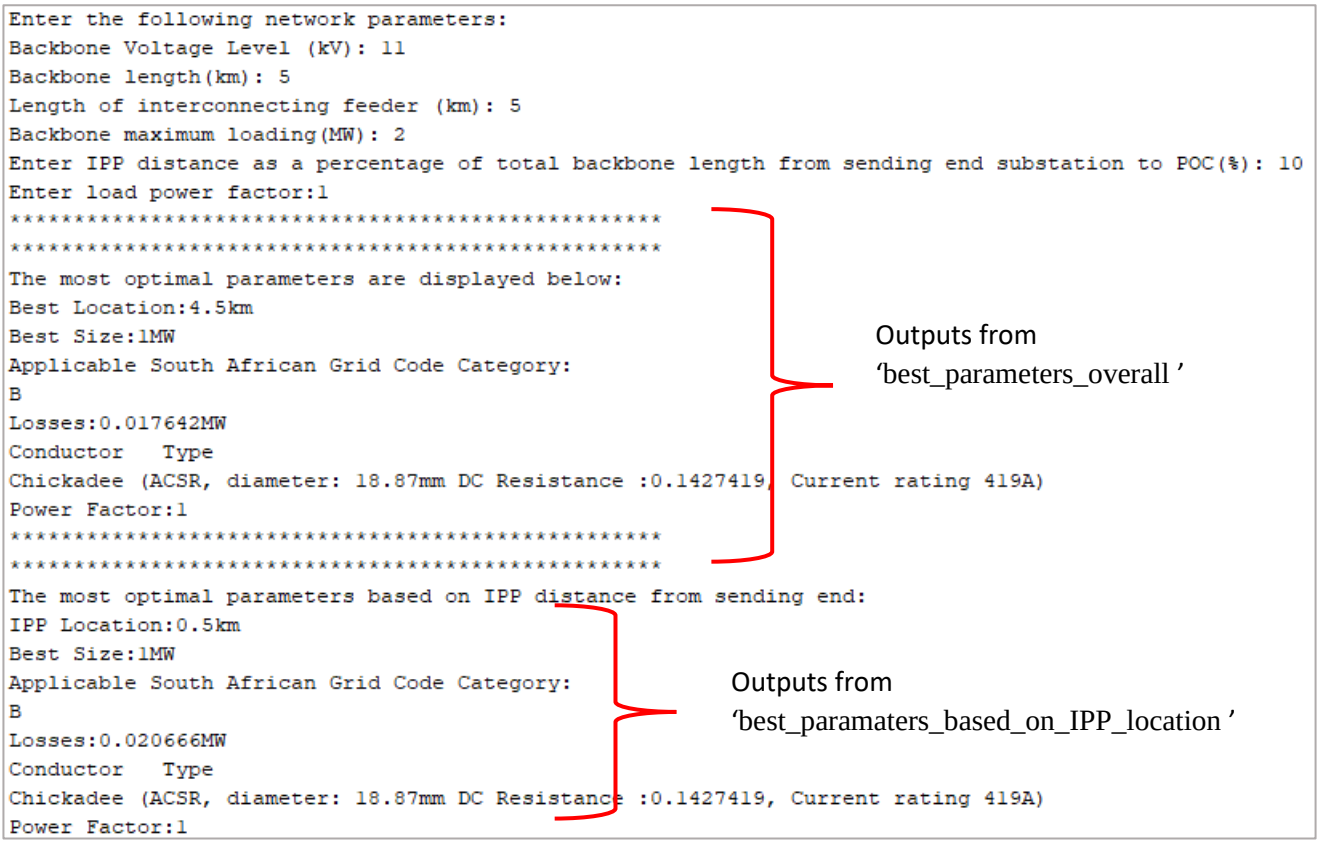

Figure 3-50:Output results indicating the recommended IPP size, location, power factor and interconnecting conductor.

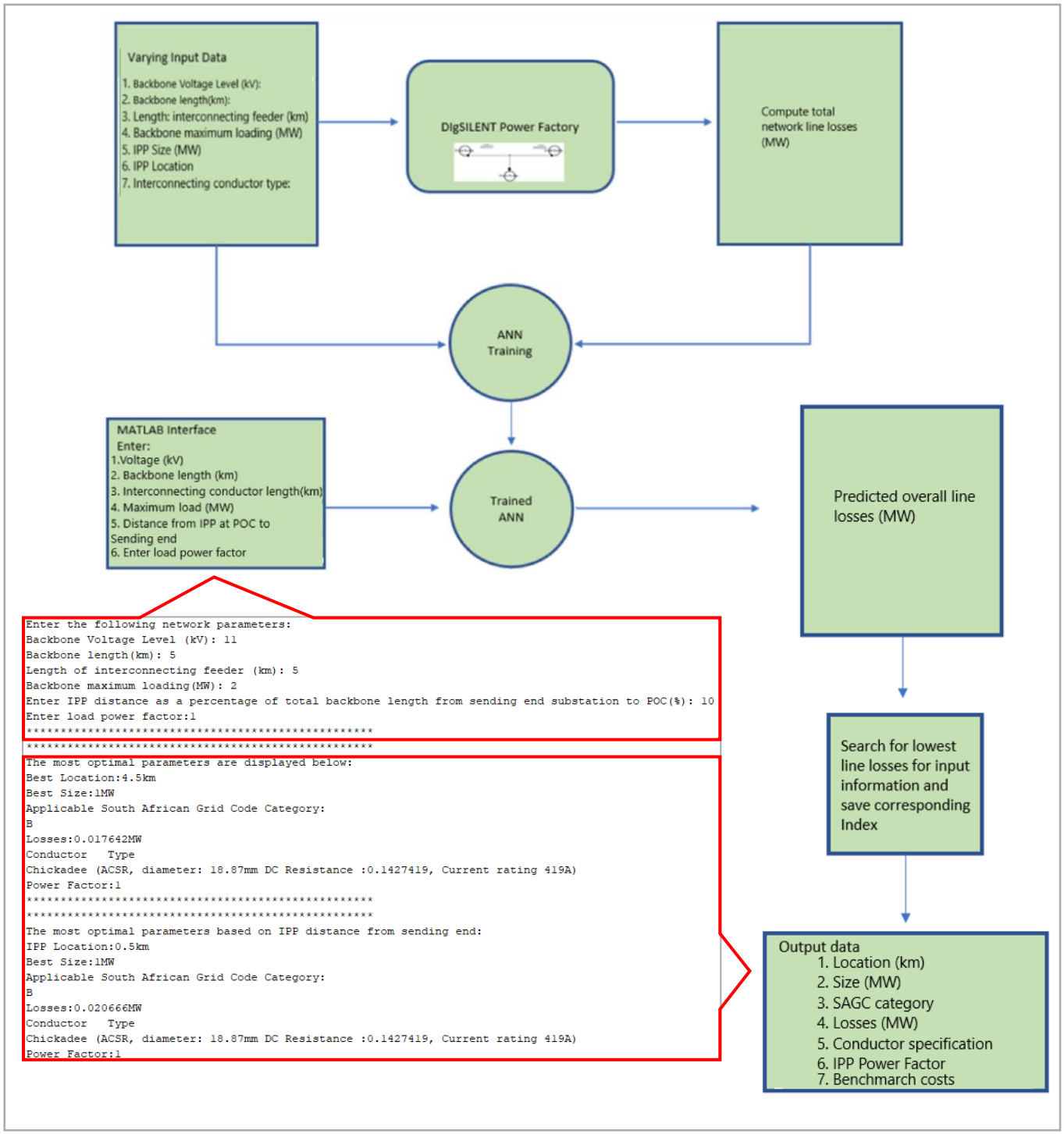

Figure 3-51:Overview of process followed from input data to output data.

3.4 Developing a Framework for Testing the ANN

Since the 7 ANN models apply specifically to 7 unique nominal voltage networks undergoing IPP interconnection, the tests to be conducted in Chapter 4 are carried out by applying each algorithm to a matching power system network using DIgSILENT Powerfactory software. Seven cases are presented starting from the lowest voltage test case (11kV) to the highest test case (400kV). Case 1 and Case 2 test the 11kV and 22kV ANNs on modified IEEE 13 – bus systems while Case 3 to Case 7 test 66kV, 132kV, 220kV, 275kV and 400kV ANNs on modified IEEE – 14 bus systems [94, 95, 98].

3.4.1 Performance Comparison of the 7 ANN models against DIgSILENT Powerfactory using IEEE 13-Bus and IEEE 14-Bus System.

In this section the modified IEEE 13-bus and IEEE 14-bus test systems are described.

3.4.1.1 IEEE 13-bus Network Description for 11kV and 22kV Test Networks

Two modified versions of the IEEE 13-bus are used to test the 11kV and 22kV ANNs as shown on Figure 3 – 52. The IEEE 13 Node Test Feeder consists of 13 nodes, 12 loads (9 of which are unbalanced), 10 overhead lines and underground cables with 1, 2, 3 phases with a varying arrangement, a single capacitor bank connected in a shunt configuration, a transformer and a per phase voltage regulator.

The standard IEEE 13-bus system operates at a nominal voltage of 4.16 kV (phase-to-phase) [94]. Since this voltage is not used in South Africa, the network is modified to suit 11kV and 22kV operation from the LV transformer terminal, connected to busbar 2 (Figure 3 – 52). The active and reactive power setpoint at bus 5 of the IEEE 13 bus system remain unchanged from the original values specified in [94]. These are: 4.05MVA operating at 0.85 lagging power factor (Active and reactive power setpoints of 3.5 MW,2.1 MVAR respectively). For both cases the length of Feeder A is set to 5 km as this is commonly seen in distribution networks in South Africa [95]. The interconnecting conductor length is set to 5 km, which is justified based on studies performed in Chapter 3, Section *3.2.3.1* :11kV Data. The MV/LV transformer connected between bus1 and bus 2 is configured as Dyn11,connecting to feeder A without a neutral conductor. This is a common setup especially in distribution networks in South Africa as seen at Moehoek substation in the Mpumalanga Province [96]. A Kingbird conductor having maximum current rating of 586A is used for both cases to safety transmit the 4.054MVA (220A) demand [97].

Table 3-8:11kV and 22kV Feeder data

Feeder Data							
Feeder name	**Length (km)**	**Rdc @ 50 dec C**	**Receiving end load (MW)**	**pf**	**Number of subconductors per bundle**	**Type**	**IEEE reference**
11kV: Feeder A	5	0.08921	3.5	0.85	1	ACSR Kingbird	[94,95,96,97,98]
22kV: Feeder A	5	0.08921	3.5	0.85	1	ACSR Kingbird	[94,95,96,97,98]

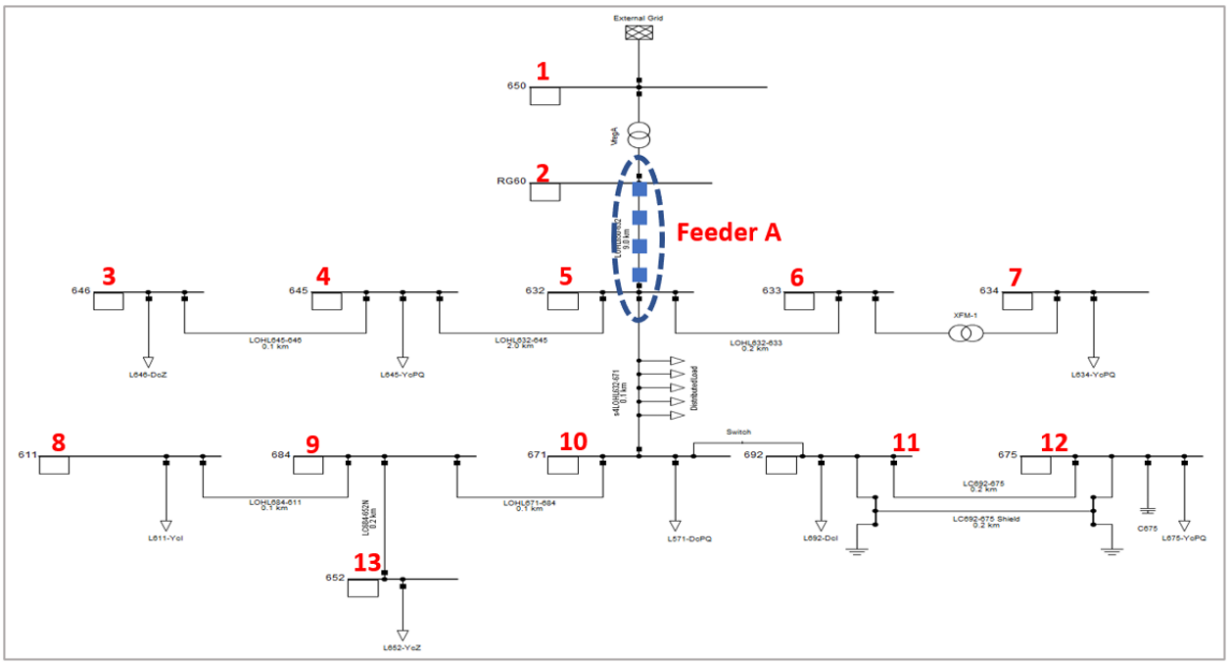

Figure 3-52:Modified IEEE 13-bus test system used to test 11kV and 22kV ANNs.

3.4.1.2 IEEE 14-bus System Network Description

The 66kV, 132kV, 220kV, 275kV and 400kV ANN models are tested using the IEEE 14 – bus system shown in Figure 3 -53 below [95]. The IEEE 14-bus system is simulated for a three-phase balanced load consisting of 14 buses (nodes), 5 generators, 11 loads, 16 lines, 5 transformers and one capacitive shunt device. Three of the 5 transformers are used to represent one single 3-winding transformer.

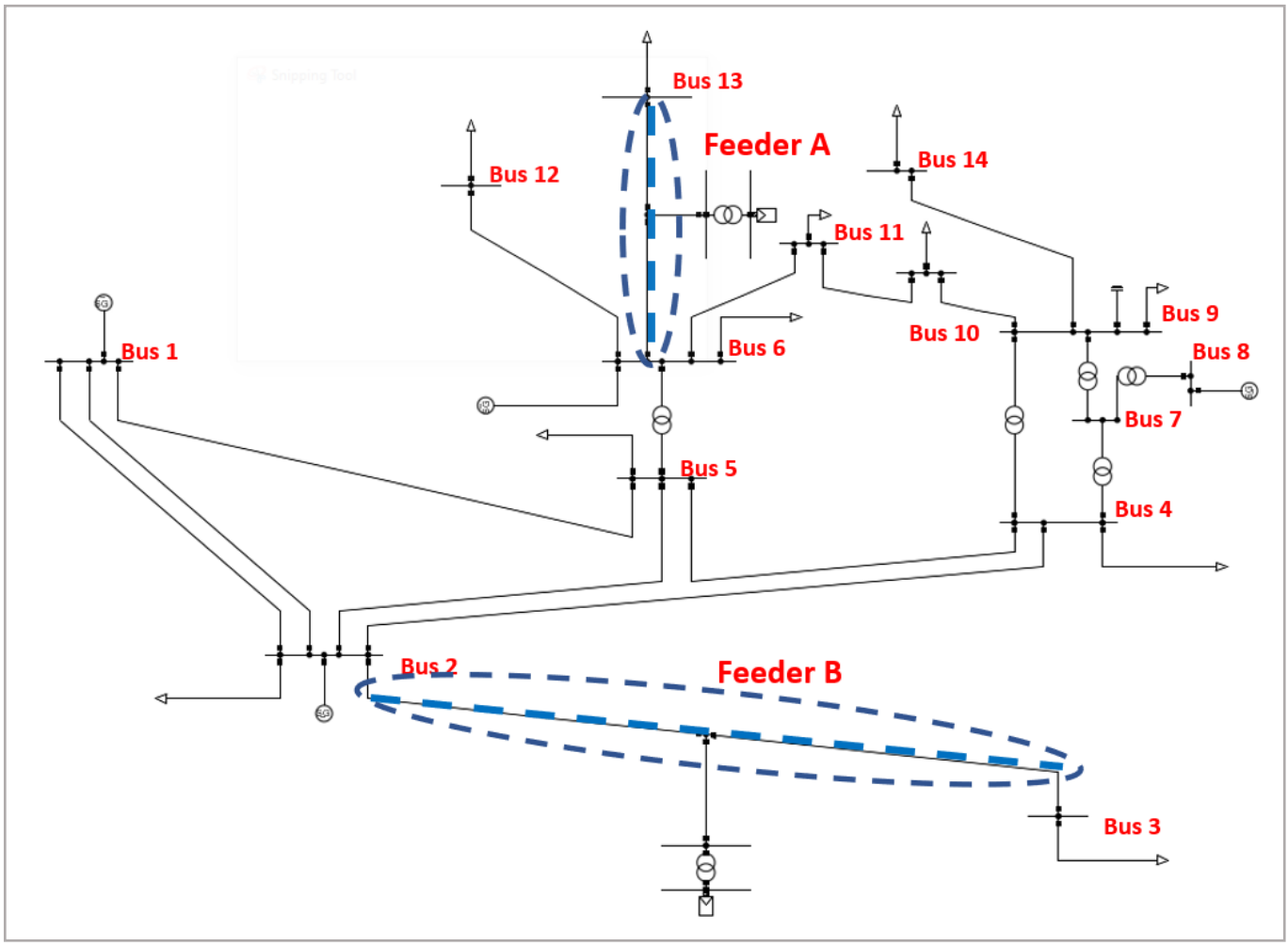

Figure 3-53:IEEE 14-bus test system used to test 66kV, 132kV 220kV, 275kV and 400kV ANNs.

3.4.2 66kV/132 kV Network Modification

Figure 3 -54 shows the modified IEEE 14-bus system used for the 132/66 kV cases. The modifications include:

- Transformers: Turns ratio 132/33 kV changed to 132/66 kV: (100MVA rating remains the same for all transformers which is same as the original value)
  - TFR between bus 5 and bus 6: 132/66 kV
  - TFR between bus 4 and bus 7: 132/1 kV
  - TFR between bus 7 and bus 8: 1/11 kV
  - TFR between bus 7 and bus 9: 1/66 kV
  - TFR between bus 4 and bus 9: 132/66 kV

- Feeder A is increased in length from 1km to 15.6 km having maximum radial load of 30MW. This is a Kingbird conductor with load value and line length taken from an existing radial feeder in the literature [99].The power factor at the load is 0.95.
- Feeder B is increased in length from 1km to 35 km having maximum radial load of 91MW operating at 0.95 pf using an ACSR Kingbird conductor – parameters taken from existing 132kV feeder specified in [100].

Table 3-9: 66/132kV Feeder data

Feeder Data							
Feeder name	**Length (km)**	**Rdc @ 50 dec C**	**Receiving end load (MW)**	**pf**	**Number of subconductors per bundle**	**Type**	**IEEE reference**
A	15.6	0.0891	30	0.95	1	ACSR Kingbird	[99]
B	35	0.0891	91	0.95	2	ACSR Kingbird	[100]

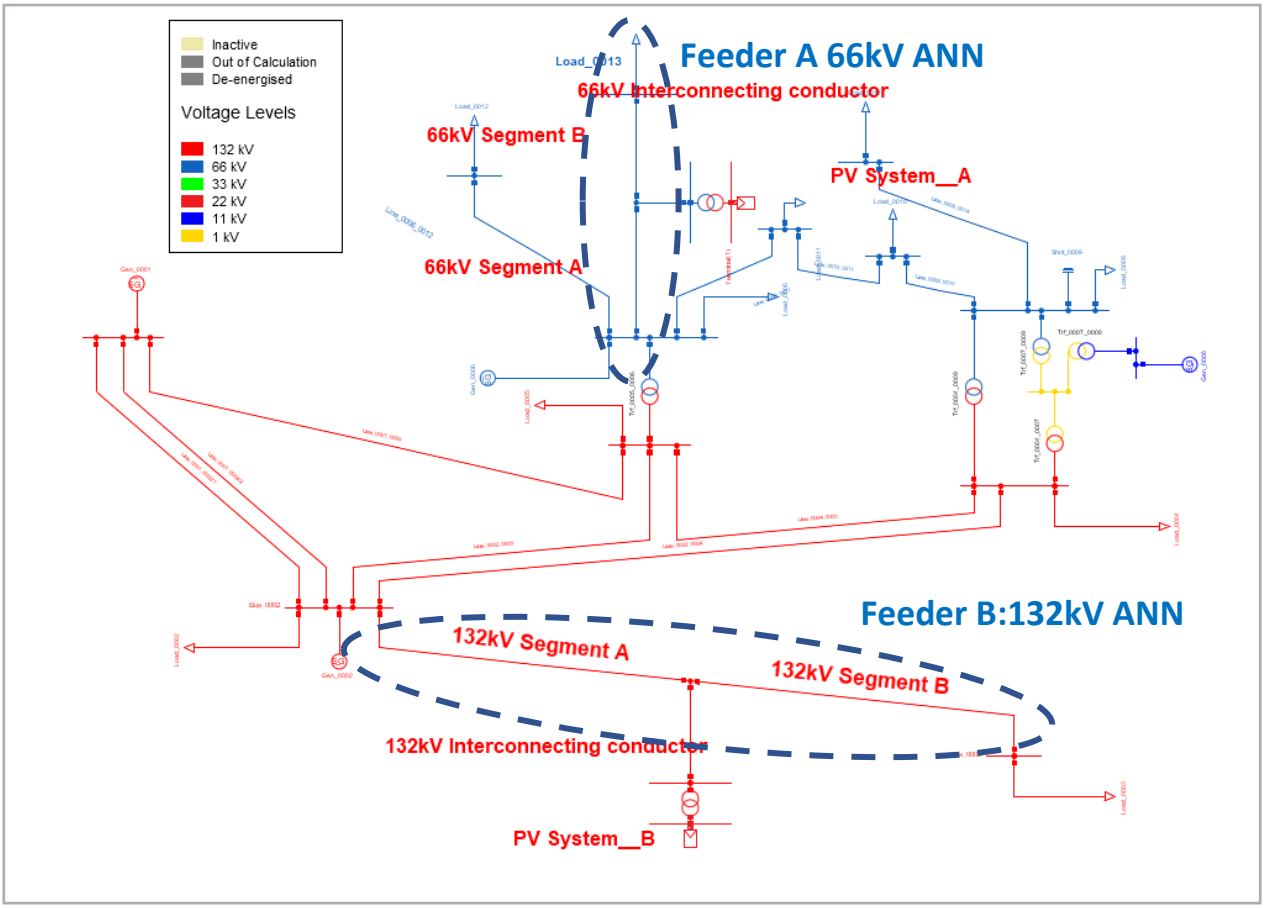

Figure 3-54:Modified IEEE 14-bus test system used to test 66k and 132kV ANNs

3.4.3 220/275kV Network

Figure 3-55 shows the modified IEEE 14 bus system used for the 275/220 kV cases. The modifications include:

- Transformers: Turns ratio 132/33 kV changed to 275/220 kV and the followings selected (100MVA rating remains the same for all transformers which is the same as the original value).
    - TFR between bus 5 and bus 6: 275/220 kV
    - TFR between bus 4 and bus 7: 275/1 kV
    - TFR between bus 7 and bus 8: 1/11 kV
    - TFR between bus 7 and bus 9: 1/220 kV
    - TFR between bus 4 and bus 9: 275/220 kV
- Feeder A is increased in length from 1km to 134 km having maximum radial load of 201 MW. This is a Single circuit Zebra conductor with load value and line length taken from an existing feeder in the literature[101-102]. The power factor at the load is 1.0.
- Feeder B is increased in length from 1km to 196km having maximum radial load of 201MW operating at 0.96 pf using an ACSR Twin-Zebra conductor – parameters taken from existing 275kV feeder specified in [103-104].

Table 3-10: 220/275kV Feeder data

Feeder Data							
Feeder name	**Length (km)**	**Rdc @ 50 dec C**	**Receiving end load (MW)**	**pf**	**Number of subconductors per bundle**	**Type**	**IEEE reference**
A	134	0.0642	201	0.95	1	ACSR Zebra	[101-102]
B	196	0.0642	201	0.96	2	ACSR Twin Zebra	[103-104]

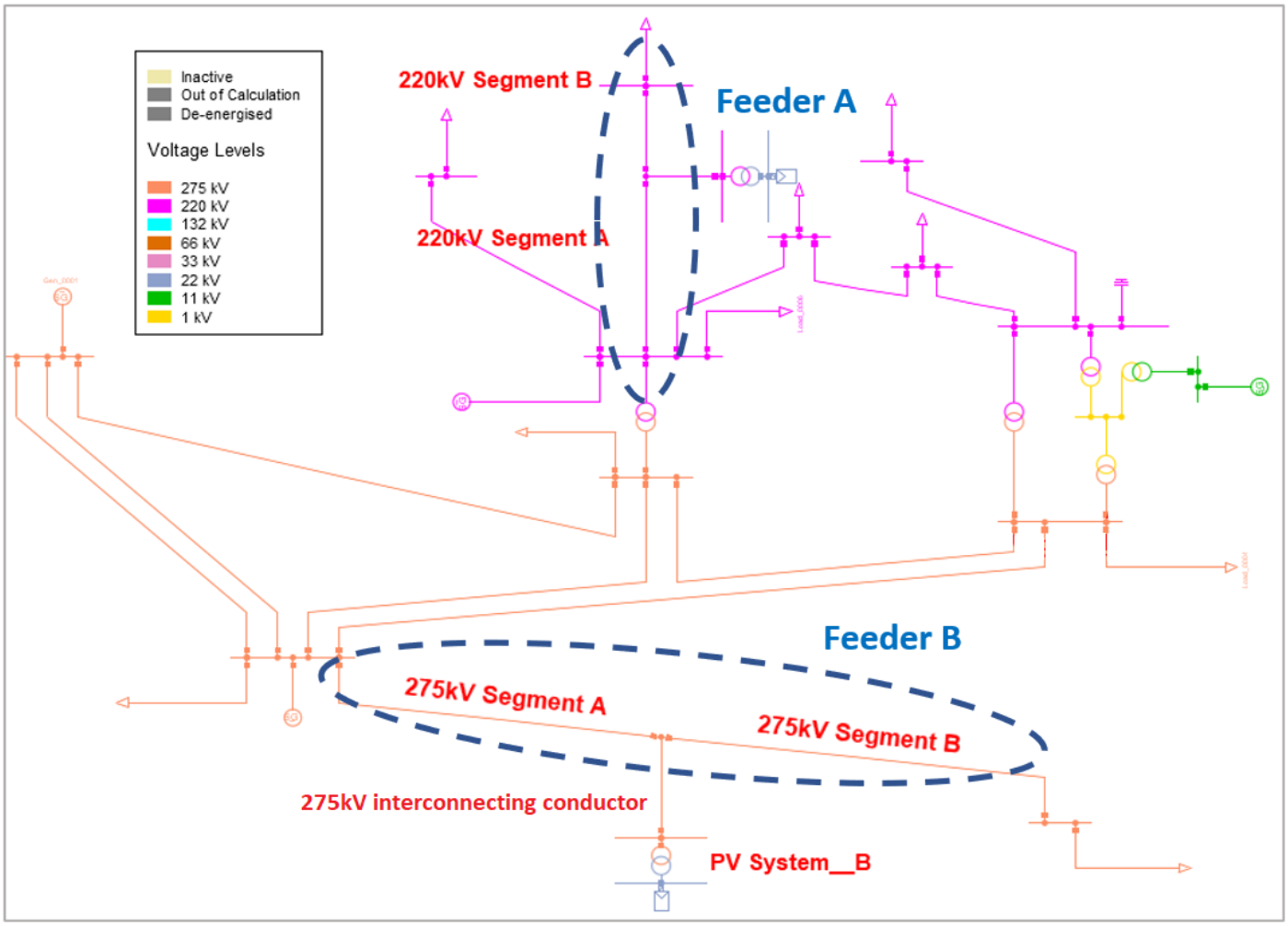

Figure 3-55:Modified IEEE 14-bus test system used to test 220k and 275kV ANNs

3.4.4 400kV Network

Figure 3 -56 shows the modified IEEE 14 bus system used for the 400/275 kV cases. The modifications include:

- Transformers: Turns ratio 132/33 kV changed to 400/275 kV(100MVA rating remains the same for all transformers which is the same as the original value):
  - TFR between bus 5 and bus 6: 400/275 kV
  - TFR between bus 4 and bus 7: 400/1 kV
  - TFR between bus 7 and bus 8: 1/11 kV
  - TFR between bus 7 and bus 9: 1/275 kV
  - TFR between bus 4 and bus 9: 400/275 kV

- Feeder B is increased in length from 1km to 138 km having maximum radial load of 150MW.This is a ACSR Zebra (x4) conductor with load value and line length taken from an existing radial feeder in the literature [105-106].The power factor at the load is unity.

Table 3-11:400kV Feeder data

Feeder Data							
Feeder name	**Length (km)**	**Rdc @ 50 dec C**	**Receiving end load (MW)**	**pf**	**Number of sub conductors per bundle**	**Type**	**IEEE reference**
B	138	0.02978	150	1	4	ACSR 4 x Zebra	[105-106]

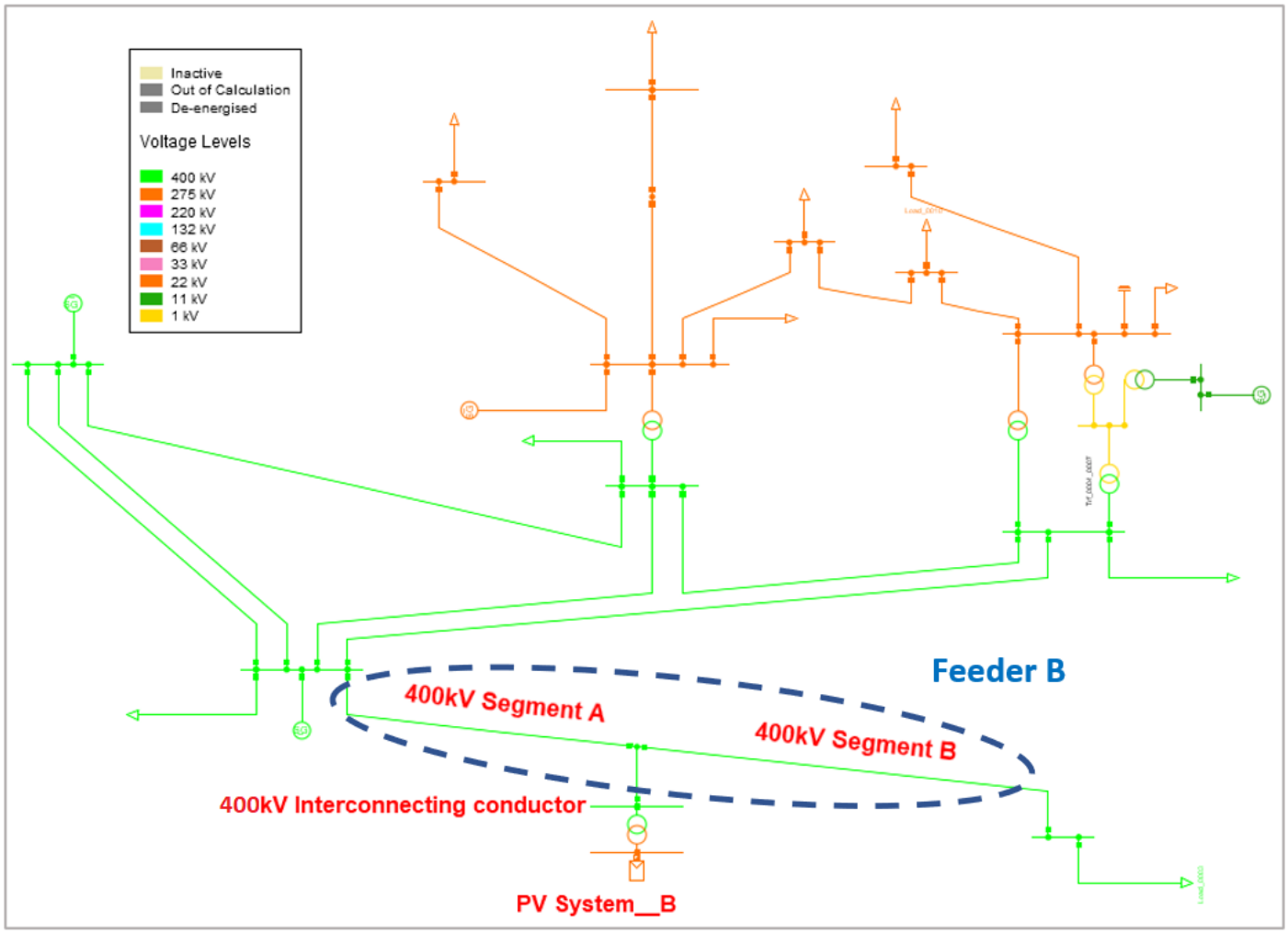

Figure 3-56:Modified IEEE 14-bus test system used to test 400kV ANN

3.5 Conclusion

Chapter 3 described the methodology and processes required for developing 7 ANN voltage specific algorithms which are designed to be used as a tool for network planners considering the integration of IPPs to the South African network in accordance with the constraints of the SAGC. The chapter ended off by presenting integrated voltage networks to be used as test networks to verify the performance and prediction accuracy of ANN models presented in chapter 3. Chapter 4 will analyse this performance in more detail by testing the model on test networks derived from IEEE 13-bus and IEEE 14-bus systems with some modifications

CHAPTER 4

CASE STUDIES AND RESULTS

As described in previous chapters, the objective of this research is to develop an ANN based algorithm to be used as a tool for providing additional support to network engineers and independent power producers (IPPs), especially for performing grid application studies. The algorithm as presented in chapter 3 caters for IPPs seeking connection to 11kV, 22kV, 66kV, 132kV, 220kV, 275kV and 400kV networks.

4.1 Case study description

Chapter 4 tests the performance and accuracy of this algorithm. Since the 7 ANN algorithms apply specifically to 7 unique nominal voltage networks undergoing IPP interconnection, the tests shown in this chapter are carried out by applying each algorithm to a matching power system network using DIgSILENT Powerfactory software. Seven cases are presented starting from the lowest voltage test case (11kV) to the highest voltage test case (400kV). Case 1 and Case 2 test the 11kV and 22kV ANNs on modified IEEE 13–bus systems, while Case 3 to Case 7 test 66kV, 132kV, 220kV, 275kV and 400kV ANNs on modified IEEE–14 bus systems. For all cases, the algorithm returns the best IPP size, location, power factor and interconnecting feeder type. Total line losses for these cases are recorded and compared to DIgSILENT Powerfactory simulation results and presented in Chapter 4 of this thesis.

4.1.1 Modifications for IEEE 13-Bus and IEEE 14-Bus Systems for Testing the ANN

Table 4-1 lists the modifications done on the IEEE 13-bus and IEEE 14-bus Systems for Testing the 7 ANNs.

Table 4-1: IEEE Test Case Modifications

IEEE Test System	Case Study with Voltage Level	Description of Modifications
13-bus	Case 1:11kV	Feeder A: length:5 km. Conductor: ACSR Kingbird. Nominal system voltage: 11 kV. MV/LV transformer: 5 MVA, 22/11 kV (Dyn11).
13-bus	Case 2: 22kV	Feeder A length:5 km. Feeder A conductor: ACSR Kingbird. Nominal voltage of network: 22 kV. MV/LV transformer: 5 MVA, 66/22 kV (Dyn11).
14-bus	Case 3: 66kV	66kV Feeder A length:15.6 km. Feeder A conductor: ACSR Kingbird (Rdc @ 50 deg C: 0.0891). Receiving end load: 30 MW @ 0.95 pf (lag).
14-bus	Case 4: 132kV	132 kV Feeder B length:35 km. Feeder B conductor: ACSR Kingbird (Rdc @ 50 deg C: 0.0891). Receiving end load: 91 MW @ 0.95 pf (lag). Intercon Twin Zebra.
14-bus	Case 5: 220kV	220 kV Feeder A length:134 km. Feeder B conductor: ACSR Zebra (Rdc @ 50 deg C: 0.0642). Receiving end load: 201 MW @ 0.95 pf.
14-bus	Case 6: 275kV	275 kV Feeder B length:196 km. Feeder B conductor: ACSR Twin Zebra (Rdc @ 50 deg C: 0.0642). Receiving end load: 201 MW @ 0.96 pf (lag).
14-bus	Case 7: 400kV	400 kV Feeder B length:138 km. Feeder B conductor: ACSR Quad Zebra (Rdc @ 50 deg C: 0.0642). Receiving end load: 150 MW @ unity pf.

4.1.2 Case 1 (11kV) and Case 2 (22kV) Networks for ANN Algorithm

Both 11kV and 22kV algorithms are tested on backbone Feeder A (the backbone feeder) of Figure 4 – 1 below. For both cases the length of backbone Feeder A (the backbone feeder) is set to 5km since this is a common length used in distribution networks South Africa, as shown in [94,95,96,97,98]. The interconnecting conductor length is set to 5km, which is justified based on studies performed in Chapter 3, Section 3.2.3.1 for 11kV Data. The active and reactive power setpoints at bus 5 of the IEEE 13-bus system remain unchanged from the original values specified in [94]. These are: 4.05MVA operating at 0.85 lagging power factor with active and reactive power setpoints of 3.5 MW,2.1 MVAR respectively. The IPP for both cases are located at positions 10%, 20%, 30%, 40%, 50%, 60%,70%, 80% and 90% of the total backbone Feeder A length as measured from sending end busbar 2.

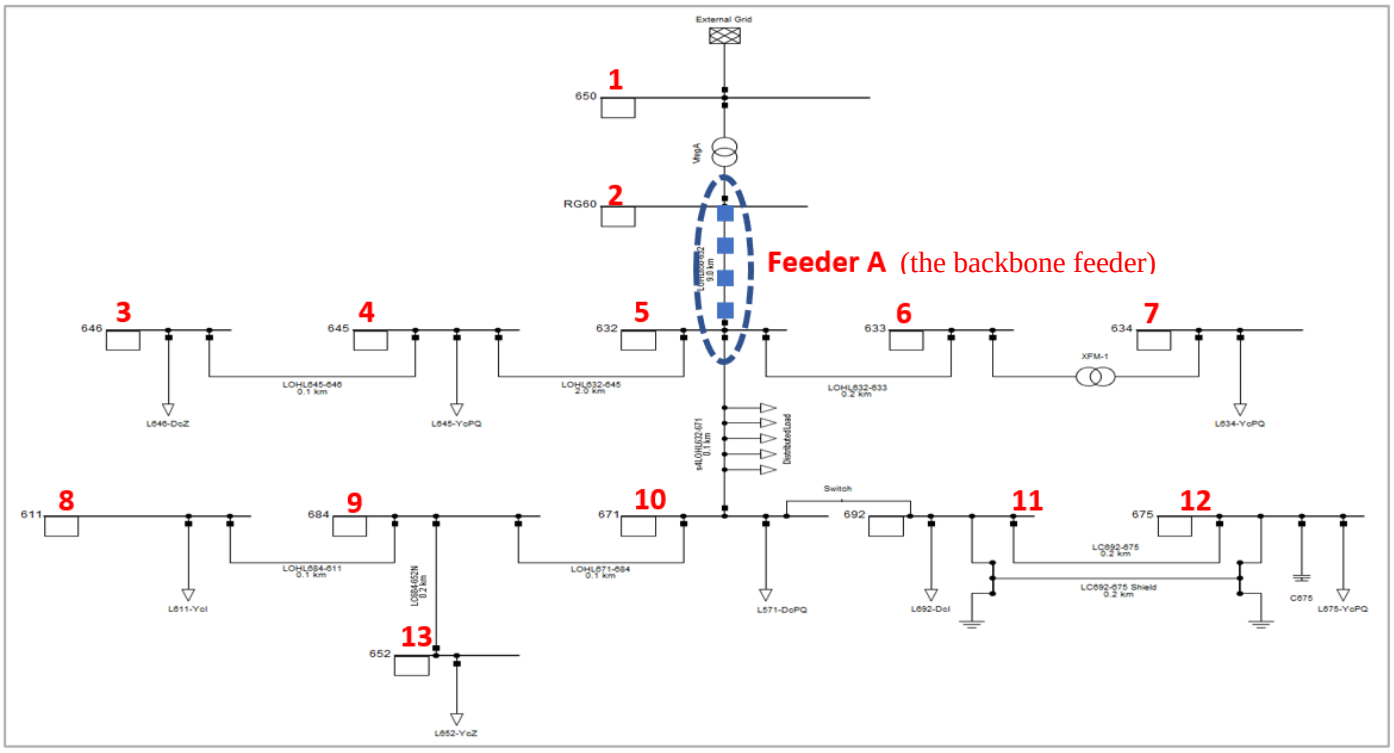

Figure 4-1:Modified IEEE – 13 bus system used for testing 11kV and 22kV ANNs.

4.1.2 Case 3 (66kV) and Case 4 (132kV) Networks for ANN Algorithm

Figure 4-2 and Table 4-2 below show the modified IEEE 14-bus system used testing the ANN for 66kV and 132kV cases. The same approach as 11kV and 22kV cases has been followed for these cases. The IPP for both cases are located at positions 10%, 20%, 30%, 40%, 50%, 60%,70%, 80% and 90% of the total backbone Feeder A and backbone Feeder B length as measured from sending end busbar 2. Interconnecting conductor lengths are set to 12km [99].

Table 4-2: 66kV and 132kV Feeder Data

Feeder Data							
Name of backbone Feeder Tested On	**Length (km)**	**Rdc @ 50 deg C**	**Receiving end load (MW)**	**pf**	**Number of subconductors per bundle**	**Type**	**IEEE reference**
A	15.6	0.0891	30	0.95	1	ACSR Kingbird	[99]
B	35	0.0891	91	0.95	2	ACSR Kingbird	[100]

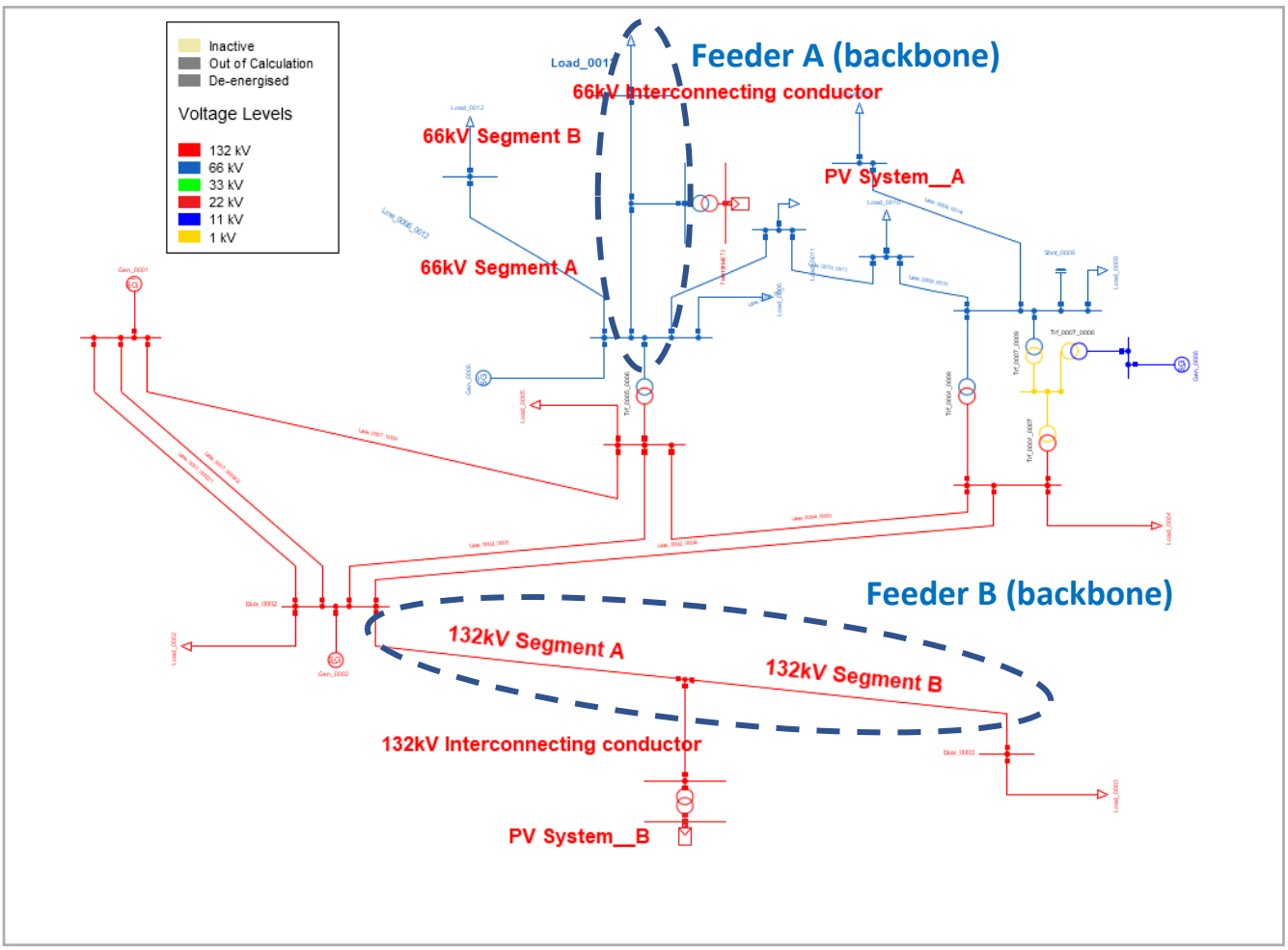

Figure 4-2:Modified IEEE 14-bus test system used to test 66k and 132kV ANNs

4.1.3 Case 5 (220kV) and Case 6 (275kV) Networks for ANN Algorithm

Figure 4 -3 and Table 4–3 show the modified IEEE 14-bus system used for the 220kV and 275 kV cases. The IPP for both cases are located at positions 10%, 20%, 30%, 40%, 50%, 60%,70%, 80% and 90% of the total backbone Feeder A and backbone Feeder B length as measured from sending end busbar 2.

Table 4-3: 220kV and 275kV Feeder Data

Feeder Data							
Backbone Feeder name	**Length (km)**	**Rdc @ 50 dec C**	**Receiving end load (MW)**	**pf**	**Number of subconductors per bundle**	**Type**	**IEEE reference**
A	134	0.0642	201	0.95	1	ACSR Zebra	[101-102]
B	196	0.0642	201	0.96	2	ACSR Twin Zebra	[103-104]

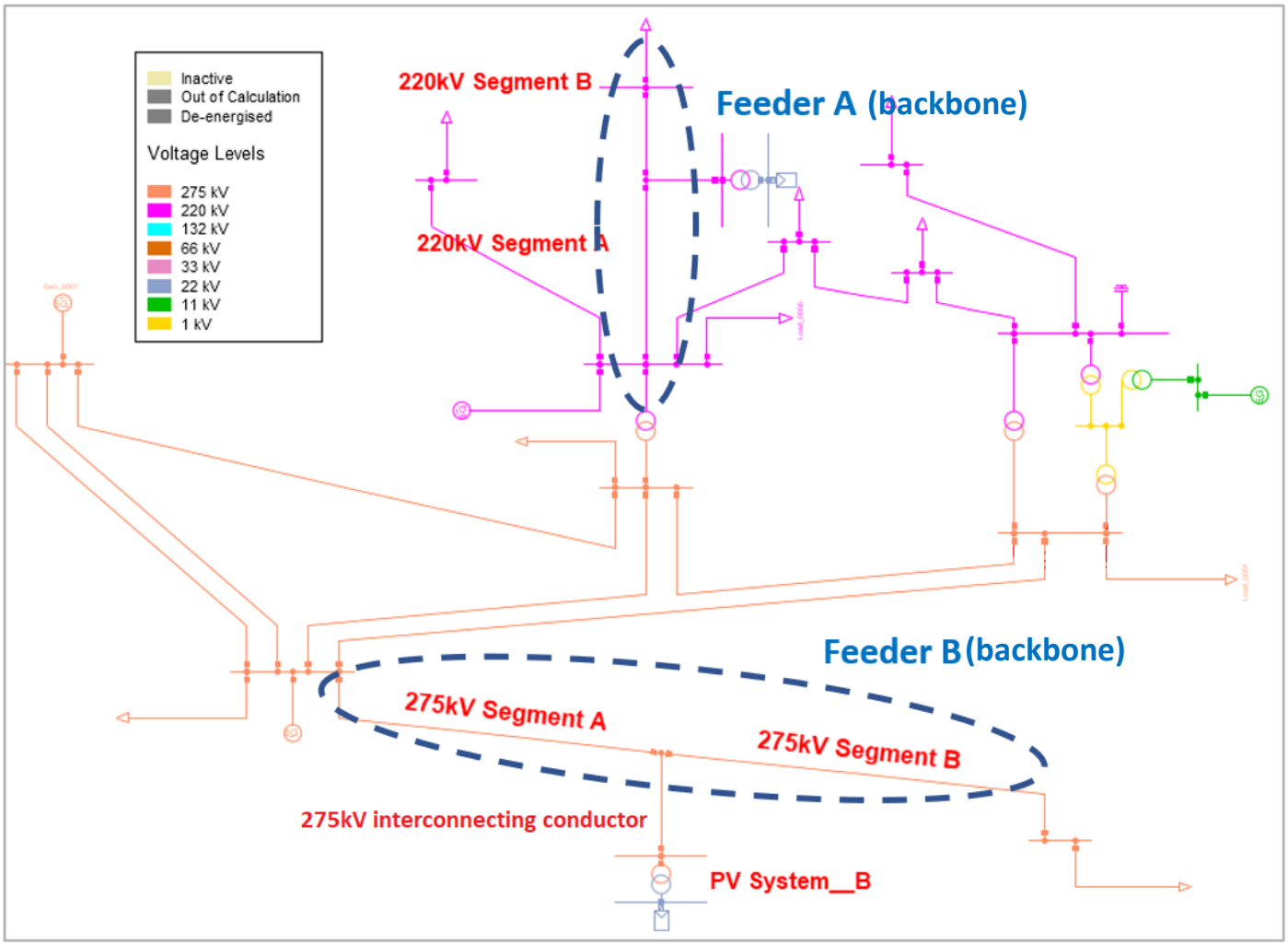

Figure 4-3:Modified IEEE 14-bus test system used to test 220k and 275kV ANNs

4.1.4 Case 7 (400kV) Network for ANN Algorithm

Figure 4-4 and Table 4–4 show the modified IEEE 14 bus system used for the 400 kV case. The IPP for both cases is located at positions 10%, 20%, 30%, 40%, 50%, 60%,70%, 80% and 90% of the total backbone Feeder A and backbone Feeder B length as measured from sending end busbar 2.

Table 4-4: 400kV Feeder data

Feeder Data							
Backbone Feeder name	**Length (km)**	**Rdc @ 50 dec C**	**Receiving end load (MW)**	**pf**	**Number of sub conductors per bundle**	**Type**	**IEEE reference**
B	138	0.0642	150	1	4	ACSR 4 x Zebra	[105-106]

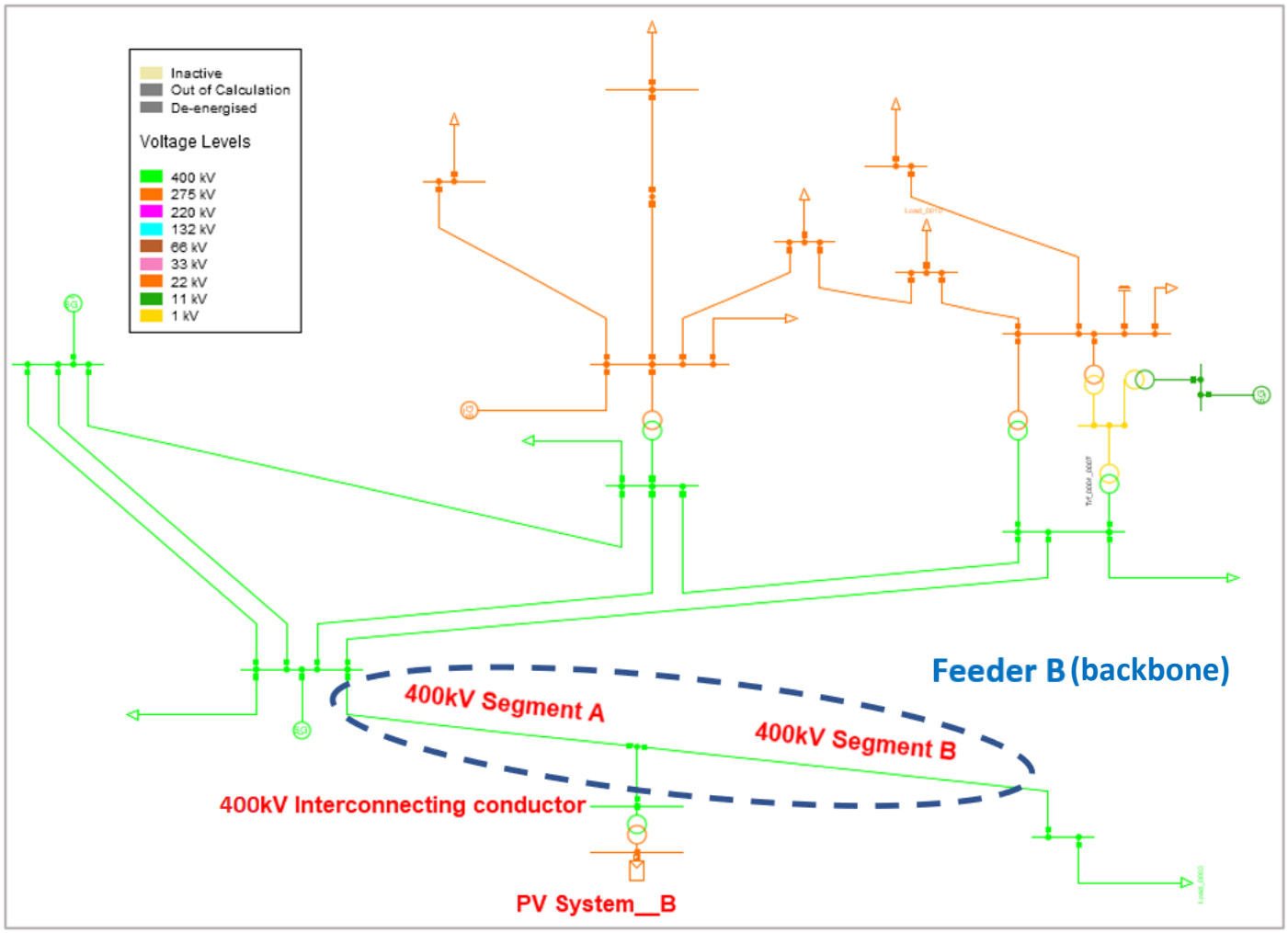

Figure 4-4:Modified IEEE 14-bus test system used to test 400kV ANN

4.2 Presentation and Analysis of Results

For all test cases, results are obtained in two steps. The first step requires the user to enter specific network parameters via the MATLAB user interface. These are:

- The backbone voltage (kV) (prompt 1)
- Backbone length (km) (prompt 2)
- Interconnecting feeder length (km) (prompt 3)
- Maximum load seen at the receiving end (MW) (prompt 4)
- Distance from IPP at the POC to the sending end busbar (Segment A length) as a percentage of the total backbone length (km) (prompt 5)
- Load power factor at the receiving end (prompt 6)

The ANN algorithm returns two sets of information below:

(a) The most favourable operating parameters resulting in the smallest line losses ***overall***

7. The best location of connection **overall** (km)
8. The best IPP size (MW) based on the best location overall.
9. The applicable IPP SAGC category (Category A,B or C) based on the best location overall
10. Overall losses (MW) based on the best location overall
11. The conductor type based on point the best location overall
12. The most suitable IPP power factor based on the best location overall.

(b) The most favourable operating parameters resulting in the smallest line losses based ***on the users proposed IPP location at the POC:***

- The proposed location of connection (km)
- The best IPP size based on proposed location (MW)
- The applicable IPP SAGC category based on proposed location (Category A,B or C)
- Overall losses (MW)
- The conductor type
- The most suitable IPP power factor

Once (a) and (b) have been determined and recorded, the second step is to analyse the accuracy and closeness of these against DIgSILENT Powerfactory results. This is done by connecting the IPP with the parameters returned in (a) and (b) above in DIgSILENT Powerfactory and then running a load flow simulation. Losses generated from DIgSILENT Powerfactory simulations are then saved and compared to the losses arising from (a) and (b). If differences in error between the ANN losses and DIgSILENT Powerfactory losses fall within 3%, the result is considered acceptable since it falls within the range of existing error values previously documented in the literature based on similar ANN based studies [65, 66, 67].

4.3 Case 1: 11kV ANN - Results

IPP is connected to the 5km backbone at the following locations measured from busbar 2 (the sending end) indicated in Figure 4-1 above and simulated in DIgSILENT Powerfactory. Testing IPP locations measured from sending end are as follows: 10% (0.5km), 20% (2.5km), 30% (1.5km) ,40% (2km), 50% (2.5km), 60% (3km),70% (3.5km), 80% (4km) and 90% (4.5km). A loss comparison between the ANN and DIgSILENT Powerfactory is shown in Figure 4–5 to Figure 4-7, listing the results for the 10%, 50% and 90% cases. The full set of results is shown in Table 4-5 for all locations.

ANN Algorithm Output Results:

```
**********   ANN prediction    **********
Enter the following network parameters:
Backbone Voltage Level (kV): 11
Backbone length(km): 5
Length of interconnecting feeder (km): 5
Backbone maximum loading(MW): 3.5
Enter IPP distance as a percentage of total backbone length from sending end substation to POC(%): 10
Enter load power factor:0.85
**************************************************
**************************************************
The most optimal parameters are displayed below:
Best Location:4.5km
Best Size:1.5MW
Applicable South African Grid Code Category:
B
Losses:0.053516MW
Conductor    Type
Chickadee (ACSR, diameter: 18.87mm DC Resistance :0.1427419, Current rating 419A)
Power Factor:0.975
**************************************************
**************************************************
The most optimal parameters based on IPP distance from sending end:
IPP Location:1km
Best Size:1MW
Applicable South African Grid Code Category:
B
Losses:0.073024MW
Conductor    Type
Chickadee (ACSR, diameter: 18.87mm DC Resistance :0.1427419, Current rating 419A)
Power Factor:0.975
```

Overall best location and IPP size.

Best size based on the proposed 10% location

ANN predicted Losses = 0.073024MW

DIgSILENT Powerfactory Simulation Results:

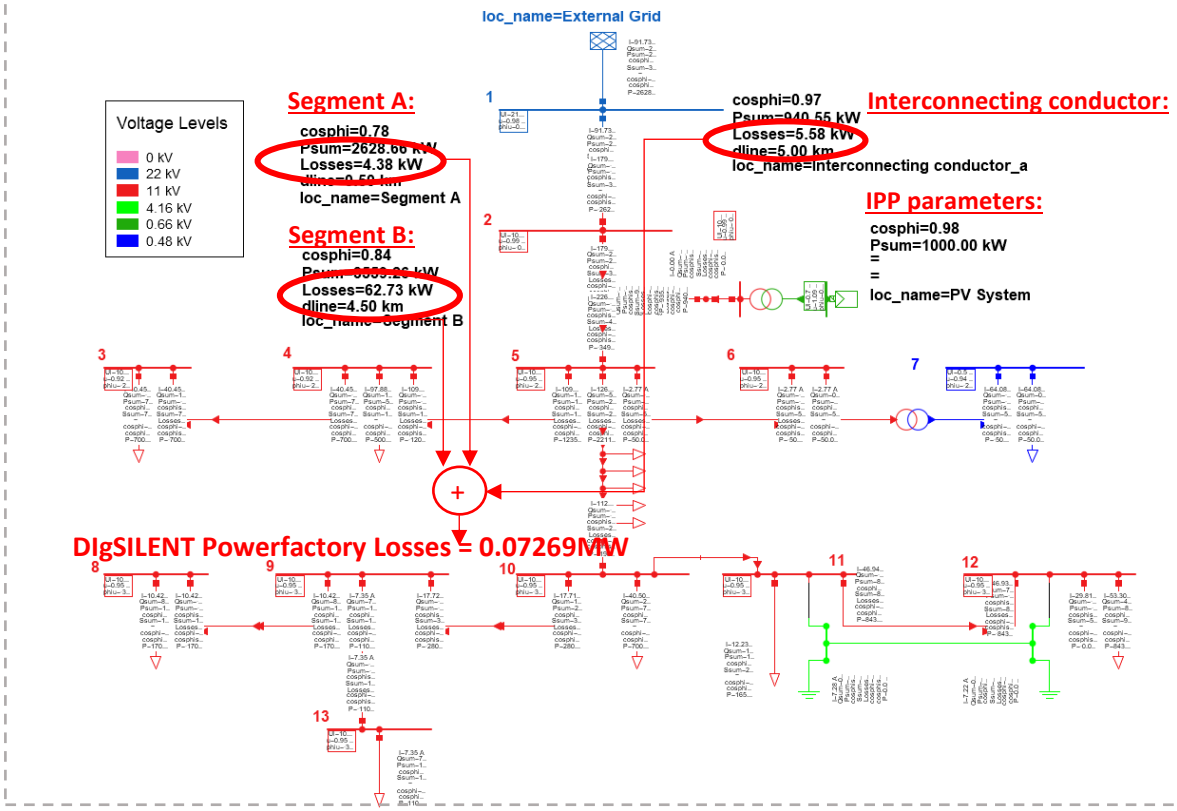

Figure 4-5: Results for Case 1 (11kV) for IPP at 10% from sending end (0.5km from busbar 2 in Figure 4-1)

ANN Algorithm Output Results:

```
********************   ANN prediction    ********************
Enter the following network parameters:
Backbone Voltage Level (kV): 11
Backbone length(km): 5
Length of interconnecting feeder (km): 5
Backbone maximum loading(MW): 3.5
Enter IPP distance as a percentage of total backbone length from sending end substation to POC(%): 50
Enter load power factor:0.85
*****************************************************
*****************************************************
The most optimal parameters are displayed below:
Best Location:4.5km
Best Size:1.5MW
Applicable South African Grid Code Category:
B
Losses:0.053516MW
Conductor   Type
Chickadee (ACSR, diameter: 18.87mm DC Resistance :0.1427419, Current rating 419A)
Power Factor:0.975
*****************************************************
*****************************************************
The most optimal parameters based on IPP distance from sending end:
IPP Location:2.5km
Best Size:1MW
Applicable South African Grid Code Category:
B
Losses:0.0651MW
Conductor   Type
Chickadee (ACSR, diameter: 18.87mm DC Resistance :0.1427419, Current rating 419A)
Power Factor:0.975
```

ANN predicted Losses = 0.0651MW

Set 1: Overall best location and IPP size.

Set 2: Based on the proposed 50%

DIgSILENT Powerfactory Simulation Results:

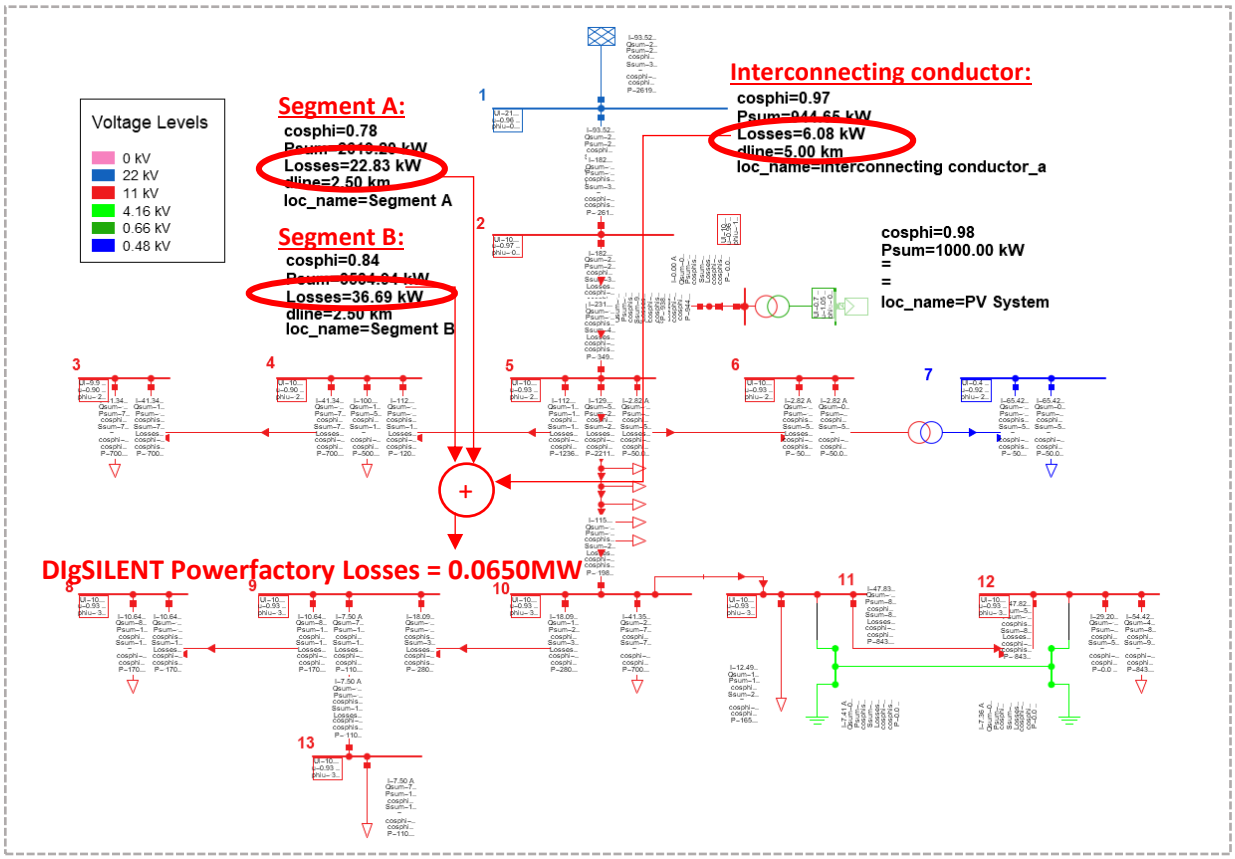

Figure 4-6: Results for Case 1 (11kV) for IPP at 50% from sending end (2.5km from busbar 2 in Figure 4-1)

ANN Algorithm Output Results:

```
********************   ANN prediction    ********************
Enter the following network parameters:
Backbone Voltage Level (kV): 11
Backbone length(km): 5
Length of interconnecting feeder (km): 5
Backbone maximum loading(MW): 3.5
Enter IPP distance as a percentage of total backbone length from sending end substation to POC(%): 90
Enter load power factor:0.85
**************************************************
**************************************************
The most optimal parameters are displayed below:
Best Location:4.5km
Best Size:1.5MW
Applicable South African Grid Code Category:
B
Losses:0.053516MW
Conductor   Type
Chickadee (ACSR, diameter: 18.87mm DC Resistance :0.1427419, Current rating 419A)
Power Factor:0.975
**************************************************
**************************************************
The most optimal parameters based on IPP distance from sending end:
IPP Location:4.5km
Best Size:1.5MW
Applicable South African Grid Code Category:
B
Losses:0.053516MW
Conductor   Type
Chickadee (ACSR, diameter: 18.87mm DC Resistance :0.1427419, Current rating 419A)
Power Factor:0.975
```

ANN predicted Losses = 0.053516MW

Set 1: Overall best location and IPP size.

Set 2: Based on the proposed 90%

DIgSILENT Powerfactory Simulation Results:

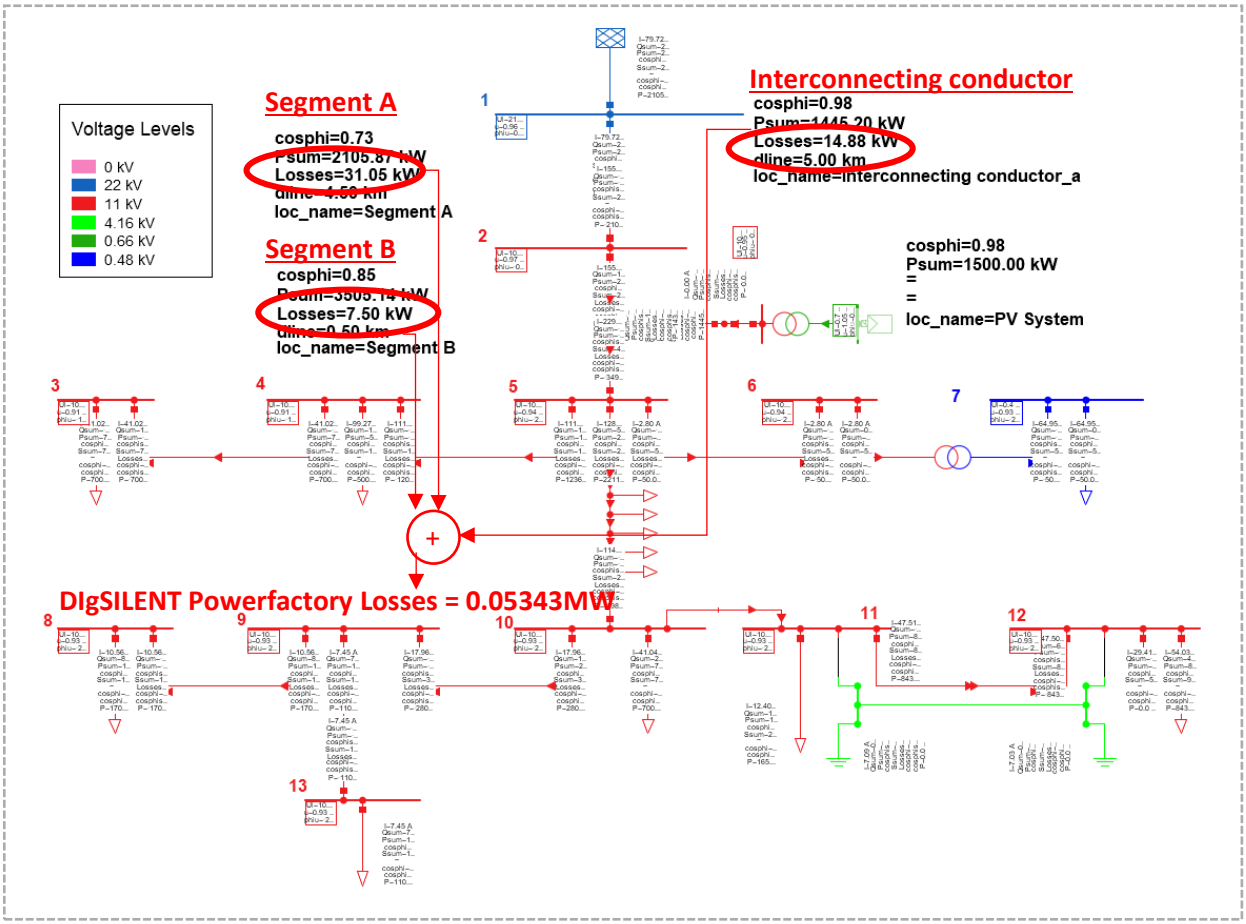

Figure 4-7: Results for Case 1 (11kV) for IPP at 90% from sending end (4.5 km from busbar 2 in Figure 4-1)

The same parameters are used as inputs to the modified IEEE 13-bus system, and the actual losses generated from the IEEE 13- bus system in DIgSILENT Powerfactory are compared to the ANN predicted losses for the same operating parameters of 3.5MW at the load receiving end, Feeder A length of 5km, and receiving end power factor 0.85 lagging. Figure 4 – 5 through Figure 4 - 7 show ANN results for cases where the IPP (connected to node X) moves from the sending end (Length of Segment A is 10% of the total line length, Length of Segment B is 90% of total line length) to the centre of backbone feeder A (Length of Segment A is 50% of total line length, Length of Segment B is 50% of the total line length) and lastly to receiving end (Length of Segment A is 90% of the total line length, Length of Segment B is 10% of total line length) on backbone Feeder A. Table 4-5 summarises the results when the IPP is located from 10% to 90% of the total backbone feeder length A, in 10% increments. Figure 4-8 shows the error between the ANN prediction and DIgSILENT Powerfactory simulations. The graph indicates the difference in total line losses between the ANN algorithm predictions and DIgSILENT Powerfactory. Ideally, both graphs would be precisely one on top of another which indicates a perfect ANN loss prediction. As can be seen, there are differences in values since they are not exactly overlapped with a worst-case difference in error of 1.44% which translates to an error of 0.91kW.

Table 4-5: Case 1 - (11kV) Comparison of ANN Loss Results with DIgSILENT Powerfactory Loss Results

Case 1 (11kV) MW Loss comparison								
IPP Location (%) from Sending End	**IPP Size**	**IPP power factor**	**Conductor**	**SAGC Category**	**ANN Losses (MW)**	**DIgSILENT Powerfactory Losses (MW)**	**Error (kW)**	**Error (%)**
Best overall location (90%)	1.5MW	0.975	Chickadee	B	0.05352	0.05343	0.09	0.1684
IPP connected at 10%	1MW	0.975	Chickadee	B	0.07302	0.07269	0.33	0.4539
IPP connected at 20%	1MW	0.975	Chickadee	B	0.07290	0.07211	0.79	1.0955
IPP connected at 30%	1MW	0.975	Chickadee	B	0.07032	0.06957	0.75	1.0780
IPP connected at 40%	1MW	0.975	Chickadee	B	0.06772	0.06755	0.17	0.2516
IPP connected at 50%	1MW	0.975	Chickadee	B	0.06510	0.06501	0.09	0.1384
IPP connected at 60%	1MW	0.975	Chickadee	B	0.06204	0.06295	0.91	1.4455
IPP connected at 70%	1.5MW	0.975	Chickadee	B	0.05945	0.059001	0.449	0.7610
IPP connected at 80%	1.5MW	0.975	Chickadee	B	0.05573	0.05608	0.35	0.6241
IPP connected at 90%	1.5MW	0.975	Chickadee	B	0.05352	0.05343	0.09	0.1684

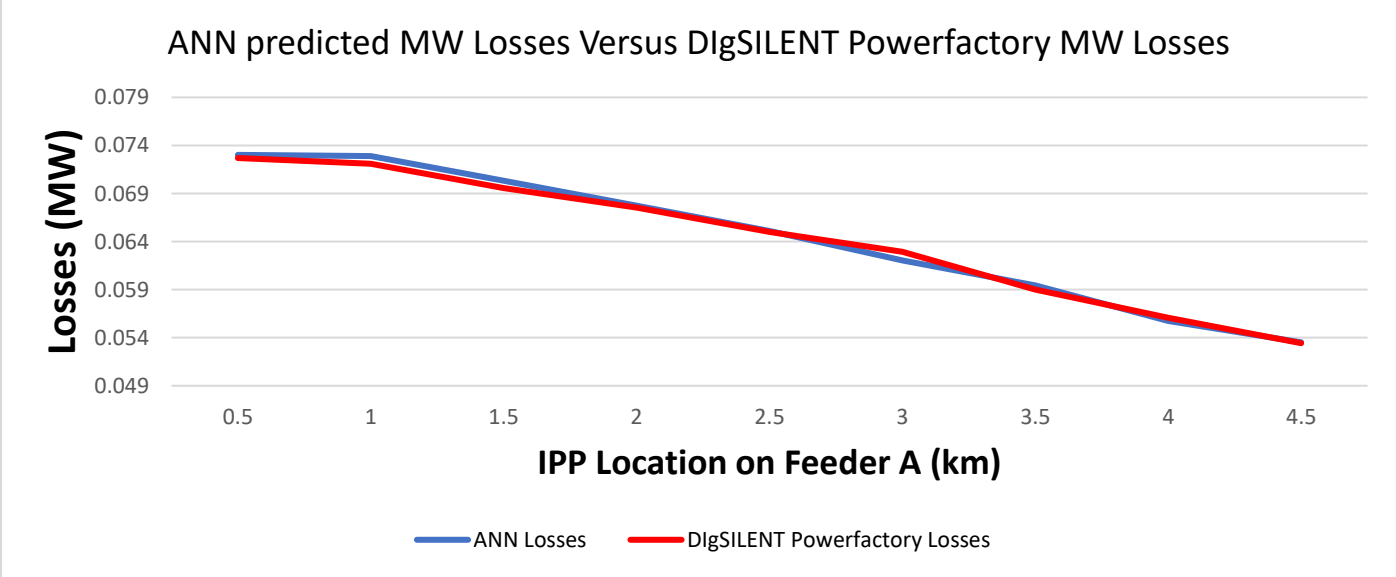

Figure 4-8:Case 1 (11kV) - Loss comparison between the ANN and DIgSILENT Powerfactory

4.4 Case 2: 22kV ANN –Results

For the 22kV case that same approach is taken as in the 11kV case and the case refers to Figure 4-1. IPP connected at the following locations on backbone Feeder A: 10% (0.5km), 20% (2.5km), 30% (1.5km) ,40% (2km), 50% (2.5km), 60% (3km),70% (3.5km), 80% (4km) and 90% (4.5km). A loss comparison between the ANN and DIgSILENT Powerfactory is shown in Figure 4 – 9 to Figure 4-11 showing the results for the 10%, 50% and 90% cases. The full set of results shown in Table 4-6 for all locations.

ANN Algorithm Output Results

```
**********************   ANN prediction    **********************
Enter the following network parameters:
Backbone Voltage Level (kV): 22
Backbone length(km): 5
Length of interconnecting feeder (km): 5
Backbone maximum loading(MW): 3.5
Enter IPP distance as a percentage of total backbone length from sending end substation to POC(%): 10
Enter load power factor:0.85
**************************************************
**************************************************
The most optimal parameters are displayed below:
Best Location:4.5km
Best Size:1.5MW
Applicable South African Grid Code Category:
B
Losses:0.013445MW
Conductor    Type
Chickadee (ACSR, diameter: 18.87mm DC Resistance :0.1427419, Current rating 419A)
Power Factor:0.975
**************************************************
**************************************************
The most optimal parameters based on IPP distance from sending end:
IPP Location:0.5km
Best Size:1MW
Applicable South African Grid Code Category:
B
Losses:0.018828MW
Conductor    Type
Chickadee (ACSR, diameter: 18.87mm DC Resistance :0.1427419, Current rating 419A)
Power Factor:0.975
```

ANN predicted Losses = 0.018828MW

Set 1: Overall best location and IPP size.

Set 2: Based on the proposed 10%

DIgSILENT Powerfactory Simulation Results:

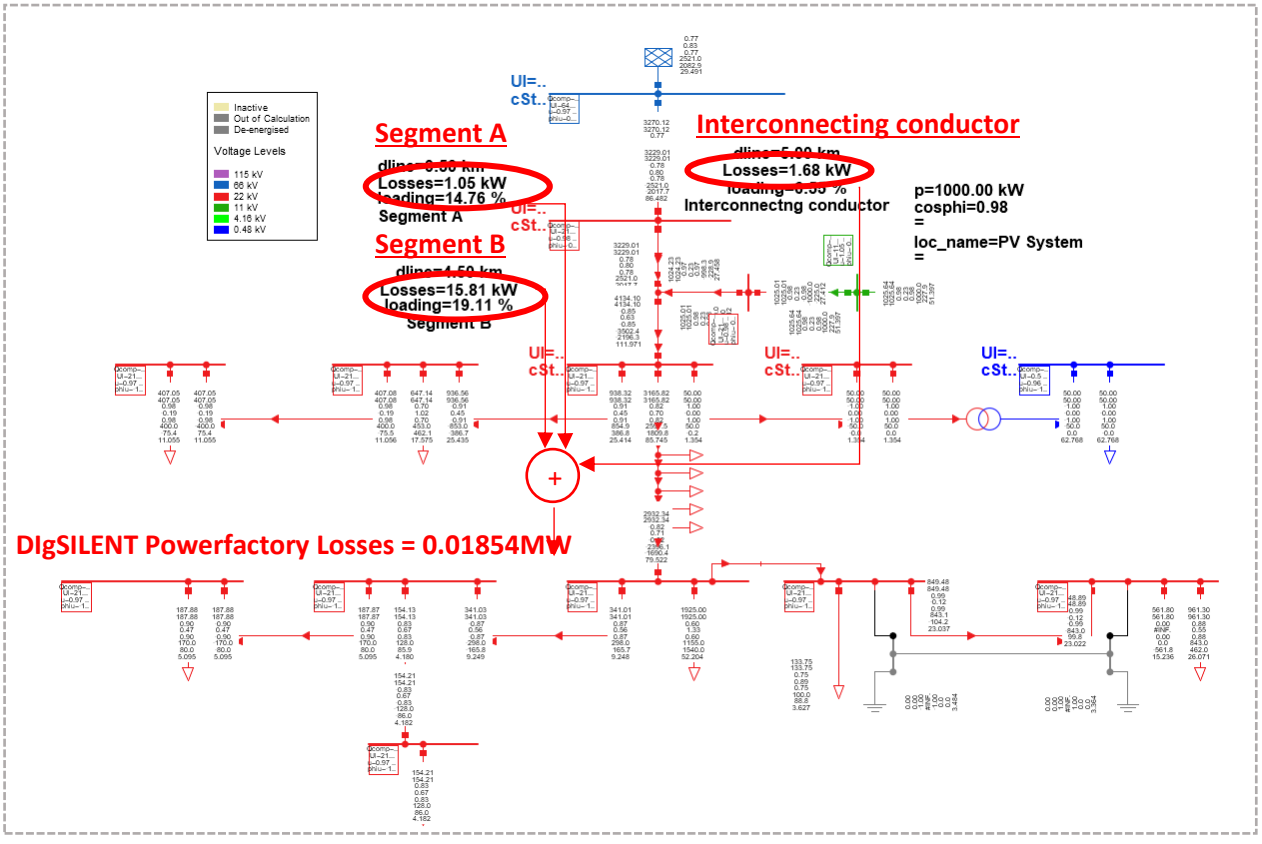

Figure 4-9: Results for Case 2 (22kV) for IPP at 10% from sending end (0.5km from busbar 2 in Figure 4-1)

ANN Algorithm Output Results

```
*********************   ANN prediction    *********************
Enter the following network parameters:
Backbone Voltage Level (kV): 22
Backbone length(km): 5
Length of interconnecting feeder (km): 5
Backbone maximum loading(MW): 3.5
Enter IPP distance as a percentage of total backbone length from sending end substation to POC(%): 50
Enter load power factor:0.85
*****************************************************
*****************************************************
The most optimal parameters are displayed below:
Best Location:4.5km
Best Size:1.5MW
Applicable South African Grid Code Category:
B
Losses:0.013445MW
Conductor    Type
Chickadee (ACSR, diameter: 18.87mm DC Resistance :0.1427419, Current rating 419A)
Power Factor:0.975
*****************************************************
*****************************************************
The most optimal parameters based on IPP distance from sending end:
IPP Location:2.5km
Best Size:1MW
Applicable South African Grid Code Category:
B
Losses:0.016331MW
Conductor    Type
Chickadee (ACSR, diameter: 18.87mm DC Resistance :0.1427419, Current rating 419A)
Power Factor:0.975
```

Set 1: Overall best location and IPP size.

Set 2: Based on the proposed 50%

ANN predicted Losses = 0.016331MW

DIgSILENT Powerfactory Simulation Results:

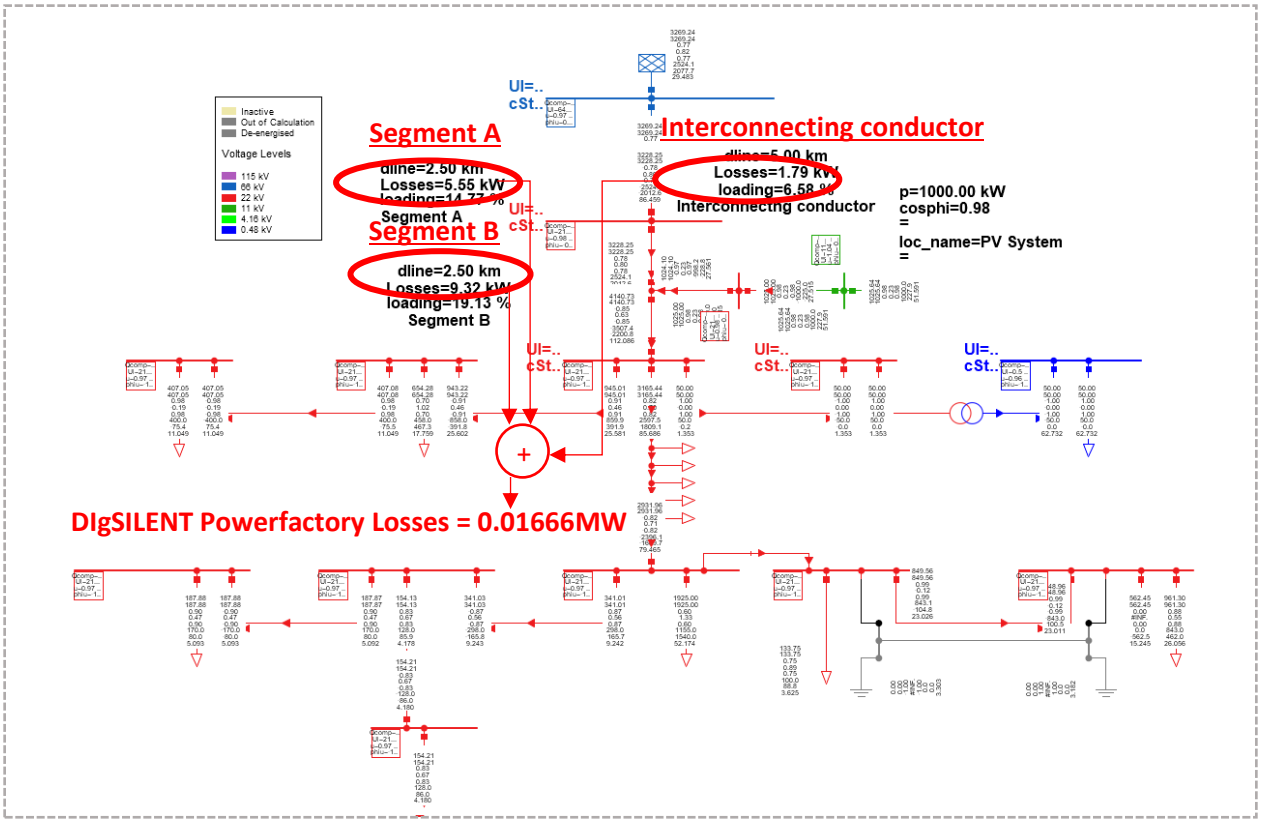

Figure 4-10: Results for Case 2 (22kV) for IPP at 50% from sending end (2.5km from busbar 2 in Figure 4-1)

ANN Algorithm Output Results

```
********************   ANN prediction    ********************
Enter the following network parameters:
Backbone Voltage Level (kV): 22
Backbone length(km): 5
Length of interconnecting feeder (km): 5
Backbone maximum loading(MW): 3.5
Enter IPP distance as a percentage of total backbone length from sending end substation to POC(%): 90
Enter load power factor:0.85
**************************************************
**************************************************
The most optimal parameters are displayed below:
Best Location:4.5km
Best Size:1.5MW
Applicable South African Grid Code Category:
B
Losses:0.013445MW
Conductor   Type
Chickadee (ACSR, diameter: 18.87mm DC Resistance :0.1427419, Current rating 419A)
Power Factor:0.975
**************************************************
**************************************************
The most optimal parameters based on IPP distance from sending end:
IPP Location:4.5km
Best Size:1.5MW
Applicable South African Grid Code Category:
B
Losses:0.013445MW
Conductor   Type
Chickadee (ACSR, diameter: 18.87mm DC Resistance :0.1427419, Current rating 419A)
Power Factor:0.975
```

Set 1: Overall best location and IPP size.

Set 2: Based on the proposed 90%

ANN predicted Losses = 0.013445MW

DIgSILENT Powerfactory Simulation Results:

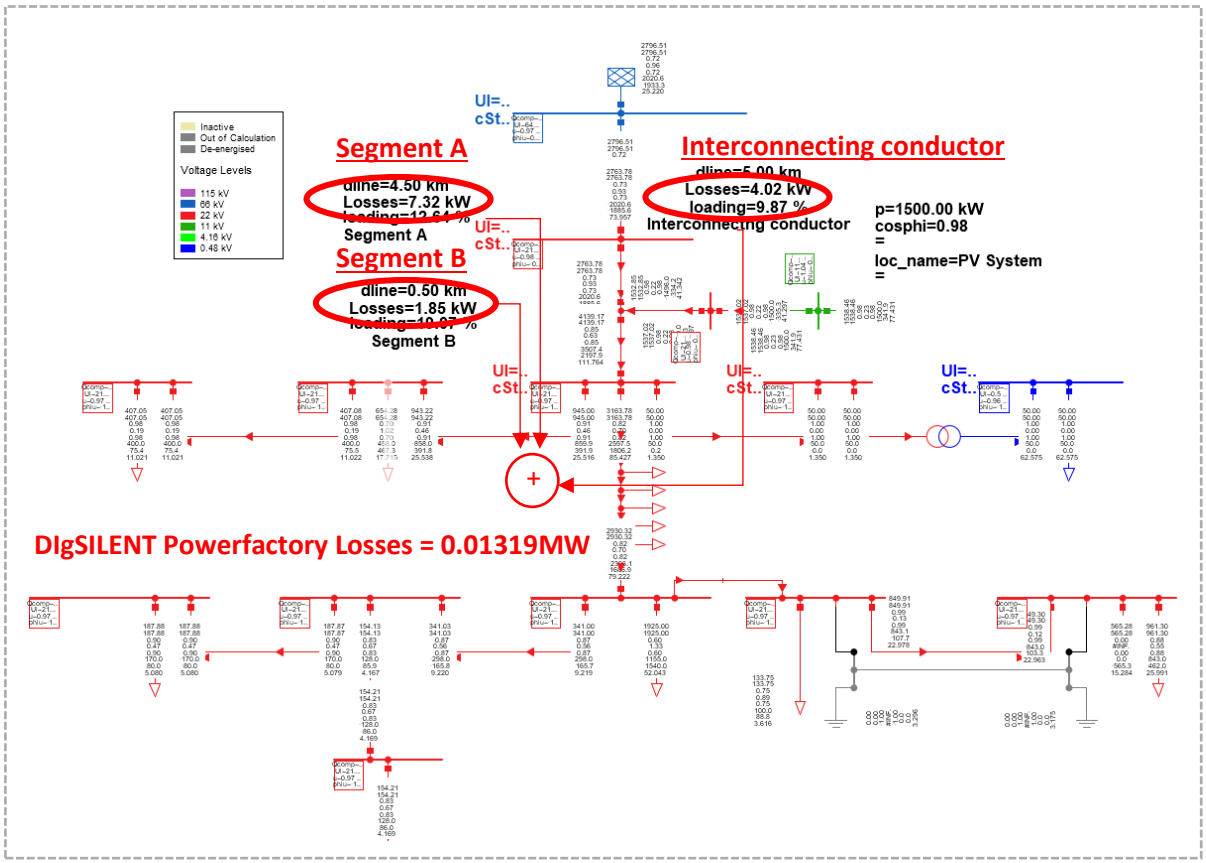

Figure 4-11: Results for Case 2 (22kV) for IPP at 90% from sending end (0.5km from busbar 2 in Figure 4-1)

Table 4 - 6 summarises the results when the IPP is located from 10% to 90% of the total backbone feeder A length, in 10% increments, with Figure 4 - 12 showing the error between the ANN prediction and DIgSILENT Powerfactory. The graph is indicating the difference in total line losses between the ANN algorithm predictions and DIgSILENT Powerfactory. Ideally, both graphs would be precisely one on top of another which indicates a perfect ANN loss prediction. As seen there are differences in values since they are not exactly overlapped with a worst-case difference in error of 1.93% which translates to an error of 0.255kW.

Table 4-6: Case 2 (22kV) – Comparison of ANN Loss Results with DIgSILENT Powerfactory Loss Results

Case 2 (22kV) MW Loss comparison								
IPP Location (%)	**IPP Size**	**IPP power factor**	**Conductor**	**SAGC Category**	**ANN Losses (MW)**	**DIgSILENT Powerfactory Losses (MW)**	**Error (kW)**	**Error (%)**
Best overall location (90%)	1.5MW	0.975	Chickadee	B	0.013445	0.013190	0.255	1.9332
IPP connected at 10%	1MW	0.975	Chickadee	B	0.018828	0.018540	0.288	1.5533
IPP connected at 20%	1MW	0.975	Chickadee	B	0.01703	0.016867	0.282	1.5188
IPP connected at 30%	1MW	0.975	Chickadee	B	0.01587	0.016085	0.02	0.1136
IPP connected at 40%	1MW	0.975	Chickadee	B	0.01505	0.015101	0.137	0.8144
IPP connected at 50%	1MW	0.975	Chickadee	B	0.016331	0.016666	0.119	0.7234
IPP connected at 60%	1MW	0.975	Chickadee	B	0.01364	0.013024	0.097	0.6245
IPP connected at 70%	1.5MW	0.975	Chickadee	B	0.01302	0.012823	0.216	1.4703
IPP connected at 80%	1.5MW	0.975	Chickadee	B	0.01264	0.012437	0.049	0.3496
IPP connected at 90%	1.5MW	0.975	Chickadee	B	0.013445	0.013190	0.255	1.9332

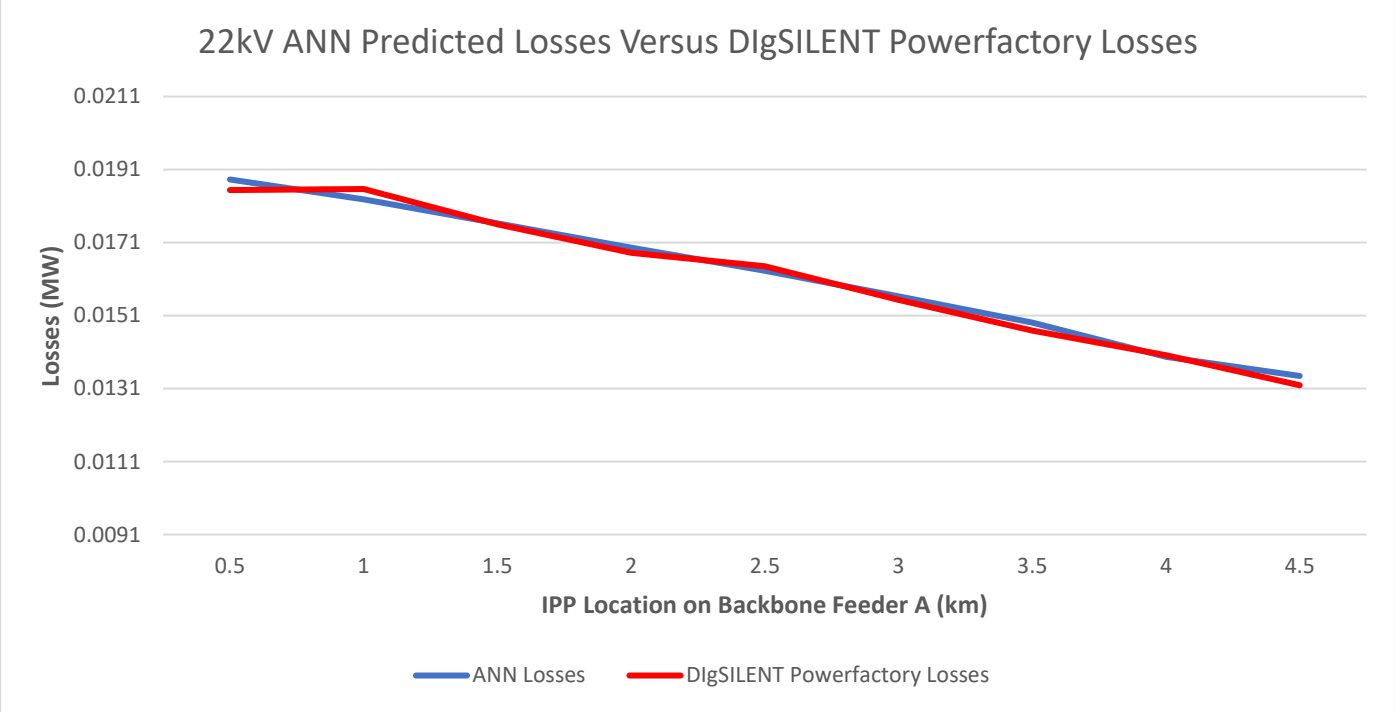

Figure 4-12: Case 2 (22kV) - Loss comparison between the ANN and DIgSILENT Powerfactory

4.5 Case 3: 66 kV ANN - Results

IPP is connected to the 15.6 km backbone at the following locations measured from busbar 2 (the sending end) indicated in Figure 4-2 above and simulated in DIgSILENT Powerfactory. Testing IPP locations measured from sending end are as follows: 10% (1.56km), 20% (3.12km), 30% (4.68km) ,40% (6.24km), 50% (7.8km), 60% (9.26km),70% (10.92km), 80% (12.48km) and 90% (14.04km). Loss comparisons between the ANN and DIgSILENT Powerfactory are shown in Figure 4-13 to Figure 4-15 listing the results for the 10%, 50% and 90% cases. The full set of results is shown in Table 4-7 for all locations.

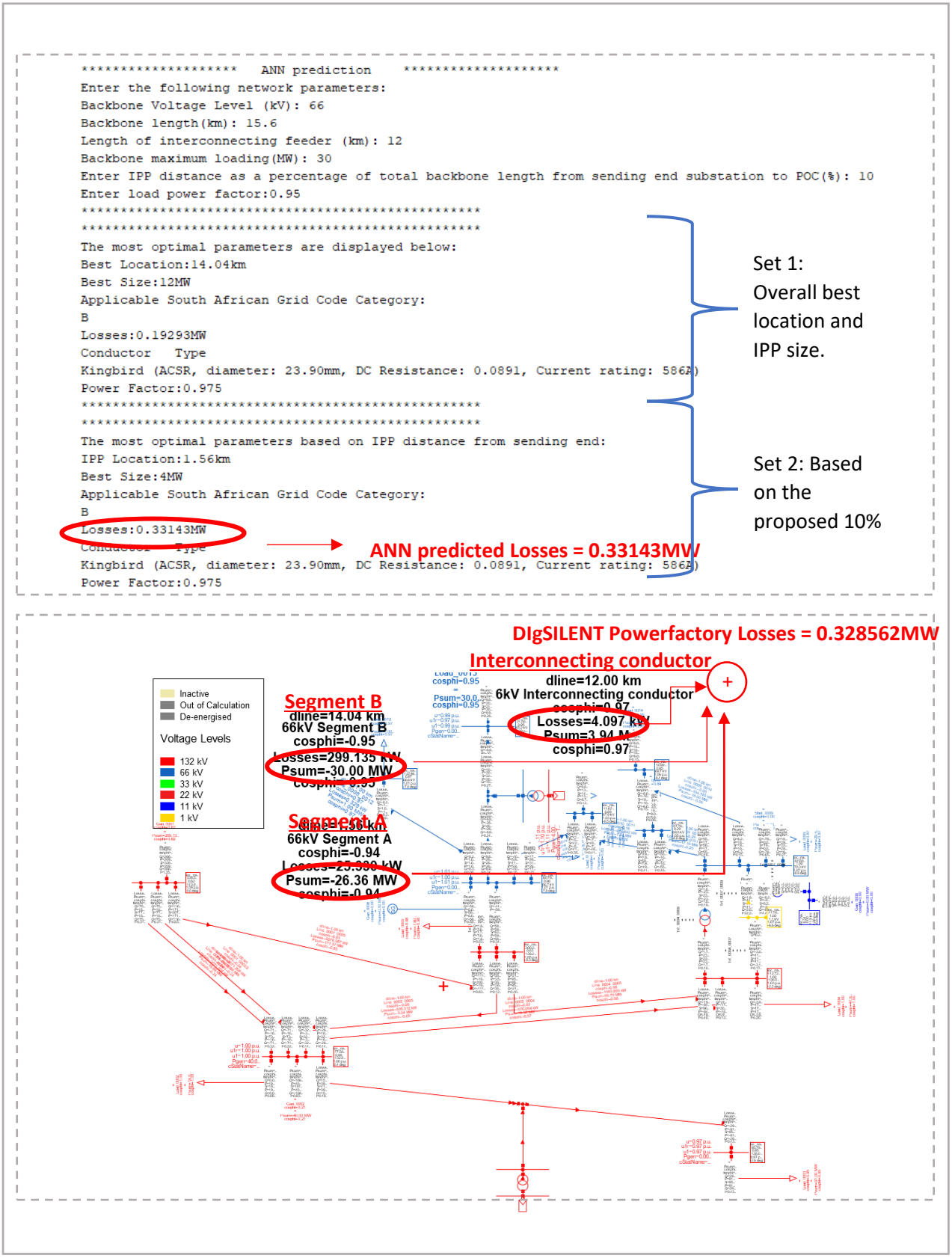

Figure 4-13: Results for Case 3 (66kV) for IPP at 10% from sending end (1.56km from busbar 2 in Figure 4-2)

```
**********   ANN prediction    **********
Enter the following network parameters:
Backbone Voltage Level (kV): 66
Backbone length(km): 15.6
Length of interconnecting feeder (km): 12
Backbone maximum loading(MW): 30
Enter IPP distance as a percentage of total backbone length from sending end substation to POC(%): 50
Enter load power factor:0.95
**************************************************
**************************************************
The most optimal parameters are displayed below:
Best Location:14.04km
Best Size:12MW
Applicable South African Grid Code Category:
B
Losses:0.19293MW
Conductor   Type
Kingbird (ACSR, diameter: 23.90mm, DC Resistance: 0.0891, Current rating: 586A)
Power Factor:0.975
**************************************************
**************************************************
The most optimal parameters based on IPP distance from sending end:
IPP Location:7.8km
Best Size:12MW
Applicable South African Grid Code Category:
B
Losses:0.27292MW
Conductor   Type
Kingbird (ACSR, diameter: 23.90mm, DC Resistance: 0.0891, Current rating: 586A)
Power Factor:0.975
```

Set 1: Overall best location and IPP size.

Set 2: Based on the proposed 50%

ANN predicted Losses = 0.27292MW

DIgSILENT Powerfactory Losses = 0.0269675MW

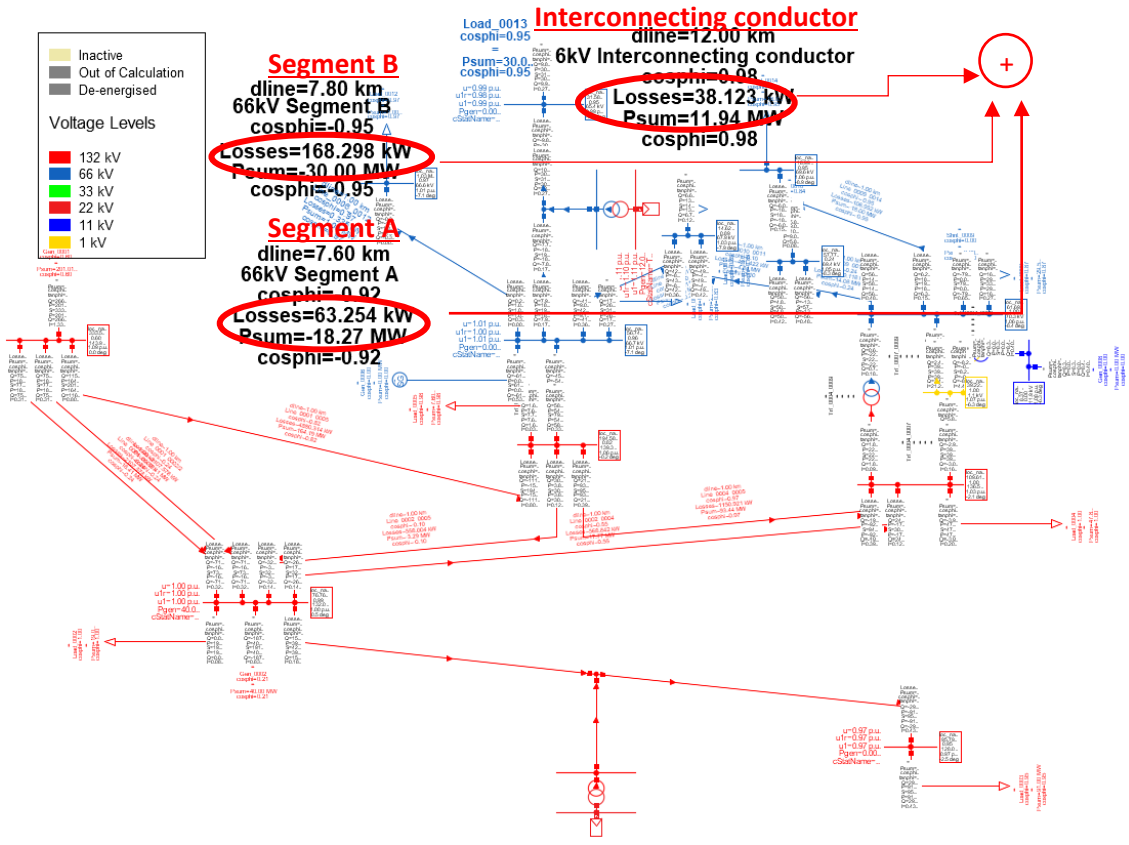

Figure 4-14: Results for Case 3 (66kV) for IPP at 50% from sending end (7.8km from busbar 2 in Figure 4-2)

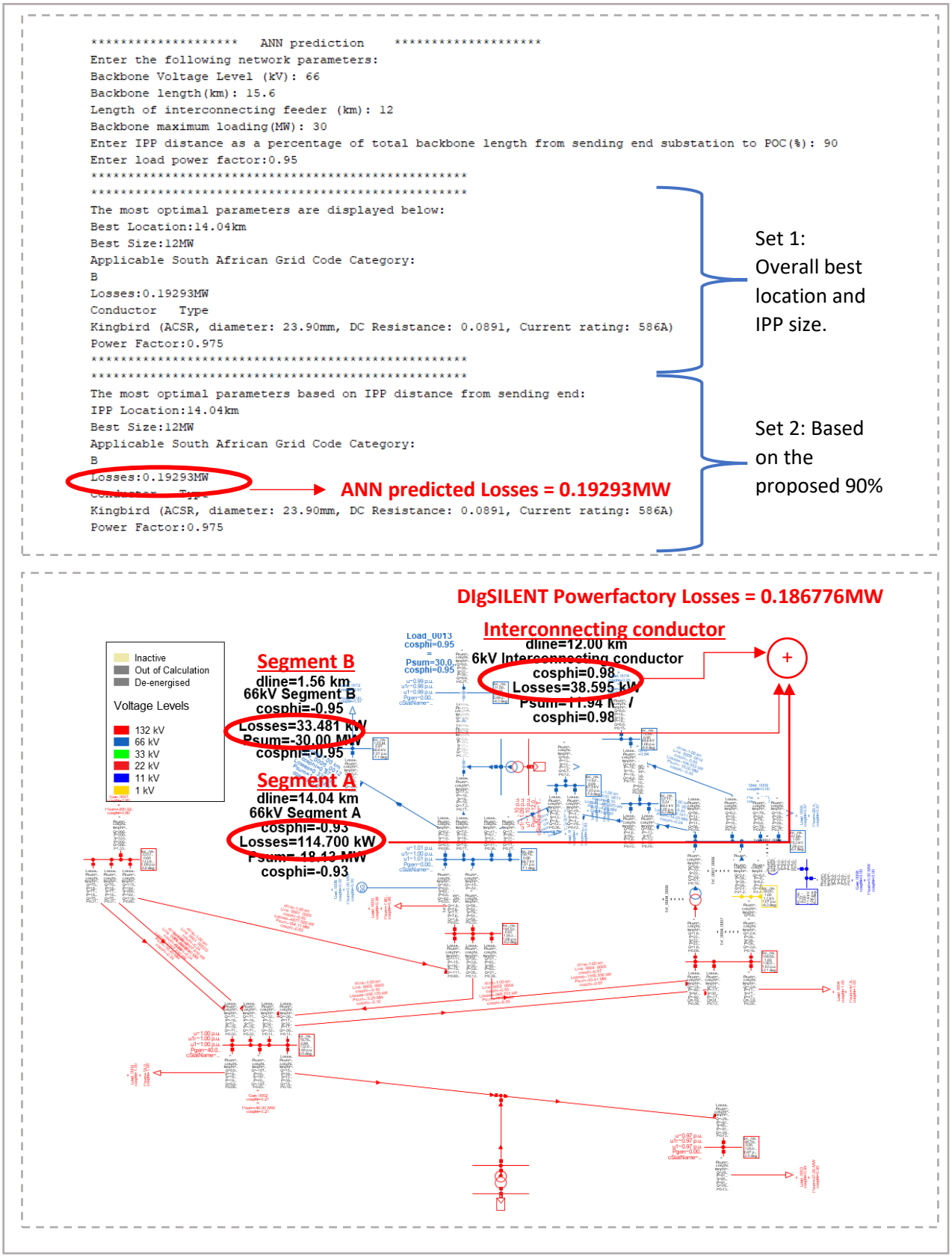

Figure 4-15: Results for Case 3 (66kV) for IPP at 90% from sending end (14.04km from busbar 2 in Figure 4-2)

The same parameters are used as inputs to the modified IEEE 14-bus system, and the actual losses generated from the IEEE 14- bus system in DIgSILENT Powerfactory are compared to the ANN predicted losses for the same operating parameters of 30MW at the load receiving end, backbone Feeder A length of 15.6km, and receiving end power factor 0.85 lagging. Figure 4-13 through Figure 4-15 show ANN results for cases where the IPP (connected to node X) moves from the sending end (Length of Segment A is 10% of the total line length, Length of Segment B is 90% of total line length) to the centre of backbone Feeder A (Length of Segment A is 50% of total line length, Length of Segment B is 50% of the total line length) and lastly to receiving end (Length of Segment A is 90% of the total line length, Length of Segment B is 10% of total line length) on Feeder A. Table 4-7 summarises the results when the IPP is located from 10% to 90% of the total feeder length A, in 10% increments. Figure 4-16 shows the error between the ANN prediction and DIgSILENT Powerfactory simulations. The graph indicates the difference in total line losses between the ANN algorithm predictions and DIgSILENT Powerfactory. Ideally, both graphs would be precisely one on top of another which indicates a perfect ANN loss prediction. As seen there are differences in values since they are not exactly overlapped with a worst-case difference in error of 3.29% which translates to an error of 0.615kW.

Table 4-7: Case 3 (66kV) – Comparison of 66kV ANN Loss Results with DIgSILENT Powerfactory Loss Results

Case 3 (66 kV) MW Loss comparison								
IPP Location (%) from Sending End	**IPP Size**	**IPP power factor**	**Conductor**	**SAGC Category**	**ANN Losses (MW)**	**DIgSILENT Powerfactory Losses (MW)**	**Error (kW)**	**Error (%)**
Best overall location (90%)	12MW	0.975	Kingbird	B	0.019293	0.0186776	0,6154	3,29
IPP connected at 10%	4MW	0.975	Kingbird	B	0.033143	0.032856	0,287	0,87
IPP connected at 20%	6MW	0.975	Kingbird	B	0.032233	0.032988	0,755	2,28
IPP connected at 30%	8MW	0.975	Kingbird	B	0.030885	0.031691	0,806	2,54
IPP connected at 40%	10MW	0.975	Kingbird	B	0.029213	0.029633	0,42	1,41
IPP connected at 50%	12MW	0.975	Kingbird	B	0.027292	0.0269675	0,3245	1,20
IPP connected at 60%	12MW	0.975	Kingbird	B	0.025365	0.025577	0,212	0,82
IPP connected at 70%	12MW	0.975	Kingbird	B	0.023318	0.023152	0,166	0,71
IPP connected at 80%	12MW	0.975	Kingbird	B	0.021329	0.021109	0,22	1,04
IPP connected at 90%	12MW	0.975	Kingbird	B	0.019293	0.0186776	0,6154	3,29

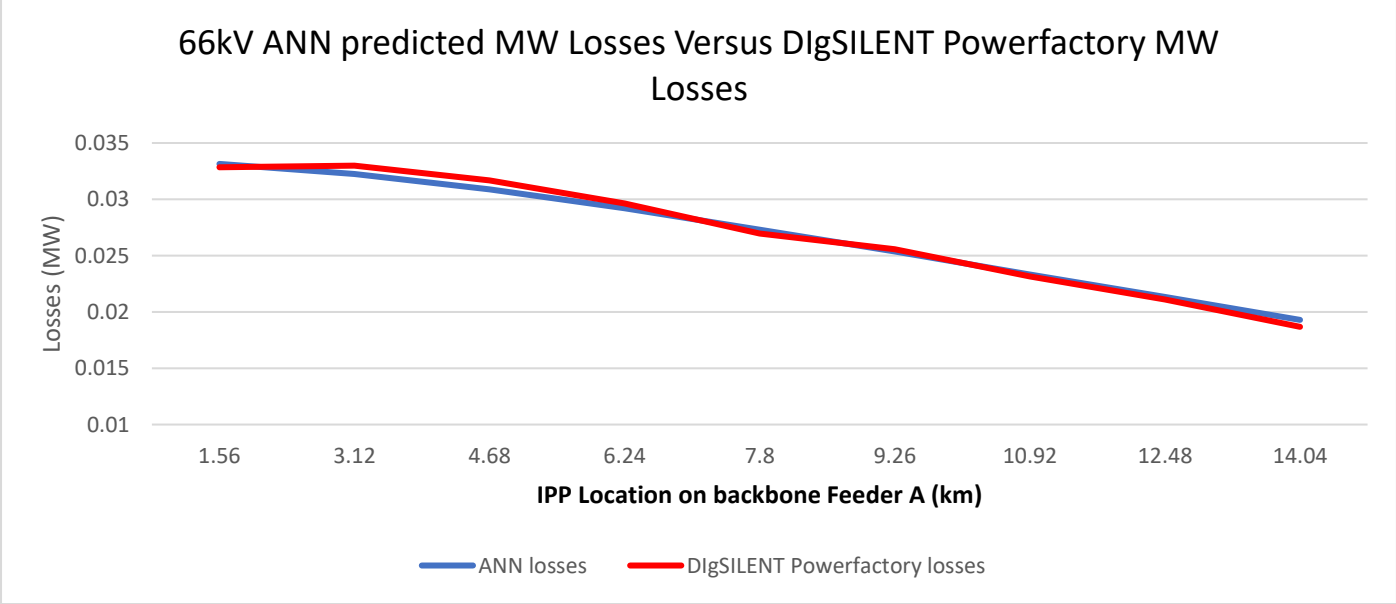

Figure 4-16:Case 3 (66kV) - Loss comparison between the ANN and DIgSILENT Powerfactory

4.6 Case 4: 132kV ANN - Results

IPP is connected to the 35km backbone at the following locations measured from busbar 2 (the sending end) indicated in Figure 4-2 above (modified IEEE 14-bus test network) and simulated in DIgSILENT Powerfactory. Testing IPP locations measured from sending end are as follows: 10% (3.5km), 20% (7km), 30% (10.5km) ,40% (14km), 50% (17.5km), 60% (21km),70% (24.5km), 80% (28km) and 90% (31.5km). A loss comparison between the ANN and DIgSILENT Powerfactory are shown in Figure 4 – 17 to Figure 4-19 listing the results for the 10%, 50% and 90% cases. The full set of results is shown in Table 4-8 for all locations.

ANN Algorithm Output Results:

```
**********************   ANN prediction    **********************
Enter the following network parameters:
Backbone Voltage Level (kV): 132
Backbone length(km): 35
Length of interconnecting feeder (km): 29
Backbone maximum loading(MW): 91
Enter IPP distance as a percentage of total backbone length from sending end substation to POC(%): 10
Enter load power factor:0.95
*****************************************************
*****************************************************
The most optimal parameters are displayed below:
Best Location:31.5km
Best Size:67.5MW
Applicable South African Grid Code Category:
C
Losses:0.55621MW
Conductor    Type
 Zebra (ACSR, diameter: 23.90mm, DC Resistance: 0.0445, Current rating: 710A)
Power Factor:0.95
*****************************************************
*****************************************************
The most optimal parameters based on IPP distance from sending end:
IPP Location:3.5km
Best Size:22MW
Applicable South African Grid Code Category:
B
Losses:1.4709MW
 Zebra (ACSR, diameter: 23.90mm, DC Resistance: 0.0445, Current rating: 710A)
Power Factor:0.95
```

Overall best location and IPP size.

Best size based on the proposed 10% location

ANN predicted Losses = 1.4709MW

DIgSILENT Powerfactory Simulation Results:

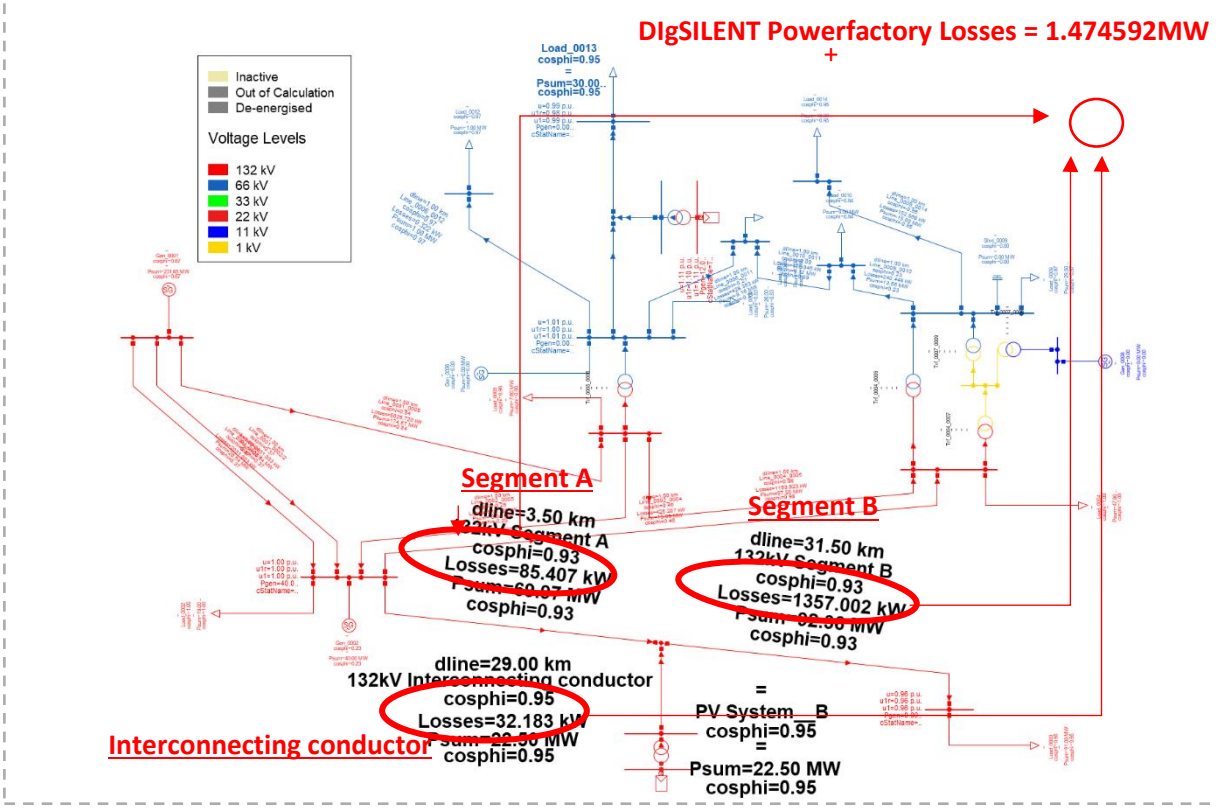

Figure 4-17: Results for Case 4 (132kV) for IPP at 10% from sending end (3.5km from busbar 2 in Figure 4-2)

ANN Algorithm Output Results:

```
********************   ANN prediction    ********************
Enter the following network parameters:
Backbone Voltage Level (kV): 132
Backbone length(km): 35
Length of interconnecting feeder (km): 29
Backbone maximum loading(MW): 91
Enter IPP distance as a percentage of total backbone length from sending end substation to POC(%): 50
Enter load power factor:0.95
**************************************************
**************************************************
The most optimal parameters are displayed below:
Best Location:31.5km
Best Size:67.5MW
Applicable South African Grid Code Category:
C
Losses:0.55621MW
Conductor    Type
 Zebra (ACSR, diameter: 23.90mm, DC Resistance: 0.0445, Current rating: 710A)
Power Factor:0.95
**************************************************
**************************************************
The most optimal parameters based on IPP distance from sending end:
IPP Location:17.5km
Best Size:53MW
Applicable South African Grid Code Category:
B
Losses:1.0733MW
Conductor    Type
 Zebra (ACSR, diameter: 23.90mm, DC Resistance: 0.0445, Current rating: 710A)
Power Factor:0.95
```

Set 1: Overall best location and IPP size.

Set 2: Based on the proposed 50%

ANN predicted Losses = 1.0733MW

DIgSILENT Powerfactory Simulation Results:

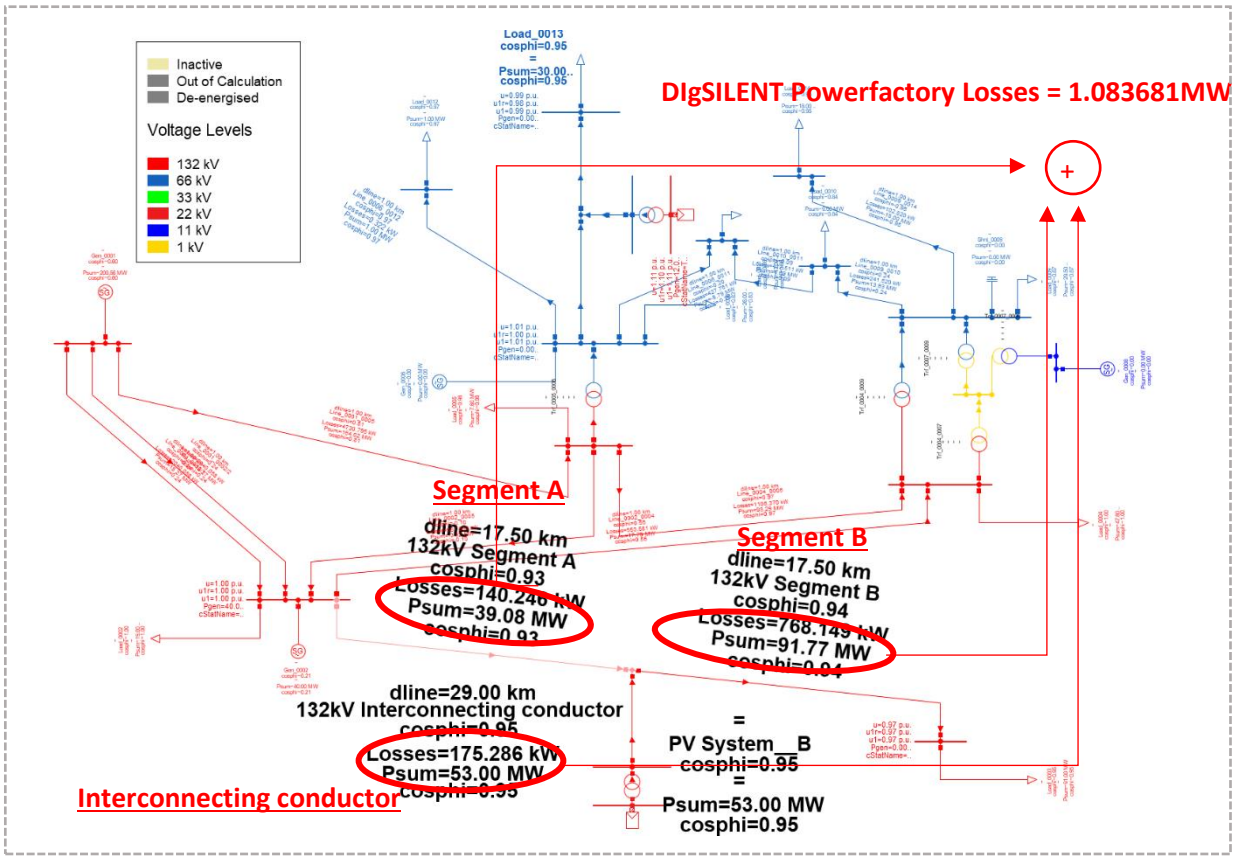

Figure 4-18: Results for Case 4 (132kV) for IPP at 50% from sending end (17.5km from busbar 2 in Figure 4-2)

ANN Algorithm Output Results:

```
**********   ANN prediction    **********
Enter the following network parameters:
Backbone Voltage Level (kV): 132
Backbone length(km): 35
Length of interconnecting feeder (km): 29
Backbone maximum loading(MW): 91
Enter IPP distance as a percentage of total backbone length from sending end substation to POC(%): 90
Enter load power factor:0.95
**************************************************
**************************************************
The most optimal parameters are displayed below:
Best Location:31.5km
Best Size:67.5MW
Applicable South African Grid Code Category:
C
Losses:0.55621MW
Conductor   Type
 Zebra (ACSR, diameter: 23.90mm, DC Resistance: 0.0445, Current rating: 710A)
Power Factor:0.95
**************************************************
**************************************************
The most optimal parameters based on IPP distance from sending end:
IPP Location:31.5km
Best Size:68MW
Applicable South African Grid Code Category:
B
Losses:0.55621MW
Conductor   Type
 Zebra (ACSR, diameter: 23.90mm, DC Resistance: 0.0445, Current rating: 710A)
Power Factor:0.95
```

ANN predicted Losses = 0.55621MW

Set 1: Overall best location and IPP size.

Set 2: Based on the proposed 90%

DIgSILENT Powerfactory Simulation Results:

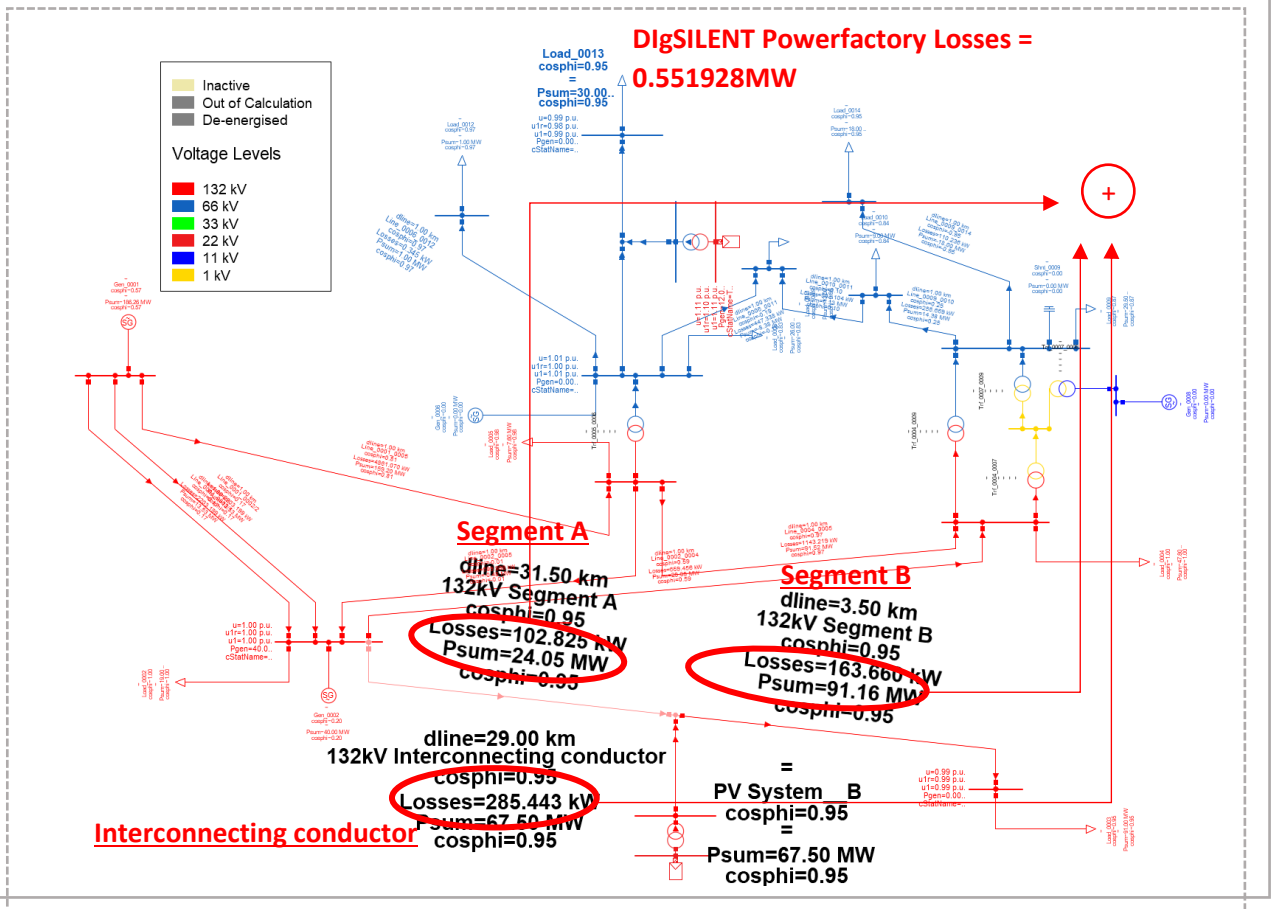

Figure 4-19: Results for Case 4 (132kV) for IPP at 90% from sending end (28km from busbar 2 in Figure 4-2)

The same parameters are used as inputs to the modified IEEE 14-bus system, and the actual losses generated from the IEEE 14- bus system in DIgSILENT Powerfactory are compared to the ANN predicted losses for the same operating parameters of 91MW at the load receiving end, Feeder A length of 35km, and receiving end power factor 0.95 lagging. Figure 4 – 17 through Figure 4 - 19 show ANN results for cases where the IPP (connected to node X) moves from the sending end (Length of Segment A is 10% of the total line length, Length of Segment B is 90% of total line length) to the centre of backbone feeder A (Length of Segment A is 50% of total line length, Length of Segment B is 50% of the total line length) and lastly to receiving end (Length of Segment A is 90% of the total line length, Length of Segment B is 10% of total line length) on backbone Feeder A. Table 4-8 summarises the results when the IPP is located from 10% to 90% of the total feeder length A, in 10% increments. Figure 4-20 shows the error between the ANN prediction and DIgSILENT Powerfactory simulations. The graph indicates the difference in total line losses between the ANN algorithm predictions and DIgSILENT Powerfactory. Ideally, both graphs would be precisely one on top of another which indicates a perfect ANN loss prediction. As seen there are differences in values since they are not exactly overlapped with a worst-case difference in error of 2.834% which translates to an error of 19.11kW.

Table 4-8:Case 4 (132kV) – Comparison of ANN Loss Results with DIgSILENT Powerfactory Loss Results

Case 4 (132kV) MW Loss comparison								
IPP Location (%) from Sending End	**IPP Size**	**IPP power factor**	**Conductor**	**SAGC Category**	**ANN Losses (MW)**	**DIgSILENT Powerfactory Losses (MW)**	**Error (kW)**	**Error (%)**
Best overall location (90%)	68MW	0.95	Zebra	C	0.55621	0.55193	4,280	0,775
IPP connected at 10%	22MW	0.95	Zebra	C	1.4709	1.47459	3,690	0,250
IPP connected at 20%	30MW	0.95	Zebra	C	1.4007	1.42738	26,680	1,869
IPP connected at 30%	37.5MW	0.95	Zebra	C	1.3054	1.31194	6,540	0,498
IPP connected at 40%	37.5MW	0.95	Zebra	C	1.20901	1.23007	21,060	1,712
IPP connected at 50%	53MW	0.95	Zebra	C	1.07330	1.08368	10,380	0,958
IPP connected at 60%	60MW	0.95	Zebra	C	0.95012	0.94866	1,460	0,154
IPP connected at 70%	68MW	0.95	Zebra	C	0.82199	0.82914	7,150	0,862
IPP connected at 80%	68MW	0.95	Zebra	C	0.69344	0.67433	19,110	2,834
IPP connected at 90%	68MW	0.95	Zebra	C	0.55621	0.55193	4,280	0,775

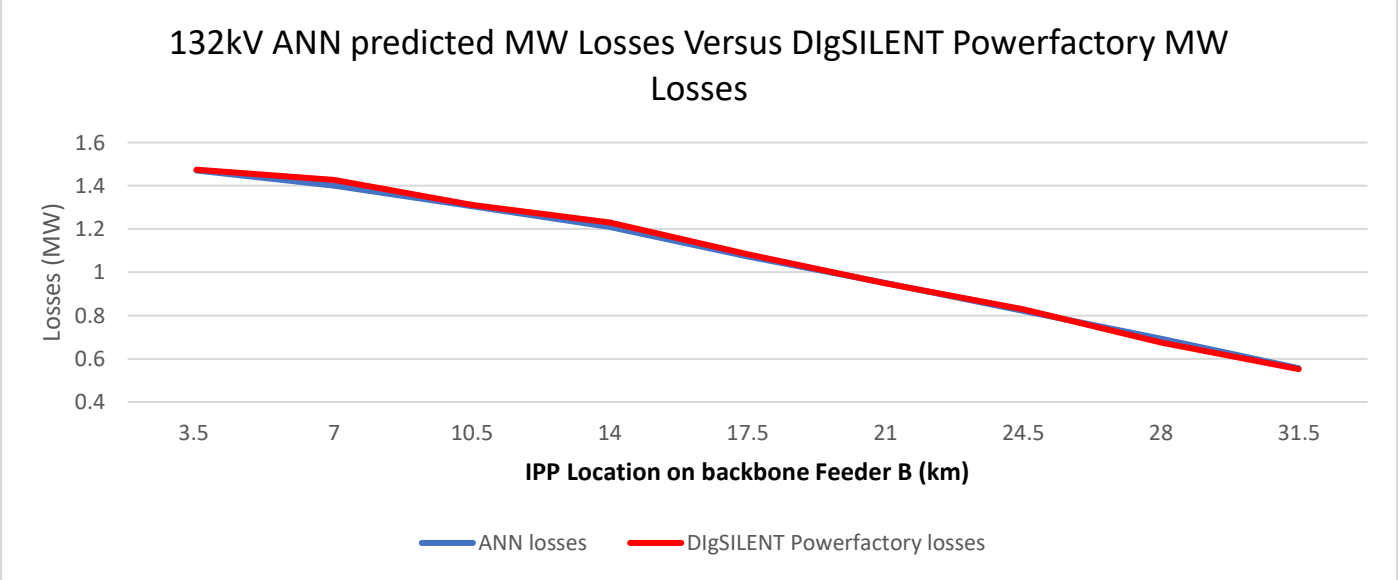

Figure 4-20:Case 4 (132kV) - Loss comparison between the ANN and DIgSILENT Powerfactory

4.7 Case 5: 220kV ANN - Results

IPP is connected to the 134km backbone at the following locations measured from busbar 2 (the sending end) indicated in Figure 4-2 above (modified IEEE 14-bus test network) and simulated in DIgSILENT Powerfactory. Testing IPP locations measured from sending end are as follows: 10% (10.34km), 20% (26.8km), 30% (40.2km) ,40% (53.6km), 50% (67km), 60% (80.4km), 70% (93.8km), 80% (107.2km) and 90% (120.6km). Loss comparisons between the ANN and DIgSILENT Powerfactory are shown in Figure 4–21 to Figure 4-23 listing the results for the 10%, 50% and 90% cases. The full set of results is shown in Table 4-9 for all locations.

ANN Algorithm Output Results:

```
**********************   ANN prediction    **********************
Enter the following network parameters:
Backbone Voltage Level (kV): 220
Backbone length(km): 134
Length of interconnecting feeder (km): 66
Backbone maximum loading(MW): 201
Enter IPP distance as a percentage of total backbone length from sending end substation to POC(%): 10
Enter load power factor:0.95
**************************************************
**************************************************
The most optimal parameters are displayed below:
Best Location:120.6km
Best Size:110MW
Applicable South African Grid Code Category:
C
Losses:3.715MW
Conductor    Type
 Zebra (ACSR, diameter: 23.90mm, DC Resistance: 0.0445, Current rating: 710A)
Power Factor:0.95
**************************************************
**************************************************
The most optimal parameters based on IPP distance from sending end:
IPP Location:13.4km
Best Size:40MW
Applicable South African Grid Code Category:
C
Losses:9.0542MW
Conductor    Type
 Zebra (ACSR, diameter: 23.90mm, DC Resistance: 0.0445, Current rating: 710A)
Power Factor:0.95
```

Overall best location and IPP size.

Best size based on the proposed 10% location

ANN predicted Losses = 9.0542MW

DIgSILENT Powerfactory Simulation Results:

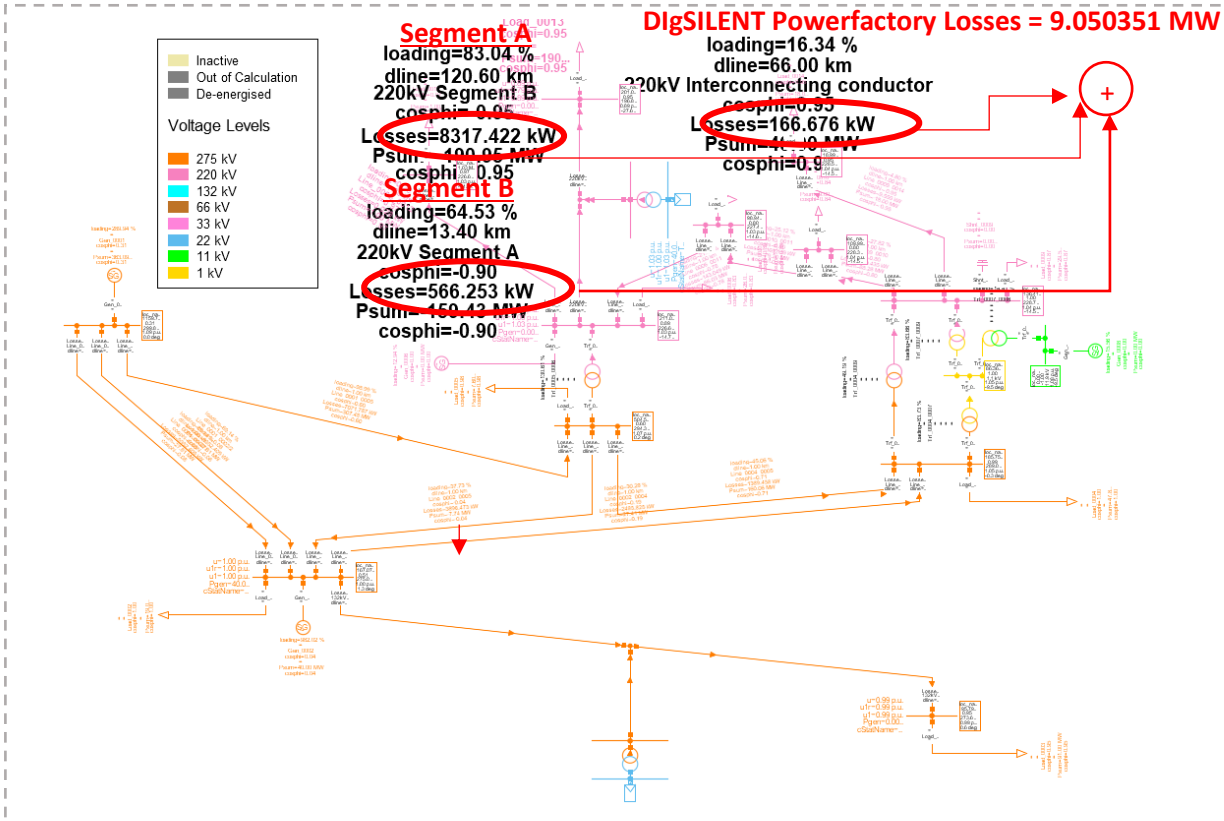

Figure 4-21: Results for Case 5 (220kV) for IPP at 10% from sending end (13.4km from busbar 2 in Figure 4-2)

ANN Algorithm Output Results:

```
**********************    ANN prediction    **********************
Enter the following network parameters:
Backbone Voltage Level (kV): 220
Backbone length(km): 134
Length of interconnecting feeder (km): 66
Backbone maximum loading(MW): 201
Enter IPP distance as a percentage of total backbone length from sending end substation to POC(%): 50
Enter load power factor:0.95
*****************************************************
*****************************************************
The most optimal parameters are displayed below:
Best Location:120.6km
Best Size:110MW
Applicable South African Grid Code Category:
C
Losses:3.715MW
Conductor    Type
 Zebra (ACSR, diameter: 23.90mm, DC Resistance: 0.0445, Current rating: 710A)
Power Factor:0.95
*****************************************************
*****************************************************
The most optimal parameters based on IPP distance from sending end:
IPP Location:67km
Best Size:110MW
Applicable South African Grid Code Category:
C
Losses:6.3936MW
Conductor    Type
 Zebra (ACSR, diameter: 23.90mm, DC Resistance: 0.0445, Current rating: 710A)
Power Factor:0.95
```

Set 1: Overall best location and IPP size.

Set 2: Based on the proposed 50%

ANN predicted Losses = 6.3936MW

DIgSILENT Powerfactory Simulation Results:

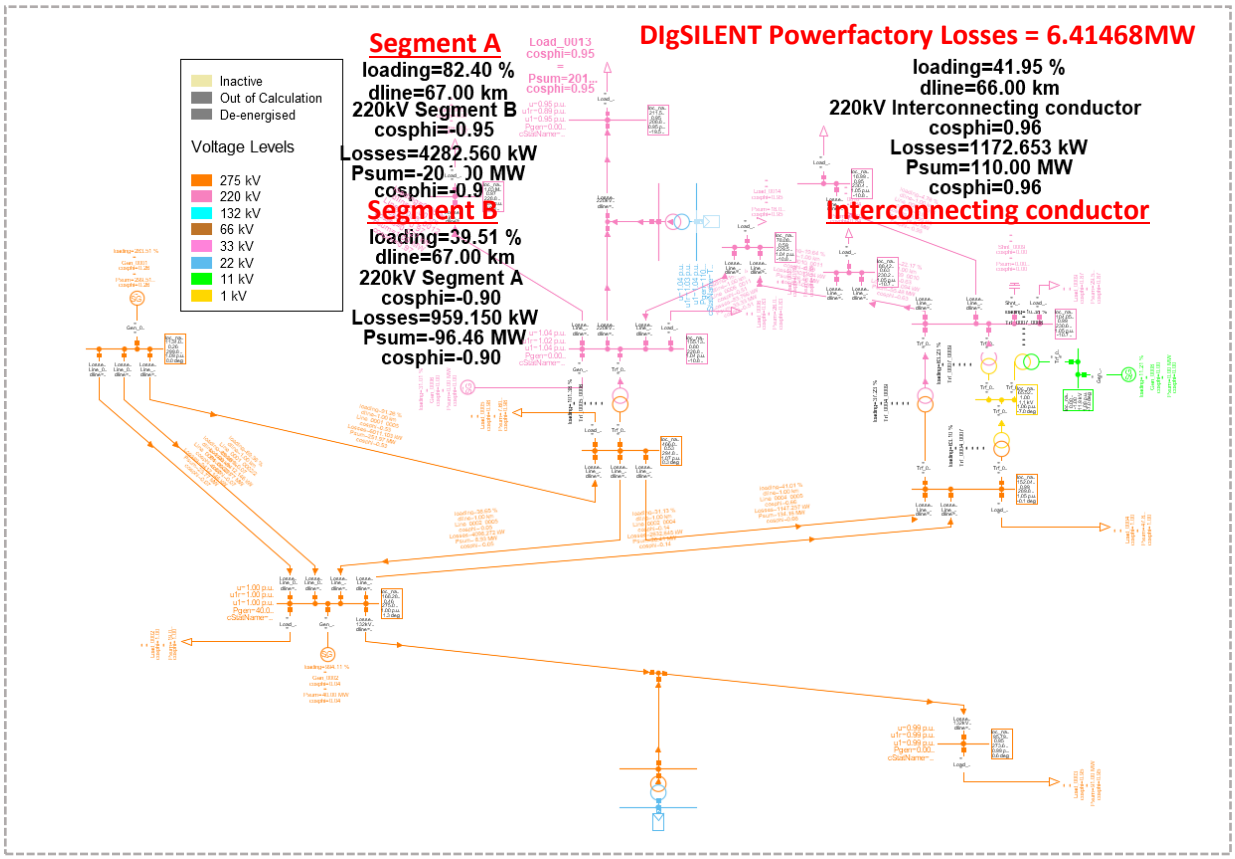

Figure 4-22: Results for Case 5 (220kV) for IPP at 50% from sending end (67km from busbar 2 in Figure 4-2)

ANN Algorithm Output Results:

```
**********************   ANN prediction    **********************
Enter the following network parameters:
Backbone Voltage Level (kV): 220
Backbone length(km): 134
Length of interconnecting feeder (km): 66
Backbone maximum loading(MW): 201
Enter IPP distance as a percentage of total backbone length from sending end substation to POC(%): 90
Enter load power factor:0.95
*****************************************************
*****************************************************
The most optimal parameters are displayed below:
Best Location:120.6km
Best Size:110MW
Applicable South African Grid Code Category:
C
Losses:3.715MW
Conductor    Type
 Zebra (ACSR, diameter: 23.90mm, DC Resistance: 0.0445, Current rating: 710A)
Power Factor:0.95
*****************************************************
*****************************************************
The most optimal parameters based on IPP distance from sending end:
IPP Location:120.6km
Best Size:110MW
Applicable South African Grid Code Category:
C
Losses:3.715MW
Conductor    Type
 Zebra (ACSR, diameter: 23.90mm, DC Resistance: 0.0445, Current rating: 710A)
Power Factor:0.95
```

Set 1: Overall best location and IPP size.

Set 2: Based on the proposed 90%

ANN predicted Losses = 3.715MW

DIgSILENT Powerfactory Simulation Results:

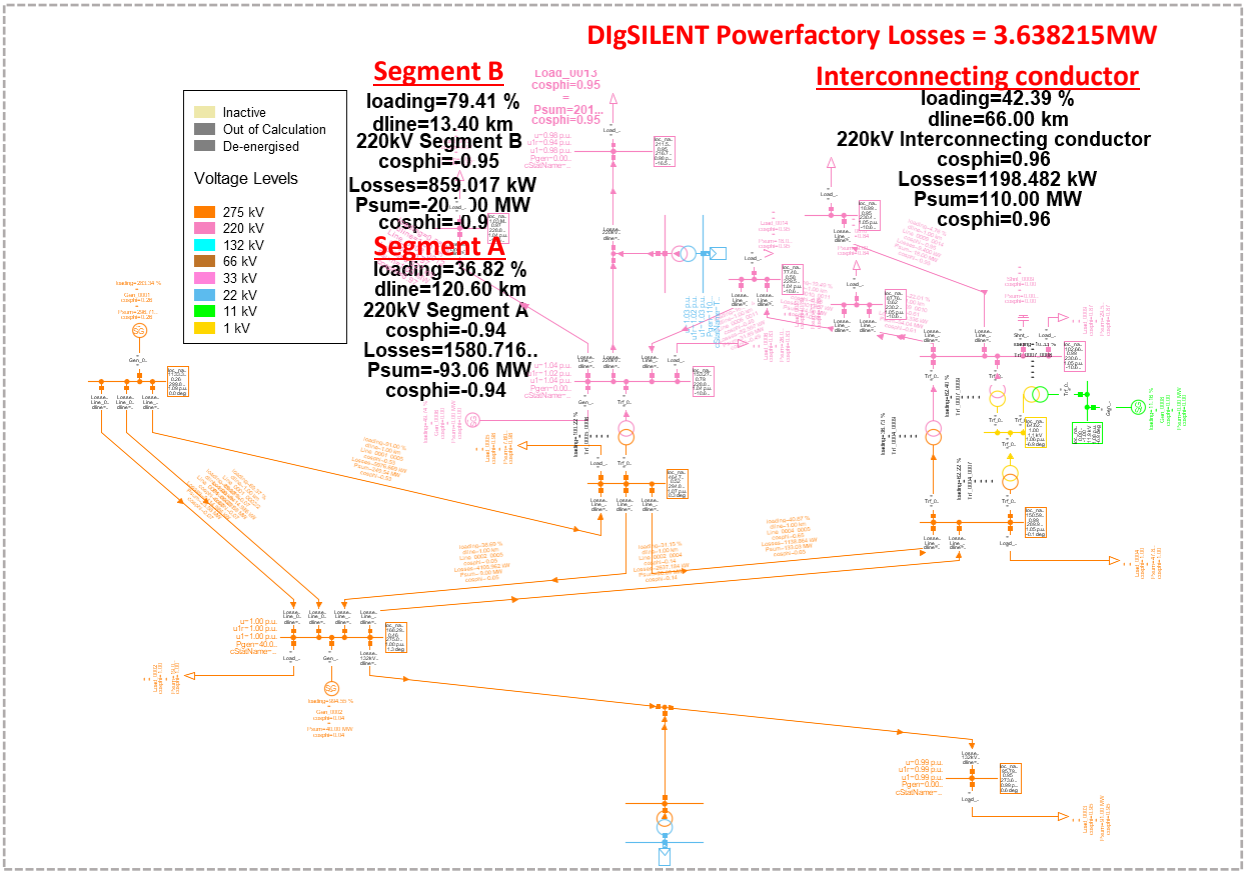

Figure 4-23: Results for Case 5 (220kV) for IPP at 90% from sending end (120.6km from busbar 2 in Figure 4-2)

The same parameters are used as inputs to the modified IEEE 14-bus system, and the actual losses generated from the IEEE 14- bus system in DIgSILENT Powerfactory are compared to the ANN predicted losses for the same operating parameters of 201MW at the load receiving end, Feeder A length of 134km, and receiving end power factor 0.95 lagging. Figure 4 – 21 through Figure 4 - 23 show ANN results for cases where the IPP (connected to node X) moves from the sending end (Length of Segment A is 10% of the total line length, Length of Segment B is 90% of total line length) to the centre of backbone feeder A (Length of Segment A is 50% of total line length, Length of Segment B is 50% of the total line length) and lastly to receiving end (Length of Segment A is 90% of the total line length, Length of Segment B is 10% of total line length) on Feeder A. Table 4-9 summarises the results when the IPP is located from 10% to 90% of the total feeder length A, in 10% increments. Figure 4-24 shows the error between the ANN prediction and DIgSILENT Powerfactory simulations. The graph indicates the difference in total line losses between the ANN algorithm predictions and DIgSILENT Powerfactory. Ideally, both graphs would be precisely one on top of another which indicates a perfect ANN loss prediction. As seen there are differences in values since they are not exactly overlapped with a worst-case difference in error of 3.186% which translates to an error of 138.08kW.

Table 4-9: Case 5 (220kV) – Comparison of ANN Loss Results with DIgSILENT Powerfactory Loss Results

Case 5 (220kV) MW Loss comparison								
IPP Location (%) from Sending End	**IPP Size**	**IPP power factor**	**Conductor**	**SAGC Category**	**ANN Losses (MW)**	**DIgSILENT Powerfactory Losses (MW)**	**Error (kW)**	**Error (%)**
Best overall location (90%)	110MW	0.95	Zebra	C	3.7150	3.68215	32,850	0,892
IPP connected at 10%	22MW	0.95	Zebra	C	9.0542	9.050315	3,885	0,043
IPP connected at 20%	70MW	0.95	Zebra	C	8.5718	8.613354	41,554	0,482
IPP connected at 30%	90MW	0.95	Zebra	C	7.9226	8.009655	87,055	1,087
IPP connected at 40%	100MW	0.95	Zebra	C	7.1924	7.352441	160,041	2,177
IPP connected at 50%	110MW	0.95	Zebra	C	6.39360	6.41468	21,080	0,329
IPP connected at 60%	110MW	0.95	Zebra	C	5.63195	5.59124	40,710	0,728
IPP connected at 70%	110MW	0.95	Zebra	C	5.04001	4.98551	54,500	1,093
IPP connected at 80%	110MW	0.95	Zebra	C	4.1965	4.33458	138,080	3,186
IPP connected at 90%	110MW	0.95	Zebra	C	3.7150	3.68215	32,850	0,892

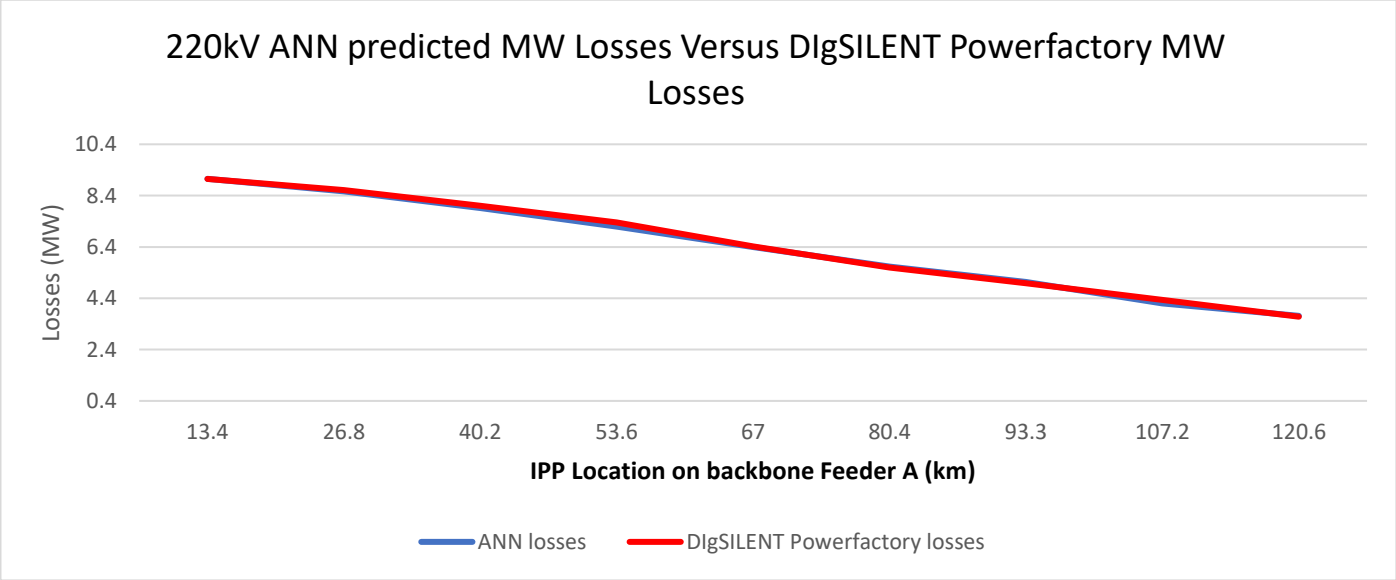

Figure 4-24: Case 5 (220kV) - Loss comparison between the ANN and DIgSILENT Powerfactory

4.8 Case 6: 275kV ANN - Results

IPP is connected to the 196km backbone at the following locations measured from busbar 2 (the sending end) indicated in Figure 4-2 above (modified IEEE 14-bus test network) and simulated in DIgSILENT Powerfactory. Testing IPP locations measured from sending end are as follows: 10% (19.6km), 20% (39.2km), 30% (58.8km) ,40% (78.4km), 50% (98km), 60% (117.6km),70% (137.2km), 80% (156.8km) and 90% (176.4km). Loss comparisons between the ANN and DIgSILENT Powerfactory are shown in Figure 4–25 to Figure 4-27, listing the results for the 10%, 50% and 90% cases. The full set of results is shown in Table 4-10 for all locations.

ANN Algorithm Output Results:

```
********************   ANN prediction    ********************
Enter the following network parameters:
Backbone Voltage Level (kV): 275
Backbone length(km): 196
Length of interconnecting feeder (km): 80
Backbone maximum loading(MW): 201
Enter IPP distance as a percentage of total backbone length from sending end substation to POC(%): 10
Enter load power factor:0.96
**************************************************
**************************************************
The most optimal parameters are displayed below:
Best Location:176.4km
Best Size:110MW
Applicable South African Grid Code Category:
C
Losses:1.818MW
Conductor   Type
 Zebra (ACSR, diameter: 23.90mm, DC Resistance: 0.0445, Current rating: 710A)
Power Factor:0.95
**************************************************
**************************************************
The most optimal parameters based on IPP distance from sending end:
IPP Location:19.6km
Best Size:40MW
Applicable South African Grid Code Category:
C
Losses:4.9191MW
Conductor   Type
 Zebra (ACSR, diameter: 23.90mm, DC Resistance: 0.0445, Current rating: 710A)
Power Factor:0.95
```

Overall best location and IPP size.

Best size based on the proposed 10% location

ANN predicted Losses = 4.9191MW

DIgSILENT Powerfactory Simulation Results:

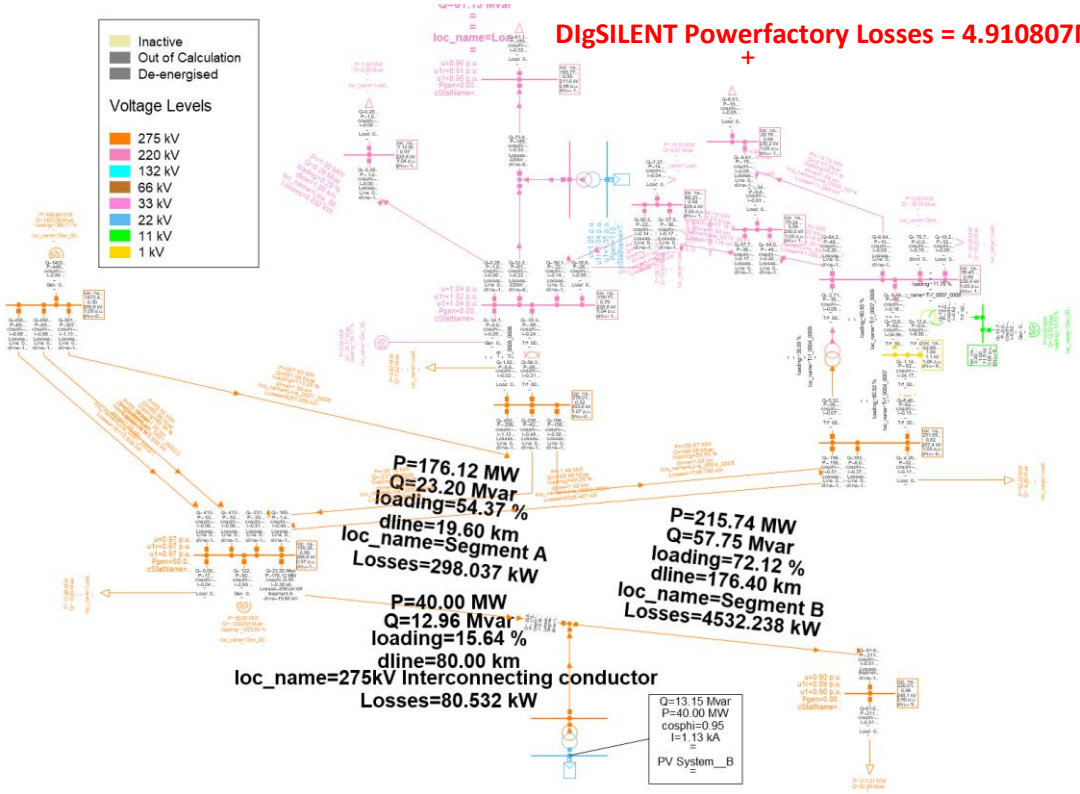

Figure 4-25: Results for Case 6 (275kV) for IPP at 10% from sending end (19.6km from busbar 2 in Figure 4-2)

ANN Algorithm Output Results:

```
**********   ANN prediction    **********
Enter the following network parameters:
Backbone Voltage Level (kV): 275
Backbone length(km): 196
Length of interconnecting feeder (km): 80
Backbone maximum loading(MW): 201
Enter IPP distance as a percentage of total backbone length from sending end substation to POC(%): 50
Enter load power factor:0.96
**************************************************
**************************************************
The most optimal parameters are displayed below:
Best Location:176.4km
Best Size:110MW
Applicable South African Grid Code Category:
C
Losses:1.818MW
Conductor   Type
 Zebra (ACSR, diameter: 23.90mm, DC Resistance: 0.0445, Current rating: 710A)
Power Factor:0.95
**************************************************
**************************************************
The most optimal parameters based on IPP distance from sending end:
IPP Location:98km
Best Size:110MW
Applicable South African Grid Code Category:
C
Losses:3.4619MW
Conductor   Type
 Zebra (ACSR, diameter: 23.90mm, DC Resistance: 0.0445, Current rating: 710A)
Power Factor:0.95
```

Set 1: Overall best location and IPP size.

Set 2: Based on the proposed 50%

ANN predicted Losses = 3.461MW

DIgSILENT Powerfactory Simulation Results:

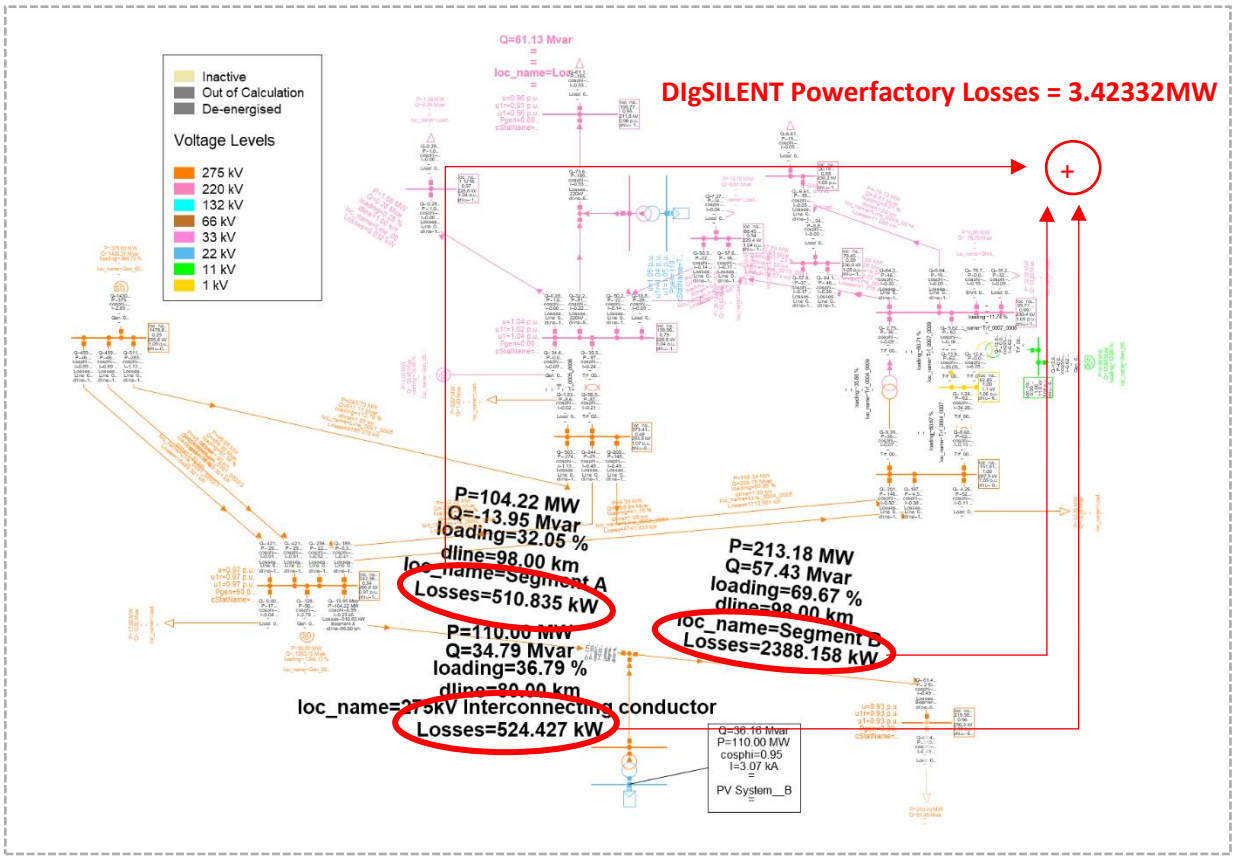

Figure 4-26: Results for Case 6 (275kV) for IPP at 50% from sending end (98km from busbar 2 in Figure 4-2)

ANN Algorithm Output Results:

```
********************   ANN prediction    ********************
Enter the following network parameters:
Backbone Voltage Level (kV): 275
Backbone length(km): 196
Length of interconnecting feeder (km): 80
Backbone maximum loading(MW): 201
Enter IPP distance as a percentage of total backbone length from sending end substation to POC(%): 90
Enter load power factor:0.96
**************************************************
**************************************************
The most optimal parameters are displayed below:
Best Location:176.4km
Best Size:110MW
Applicable South African Grid Code Category:
C
Losses:1.818MW
Conductor   Type
 Zebra (ACSR, diameter: 23.90mm, DC Resistance: 0.0445, Current rating: 710A)
Power Factor:0.95
**************************************************
**************************************************
The most optimal parameters based on IPP distance from sending end:
IPP Location:176.4km
Best Size:110MW
Applicable South African Grid Code Category:
C
Losses:1.818MW
Conductor   Type
 Zebra (ACSR, diameter: 23.90mm, DC Resistance: 0.0445, Current rating: 710A)
Power Factor:0.95
```

ANN predicted Losses = 1.818MW

Set 1: Overall best location and IPP size.

Set 2: Based on the proposed 90%

DIgSILENT Powerfactory Simulation Results:

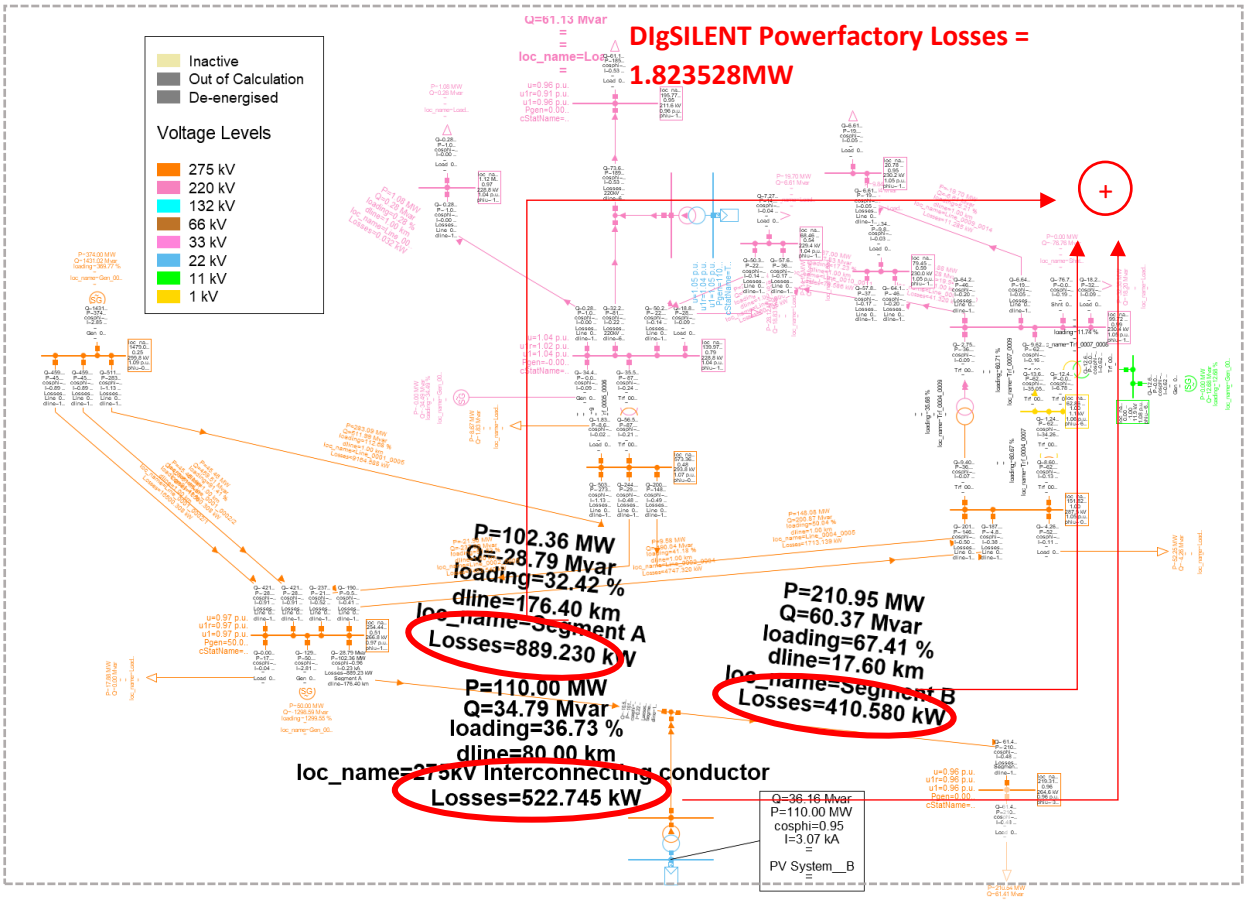

Figure 4-27: Results for Case 6 (275kV) for IPP at 90% from sending end (176.4km from busbar 2 in Figure 4-2)

The same parameters are used as inputs to the modified IEEE 14-bus system, and the actual losses generated from the IEEE 14- bus system in DIgSILENT Powerfactory are compared to the ANN predicted losses for the same operating parameters of 201MW at the load receiving end, Feeder A length of 196km, and receiving end power factor 0.96 lagging. Figure 4–25 through Figure 4-27 show ANN results for cases where the IPP (connected to node X) moves from the sending end (Length of Segment A is 10% of the total line length, Length of Segment B is 90% of total line length) to the centre of Feeder A (Length of Segment A is 50% of total line length, Length of Segment B is 50% of the total line length) and lastly to receiving end (Length of Segment A is 90% of the total line length, Length of Segment B is 10% of total line length) on Backbone Feeder B. Table 4-10 summarises the results when the IPP is located from 10% to 90% of the total feeder length A, in 10% increments. Figure 4-28 shows the error between the ANN prediction and DIgSILENT Powerfactory simulations. The graph indicates the difference in total line losses between the ANN algorithm predictions and DIgSILENT Powerfactory. Ideally, both graphs would be precisely one on top of another which indicates a perfect ANN loss prediction. As seen there are differences in values since they are not exactly overlapped with a worst-case difference in error of 1.4% which translates to an error of 31.3kW.

Table 4-10: Case 6 (275kV) – Comparison of ANN Loss Results with DIgSILENT Powerfactory Loss Results

Case 6 (275kV) MW Loss comparison								
IPP Location (%) from Sending End	**IPP Size**	**IPP power factor**	**Conductor**	**SAGC Category**	**ANN Losses (MW)**	**DIgSILENT Powerfactory Losses (MW)**	**Error (kW)**	**Error (%)**
Best overall location (90%)	110MW	0.95	2xZebra	C	1.8180	1.8235	5.500	0.3
IPP connected at 10%	40MW	0.95	2xZebra	C	4.9191	4.9108	8,300	0,2
IPP connected at 20%	50MW	0.95	2xZebra	C	4.7988	4.7895	9,300	0,2
IPP connected at 30%	60MW	0.95	2xZebra	C	4.5321	4.5297	2,400	0,1
IPP connected at 40%	80MW	0.95	2xZebra	C	3.9113	3.9153	4,000	0,1
IPP connected at 50%	110MW	0.95	2xZebra	C	3.1243	3.1193	5,000	0,2
IPP connected at 60%	100MW	0.95	2xZebra	C	2.7196	2.7421	22,500	0,8
IPP connected at 70%	100MW	0.95	2xZebra	C	2.3604	2.3407	19,700	0,8
IPP connected at 80%	110MW	0.95	2xZebra	C	2.2149	2.2462	31,300	1,4
IPP connected at 90%	110MW	0.95	2xZebra	C	1.8180	1.8235	5,500	0,3

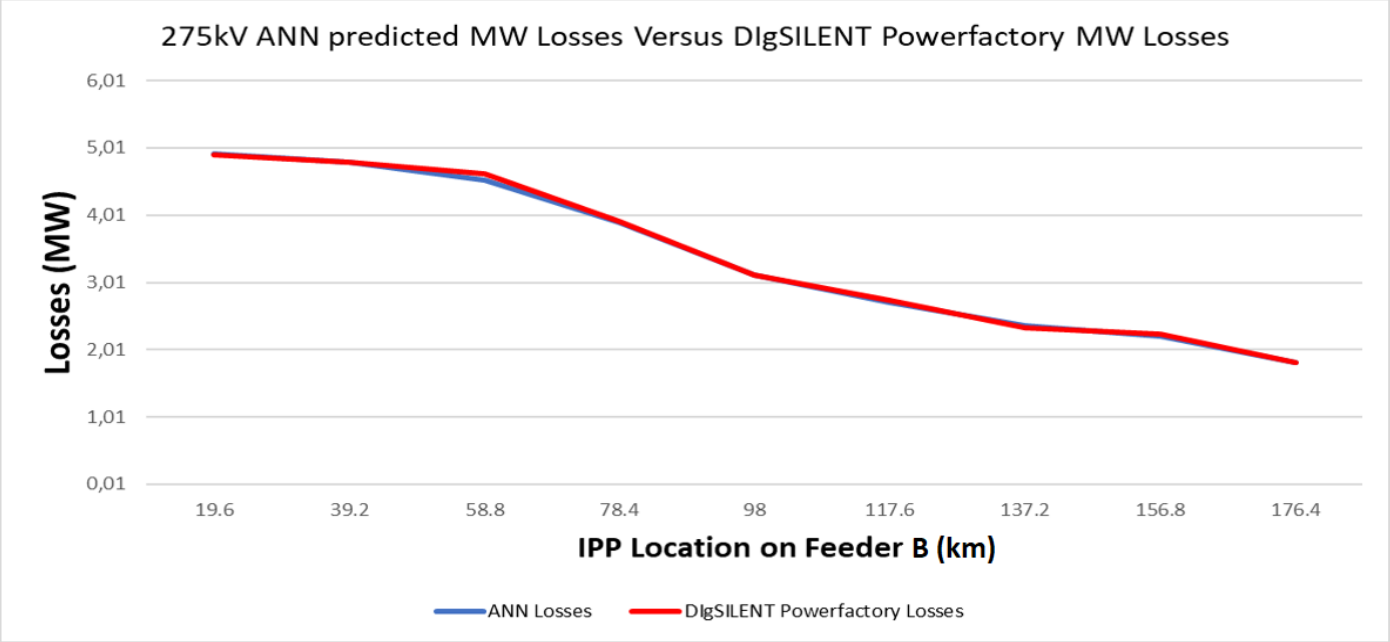

Figure 4-28: Case 6 (275kV) - Loss comparison between the ANN and DIgSILENT Powerfactory

4.9 Case 7: 400kV ANN - Results

IPP is connected to the 138km backbone at the following locations measured from busbar 2 (the sending end) indicated in Figure 4-11 above (modified IEEE 14-bus test network) and simulated in DIgSILENT Powerfactory. Testing IPP locations measured from sending end are as follows: 10% (13.8km), 20% (27.6km), 30% (41.4km) ,40% (55.2km), 50% (69km), 60% (82.8km),70% (96.6km), 80% (110.4km) and 90% (124.2km). Loss comparisons between the ANN and DIgSILENT Powerfactory are shown in Figure 4 – 29 to Figure 4-31 listing the results for the 10%, 50% and 90% cases. The full set of results is shown in Table 4-11 for all locations.

ANN Algorithm Output Results:

```
**********************   ANN prediction    **********************
Enter the following network parameters:
Backbone Voltage Level (kV): 400
Backbone length(km): 138
Length of interconnecting feeder (km): 90
Backbone maximum loading(MW): 150
Enter IPP distance as a percentage of total backbone length from sending end substation to POC(%): 10
Enter load power factor:1
*****************************************************
*****************************************************
The most optimal parameters are displayed below:
Best Location:124.2km
Best Size:90MW
Applicable South African Grid Code Category:
C
Losses:0.17937MW
Conductor   Type
Twin Tern  (ACSR, diameter: 23.90mm, DC Resistance: 0.0445, Current rating: 1172A)
Power Factor:-0.95
*****************************************************
*****************************************************
The most optimal parameters based on IPP distance from sending end:
IPP Location:13.8km
Best Size:30MW
Applicable South African Grid Code Category:
B
Losses:0.37736MW
Conductor   Type
Quad Zebra  (ACSR, diameter: 23.90mm, DC Resistance: 0.0674, Current rating: 2840A)
Power Factor:-0.95
```

ANN predicted Losses = 0.37736MW

Overall best location and IPP size.

Best size based on the proposed 10% location

DIgSILENT Powerfactory Simulation Results:

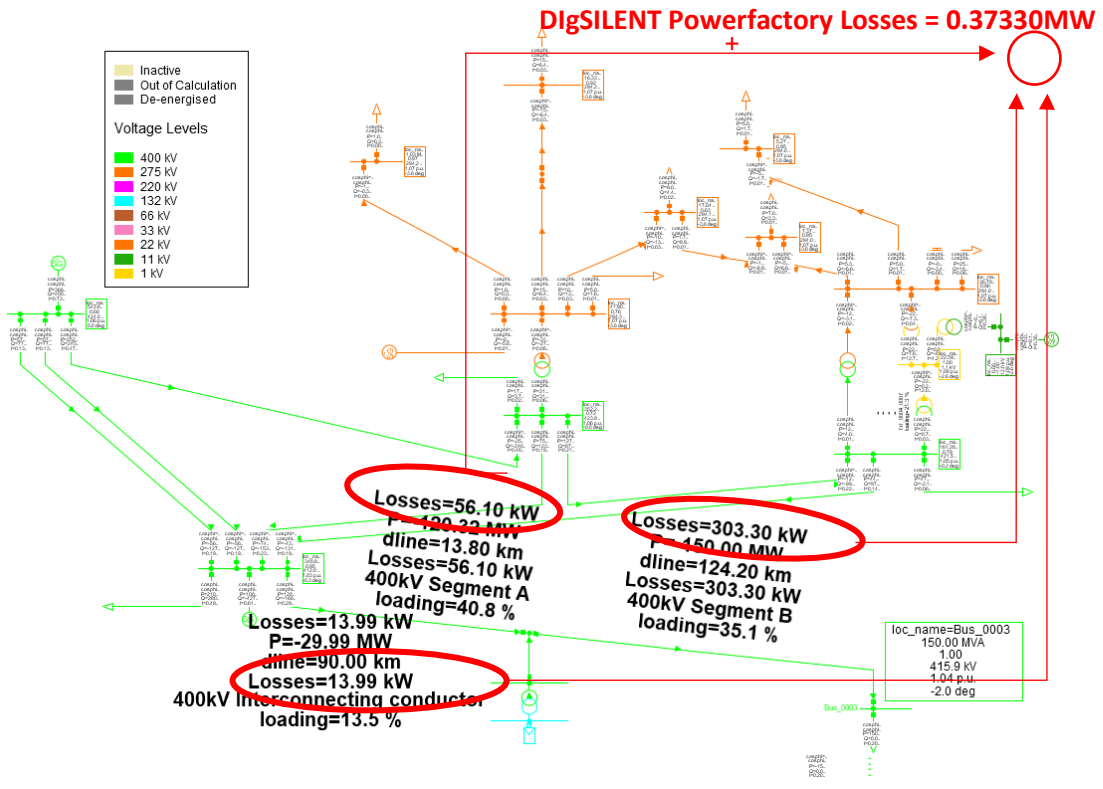

Figure 4-29: Results for Case 7 (400kV) for IPP at 10% from sending end (13.8km from busbar 2 in Figure 4-2)

ANN Algorithm Output Results:

```
********************   ANN prediction    ********************
Enter the following network parameters:
Backbone Voltage Level (kV): 400
Backbone length(km): 138
Length of interconnecting feeder (km): 90
Backbone maximum loading(MW): 150
Enter IPP distance as a percentage of total backbone length from sending end substation to POC(%): 50
Enter load power factor:1
*****************************************************
*****************************************************
The most optimal parameters are displayed below:
Best Location:124.2km
Best Size:90MW
Applicable South African Grid Code Category:
C
Losses:0.17937MW
Conductor    Type
Twin Tern   (ACSR, diameter: 23.90mm, DC Resistance: 0.0445, Current rating: 1172A)
Power Factor:-0.95
*****************************************************
*****************************************************
The most optimal parameters based on IPP distance from sending end:
IPP Location:69km
Best Size:70MW
Applicable South African Grid Code Category:
B
Losses:0.30211MW
Conductor    Type
Quad Zebra   (ACSR, diameter: 23.90mm, DC Resistance: 0.0674, Current rating: 2840A)
Power Factor:-0.95
```

Set 1: Overall best location and IPP size.

Set 2: Based on the proposed 50%

ANN predicted Losses = 0.3021MW

DIgSILENT Powerfactory Simulation Results:

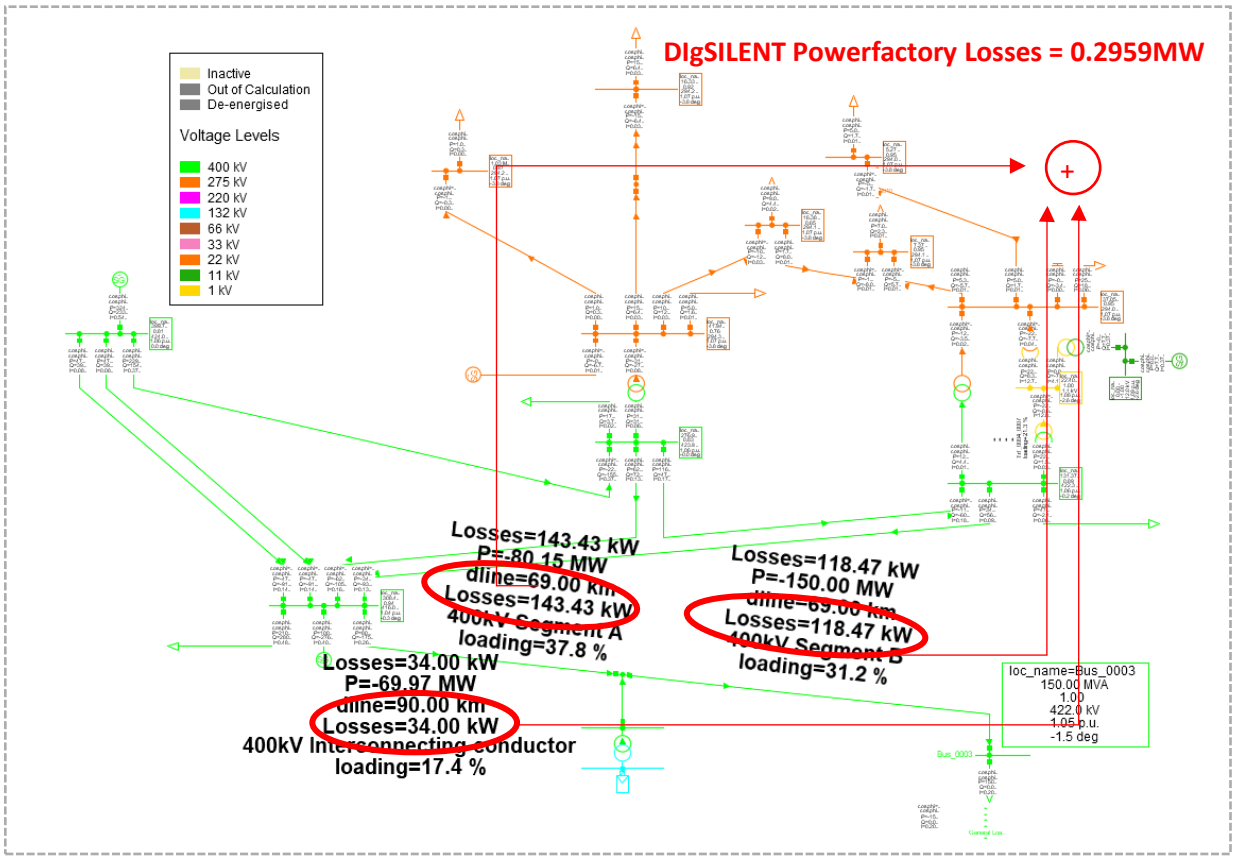

Figure 4-30: Results for Case 7 (400kV) for IPP at 50% from sending end (69km from busbar 2 in Figure 4-2)

ANN Algorithm Output Results:

```
********************   ANN prediction    ********************
Enter the following network parameters:
Backbone Voltage Level (kV): 400
Backbone length(km): 138
Length of interconnecting feeder (km): 90
Backbone maximum loading(MW): 150
Enter IPP distance as a percentage of total backbone length from sending end substation to POC(%): 90
Enter load power factor:1
**************************************************
**************************************************
The most optimal parameters are displayed below:
Best Location:124.2km
Best Size:90MW
Applicable South African Grid Code Category:
C
Losses:0.17937MW
Conductor   Type
Twin Tern  (ACSR, diameter: 23.90mm, DC Resistance: 0.0445, Current rating: 1172A)
Power Factor:-0.95
**************************************************
**************************************************
The most optimal parameters based on IPP distance from sending end:
IPP Location:124.2km
Best Size:90MW
Applicable South African Grid Code Category:
B
Losses:0.17937MW
Conductor   Type
Quad Zebra  (ACSR, diameter: 23.90mm, DC Resistance: 0.0674, Current rating: 2840A)
Power Factor:-0.95
```

Set 1: Overall best location and IPP size.

Set 2: Based on the proposed 90%

ANN predicted Losses = 0.17937MW

DIgSILENT Powerfactory Simulation Results:

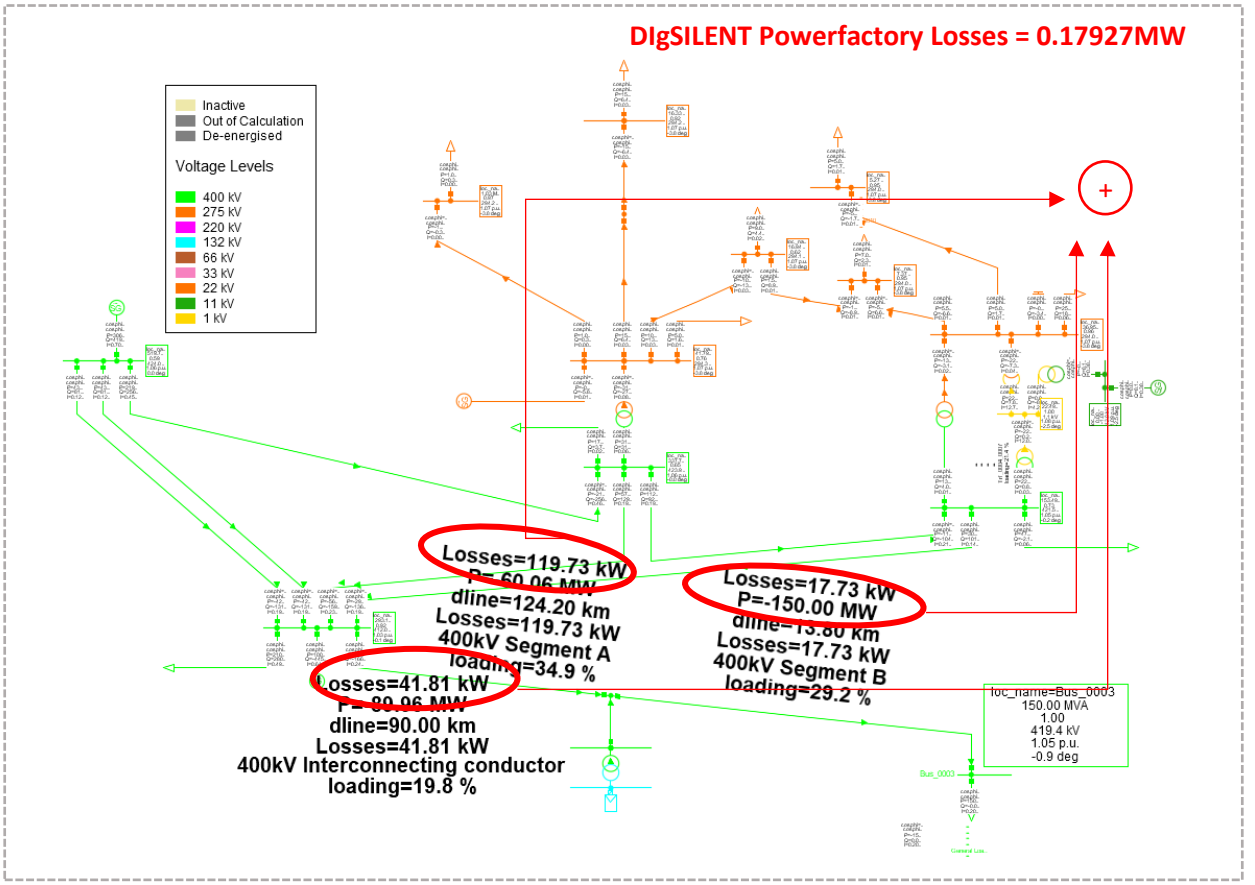

Figure 4-31: Results for Case 7 (400kV) for IPP at 90% from sending end (124.2km from busbar 2 in Figure 4-2)

The same parameters are used as inputs to the modified IEEE 14-bus system, and the actual losses generated from the IEEE 14- bus system in DIgSILENT Powerfactory are compared to the ANN predicted losses for the same operating parameters of 150MW at the load receiving end, Feeder A length of 138km, and receiving end power factor of unity. Figure 4 – 29 through Figure 4 - 31 show ANN results for cases where the IPP (connected to node X) moves from the sending end (Length of Segment A is 10% of the total line length, Length of Segment B is 90% of total line length) to the centre of feeder A (Length of Segment A is 50% of total line length, Length of Segment B is 50% of the total line length) and lastly to receiving end (Length of Segment A is 90% of the total line length, Length of Segment B is 10% of total line length) on backbone Feeder B. Table 4-11 summarises the results when the IPP is located from 10% to 90% of the total feeder length A, in 10% increments. Figure 4-32 shows the error between the ANN prediction and DIgSILENT Powerfactory simulations. The graph indicates the difference in total line losses between the ANN algorithm predictions and DIgSILENT Powerfactory. Ideally, both graphs would be precisely one on top of another which indicates a perfect ANN loss prediction. As seen there are differences in values since they are not exactly overlapped with a worst-case difference in error of 2.098% which translates to an error of 6.21kW.

Table 4-11:Case 7 (400kV) – Comparison of ANN Loss Results with DIgSILENT Powerfactory Loss Results

Case 7 (400kV) MW Loss comparison								
IPP Location (%) from Sending End	**IPP Size**	**IPP power factor**	**Conductor**	**SAGC Category**	**ANN Losses (MW)**	**DIgSILENT Powerfactory Losses (MW)**	**Error (kW)**	**Error (%)**
Best overall location (90%)	90MW	-0.95	4 x Zebra	C	0.17937	0.17927	0.1	0.0557
IPP connected at 10%	30MW	-0.95	4 x Zebra	C	0.37736	0.37330	4,06	1,087
IPP connected at 20%	40MW	-0.95	4 x Zebra	C	0.37698	0.37334	3,64	0,974
IPP connected at 30%	50MW	-0.95	4 x Zebra	C	0.35036	0.35107	0,71	0,202
IPP connected at 40%	60MW	-0.95	4 x Zebra	C	0.32837	0.32706	1,31	0,400
IPP connected at 50%	70MW	-0.95	4 x Zebra	C	0.30211	0.29590	6,21	2,098
IPP connected at 60%	80MW	-0.95	4 x Zebra	C	0.27403	0.26980	4,23	1,567
IPP connected at 70%	80MW	-0.95	4 x Zebra	C	0.24169	0.23890	2,79	1,167
IPP connected at 80%	80MW	-0.95	4 x Zebra	C	0.20758	0.20477	2,81	1,3722
IPP connected at 90%	90MW	-0.95	4 x Zebra	C	0.17937	0.17927	0,1	0,0557

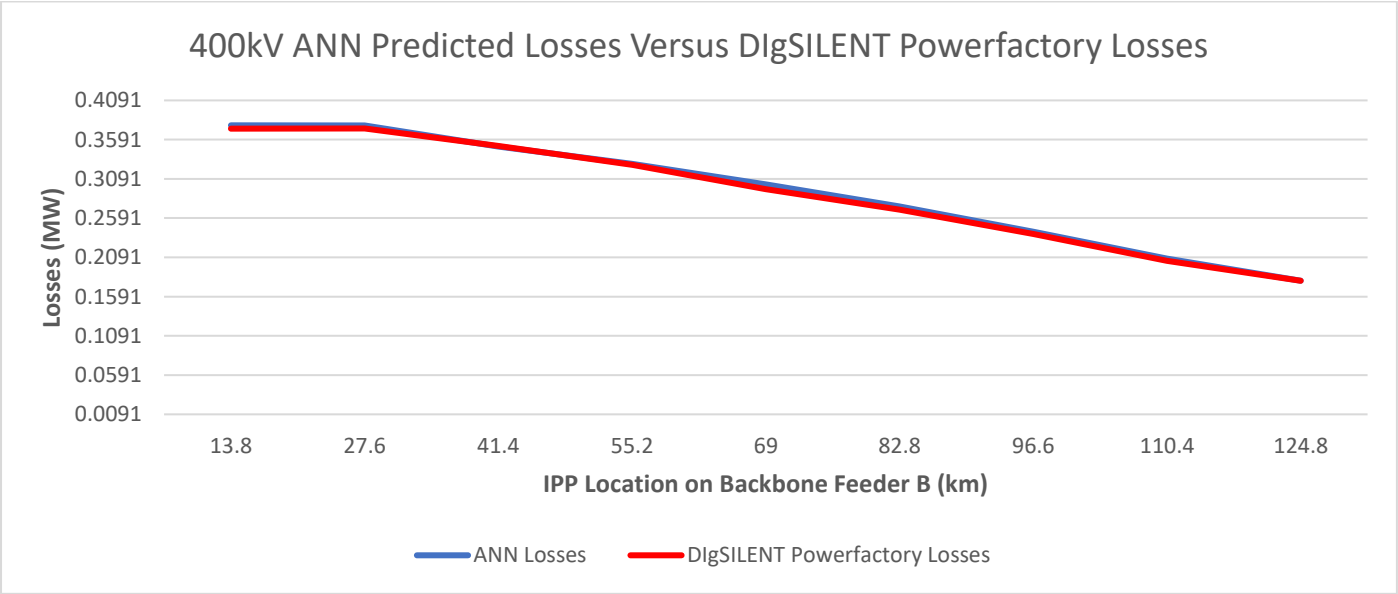

Figure 4-32:Case 7 (400kV) - Loss comparison between the ANN and DIgSILENT Powerfactory

4.10 Factors impacting the accuracy of results

For testing the performance of the ANN model, the original IEEE-13 and IEEE–14 network parameters were set based on existing data obtained from literature. This was done to correctly validate the accuracy and precision of the ANN from a practical and realistic perspective. During the ANN training phase - in order to simplify the input data set, the input data values used were chosen to be discrete in nature. Considering the 132kV ANN input data for example segment A line lengths were varied in 10 km increments. This allowed for a wider range/spread of input scenarios while also enabling the ANN to consider larger backbone feeder lengths. Ideally, training the ANN with all values in between the actual 10km discrete values would make the ANN stronger since it would be trained with a more comprehensive dataset. This, however, would be impractical from a data storage perspective and moreover make data processing more complicated and time-consuming. The discrete organisation of input data was also applied to receiving end load values, interconnecting conductor length values, IPP export power values and load power factor values. In order to capture the line losses for these cases, the sending end voltages were also set between 1.0pu and 1.03pu when simulated in DIgSILENT Powerfactory software. But in reality and as was shown in the IEEE-13 and IEEE-14 cases, sending end voltages were sometimes higher (for the 11kV, 22kV and cases greater than 132kV) – as high as 1.05pu.

This can explain why all ANNs had slight errors in prediction – up to 3% in some cases. Although minimal, it is suggested to include a smaller input data range to strengthen the ANN prediction model. Considering the ANN structure itself, limiting the hidden layer size to 3 layers resulted in the smallest error in prediction overall. It was observed that increasing the ANN hidden layer size to greater than 3 layers, resulted in the ANN overfitting the data which resulted in larger prediction errors. Having a smaller hidden layer size would result in the ANN underfitting the data, which means that it was not trained adequately enough, furthermore creating predictive deviation from the true output loss values. The ANN hidden layer size had to be tentatively selected for each voltage ANN in order to achieve the smallest loss difference when compared against DIgSILENT Powerfactory.

4.11 Impact of Power Factor on Results

As observed, the addition of an IPP to the network creates reactive power changes across the network. This change in reactive power will result in an increase or decrease in the reactive power flow on Segment A ,Segment B and the interconnecting conductor depending on the power factor at the load (receiving end).

For the 11kV network, the backbone conductor (Feeder A) is 5 km ACSR Kingbird. The receiving end power is 4.05MVA operating at 0.85 lagging power factor with active and reactive power setpoints of 3.5 MW, 2.1 MVAR respectively. The algorithm recommends an IPP size of 1.5MW operating at 0.975 (lagging) power factor, located at the 4.5km from the sending end substation using an ACSR Chickadee conductor. The ANN predicted total line losses of 0.05351MW while the true loss value is 0.05343MW (when checked using DIgSILENT Powerfactory). There is an error of 0.1684%. To further justify the accuracy of the algorithm, a 1MW and 2MW IPP size was used as the export capacity operating at different power factors (unity, lead and lagging). Figure 4 -33 clearly indicates the correctness of the 11kV ANN by selecting a 1.5MW IPP capacity operating at 0.975. As seen, the greatest loss impact is strongly related to the IPP size, location and power factor. The same results were seen when comparing the accuracy of the 11kV ANN to all other locations on the backbone, where the trend suggests that smaller IPP maximum export power ratings (measured in MW) are preferred when connections occur closer to the sending end, while larger sizes are preferred when connecting closer to the receiving end.

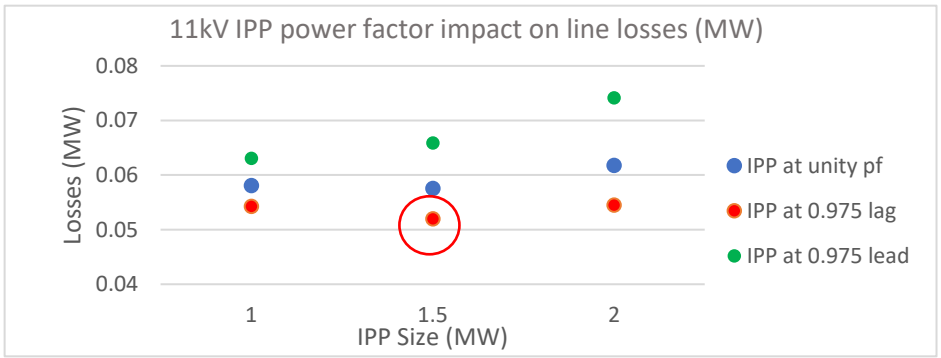

Figure 4-33:Case 1 (11kV) – Losses when IPP is located at 4.5km from the sending end.

The 22kV case was then presented and modelled using the same network as the 11kV case, but for a higher nominal voltage of 22kV. The same trend is seen for the 22kV case but with total losses significantly less than the 11kV case due to increased voltage. Results showed that when connecting a 1.5MW IPP 4.5km from the sending end, the algorithm suggests a power factor setpoint of 0.975 lagging which generates 13kW of line losses. This is in comparison to a leading power factor that results in 16kW losses. This lagging pf gives 3kW loss savings with respect to a leading pf for the 1.5MW IPP capacity. Figure 4 - 34 shows that for a 2MW IPP capacity, the capacitive setpoint enhances total system losses even more to 18kW.

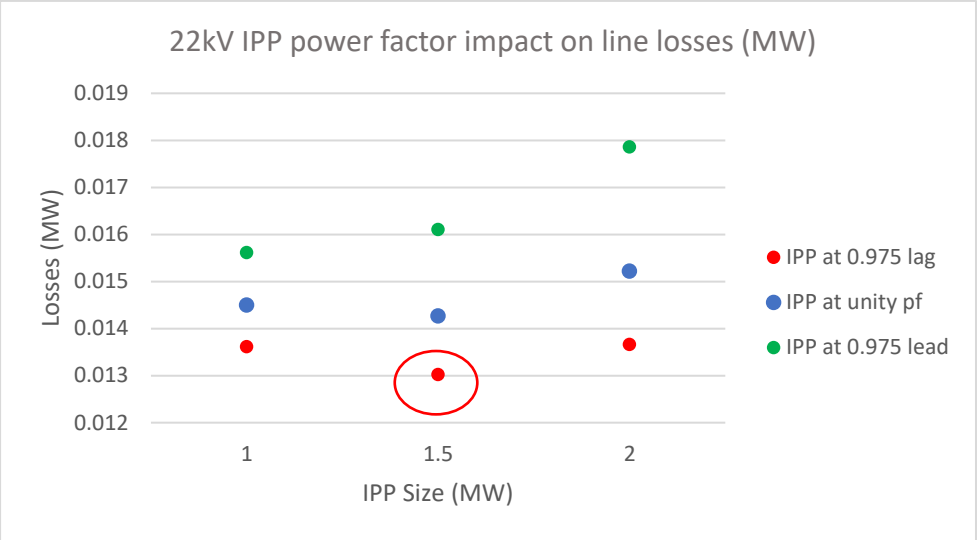

Figure 4-34:Case 2 (22kV) – Losses when IPP is located at 4.5km from the sending end. A 0.975 lagging pf setpoint results in lowest losses overall with an IPP size of 1.5MW capacity.

For cases with voltages of 66kV and above, the algorithm was tested using the IEEE14-bus system. The 66kV ANN had a predicative error of 3.21% for the IPP located 14.04km from the sending end (for a backbone length of 15.6km). Figure 4-35 is shown below, indicating smaller differences in losses regardless of IPP power factor for a 2MW export capacity. It is also observed that as the IPP size increases, the losses become more pronounced depending on the IPP power factor. As seen, for a lagging setpoint and IPP export capacity of 12MW, total losses amount to 193kW, while for the leading power factor case, 238kW of losses are generated.

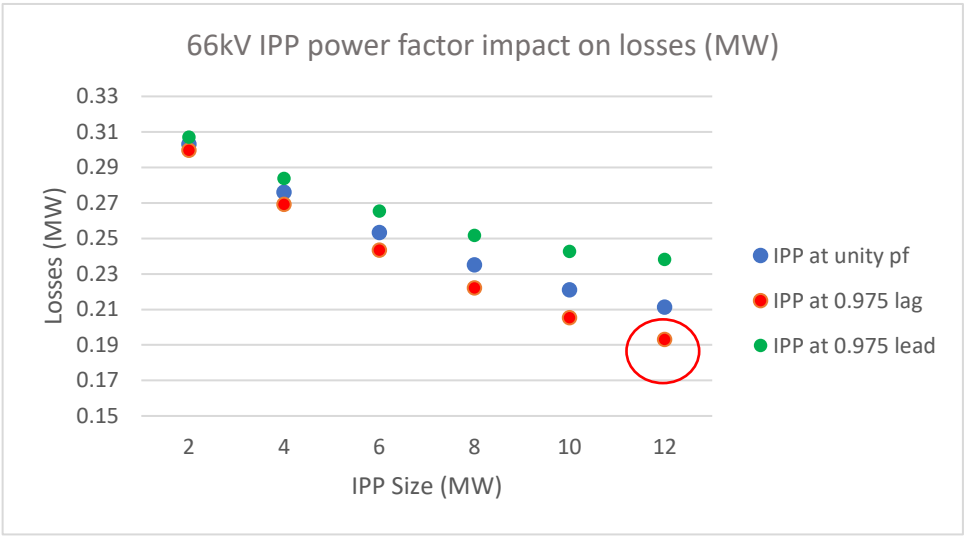

Figure 4-35:Case 3 (66kV) – Losses when IPP is located at 14.04km from the sending end. A 0.975 lagging pf setpoint results in lowest losses overall with an IPP size of 12MW capacity.

The 132kV ANN achieves a prediction error of 0.755% when connecting a 67.5MW IPP, 31.5km from the sending ending end on the 35km backbone, operating at 0.95 lagging power factor – this location and size is the most optimal for line loss reduction. When operating at an inductive setpoint of 0.95, the IPP reduces total line losses to generates 0.55MW, which is 450kW lower than the capacitive setpoint. This is because the load (operating at 0.95 lag) requires more reactive power from the IPP to overcome the VAR deficit. This difference is indicated in Figure 3–36, which also shows lowest losses are generated for 0.975 lagging setpoint.

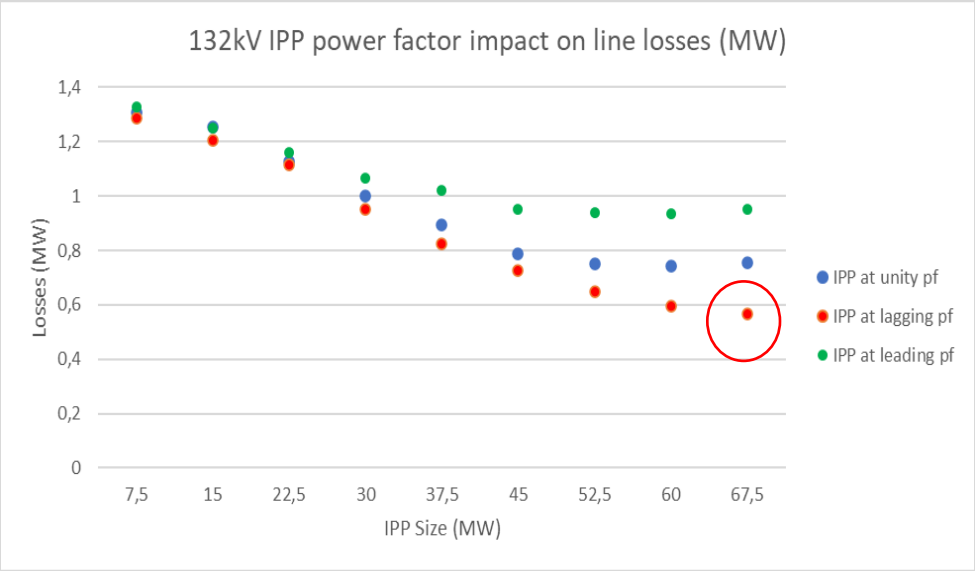

Figure 4-36:Case 4 (132kV) – Losses when IPP is located 31.5km from the sending end. A 0.975 lagging pf setpoint results in lowest losses overall with an IPP size of 67.5MW capacity.

For the EHV cases (220kV – 400kV), the same trend is seen. For the 220kV network, the lowest losses are seen for an IPP connected furthest away from the sending end (120.9km) along the 134km backbone. This requires a 110MW IPP at operating at 0.95 lagging pf resulting in 3.7MW of line losses. For a 0.95 leading power factor, the total system losses increase to 5MW, indicating that the algorithm predicted correctly. These losses, however, are significantly lower when compared to connecting at 10% (13.4km from sending end) on the 134km backbone which results in 9MW of generated line losses since the VARs need to now be transferred over a longer line length, rather than being supplied closer to the load end (which is why losses are lower for the IPP connecting closer to the receiving end). For this location the algorithm correctly sizes the IPP export capacity to be 22MW at a lagging power factor.

The 275kV case has lowest losses for a 110MW IPP size operating at a lagging power factor of 0.95. This generates 1.8MW of losses (approximately 500kW lower than the capacitive case), but also is significantly lower than the 220kW case since a twin conductor Zebra bundle is used for the interconnecting feeder.

Since the 400kV network is modelled using quad Zebra conductors, losses are much smaller than the 220kV and 275kV cases, which only used a Twin bundle conductor geometry per phase. This increased the geometric mean radius which increased the maximum power transfer of 150MW required at the receiving end. Since the power factor at the 400kV receiving end load is unity, the required reactive VAR support, in addition to the high voltage level (400kV at 1.04pu), saw an optimal IPP power factor setpoint of 0.95 (leading) resulting in a surplus of VARs. In this case, a leading IPP power factor would have more of an effect on line loss reduction than the lagging setpoint since it would consume the excess reactive power required at the load end.

In general, smaller IPP sizes are more beneficial for minimising line losses when connecting closer to the sending end, since the required transfer of VARS over a longer distance (in order to get VAR supply to the load) will increase power line losses as shown in Figures 4-34 to 4-36 above. Power factor in this case also has less of an effect on line losses when compared to connecting directly to the receiving end (or further away from the sending end) since the power transfer is directly consumed by the load itself without the influence of backbone losses. An IPP connecting to the network with a capacitive power factor will reduce the line current and therefore reduce the total system losses seen on

Segment A and Segment B when the load is in excess of reactive power as was the case for the 400kV network. For cases that are lightly loaded at the receiving end, the line charging current (due to the Ferranti effect) is essentially constant and will only depend on the network voltage level. This will cause the charging current to be higher and in turn the total system losses larger than the inductive setpoint of the IPP. In such events, the inductive power factor will absorb the reactive power and help to reduce the line currents seen on Segment A, Segment B and the interconnecting conductor, thus reducing power losses overall.

4.12 Conclusion

The trend for all cases strongly suggests that the most optimal location of IPPs is closer to the receiving end since this is where reactive power is consumed. If not the reactive power needs to be transferred from the sending end of the line which will increase currents flowing through Segment B (current through Segment A combined with IPP current) and therefore increase the power line losses overall. Although this effect is not as enhanced as when connecting a capacitor bank or reactor (reactive power source) at the load, it is clear from the cases presented above that the power factor setpoint of the IPP still has considerable impact on the total power line losses. In terms of flexibility and adaptability, the proposed model considers only solar PV IPPs and no other sources of energy such as battery energy storage, wind energy or diesel co-generation seeking connection to the grid. Since these other sources have different operating modes and setpoints, the existing model would require an additional programming function for this. Since a static study is considered, in order to make the model more practical, a dynamic model would need to be implemented. This can be achieved by incorporating a range of datapoints into the input dataset for a single IPP case study, which takes into account not only the maximum peak load seen at the receiving end, but also daily load fluctuations to paint a more realistic picture of how the receiving end load behaves. For instance, under lightly loaded conditions, the receiving end voltage will see significantly higher voltages due to Ferranti effect – especially for longer lines operating at EHV. The algorithm in this sense lacks flexibility because the entire input dataset and programming required for this would require adjustment – storage concerns and more rigorous test would also need to be included for this. The model is also specific to the South African network, in order to use it on networks outside of South Africa – which possibly have alternative network nominal voltages - input and target data would need to be re-calculated since the voltage change will have a direct influence on line losses. The model is flexible in the sense that a more comprehensive conductor set can be added by simply increasing the input data size and consequentially increasing the target data size to accommodate for more conductor options.

In this section, the performance and accuracy of the ANN algorithm was tested. Seven cases were presented starting from the lowest voltage test case (11kV) to the highest test case (400kV). Case 1 and Case 2 tested the 11kV and 22kV ANNs on modified IEEE–13 bus systems while Case 3 to Case 7 tested the 66kV, 132kV, 220kV, 275kV and 400kV ANNs on modified IEEE–14 bus systems. For all cases, the algorithm returns the best IPP size, location, power factor and interconnecting feeder. Total line losses for these cases are recorded and compared to DIgSILENT Powerfactory results and presented in Chapter 4 of this thesis. The results indicate high levels of accuracy when compared with DIgSILENT Powerfactory. Chapter 5 will present the benefits of this work in the energy and power sector, and advances as well as recommendations for future work in terms of both expanding and improving.

CHAPTER 5

CONCLUSION AND RECOMMENDATIONS

Having so far presented, tested and verified the performance of the 7 ANN algorithms on modified IEEE-13 and IEEE-14 bus test networks in the form of 7 case studies, this chapter will present the overall results summary, a critical reflection of the results, and future recommendations and benefits of this work to industry from both an expanding and improving perspective - when developing an ANN model to be used for the integration of solar plants to distribution or transmission networks.

5.1 Conclusion and critical reflection of results

This research presented an ANN design tool used for the initial planning phase of solar plants seeking connection to the grid for minimising power line losses. This is done by optimising the IPP size, IPP location, interconnecting conductor as well as IPP power factor. The algorithm determines the most optimal combination of these parameters in order to ensure conductor losses are as small as possible. Seven cases are presented starting from the lowest voltage test case (11kV) to the highest test case (400kV). Case 1 and Case 2 test the 11kV and 22kV ANNs on modified IEEE-13 bus systems while Case 3 to Case 7 test 66kV, 132kV, 220kV, 275kV and 400kV ANNs on modified IEEE-14 bus systems.

In Chapter 1, a brief discussion of the research objectives and outlines were discussed. The processes to be carried out for later chapters were presented. Chapter 2 introduced the development of solar PV plants, solar PV components and the principles of solar power generation. The integration of solar PV to the grid from a mathematical perspective was given, with emphasis on line losses generated. The technical standards and requirements of the South African Grid code were highlighted. The chapter concluded with existing research conducted specifically to IPP placement on power lines for minimizing line losses.

Chapter 3 discussed selection of input data and target data used for ANN training. The modelling of a test bed network in DIgSILENT Powerfactory was shown. The test bed consisted of an IPP directly connecting (tying-in) to a backbone feeder (representing the grid) via a suitable interconnecting conductor. Collection of target data (total line losses) was presented. The input and output data for all voltage levels were discussed. The ANN model structure which was developed within MATLAB software was discussed.

Chapter 4 presented 7 cases which verified the validating and accuracy of the ANN model of the ANN models developed. The networks used were modified versions of the IEEE 13-bus and IEEE 14-bus systems. Results were cross-examined using DIgSILENT Powerfactory.

The research undertaken proved to be a success, with the ANN model showing limited prediction error, when compared to DIgSILENT Powerfactory software. Although much improvement to the model can be achieved, it serves as a starting point for a more automated approach towards the IPP sizing and placement problem, especially from a South African

perspective, since it was developed based on the limitations and requirements of the SAGC. Before it can be fully integrated within industry, it would require strenuous testing, in order to recognise and immediately reject invalid inputs from the user. An additional programming function would be needed for this to work. The final result would be more robust if it incorporated a financial element, which justified the best IPP location based not only on total line losses but costs required for installation. For example, the best IPP location based on line losses, may require greater costs of installation due a harsh/impassable surrounding terrain - a wetland or restricted area for example, would have greater costs associated with bypassing the area as per legal requirements. A 100km interconnecting conductor cannot perpendicularly intersect the backbone feeder from the IPP plant itself, since the nature of the terrain will not in many cases allow for this. In this sense, the model is one dimensional and can be strengthened by adding these additional features.

Since Eskom (the South African utility provider), owns the network infrastructure, the biggest challenge in this research was the availability and access to Eskom data, which was needed in order to train the 7 ANN models according to the SAGC. All data used in this research had to be derived from open-source platforms only, which extended research time. Information had to be verified by taking into account the limits specified in the South African National Standards (SANS 182) [70, 71], SAGC [7], NRS048 (Compatibility levels, limits, and voltage characteristics for utilities, their customers, and the National Energy Regulator in managing power quality issues parts 2) [23], IEEE Guide for the Installation of Overhead Transmission Line Conductors (524-16) [72], and reference [73].

5.2 Future recommendations

- Incorporating a costing feature to the ANN. This is the biggest improvement that can be made since the acquisition cost of installation during the planning phase is a key parameter. The cost of installation considering only line losses will also need to be justified by considering the initial cost of installation at the most optimal location on the line. It may be that even in cases where the line losses are the smallest, from a financial perspective is not viable, when considering the return on the investment.
- Only maximum loading at the receiving end was considered as an input to the ANN user interface. Considering load fluctuations for lightly loaded and well as heavily loaded lines will need to be incorporated into the ANN tool to make it more comprehensive and realistic.
- Voltages at the sending and receiving end as inputs to the ANN model will add additional accuracy to the model, since these parameters also influence line losses.
- A more comprehensive conductor range for the interconnecting conductor selection can be added to the input data to optimise this feature further. Only a limited number of conductor types per voltage level were used for the interconnecting conductor set. Adding a larger range would have a greater impact on the line losses.
- Training the ANN to consider integration of IPPs to ring network topologies in addition to radial feeders.
- Incorporating unbalanced loading conditions since the study only focussed on balanced networks.
- A methodology which incorporates battery storage and generator integration in conjunction with solar PV integration would be beneficial, especially for IPPs.

5.3 Benefits to the power and energy sector

- The model can be used as a tool for providing additional support to network engineers and independent power producers (IPPs), especially for performing grid application studies.
- The tool accurately locates and sizes IPPs seeking connection to MV/HV/EHV backbone feeders, from geographical locations far from the Point of Connection (POC).
- It additionally determines the most suitable interconnecting conductor and IPP power factor setpoint.
- With a drive to enhance greener energy storage of power, this tool will assist the IPP developer and network planner in supporting and contributing to this initiative.
- The tool will prevent overloading of the network infrastructure since it is compliant with the South African Grid Code and in line with the requirements of the NRS 048.

REFERENCES

[1] C. Moldoveanu et al., "Romanian innovative system for power losses real time monitoring and analysis in electrical transmission and distribution systems," *2021 9th International Conference on Modern Power Systems (MPS)*, Cluj-Napoca, Romania, 2021, pp. 1-6, doi: 10.1109/MPS52805.2021.9492696.

[2] A. Singh, R. S. Bhatia and S. Chanana, "An Anti-Islanding Technique for Grid-Connected DG and Multi DG System," *2018 International Conference on Emerging Trends and Innovations In Engineering And Technological Research (ICETIETR)*, Ernakulam, India, 2018, pp. 1-6, doi: 10.1109/ICETIETR.2018.8529035.

[3] K. Pal, B. kumar Panigrahi, S. Mohapatra and A. Mohapatra, "Impact of STATCOM on voltage profile in a DG penetrated grid connected system," *2017 International Conference on Circuit ,Power and Computing Technologies (ICCPCT)*, Kollam, India, 2017, pp. 1-5, doi: 10.1109/ICCPCT.2017.8074213.

[4] E. Šemić, T. Hubana and M. Šarić, "Distributed Generation Allocation in Low Voltage Distribution Network Using Artificial Neural Network," *IEEE EUROCON 2019 -18th International Conference on Smart Technologies*, Novi Sad, Serbia, 2019, pp. 1-6, doi: 10.1109/EUROCON.2019.8861816.

[5] DIgSILENT PowerFactory Software. Thesis Licence.

[6] MATLAB Version: 9.13.0 (R2022b) Update 2.

[7] NERSA, "Grid Connection Code for Renewable Power Plants (RPPs) connected to the Electricity Transmission System (TS) or Distribution System (DS) in South Africa," National Energy Regulator of South Africa, Version 3.0, August 2019.

[8] M. A. Khabarova, O. V. Novikova and A. A. Khabarov, "State and Perspectives of Power and Industry Applications of Coal," *2019 IEEE Conference of Russian Young Researchers in Electrical and Electronic Engineering (EIConRus)*, Saint Petersburg and Moscow, Russia, 2019, pp. 985-987, doi: 10.1109/EIConRus.2019.8656860.

[9] R. Mehta, D. Oyedokun, B. Merven and R. Larmour, "Multi-Nodal Energy Systems Modelling Scenarios of South Africa's Power Sector," *2023 31st Southern African Universities Power Engineering Conference (SAUPEC)*, Johannesburg, South Africa, 2023, pp. 1-6, doi: 10.1109/SAUPEC57889.2023.10057721.

[10] S. Sewchurran and I. E. Davidson, "Introduction to the South African Renewable Energy Grid Code version 2.9 requirements (Part I — Introduction)," *2017 IEEE AFRICON*, Cape Town, South Africa, 2017, pp. 1220-1224, doi: 10.1109/AFRCON.2017.8095656.

[11] S. Sewchurran and I. E. Davidson, "Introduction to the South African Renewable Energy Grid Code version 2.9 requirements (Part II — Grid code technical requirements)," *2017 IEEE AFRICON*, Cape Town, South Africa, 2017, pp. 1225-1230, doi: 10.1109/AFRCON.2017.8095657.

[12] A. Eberhard and R. Naude, "The South African Renewable Energy Procurement Program - Review, Lessons Learned & Proposals to Reduce Transaction Costs", Graduate School of Business, University of Cape Town, Cape Town, South Africa, 2017.

[13] S. Sewchurran and I. E. Davidson, "Introduction to the South African Renewable Energy Grid Code version 2.9 requirements (Part III — Discussions and conclusions)," *2017 IEEE AFRICON*, Cape Town, South Africa, 2017, pp. 1231-1235, doi: 10.1109/AFRCON.2017.8095658.

[14] S. Sewchurran and I. E. Davidson, "Guiding principles for grid code compliance of large utility scale renewable power plant intergration onto south africa's transmission/distribution networks," *2016 IEEE International Conference on Renewable Energy Research and Applications (ICRERA)*, Birmingham, UK, 2016, pp. 528-537, doi: 10.1109/ICRERA.2016.7884392.

[15] A. Pandarum, G. Lekoloane and D. Milazi, "Trends and statistics of Solar PV Distributed Generation in South Africa," *SA Energy Storage Conference & Ehibition 2018*, South Africa, 2018.

[16] J. Calitz, and J. Wright. Statistics Of Utility-Scale power generation in South Africa 2020. Cigre Energy Centre. March 2021.

[17] C. A. Vigneshwari, S. S. S. Velan, M. Venkateshwaran, M. A. Mydeen and V. Kirubakaran, "Performance and economic study of on-grid and off-grid solar photovoltaic system," *2016 International Conference on Energy Efficient Technologies for Sustainability (ICEETS)*, Nagercoil, India, 2016, pp. 239-244, doi: 10.1109/ICEETS.2016.7582933.

[18] J.W. Simatupang, and D.A. Faskayana, "Feasibility Study of Photovoltaic - Diesel Hybrid Power System as Renewable Energy Source," *International Journal of Innovative Research in Electrical, Electronics, Instrumentation and Control Engineering*, Vol. 7, Issue 3, 2019, pp.56-63, DOI 10.17148/IJIREEICE.2019.7312.

[19] N. H. Zaini, M. Z. Ab Kadir, M. Izadi, N. I. Ahmad, M. A. M. Radzi and N. Azis, "The effect of temperature on a mono-crystalline solar PV panel," *2015 IEEE Conference on Energy Conversion (CENCON)*, Johor Bahru, Malaysia, 2015, pp. 249-253, doi: 10.1109/CENCON.2015.7409548.

[20] A. Cabrera-Tobar, E. Bullich-Massagué, M. Aragüés-Peñalba, and O. Gomis-Bellmunt, "Topologies for large scale photovoltaic power plants," *Renewable and Sustainable Energy Reviews*, Vol. 59, 2016, pp.309-319, https://doi.org/10.1016/j.rser.2015.12.362.

[21] Al Smadi, Hamza. (2018). Overview of Grid-Connected PV Systems Challenges with Regards to Grid Stability.

[22] F. Viawan and A. Sannino, "Voltage control with distributed generation and its impact on losses in LV distribution systems," *2005 IEEE Russia Power Tech*, St. Petersburg, Russia, 2005, pp. 1-7, doi: 10.1109/PTC.2005.4524718.

[23] NRS 048-2:2003. ELECTRICITY SUPPLY — QUALITY OF SUPPLY, Part 2: Voltage characteristics, compatibility levels, limits and assessment methods ISBN 0-626-15179-1.

[24] Y. Yan, W. Bao, J. Xin, H. Lin, Z. Li and H. Zhong, "A thermal model based dynamic rating system for overhead transmission lines," *2015 5th International Conference on Electric Utility Deregulation and Restructuring and Power Technologies (DRPT)*, Changsha, China, 2015, pp. 2758-2763, doi: 10.1109/DRPT.2015.7432718.

[25] U. Jamil, A. Amin and A. Mahmood, "A comparative study of control techniques for power loss minimization in a distribution network," *2018 1st International Conference on Power, Energy and Smart Grid (ICPESG)*, Mirpur Azad Kashmir, Pakistan, 2018, pp. 1-5, doi: 10.1109/ICPESG.2018.8384524.

[26] M. Khasanov, S. Kamel and H. Abdel-Mawgoud, "Minimizing Power Loss and Improving Voltage Stability in Distribution System Through Optimal Allocation of Distributed Generation Using Electrostatic Discharge Algorithm," *2019 21st International Middle East Power Systems Conference (MEPCON)*, Cairo, Egypt, 2019, pp. 354-359, doi: 10.1109/MEPCON47431.2019.9007943.

[27] S. S. Alkaabi, H. H. Zeineldin and V. Khadkikar, "Short-Term Reactive Power Planning to Minimize Cost of Energy Losses Considering PV Systems," *IEEE Transactions on Smart Grid*, vol. 10, no. 3, pp. 2923-2935, May 2019, doi: 10.1109/TSG.2018.2815434.

[28] Y. Yang, E. UI Haq and Y. Jia, "A Deep Convolutional Neural Network Technique for Power Losses Estimation in Distribution Grid," *2020 IEEE/IAS Industrial and Commercial Power System Asia (I&CPS Asia)*, Weihai, China, 2020, pp. 1461-1468, doi: 10.1109/ICPSAsia48933.2020.9208474.

[29] V.S. Bhadoria, et al. "Comparison of Analytical and Heuristic Techniques for Multiobjective Optimization in Power System." *Problem Solving and Uncertainty Modeling through Optimization and Soft Computing Applications*, edited by Pratiksha Saxena, et al., IGI Global, 2016, pp. 264-291. https://doi.org/10.4018/978-1-4666-9885-7.ch013.

[30] M. M. Ansari, C. Guo, M. S. Shaikh, M. Ali Jatoi, C. Yang and J. Zhang, "A Review of Technical Methods for Distributed Systems with Distributed Generation (DG)," *2019 2nd International Conference on Computing, Mathematics and Engineering Technologies (iCoMET)*, Sukkur, Pakistan, 2019, pp. 1-7, doi: 10.1109/ICOMET.2019.8673475.

[31] B. Venkatesh Reddy, "Sizing of DG Units Using Exact Loss Formula to Improve Efficiency of Radial Distribution System," *International Journal of Emerging Trends in Electrical and Electronics*, Vol. 10, Issue 1, 2014, pp.13-17.

[32] N. Acharya, P. Mahat and N. Mithulananthan, "An analytical approach for DG allocation in primary distribution network," *International Journal of Electrical Power & Energy Systems*, Vol. 28, Issue 10, 2006, pp.669-678, https://doi.org/10.1016/j.ijepes.2006.02.013.

[33] D. Q. Hung, N. Mithulananthan and R. C. Bansal, "Analytical Expressions for DG Allocation in Primary Distribution Networks," *IEEE Transactions on Energy Conversion*, vol. 25, no. 3, pp. 814-820, Sept. 2010, doi: 10.1109/TEC.2010.2044414.

[34] G. A. S. Gandhi, R. Prakash and S. Sivasubramani, "Optimal Allocation of DG for Minimization of Power Loss and Total Investment Cost using an Analytical Approach," *2020 21st National Power Systems Conference (NPSC)*, Gandhinagar, India, 2020, pp. 1-6, doi: 10.1109/NPSC49263.2020.9331891.

[35] S. -H. Lee and J. -W. Park, "Selection of Optimal Location and Size of Multiple Distributed Generations by Using Kalman Filter Algorithm," *IEEE Transactions on Power Systems*, Vol. 24, No. 3, pp. 1393-1400, Aug. 2009, doi: 10.1109/TPWRS.2009.2016540.

[36] A. Kumar, P. Vijay Babu, and V.V.S.N. Murty, "Distributed Generators Allocation in Radial Distribution Systems with Load Growth using Loss Sensitivity Approach," *Journal of The Institution of Engineers (India): Series B*, Vol. 98, 2017, pp.275–287, https://doi.org/10.1007/s40031-016-0242-8.

[37] A. Bagheri, M. Bagheri, and A. Lorestani, "Optimal reconfiguration and DG integration in distribution networks considering switching actions costs using tabu search algorithm", *Journal of Ambient Intelligence and Humanized Computing*, Vol. 12, 2021, pp. 7837–7856, https://doi.org/10.1007/s12652-020-02511-z.

[38] N. C. Koutsoukis, P. S. Georgilakis and N. D. Hatziargyriou, "A Tabu search method for distribution network planning considering distributed generation and uncertainties," *2014 International Conference on Probabilistic Methods Applied to Power Systems (PMAPS)*, Durham, UK, 2014, pp. 1-6, doi: 10.1109/PMAPS.2014.6960627.

[39] A. Keane and M. O'Malley, "Optimal allocation of embedded generation on distribution networks," *IEEE Transactions on Power Systems*, Vol. 20, No. 3, pp. 1640-1646, Aug. 2005, doi: 10.1109/TPWRS.2005.852115.

[40] M. Kumar, A. Kumar, and K.S. Sandhu, "Optimal Location of WT based Distributed Generation in Pool based Electricity Market using Mixed Integer Non Linear Programming," *Materials Today: Proceedings*, Vol. 5, Issue 1, Part 1, 2018, pp.445-457, https://doi.org/10.1016/j.matpr.2017.11.104.

[41] B. Pawar, S. Kaur and G. B. Kumbhar, "An integrated approach for power loss reduction in primary distribution system," *2016 IEEE 6th International Conference on Power Systems (ICPS)*, New Delhi, India, 2016, pp. 1-6, doi: 10.1109/ICPES.2016.7584049.

[42] A. Heidari, V. G. Agelidis, M. Kia and M. Setayeshnazar, "Mixed-integer programming optimization-based method for switch device placement in distribution systems considering distributed generation," *2013 Australasian Universities Power Engineering Conference (AUPEC)*, Hobart, TAS, Australia, 2013, pp. 1-5, doi: 10.1109/AUPEC.2013.6725352.

[43] E. Karunarathne, J. Pasupuleti, J. Ekanayake and D. Almeida, "Optimal Placement and Sizing of DGs in Distribution Networks Using MLPSO Algorithm," *Energies 2020*, Vol. 13, 6185. https://doi.org/10.3390/en13236185.

[44] N. Vijayalaksmi and K. Gayathri, "Optimal placement of DG Units and Network Reconfiguration for Power Loss Minimization and Voltage Profile Improvement in Distribution Network," *2020 IEEE International Conference on Advances and Developments in Electrical and Electronics Engineering (ICADEE)*, Coimbatore, India, 2020, pp. 1-5, doi: 10.1109/ICADEE51157.2020.9368909.

[45] A. A. Raouf Mohamed, "A multi-objective distributed generation allocation and sizing using swarm intelligence based algorithms," *2018 19th IEEE Mediterranean Electrotechnical Conference (MELECON)*, Marrakech, Morocco, 2018, pp. 281-286, doi: 10.1109/MELCON.2018.8379108.

[46] N. Jangir, P. Kumar, N. Gupta, K. R. Niazi and A. Swarnkar, "Robust allocation of DGs integrated with distribution network reconfiguration," *2015 Annual IEEE India Conference (INDICON)*, New Delhi, India, 2015, pp. 1-6, doi: 10.1109/INDICON.2015.7443411.

[47] B. Ahmadi, O. Ceylan and A. Ozdemir, "Optimal allocation of multi-type distributed generators for minimization of power losses in distribution systems," *2019 20th International Conference on Intelligent System Application to Power Systems (ISAP)*, New Delhi, India, 2019, pp. 1-6, doi: 10.1109/ISAP48318.2019.9065974.

[48] M. G. Naguib, W. A. Omran and H. E. A. Talaat, "Optimal reconfiguration and DG allocation in active distribution networks using a probabilistic approach," *2017 IEEE PES Innovative Smart Grid Technologies Conference Europe (ISGT-Europe)*, Turin, Italy, 2017, pp. 1-6, doi: 10.1109/ISGTEurope.2017.8260224.

[49] M. NageswaraRao, N. Sumathi, V. S. N. K. Chaitanya and K. Amarendranath, "Multiple DG allocation by crow search algorithm for power loss reduction," *2017 IEEE International Conference on Power, Control, Signals and Instrumentation Engineering (ICPCSI)*, Chennai, India, 2017, pp. 790-795, doi: 10.1109/ICPCSI.2017.8391822.

[50] R. Rakesh, P. VenkataPapana and S. Keerthi, "A hybrid algorithm for optimal allocation of DG in radial distribution system," *2017 IEEE Region 10 Symposium (TENSYMP)*, Cochin, India, 2017, pp. 1-5, doi: 10.1109/TENCONSpring.2017.8070009.

[51] A. Alhamali, M. E. Farrag, G. Bevan and D. M. Hepburn, "Determination of optimal site and capacity of DG systems in distribution network based on genetic algorithm," *2017 52nd International Universities Power Engineering Conference (UPEC)*, Heraklion, Greece, 2017, pp. 1-6, doi: 10.1109/UPEC.2017.8231996.

[52] W. Sheng, K. -Y. Liu, Y. Liu, X. Meng and Y. Li, "Optimal Placement and Sizing of Distributed Generation via an Improved Nondominated Sorting Genetic Algorithm II," *IEEE Transactions on Power Delivery*, Vol. 30, No. 2, pp. 569-578, April 2015, doi: 10.1109/TPWRD.2014.2325938.

[53] M. Saric, J. Hivziefendic and M. Tesanovic, "Optimal DG Allocation for Power Loss Reduction Considering Load and Generation Uncertainties," *2019 11th International Symposium on Advanced Topics in Electrical Engineering (ATEE)*, Bucharest, Romania, 2019, pp. 1-6, doi: 10.1109/ATEE.2019.8724911.

[54] S. Bhuyan, M. Das and K. C. Bhuyan, "Particle Swarm Optimizations Based DG Allocation in Local PV Distribution Networks for Voltage Profile Improvement," *2017 International Conference on Computer, Electrical & Communication Engineering (ICCECE)*, Kolkata, India, 2017, pp. 1-4, doi: 10.1109/ICCECE.2017.8526201.

[55] S. Mahajan and S. Vadhera, "Optimal sizing and deploying of distributed generation unit using a modified multiobjective Particle Swarm Optimization," *2016 IEEE 6th International Conference on Power Systems (ICPS)*, New Delhi, India, 2016, pp. 1-6, doi: 10.1109/ICPES.2016.7584092.

[56] S. L. Mhetre, I. M. Korachagaon and R. J. Kulkarni, "Optimum DG Placement Based on Voltage Stability Increment and Reduction in Power Losses Using Particle Swarm Optimization," *2018 IEEE Global Conference on Wireless Computing and Networking (GCWCN)*, Lonavala, India, 2018, pp. 192-195, doi: 10.1109/GCWCN.2018.8668582.

[57] A. Jalali, S. K. Mohammadi, H. Sangrody and A. Rahimzadegan, "DG-embedded radial distribution system planning using binary-selective PSO," *2016 IEEE Innovative Smart Grid Technologies - Asia (ISGT-Asia)*, Melbourne, VIC, Australia, 2016, pp. 996-1001, doi: 10.1109/ISGT-Asia.2016.7796521.

[58] J. Yang, "Research on Optimized Reconfiguration of Distributed Distribution Network Based on Ant Colony Optimization Algorithm," *2020 International Conference on Computer Engineering and Application (ICCEA)*, Guangzhou, China, 2020, pp. 20-23, doi: 10.1109/ICCEA50009.2020.00012.
[59] P. Goli, S. Makkena, S. R. Gampa and D. Das, "Fuzzy Ant Colony Optimization Technique for Predefined Performance of Distribution Systems Considering DGs and Shunt Capacitors," *2019 North American Power Symposium (NAPS)*, Wichita, KS, USA, 2019, pp. 1-6, doi: 10.1109/NAPS46351.2019.9000250.
[60] H. Li, A. Wang, Y. Zhang and B. Guo, "Dynamic Reconfiguration of Distribution Network Considering Time-varying Characteristics of DG," *2019 6th International Conference on Systems and Informatics (ICSAI)*, Shanghai, China, 2019, pp. 274-279, doi: 10.1109/ICSAI48974.2019.9010140.
[61] N. Chakraborty, S. Chandra, A. Banerji and S. K. Biswas, "Optimal placement of DG using Swarm intelligence approach in distributed network: Status & challenges," *2016 21st Century Energy Needs - Materials, Systems and Applications (ICTFCEN)*, Kharagpur, India, 2016, pp. 1-5, doi: 10.1109/ICTFCEN.2016.8052746.
[62] B. Zhang et al., "Minimisation of distribution feeder loss using ant colony optimisation applied to network reconfiguration and distributed generations placement," *8th Renewable Power Generation Conference (RPG 2019)*, Shanghai, China, 2019, pp. 1-7, doi: 10.1049/cp.2019.0277.
[63] B. K. Sahoo, S. Pradhan, B. K. Panigrahi, B. Biswal, N. C. Patel and S. Das, "Fault detection in Electrical Power Transmission System using Artificial Neural Network," *2020 International Conference on Computational Intelligence for Smart Power System and Sustainable Energy (CISPSSE)*, Keonjhar, India, 2020, pp. 1-4, doi: 10.1109/CISPSSE49931.2020.9212274.
[64] T. A. Kumar and L. S. Rao, "Improvement of power quality of distribution system using ANN-LMBNN based D-STATCOM," *2017 Innovations in Power and Advanced Computing Technologies (i-PACT)*, Vellore, India, 2017, pp. 1-6, doi: 10.1109/IPACT.2017.8245211.
[65] S. Kumar, S. Mishra and S. Gupta, "Short Term Load Forecasting Using ANN and Multiple Linear Regression," *2016 Second International Conference on Computational Intelligence & Communication Technology (CICT)*, Ghaziabad, India, 2016, pp. 184-186, doi: 10.1109/CICT.2016.44.
[66] B. Yang, L. Yu, Y. Chen, H. Ye, R. Shao, H. Shu, T. Yu, X. Zhang and L. Sun, "Modelling, applications, and evaluations of optimal sizing and placement of distributed generations: A critical state-of-the-art survey", *International Journal of Energy Research*, Vol.45, No.3, 2021, pp.3615.
[67] Lanovaz, Marc & Bailey, Jordan. (2020). Tutorial: Artificial Neural Networks to Analyze Single-Case Experimental Designs. 10.31234/osf.io/3qzhp.
[68] N.Z.M. Ali, I. Musirin and S. I. Suliman, "Effect of Multi-DG Installation to Loss Reduction in Distribution System," *Journal of Electrical Systems*, Vol. 12, Issue 1, 2016, pp.187-196.
[69] P. M. J. Roque and S. P. Chowdhury, "Expansion of wind power technology in South Africa: Challenges and opportunities," *2017 IEEE PES Power Africa*, Accra, Ghana, 2017, pp. 560-565, doi: 10.1109/PowerAfrica.2017.7991287.
[70] SANS 182-1:2021, (Ed. 1.03). Conductors for overhead electrical transmission lines Part 1: Copper wires and stranded copper conductors.
[71] SANS 10280-1:2017 (Ed. 2.01). Overhead power lines for conditions prevailing in South Africa Part 1: Safety. 2017.
[72] "IEEE Guide for the Installation of Overhead Transmission Line Conductors," in IEEE Std 524-2016 (Revision of IEEE Std 524-2003) , pp.1-162, 2017, doi: 10.1109/IEEESTD.2017.7912224.
[73] S. Bisnath et al. The Planning Design and Construction of Overhead Power Lines. Crown Publications 2005.
[74] I. Hathout, K. Callery, J. Trac and T. Hathout, "Impact of Thermal Stresses on the End of Life of Overhead Transmission Conductors," *2018 IEEE Power & Energy Society General Meeting (PESGM)*, Portland, OR, USA, 2018, pp. 1-5, doi: 10.1109/PESGM.2018.8586574.
[75] Glover, J. Duncan, Mulukutla S. Sarma, and Thomas J. Overbye. Power System Analysis and Design. Australia: Thomson, 2008.
[76] E. Rosales-Asensio, A.Colmenar-Santos and J. Rosales. Transmission Line Design Manual, Series: Electrical Engineering Developments. Nova Science Pub Inc., 2020, DOI: 10.52305/MLRQ2123
[77] K. O. Papailiou. International Council on Large Electric Systems (CIGRE) Study Committee B2: Overhead Lines. CIGRE Green Book, Springer, 1st ed. 2017..
[78] CBI Electric, African Cables. ACSR Conductor Data Sheet, DISSCAAY5/BS215/IEC61089,3 April 2019.
[79] DIgSILENT Powerfactory 2020. Technical Reference Manual. DIgSILENT GmbH. Revision 2.
[80] V. Yarlagadda, G. Lakshminarayana, G. Ambati, T. Nireekshana and G. A. Karthika, "Mitigation of Ferranti Effect and Voltage Control in Transmission Systems Using Fuzzy Logic Controlled SVC," *2022 International Conference on Smart Technologies and Systems for Next Generation Computing (ICSTSN)*, Villupuram, India, 2022, pp. 1-6, doi: 10.1109/ICSTSN53084.2022.9761300.
[81] B.A. Thango and P.N. Bokoro, "Defining and Specifying Design Considerations for Distribution Transformers in Large-Scale Solar Photovoltaic Plants," *Energies 2022*, Vol. 15, 2773. https://doi.org/10.3390/en15082773
[82] IEC 60076 International Standard, "Power Transformer," 2000. V
[83] R. Saravanan and P. Sujatha, "A State of Art Techniques on Machine Learning Algorithms: A Perspective of Supervised Learning Approaches in Data Classification," *2018 Second International Conference on Intelligent Computing and Control Systems (ICICCS)*, Madurai, India, 2018, pp. 945-949, doi: 10.1109/ICCONS.2018.8663155.
[84] D. O. Anggriawan, A. Luki Satriawan, I. Sudiharto, E. Wahjono, E. Prasetyono and A. Tjahjono, "Levenberg Marquardt Backpropagation Neural Network for Harmonic Detection," *2018 International Electronics Symposium on Engineering Technology and Applications (IES-ETA)*, Bali, Indonesia, 2018, pp. 129-132, doi: 10.1109/ELECSYM.2018.8615531.
[85] S. S. Hussain, M. A. Sultan, S. Qazi and M. Ameer, "Intelligent Traffic Matrix Estimation Using LevenBerg-Marquardt Artificial Neural Network of Large Scale IP Network," *2019 13th International Conference on Mathematics, Actuarial Science, Computer Science and Statistics (MACS)*, Karachi, Pakistan, 2019, pp. 1-5, doi: 10.1109/MACS48846.2019.9024765.
[86] V. Gupta, V.K. Mishra, P. Singhal and A. Kumar, "An Overview of Supervised Machine Learning Algorithm", 2022 11th International Conference on System Modeling & Advancement in Research Trends (SMART), pp.87-92, 2022.
[87] M. T. Yildirim and B. Kurt, "Engine health monitoring in an aircraft by using Levenberg-Marquardt Feedforward Neural Network and Radial Basis Function Network," *2016 International Symposium on INnovations in Intelligent SysTems and Applications (INISTA)*, Sinaia, Romania, 2016, pp. 1-5, doi: 10.1109/INISTA.2016.7571847.
[88] D.N.Pham et al., "An Efficient Method to Predict Dengue Outbreaks in Kuala Lumpur," *3rd International Conference on Artificial Intelligence and Computer Science (AICS2015)*, Penang, Malayasia, 2015.
[89] V. Roshan Joseph, "Optimal ratio for data splitting," Statistical Analysis and Data Mining, Vol. 15, Issue 1, 2015, pp. 531–538. DOI: 10.1002/sam.11583.
[90] Z. Boger and H. Guterman, "Knowledge extraction from artificial neural network models," *1997 IEEE International Conference on Systems, Man, and Cybernetics*. Computational Cybernetics and Simulation, Orlando, FL, USA, 1997, pp. 3030-3035 vol.4, doi: 10.1109/ICSMC.1997.633051.
[91] M.J.A, Berry and G. Linoff, G. Data Mining Techniques, NY: John Wiley & SonsDeep Learning Toolbox™ Reference. Mark Hudson Beale. Martin T. Hagan. Howard B. Demuth. MATLAB 2022a.
[92] S. Karsoliya. "Approximating Number of Hidden layer neurons in Multiple Hidden Layer BPNN Architecture," *International Journal of Engineering Trends and Technology*, Vol. 3, Issue 6, 2012, pp.714-717.
[93] Deep Learning Toolbox™ User guide. Mark Hudson Beale. Martin T. Hagan. Howard B. Demuth. MATLAB 2022a.
[94] K. P. Schneider et al., "Analytic Considerations and Design Basis for the IEEE Distribution Test Feeders," *IEEE Transactions on Power Systems*, vol. 33, no. 3, pp. 3181-3188, May 2018, doi: 10.1109/TPWRS.2017.2760011.

[95] S. Monemi, T. Dent and A. Nunez, "A Model of System Protection in IEEE 14-bus Power Grid," *2022 IEEE International Conference in Power Engineering Application (ICPEA)*, Shah Alam, Malaysia, 2022, pp. 1-5, doi: 10.1109/ICPEA53519.2022.9744697.

[96] K. Moloi and A. A. Yusuff, "Moehoek 22 kV Power Distribution Feeder Reliability Assessment," *2018 IEEE PES/IAS PowerAfrica*, Cape Town, South Africa, 2018, pp. 53-57, doi: 10.1109/PowerAfrica.2018.8521020.

[97] "IEEE Guide for the Installation of Overhead Transmission Line Conductors," in IEEE Std 524-2016 (Revision of IEEE Std 524-2003) , pp.1-162, 2017, doi: 10.1109/IEEESTD.2017.7912224.

[98] A. A. Adebiyi, I. Lazaru, A. K. Saha and E. Eshiemogie Ojo, "High PV Penetration Impact on an Unbalanced Distribution Network," *2019 IEEE PES/IAS PowerAfrica*, Abuja, Nigeria, 2019, pp. 706-710, doi: 10.1109/PowerAfrica.2019.8928932.

[99] R. Varghese, R. Mathew and L. N. Shan, "Meeting additional power demand and improving power system reliability and availability," *5th Brunei International Conference on Engineering and Technology (BICET 2014)*, Bandar Seri Begawan, 2014, pp. 1-7, doi: 10.1049/cp.2014.1117.

[100] S. Ncwane, L. A. Arakkal, I. G. Mokwena and S. G. Satimburwa, "Sizing and Locating Shunt Capacitors in a Voltage Constrained South African Distribution Network," *2020 IEEE PES/IAS PowerAfrica*, Nairobi, Kenya, 2020, pp. 1-5, doi: 10.1109/PowerAfrica49420.2020.9219907.

[101] Technical Brochure, Conductors for the Uprating of Overhead Lines. Study Committee B2, CIGRE, 2004.

[102] I. S. H. Alajab, D. G. H. M. Omer and A. A. -E. E. -Z. Sam, "Comparative Study for Evacuation of Roseiries Re-Habitation 440MW Via Three Transmission Lines On Sudanese Electricity Network," *2022 International Conference on Electrical, Computer and Energy Technologies (ICECET)*, Prague, Czech Republic, 2022, pp. 1-6, doi: 10.1109/ICECET55527.2022.9872608.

[103] D.F. Hakam, R. Wahyuni and E. Y. Pramono, "Switching study for 275 kV Padang Sidempuan - Payakumbuh transmission line," *2011 International Conference on Electrical Engineering and Informatics*, Bandung, Indonesia, 2011, pp. 1-6, doi: 10.1109/ICEEI.2011.6021652.

[104] S. A. Ghani, M. S. Ahmad Khiar, I. S. Chairul, M. Y. Lada and N. H. Rahim, "Study of magnetic fields produced by transmission line tower using finite element method (FEM)," *2014 2nd International Conference on Technology, Informatics, Management, Engineering & Environment*, Bandung, Indonesia, 2014, pp. 64-68, doi: 10.1109/TIME-E.2014.7011593.

[105] S. Narain, D. Muftic, B. Jacobs and P. Naidoo, "Uprating of 275kV Lines to 400kV as Part of a Contingency Plan for Generation Integration," *2006 IEEE/PES Transmission & Distribution Conference and Exposition: Latin America*, Caracas, Venezuela, 2006, pp. 1-6, doi: 10.1109/TDCLA.2006.311548.

[106] H. Amreiz, A. Janbey and M. Darwish, "Simulation of HVAC Transmission Line," *2019 54th International Universities Power Engineering Conference (UPEC)*, Bucharest, Romania, 2019, pp. 1-6, doi: 10.1109/UPEC.2019.8893642.

[107] J. Lombard and S. Chowdhury, "Optimal Size and Placement of Independent Power Producers on MV/HV/EHV Lines For Minimizing Power Line Losses Using Artificial Neural Networks," *2022 IEEE 7th International Energy Conference (ENERGYCON)*, Riga, Latvia, 2022, pp. 1-6, doi: 10.1109/ENERGYCON53164.2022.9830217.

APPENDIX A: 22kV – 400kV Data

This appendix provides the remaining 22kV, 66kV, 132kV, 220kV, 275kV and 400kV network input and target data used for ANN training.

22kV Data

The same method used to generate 11kV network data is applied to a 22kV network: both Segment A and B use ACSR Single-Kingbird conductors per phase, having individual current ratings of 586A, with a maximum phase-to-phase separation of 1.5m. A horizontal intermediate structure geometry is used in the DIgSILENT Powerfactory simulation model, included with transposition, shown in Figure A-1. Interconnecting conductors are ACSR type Chickadee, having individual current rating of 419A. For both receiving end and IPP substations, a single transformer substation topology is used. The IPP model transfers its power via a single 20MVA 22/0.66 kV step up transformer in order to transfer the maximum export power of 8.5MW. The receiving end makes use of a single 50MVA transformer (Figure A-2).

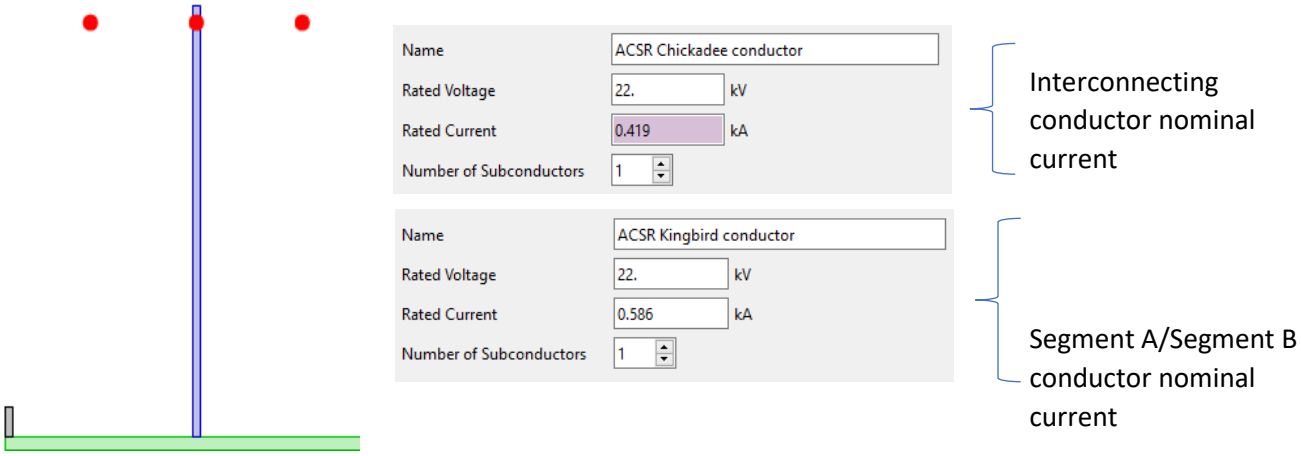

Figure A-1: 22 kV Interconnecting conductor current rating and Segment A, Segment B current rating, with horizontal intermediate structure used for the 22kV network simulation.

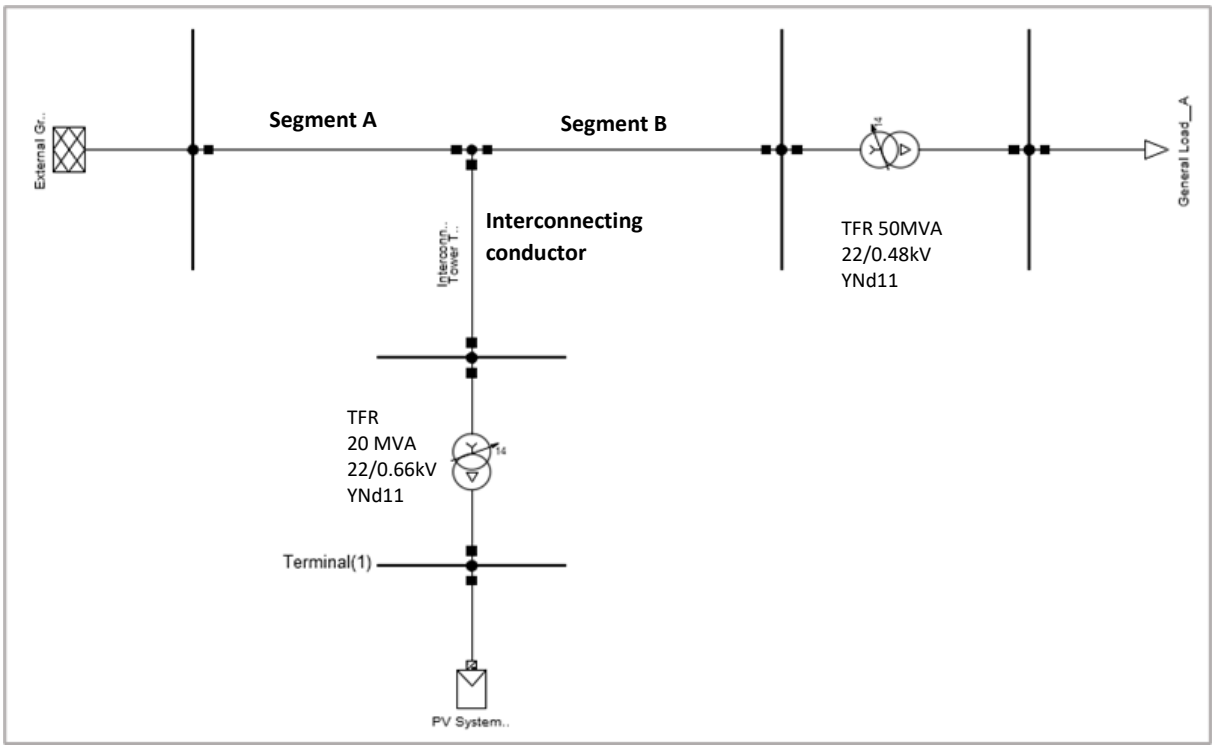

Figure A-2: 22kV network DIgSILENT Powerfactory model.

A. Interconnecting conductor location on backbone graph

The interconnecting conductor location at the POC, at a distance defined by the length of Segment A on the backbone feeder, is shown in Figure A-3. Segment A is varied in length to ensure the POC of the interconnecting feeder changes its location in equal increments corresponding to three backbone lengths of 20km (Data values 1 – 1264), 40km (Data values 1265 – 1697) and 60km (Data values 1698 – 1980).

For the 20km backbone section, three interconnecting conductor lengths of 5km, 7km and 10km are used. For the 5km interconnecting conductor section highlighted in Figure A-3 and Figure A-4, 10 different receiving end loads are applied, ranging from 2MW to 17MW. For this load range, corresponding IPP sizes are varied from 1MW to 8.5MW in 1MW increments for every 2km to 18km sweep of the POC from the sending to receiving end. This accounts for a total of 90 data points when the receiving end is loaded to 17MW (9 data points per POC sweep from sending to receiving end, with 10 IPP sizes for 9 sweep operations). This is done for a single IPP power factor setpoint.

This principle is applied to the 40km backbone (points 1265 – 1697), where the POC is located 4km from the sending end, increasing in 4km increments until Segment A is 36km in length, and also to the 60km backbone (points 1698 – 1980), where the POC is located 6km from the sending end and increased by 6km until 54km in length, for the same interconnecting feeder lengths of 5km, 7km and 10km.

Since the available maximum load is forced to be reduced for longer backbones, the set of associated maximum IPP power data values is also limited, resulting in a decreasing trend of data values, as seen from left (more data per backbone length) to right (less data per backbone length) in Figure A-4.

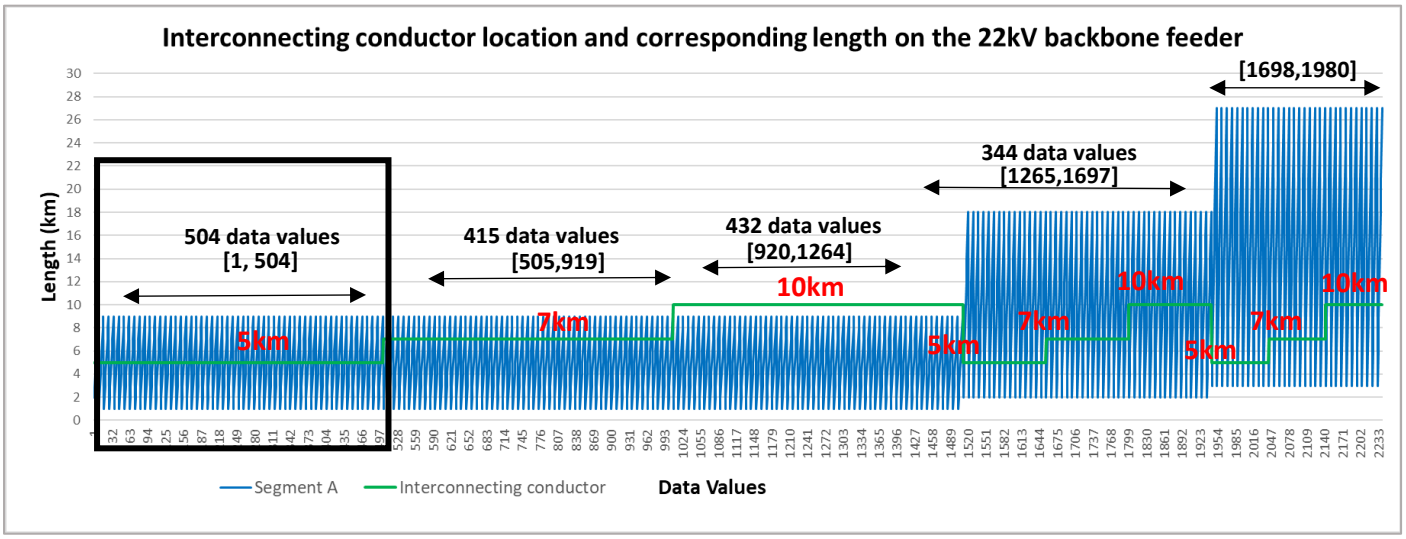

Figure A-3: 22 kV Interconnecting conductor length and location on backbone graph

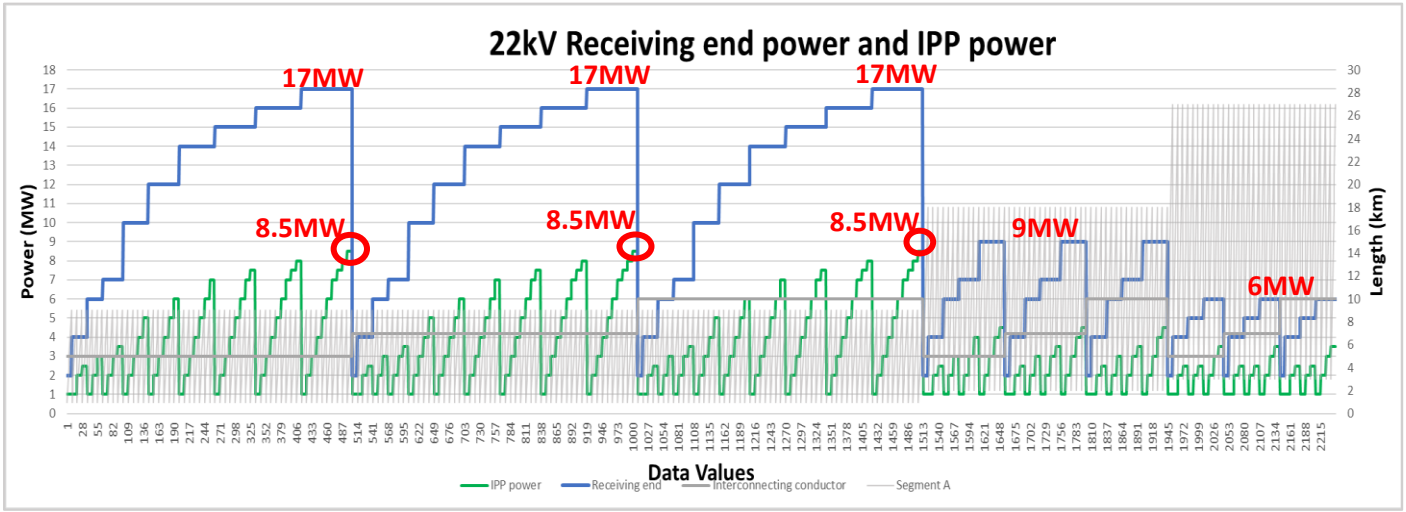

Figure A-4: 22 kV Interconnecting conductor length and its location on backbone graph, with receiving end power and IPP power curves

B Maximum MVA loading graph for the interconnecting conductor, and segments A and B of the backbone for loads operating at unity power factor.

Figure A-5 shows the sending end power required (red curve) for the 22kV network. As seen, this is the difference between load receiving end power and the power supplied by the IPP.

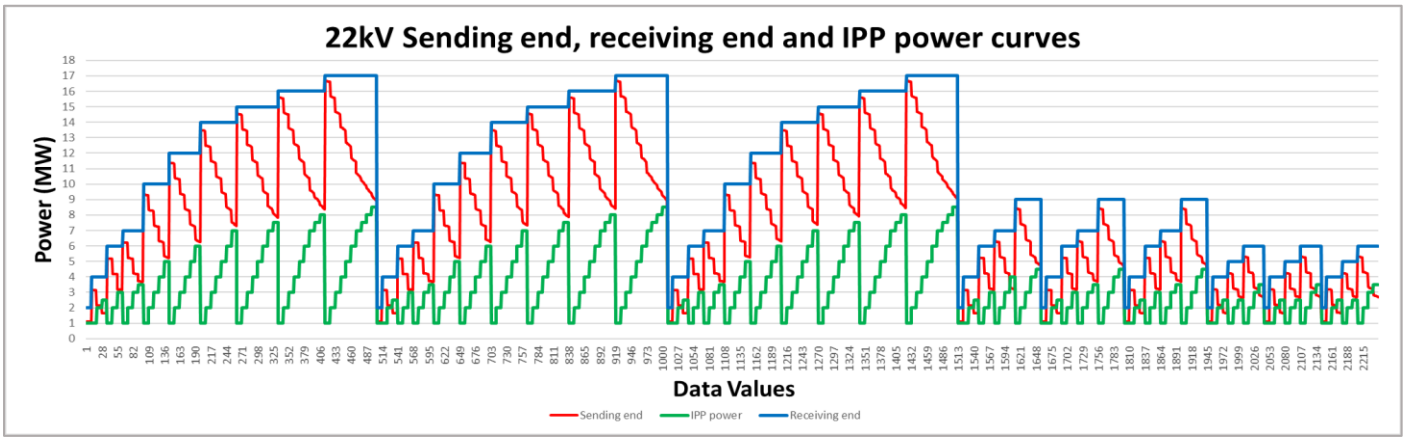

Figure A-5: 22 kV Receiving end, sending end and IPP power curves

C. Maximum and minimum voltage graphs at the load end of the network and as well as POC.

Figure A-6, Figure A-7 and Figure A-8 show the receiving end voltage, POC voltage and IPP 22kV sending voltage against Segment A lengths and the interconnecting feeder lengths for the IPP operating at unity, capacitive and inductive power factor setpoints. For both curves, the 0.975 inductive power factor setpoint of the IPP achieves the greatest increase in voltage at the receiving end and POC (as is expected). But as seen in Figures A-9 and A-10, for an increased load there is a decreased trend of voltage at both the receiving end and POC, regardless of backbone length. In addition, as the backbone length is increased, the load is forced to be reduced, in order to the ensure the POC and recieiving end voltages remain within the SAGC limit.

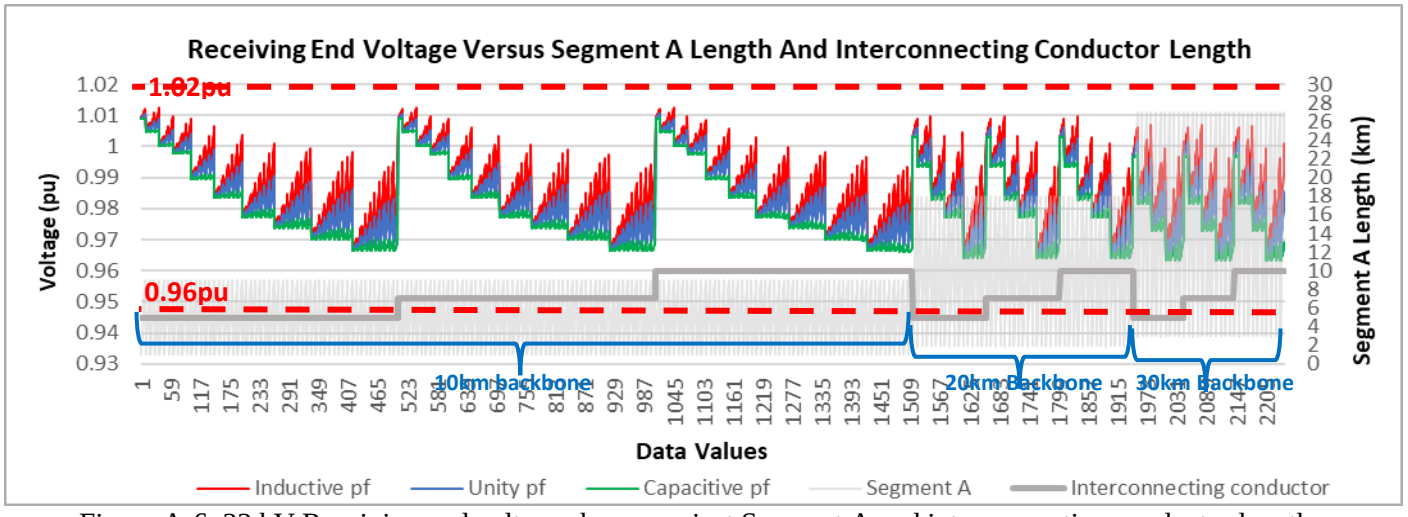

Figure A-6: 22 kV Receiving end voltage shown against Segment A and interconnecting conductor lengths

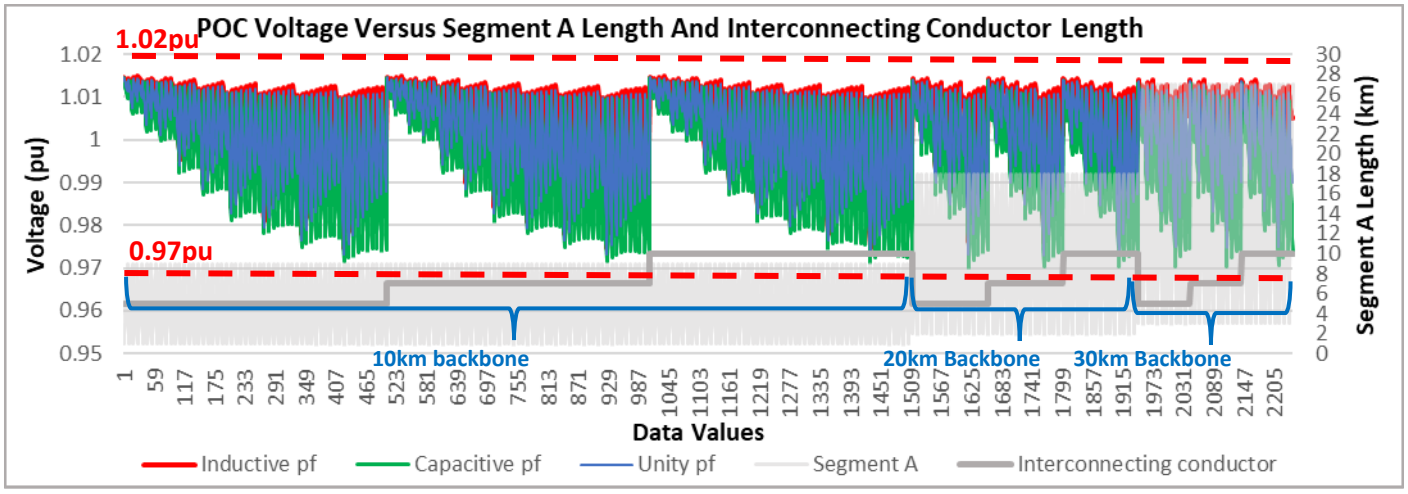

Figure A-7: 22 kV POC voltage shown against Segment A and interconnecting conductor lengths

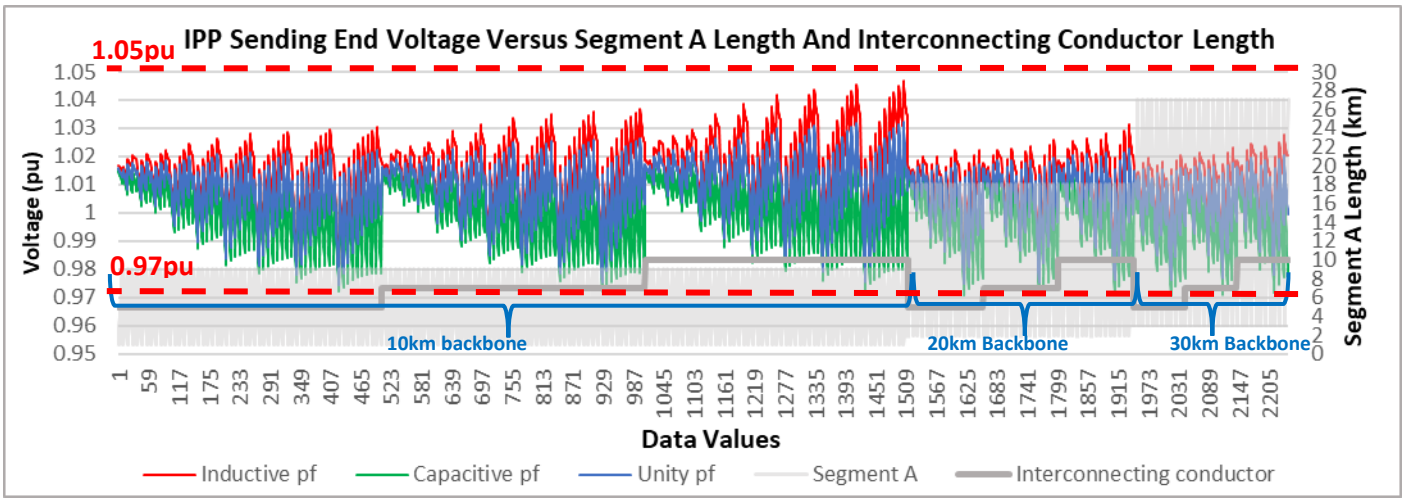

Figure A-8: 22 kV IPP sending end voltage shown against Segment A and interconnecting conductor lengths.

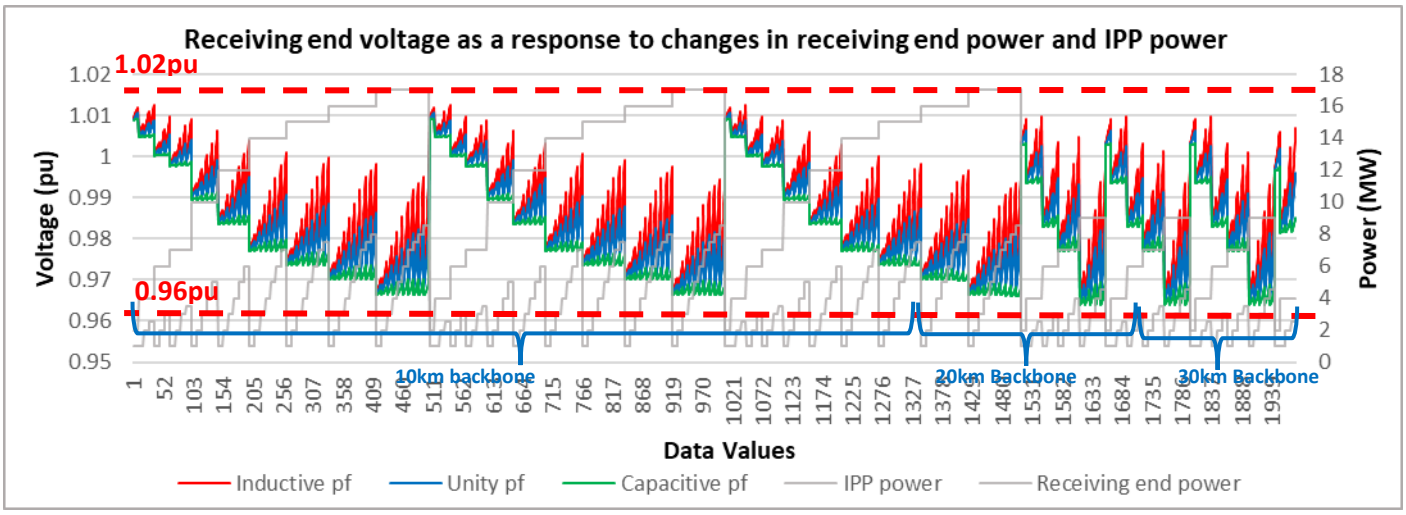

Figure A-9: 22 kV Receiving end voltage response to changes in IPP and receiving end load power.

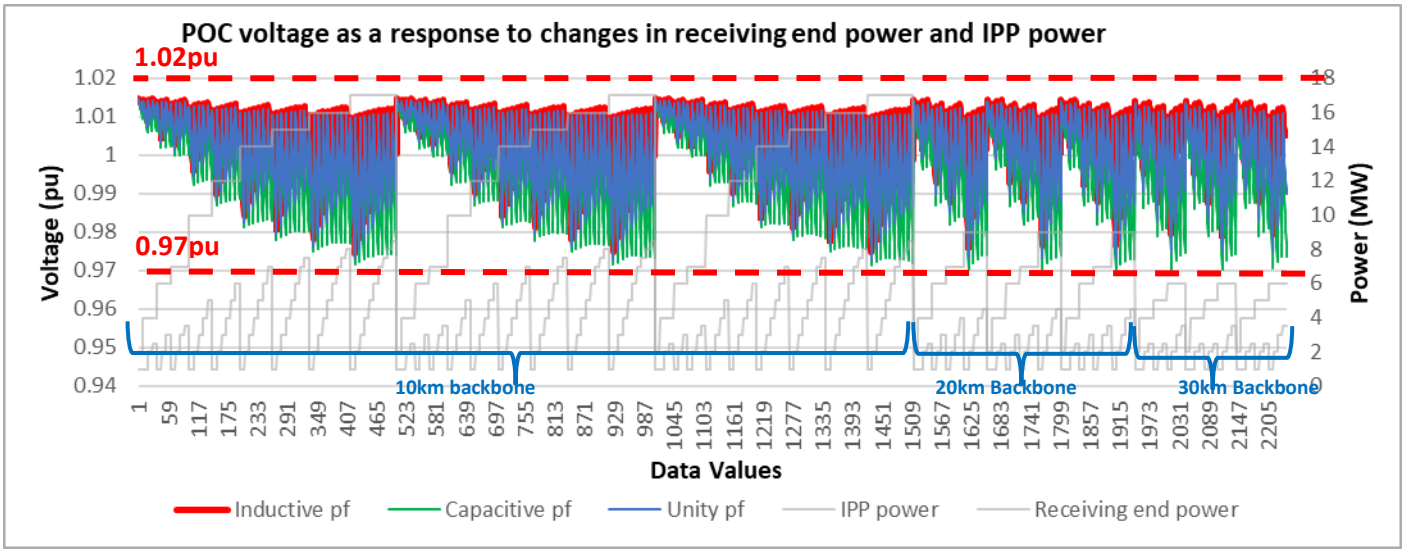

Figure A - 10: 22 kV POC voltage response to changes in IPP size receiving end load power.

D. Thermal loading graphs for interconnecting conductor, and backbone conductors (Segments A and B).

The thermal loading of the backbone (Segment A and Segment B), and the interconnecting conductor are shown by Figures A-11 to A-13. As seen, for all simulations there is again no excessive thermal stress on all conductors in the network, with the maximum loading value not exceeding 90%. Thermal loading graphs are produced for IPP setpoints of unity, 0.975 capacitive and 0.975 inductive power factors, as well as for unity power factor.

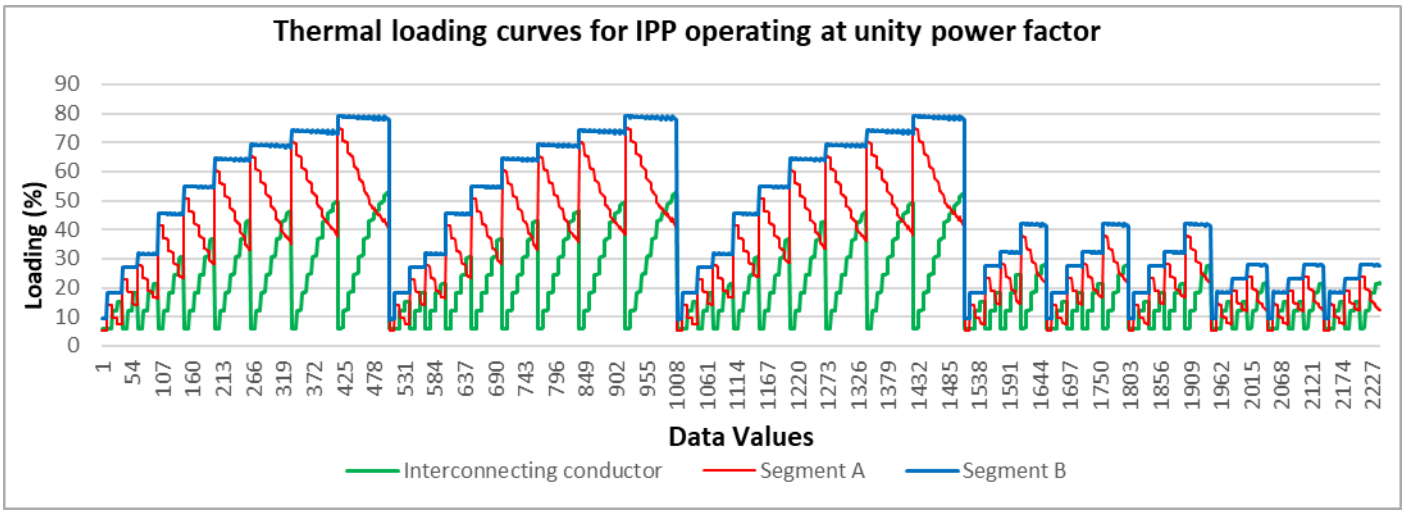

Figure A-11: 22 kV thermal loading for Segment A, Segment B and interconnecting conductor while IPP operates at unity pf

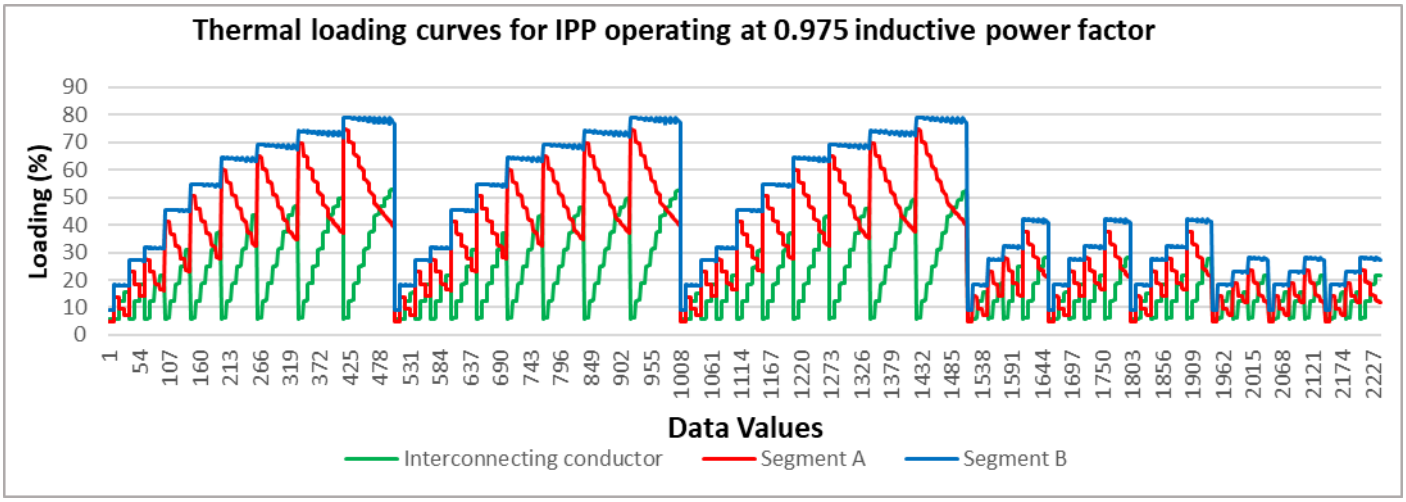

Figure A-12: 22 kV thermal loading for Segment A, Segment B and interconnecting conductor while IPP operates at 0.975 inductive pf

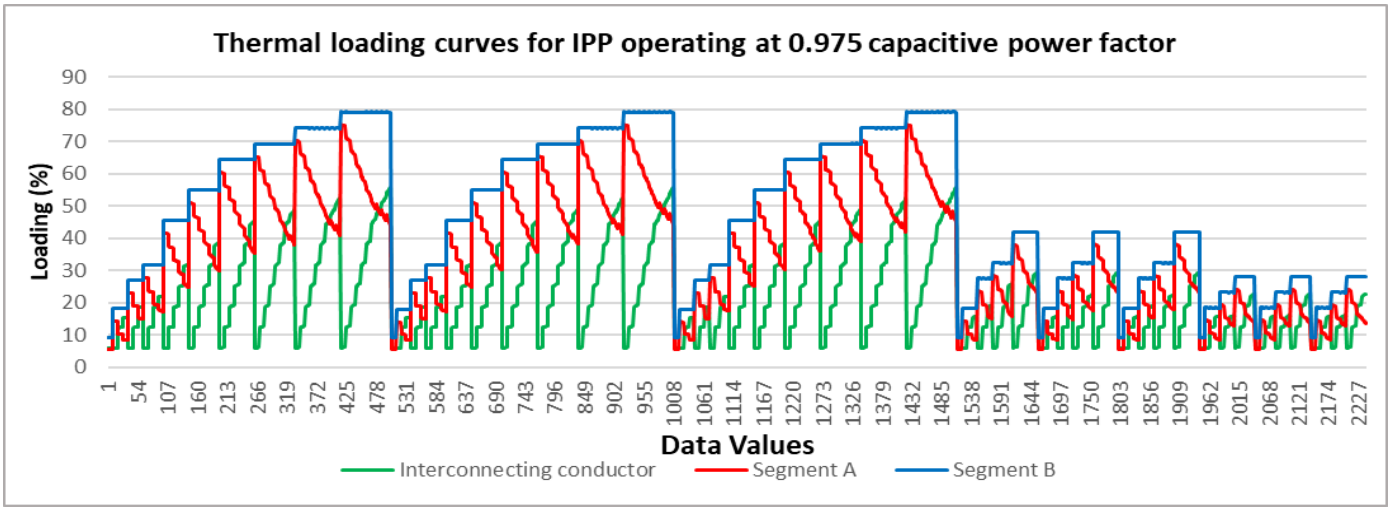

Figure A-13: 22 kV thermal loading for segment A, segment B and interconnecting conductor while IPP operates at 0.975 capacitive pf

E. Interconnecting conductor DC resistance at 20℃.

Figure A-14 shows the interconnecting conductor DC resistance at 20 deg C against IPP power. As seen, the standard Chickadee conductor is used for the interconnecting feeder at 22 kV.

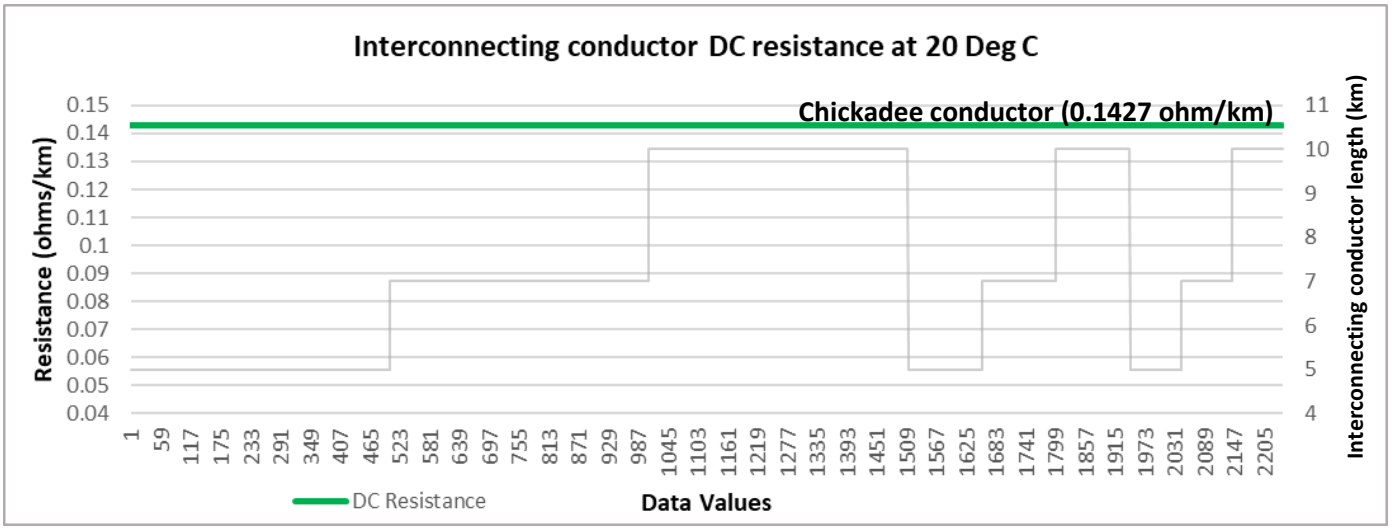

Figure A-14: 22 kV Interconnecting conductor DC resistance at 20 deg C (green), interconnecting conductor length (grey).

F. Interconnecting conductor diameter and Geometric mean radius graph.

For the 22kV interconnecting conductor, the diameter and GMR are shown in Figure A – 15.

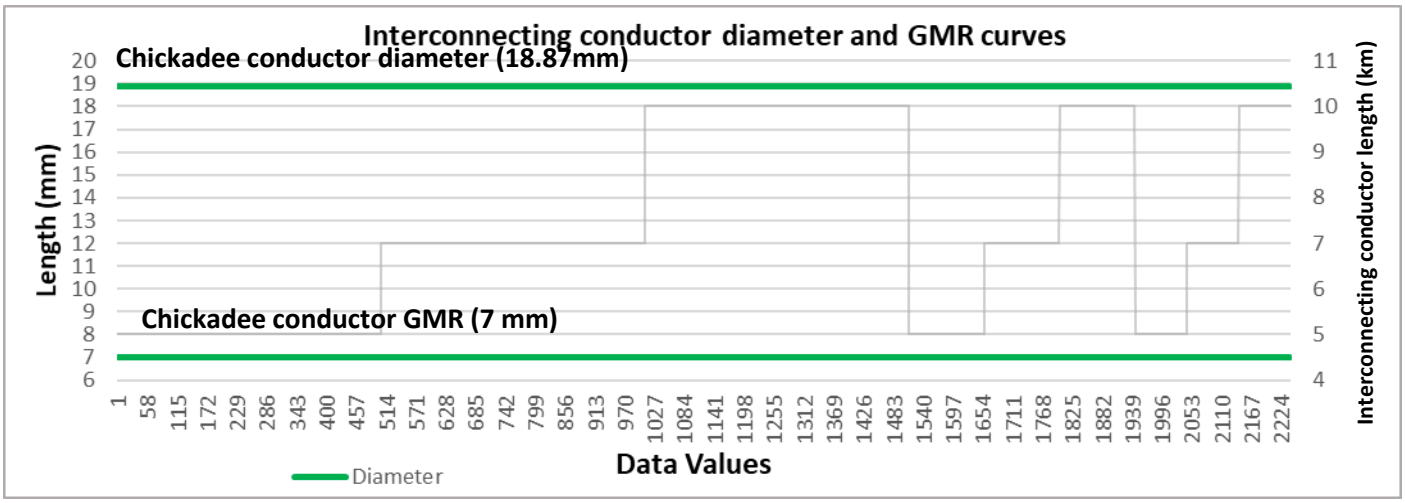

Figure A-15: 22kV Interconnecting Conductor diameter versus GMR values (green), interconnecting conductor length (grey).

G. Interconnecting conductor nominal current graph.

The interconnecting conductor nominal current values are superimposed onto the interconnecting conductor length curve as shown in Figure A-16.

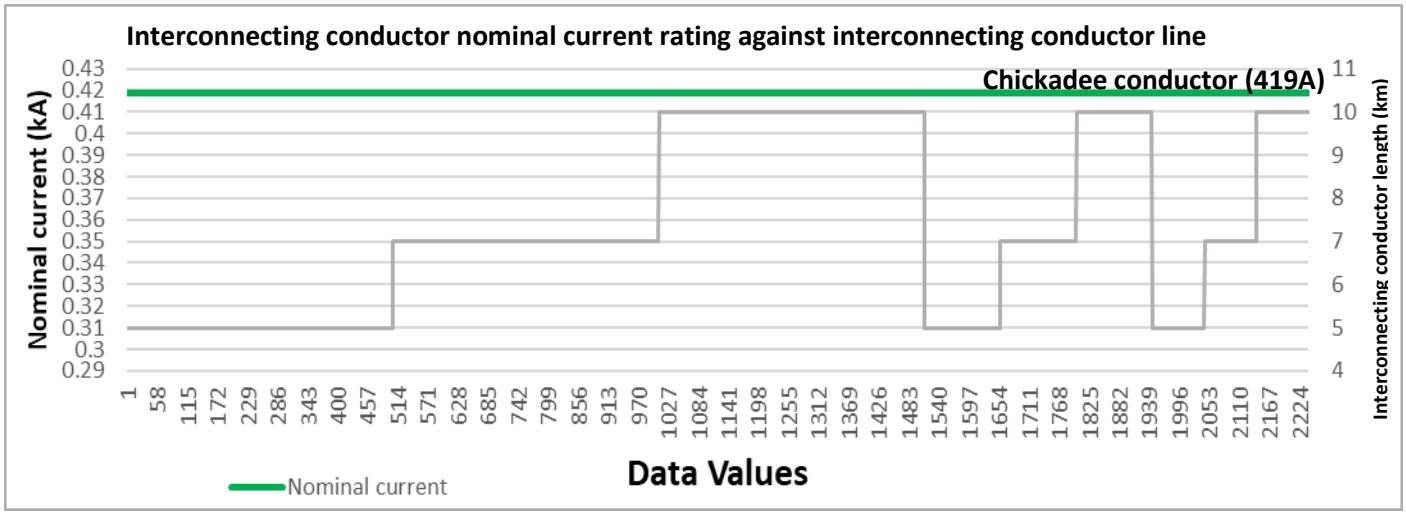

Figure A-16: 22kV interconnecting conductor nominal current rating (green) applicable to Single Chickadee conductor. Interconnecting conductor length (grey).

H. Interconnecting conductor rated power versus IPP power graph.

Figure A-17 shows the interconnecting conductor power rating and the IPP export power. This curve indicates that for all changes in IPP sizes, the interconnecting conductor rating is adequately rated to safely transfer all IPP exported power onto the network.

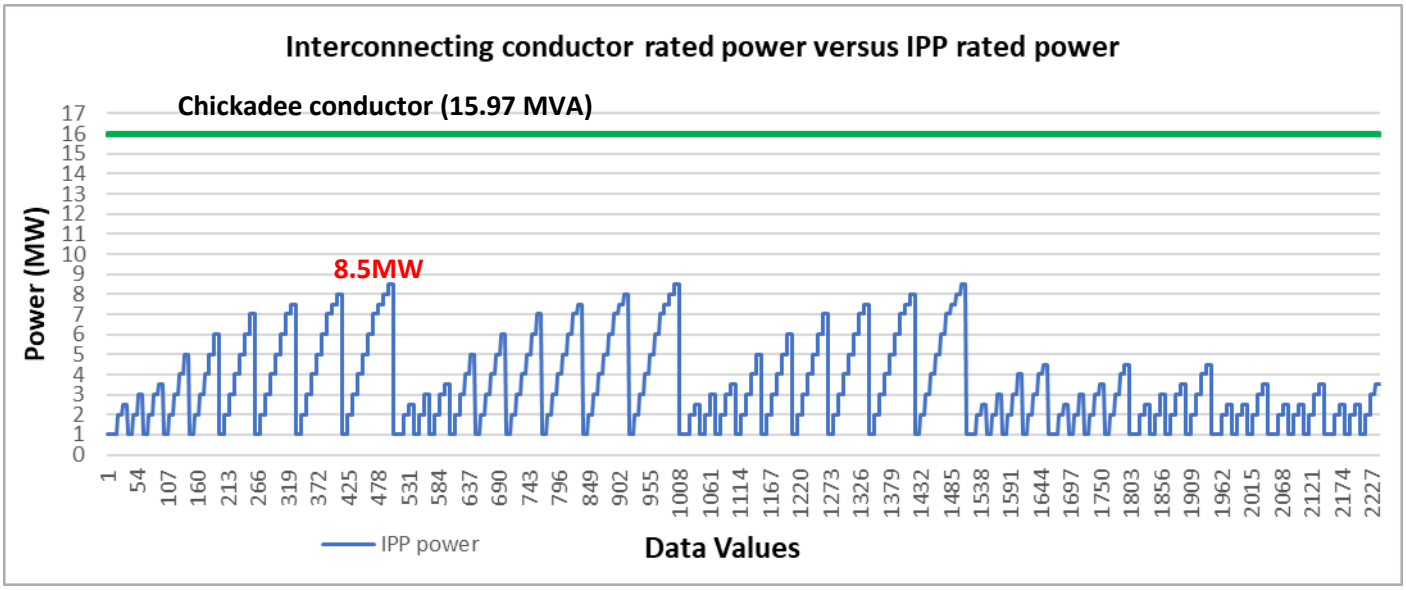

Figure A-17: 22 kV Interconnecting conductor power rating against IPP export power

I. IPP power factor variation graphs for unity, leading and lagging setpoints applicable to Category B (0.975) and Category C (0.95).

For this case, since at 22kV all IPP sizes are limited to 8.5MW (category B of the SAGC), the power factor setpoints used are as per Table 3-4 and shown in Figure 3-61.

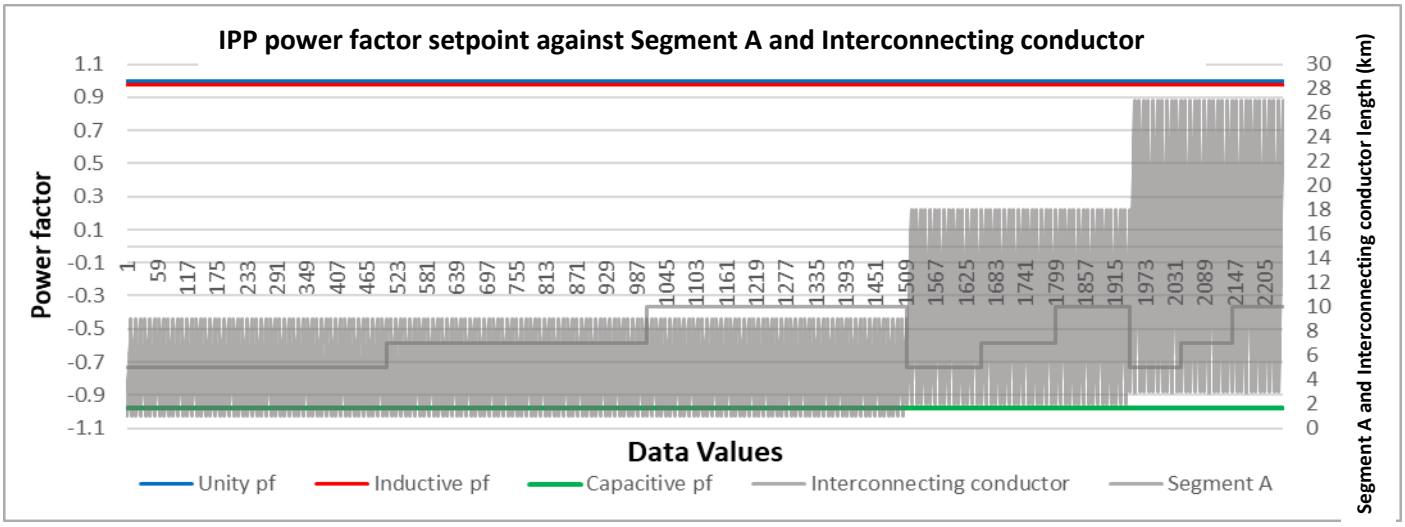

Figure A-18: 22kV IPP variations in power factor

J. Power line loss graphs corresponding to IPP power factor variation graphs.

The corresponding power line losses curves are shown in Figures A-19 to A-21.

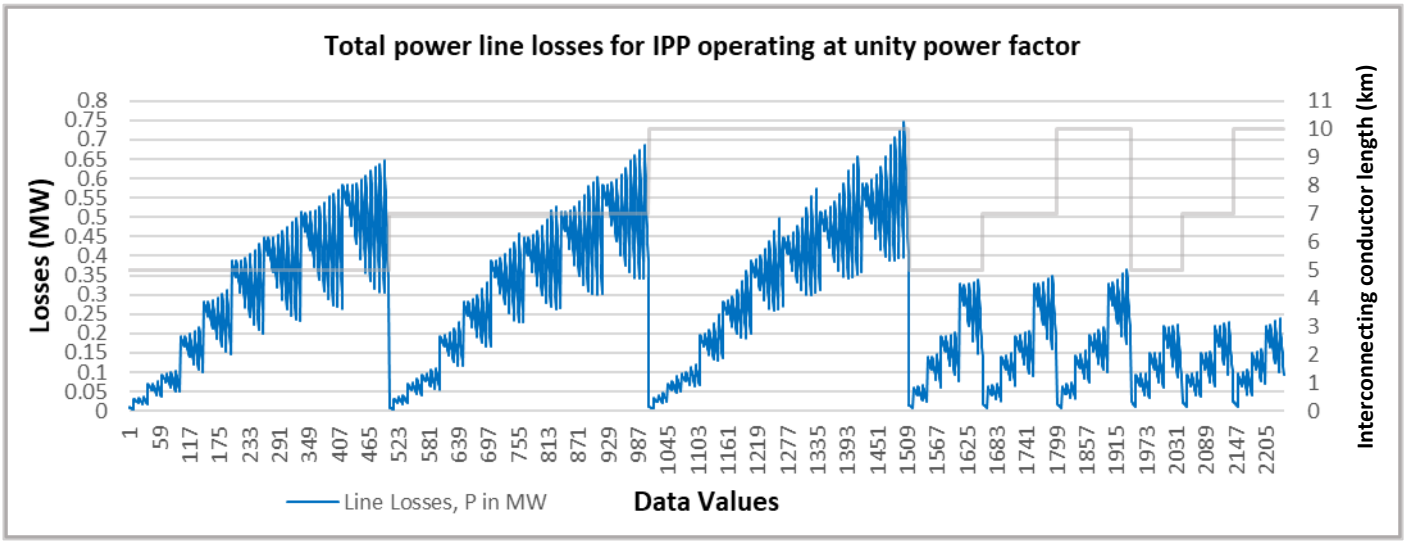

Figure A-19: 22kV Total power line losses (blue) for IPP operating at unity pf. Interconnecting conductor length (grey).

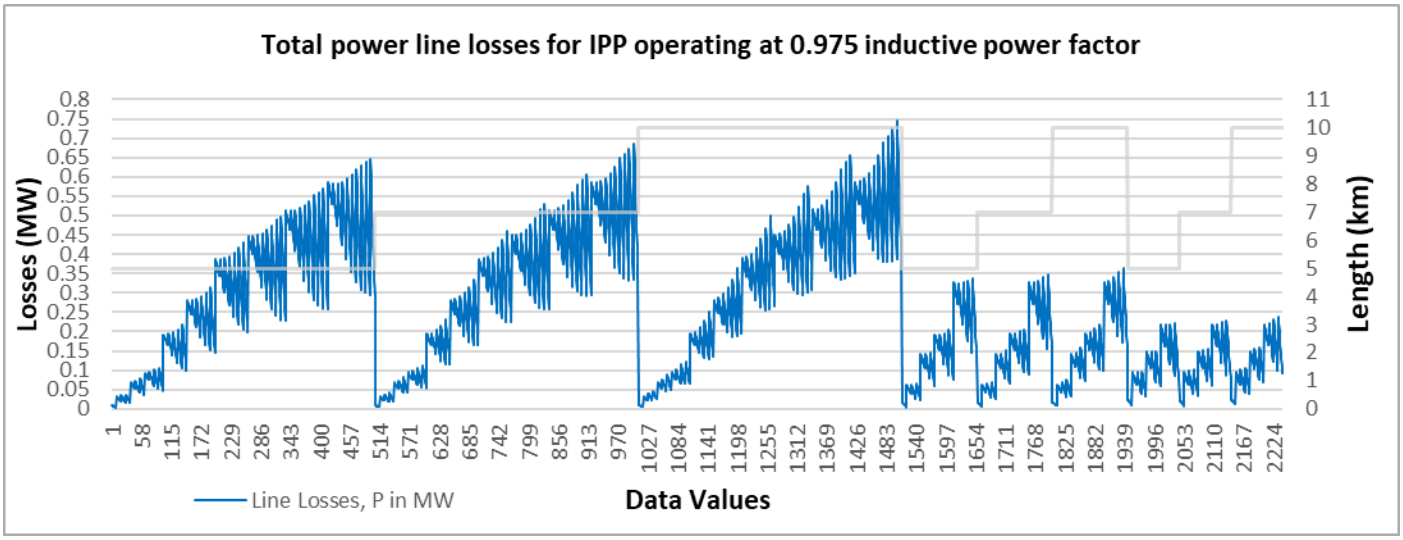

Figure A-20: 22kV Line losses (blue) for IPP operating at 0.975 inductive pf. Interconnecting conductor length (grey).

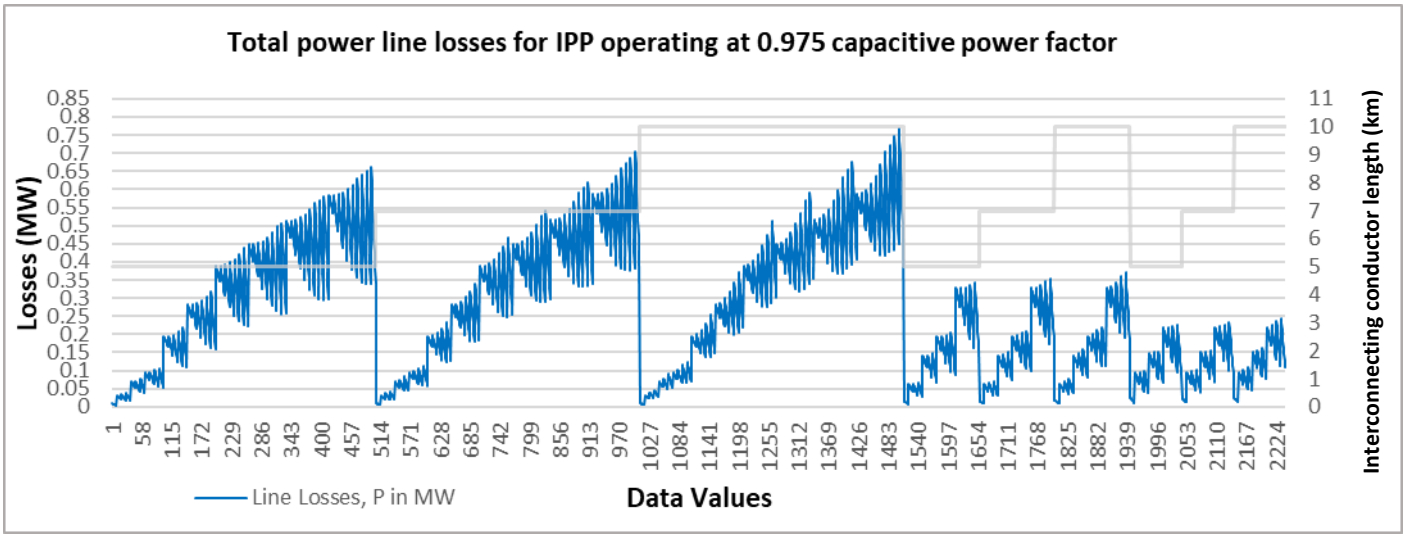

Figure A-21: 22kV Line losses (blue), for IPP operating at 0.975 capacitive pf. Interconnecting conductor length (grey).

For the 22kV technology, data shown from Sections (A) – (J) above is saved into three 2241x8 input data matrices, one representing the unity power factor IPP setpoint, another representing the 0.975 lagging IPP setpoint, and another representing the 0.975 leading power factor setpoint. When combined, a 6723 x 8 input data matrix (2241x3) is saved along with a 6723x1 target data matrix, and these will be used in the ANN design and modelling section to follow in Section 3.3. In order to capture losses for the scenarios in which the load is non-unity, the above simulations are redone in the same fashion as before, but for a receiving end (load) power factor setpoint of 0.975 (inductive) as well as 0.975 (capacitive). This means that the combined input data matrix to be used in the ANN design and modelling section expands in size from 6723x8 to 20169x8 and a target data size of 20169x1.

66 kV Data

For the 11 kV and 22 kV networks, IPPs are limited to category B (< 20 MW) of the SAGC. This requires a power factor setpoint limit of 0.975 for both inductive (+0.975) and capacitive (-0.975) modes of operation. For 66 kV and higher, both Category B ($\pm$0.975 for IPP Size < 20 MW) and Category C ($\pm$0.95 for IPP Size > 20 MW) are introduced. This is because as the load increases beyond 40MW, the maximum IPP size will also increase beyond 20 MW (in order to maintain 50% of 40MW load), requiring a power factor change from $\pm$0.975 to $\pm$0.95. A third power factor set point of unity will again be included, as was done for 11 kV and 22 kV, in order to have a more comprehensive data set. This means that there will still be three power factor operating modes: one for the IPP at unity, one for the IPP at (0.975/0.95) capacitive and one for the IPP at (0.975/0.95) inductive, with the value of 0.975 or 0.95 assigned depending on the IPP size. Loading at the receiving end is also increased to 45MW, with a corresponding maximum IPP export capacity of 28MW for backbone lengths up to 40km. For backbone lengths of 60km, 30MW is applied to the receiving end with a

corresponding maximum IPP export capacity of 16.5MW. Backbone lengths of 80km and 100km are loaded to 25MW and 19MW respectively with maximum IPP export power of 14MW and 13MW, respectively. 120km and 140km backbones are loaded to 15MW with maximum IPP power of 10MW.

For all cases, both Segment A and Segment B use ACSR Twin-Berfort conductors per phase, having individual current ratings of 965A (1.93 kA per phase). Sub conductor bundle separation distances are set to 200mm, with a maximum phase-to-phase separation of 3m. A horizontal geometry is used in the DIgSILENT Powerfactory simulation model, included with transposition as shown in Figure A-22. Interconnecting conductors are ACSR type Twin-Kingbird and Single Kingbird, having individual current ratings of 586A respectively. Twin-Kingbird conductors are used for the integration of IPPs up to 32MW – which only apply to backbone lengths up to 60km, while Single Kingbird conductors are used for the integration of IPPs of lower capacity which apply to backbone lengths greater than 60km. For both receiving end and IPP substations, a single transformer substation topology is used.The IPP model transfers its power via a single 50MVA 66/22kV step up transformer in order to transfer the maximum export power of 28MW. This is used to ensure that the IPP sending end voltage is controlled within required pu limit. The receiving end makes use of a single 100MVA transformer (Figure A-23).

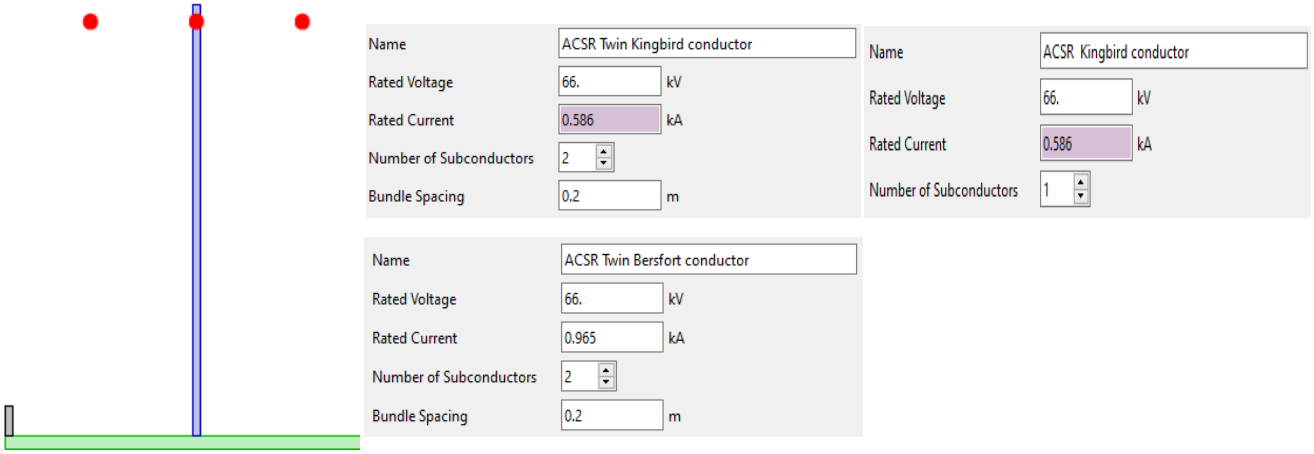

Figure A-22: 66 kV Interconnecting conductor current rating and Segment A, Segment B current rating, with horizontal intermediate structure used for the 66kV network simulation.

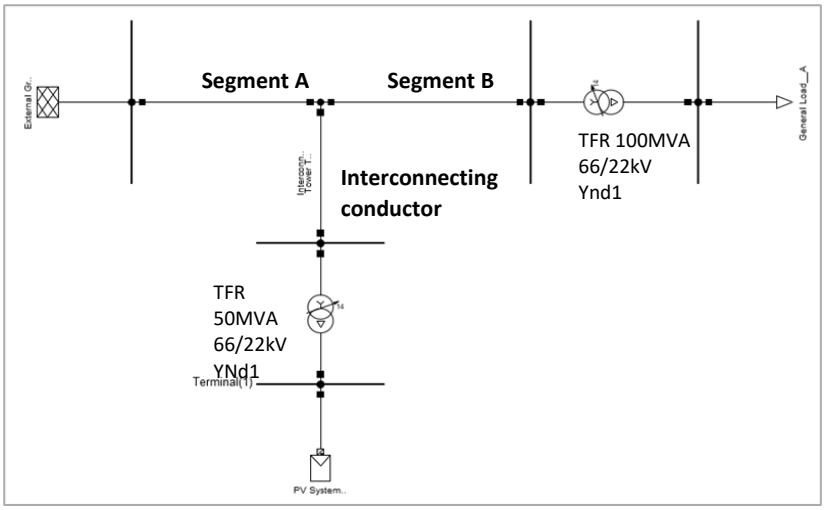

Figure A-23: 66 kV network DIgSILENT Powerfactory model

A. Interconnecting conductor location on backbone graph

Figure A-24 shows changes in Segment A length to ensure the POC of the interconnecting feeder changes its location in equal increments corresponding to six backbone lengths of 20 km (Data values 1 – 3996), 40 km (Data values 3997 – 7992), 60 km (Data values 7993 – 11070), 80 km (11071 - 13338), 100 km (13339 - 14958) and 120 km (14959 - 16038) respectively.

All backbone lengths have 6 different interconnecting conductor lengths connecting to the POC. Interconnecting conductor lengths used are 6km, 13km, 20km, 26km,33km and 40km in length. This divides every backbone length into 6 sets, one set for every interconnecting conductor length. Within each set, different receiving end loads are applied (Figure A-24). As seen, for the 20km backbone, the first set of six corresponds to an interconnecting conductor length of 6km, which has associated loads ranging from 5 MW to 45 MW (Data values 1 – 3996). For the 60km backbone, the first of six sets also corresponds to an interconnecting conductor length of 6km and has associated loads that range from 5 MW to 30 MW (Data values 7933 – 11070). For the 120km backbone, the first of six sets correspond to an interconnecting conductor length of 6km has associated loads that range from 5 MW to 15 MW (Data values 14960 – 16038). As was previously done, each IPP size is assigned a value for exactly 9 data points at a time as the POC moves from the sending to the receiving end on the backbone. For the 20km backbone, load values and IPP sizes are summarized in point form below, to ensure that the correct POC voltage and receiving end voltage is within the limits stipulated within the SAGC:

- 5 MW loads:27 data values, IPP sizes of 1 MW, 2 MW 3 MW, each occupying 9 data points.
- 10 MW loads:45 data values, IPP sizes of 1 MW, 2 MW 3 MW, 4 MW and 5 MW, each occupying 9 data points.
- 15 MW loads:45 data values, IPP sizes 2 MW – 10 MW in 2MW steps, each occupying 9 data points.
- 20 MW loads:63 data values, IPP sizes 2 MW – 14 MW in 2MW steps, each occupying 9 data points.
- 25 MW loads:90 data values, IPP sizes 2 MW – 14 MW in 2MW steps, each occupying 9 data points.
- 30 MW loads:108 data values, IPP sizes 2 MW – 24 MW in 2MW steps, each occupying 9 data points.
- 35 MW loads:135 data values, IPP sizes 2 MW – 26 MW in 2MW steps, each occupying 9 data points.
- 45 MW loads:153 data values, IPP sizes 2 MW – 28 MW in 2MW steps, each occupying 9 data points.

This principle is applied to the 40km backbone, where the POC starts at 4km from the sending end, increasing in 4km increments until Segment A is 36km in length; and to the 60km backbone, where the POC is located 6km from the sending end and increased by 6km until 54km in length, up until the backbone is 120km in length. As seen in Figure A-25, as the backbone increases in length, the load at the receiving end decreases in magnitude in order for the voltage at the POC and receiving end to be SAGC compliant.

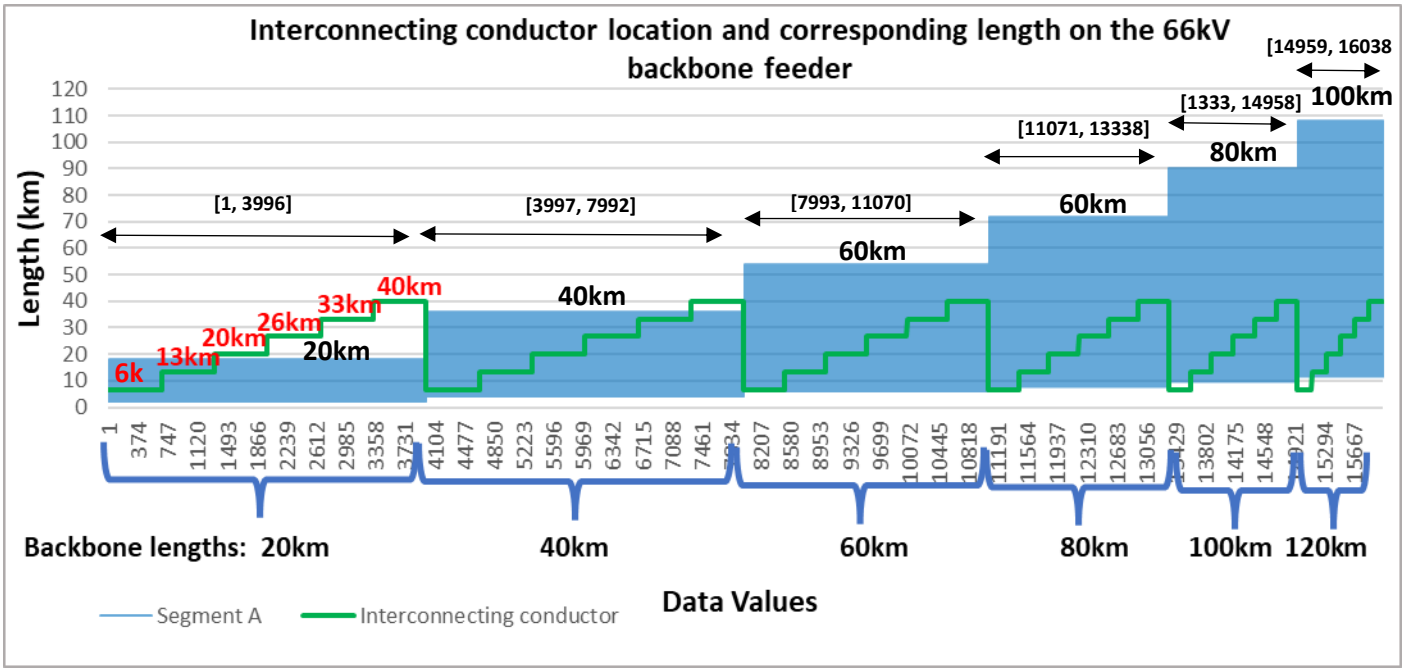

Figure A 24: 66kV interconnecting conductor length and backbone length data.

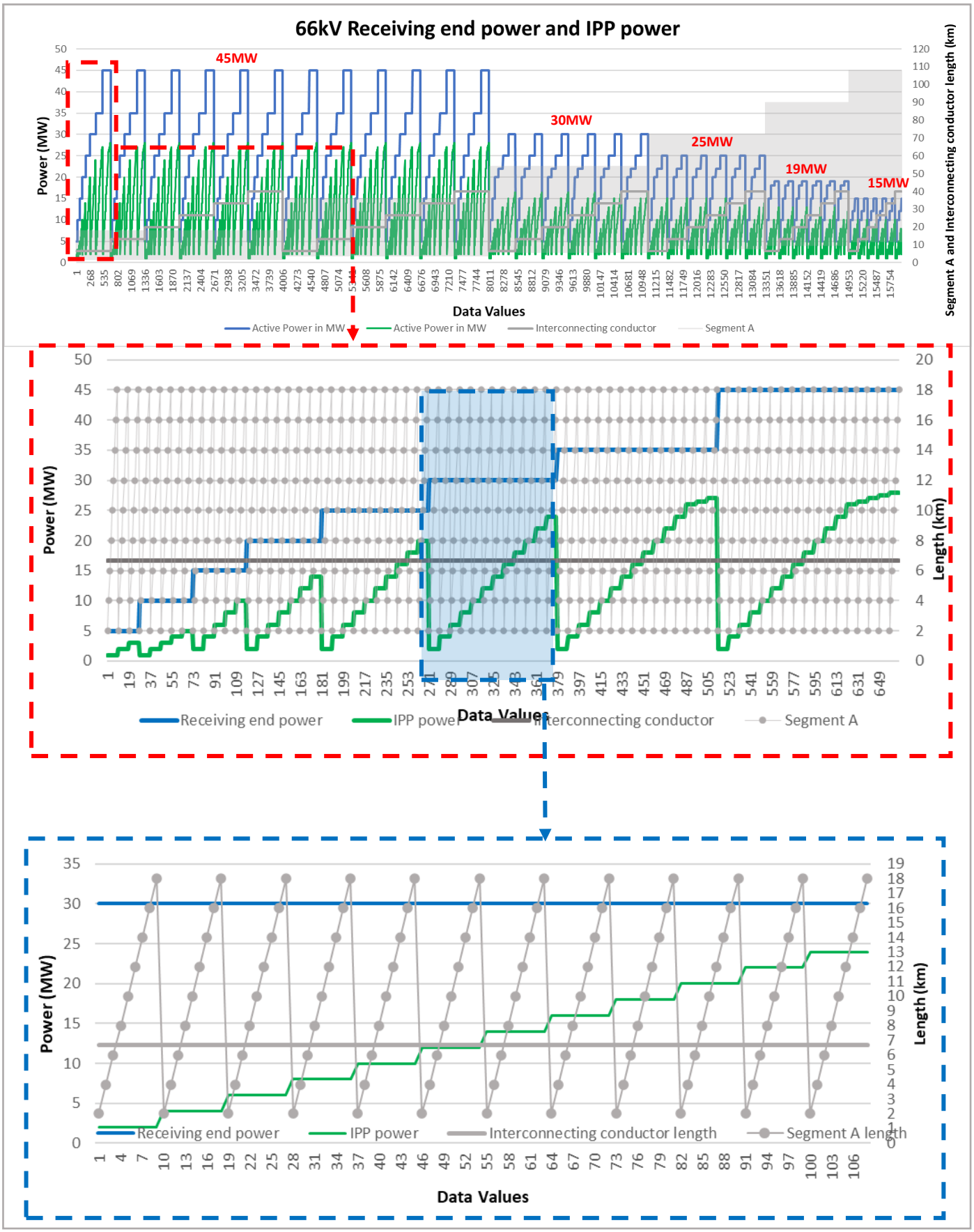

Figure A-25: 66 kV Interconnecting conductor length (grey solid line) and its location on backbone graph (grey dotted line), with receiving end power (blue) and IPP power curves (green).

B Maximum MVA loading graph for the interconnecting conductor, and Segments A and B of the backbone for loads operating at unity power factor.

Figure A-26 shows the sending end power required (red curve) for the 66kV network. As seen again, this is the difference between load receiving end power and the power supplied by the IPP.

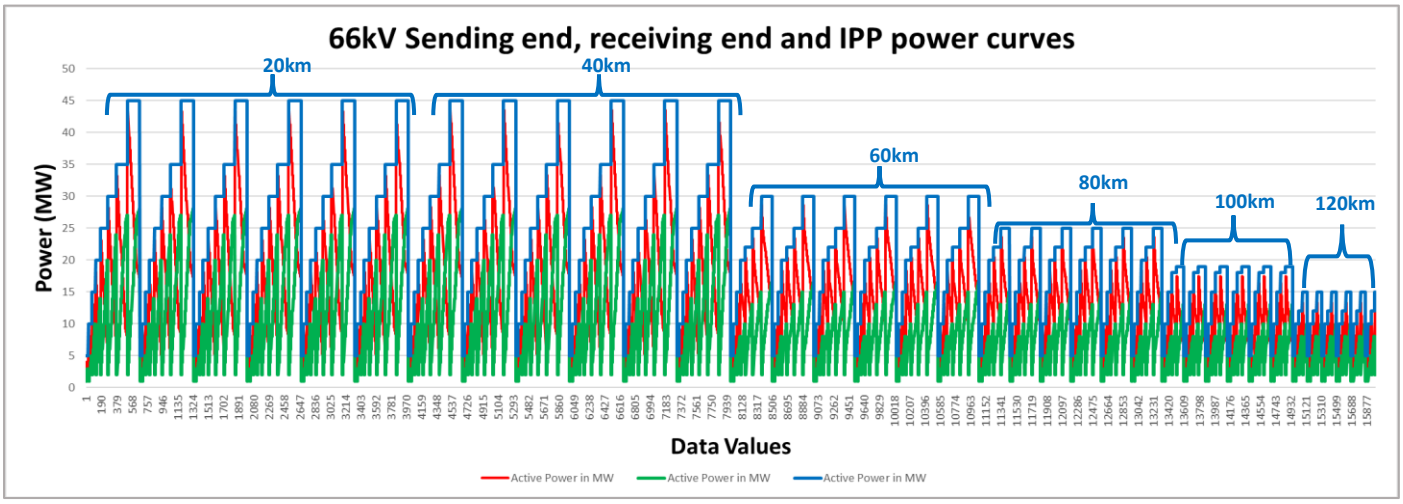

Figure A-26: 66 kV Receiving end, sending end and IPP power curves.

C. Maximum and minimum voltage graphs at the load end of the network and as well as POC.

Figure A-27, Figure A-28 and Figure A-29 show the receiving end, POC and 66kV IPP sending end voltage graphs against Segment A lengths and the interconnecting feeder lengths for the IPP operating at unity, capacitive and inductive power factor setpoints. For all curves, the inductive power factor setpoint corresponding to all IPPs (regardless of size), achieves the greatest increase in voltage at the receiving end and POC (as is expected). But as seen in Figures 3-30 to 3-31, for an increased load there is a decreased trend of voltage at both the receiving end and POC, regardless of backbone length. In addition, as the backbone length is increased, the load is forced to be reduced in order to the ensure the POC and receiving end voltages remain within the SAGC limit.

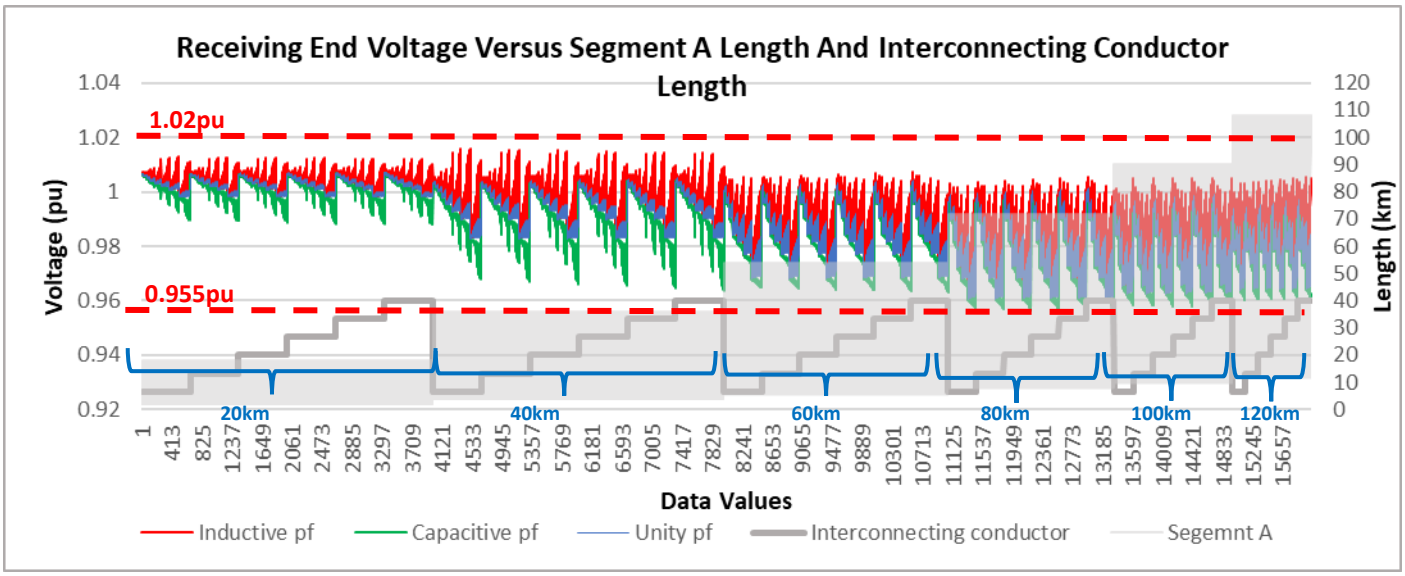

Figure A-27: 66 kV Receiving end voltage as a response to changes in IPP Sizes with varying power factor setpoints.

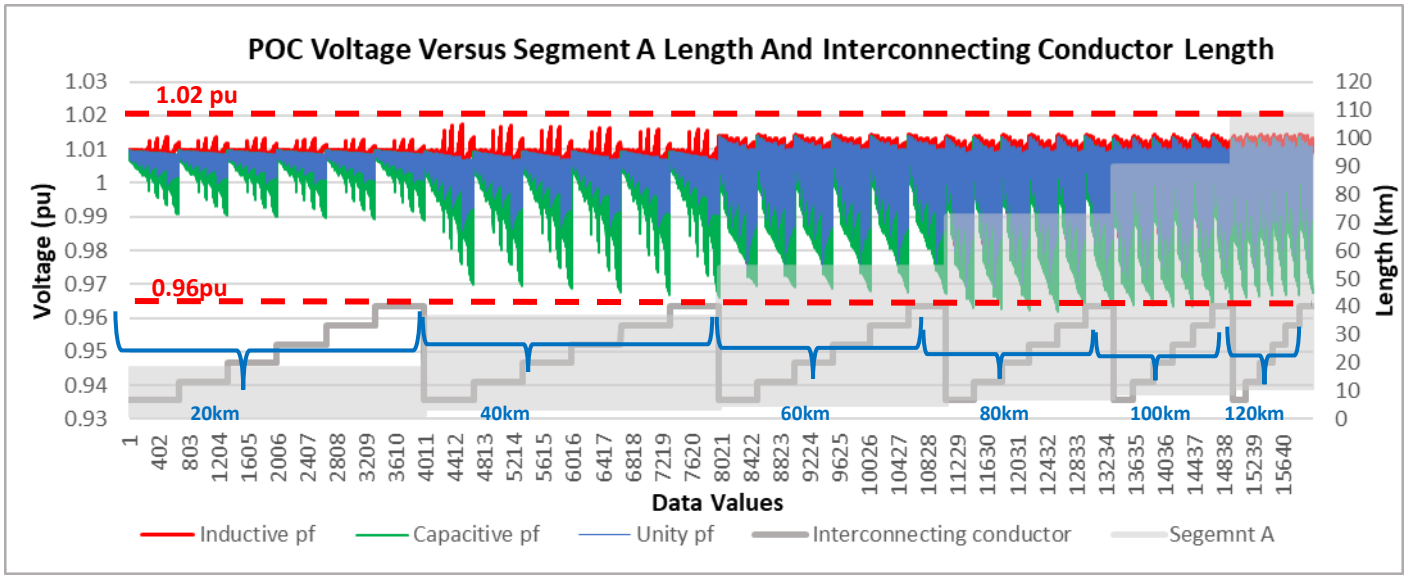

Figure A-28: 66 kV POC voltage as a response to changes in IPP Sizes with varying power factor setpoints

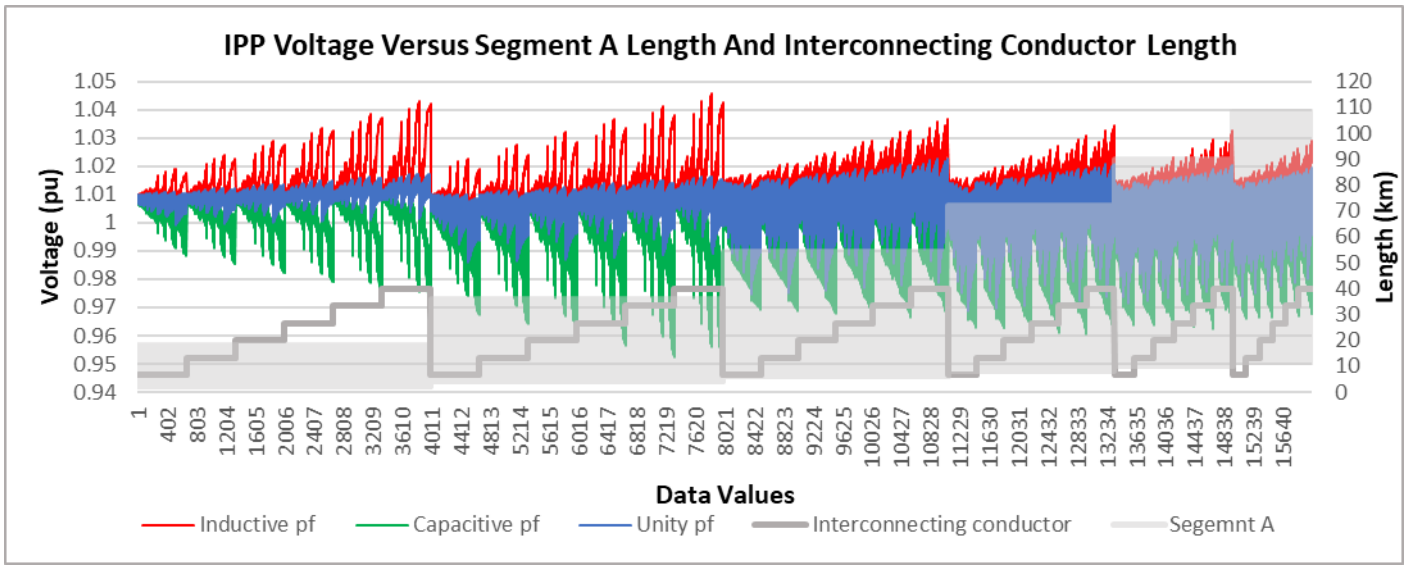

Figure A-29: 66 kV IPP Sending End Voltage Versus Segment A Length And Interconnecting Conductor Length

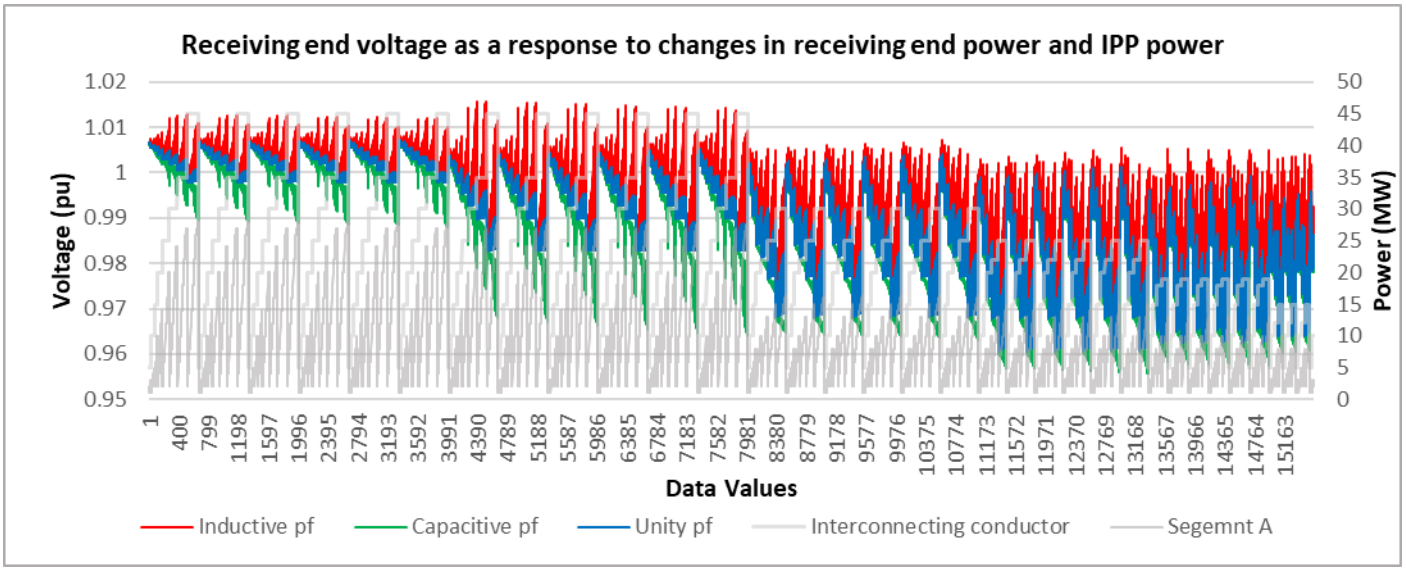

Figure A-30: 66 kV Receiving end voltage response to changes in IPP size.

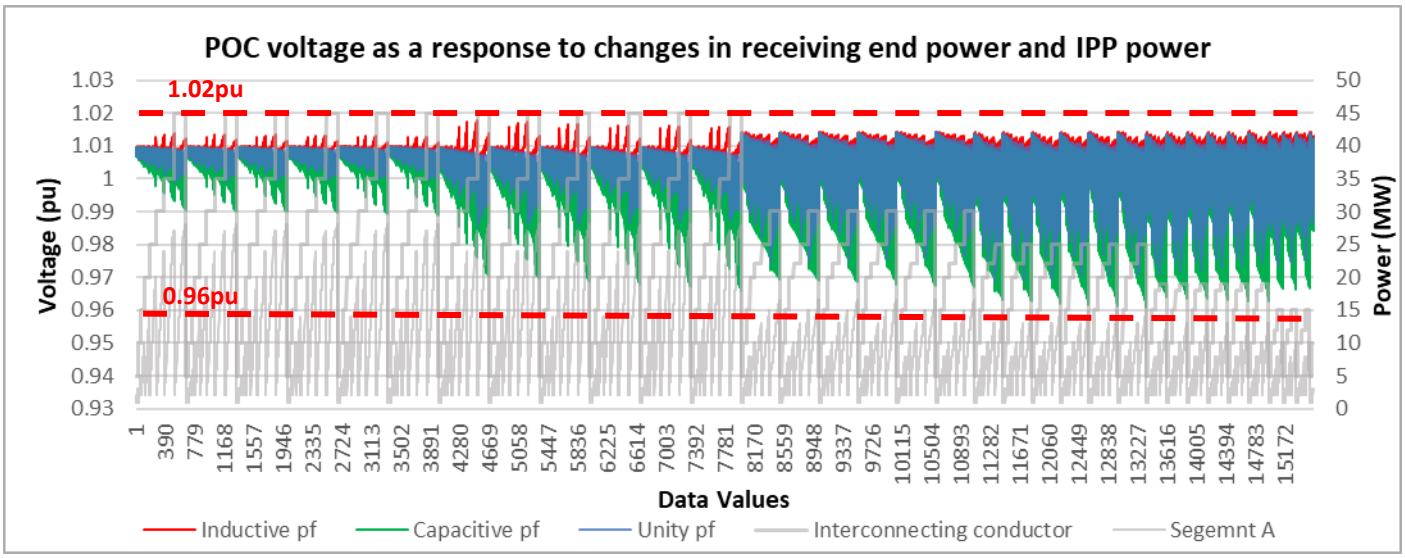

Figure A - 31: 66 kV POC voltage response to changes in load demand and IPP power.

D. Thermal loading graphs for interconnecting conductor, and backbone conductors (Segments A and B).

The thermal loading of the backbone (Segment A and Segment B), and the interconnecting conductor are shown by Figures A-32 to 3-34. As seen, for all simulations, there is again no excessive thermal stress on all conductors in the network, with the maximum loading value not exceeding 90%. Thermal loading graphs are produced for IPP setpoints of unity, 0.975 capacitive and 0.975 inductive power factors, as well as for unity power factor.

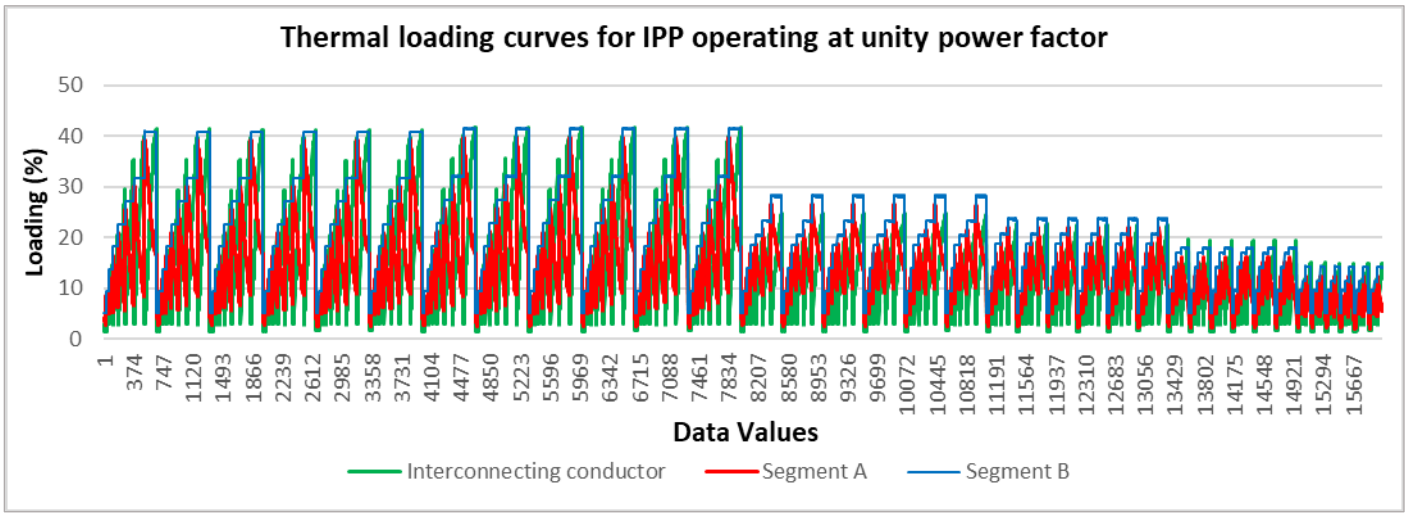

Figure A-32: 66kV thermal loading for Segment A, Segment B and interconnecting conductor while IPP at unity pf

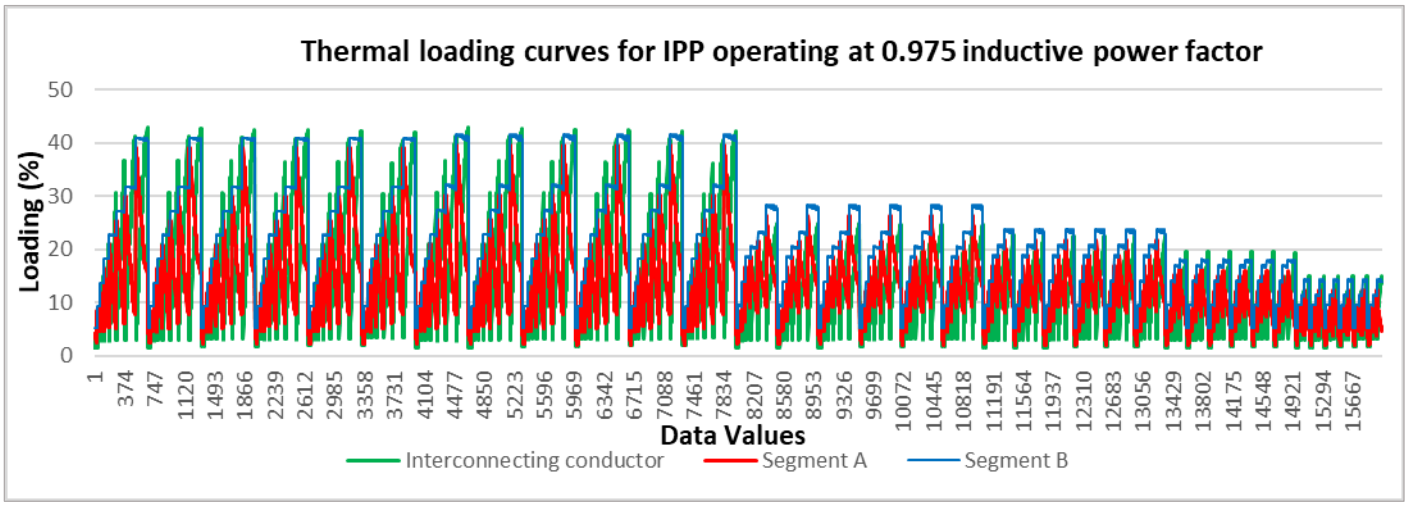

Figure A-33: 66kV thermal loading for Segment A, Segment B and interconnecting conductor while IPP operates at inductive pf

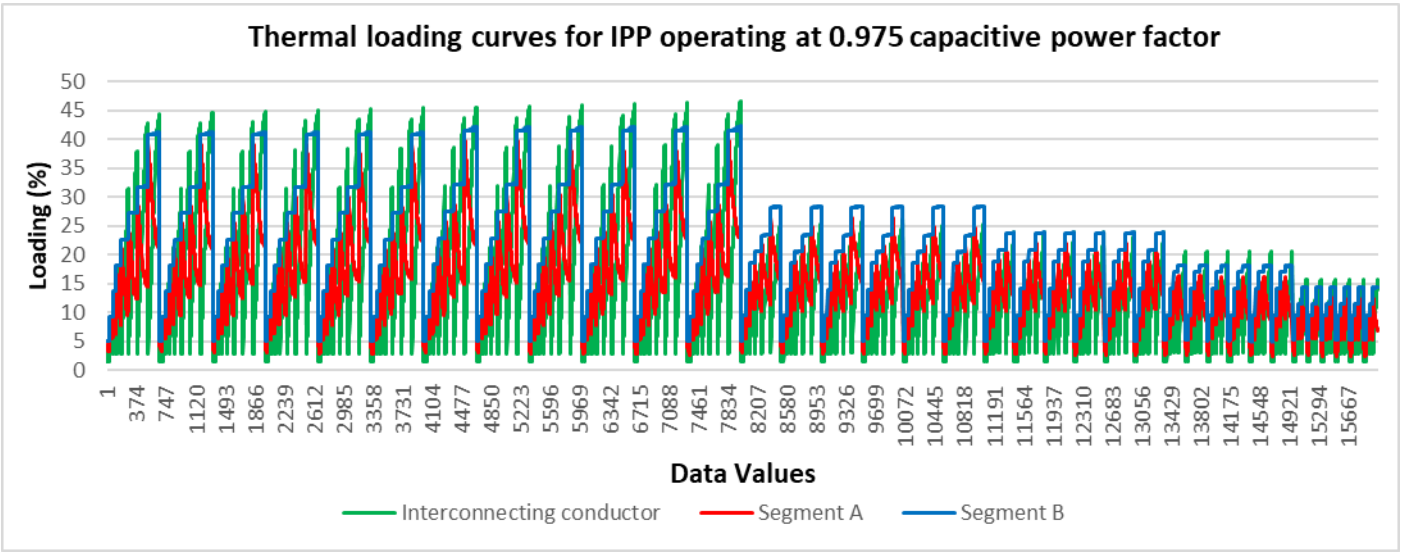

Figure A-34: 66kV thermal loading for Segment A, Segment B and interconnecting conductor while IPP operates at capacitive pf

E. Interconnecting conductor DC resistance at 20℃.

Figure A-35 shows the interconnecting conductor DC resistance at 20 deg. As seen, the standard Twin Kingbird and Single Kingbird conductors are used for the interconnecting feeder at 66kV.

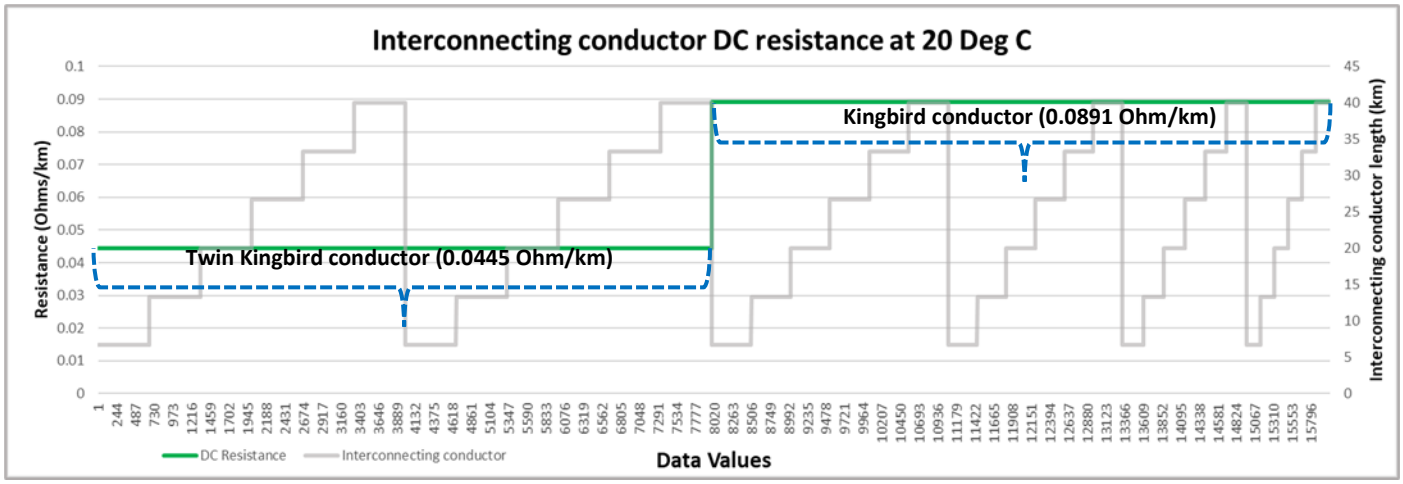

Figure A-35: 66kV Interconnecting conductor DC resistance (green) at 20 deg C, Interconnecting conductor length (grey).

F. Interconnecting conductor diameter and Geometric mean radius graph.

For the 66kV interconnecting conductor, the diameter and GMR are plotted as shown in Figure A – 36.

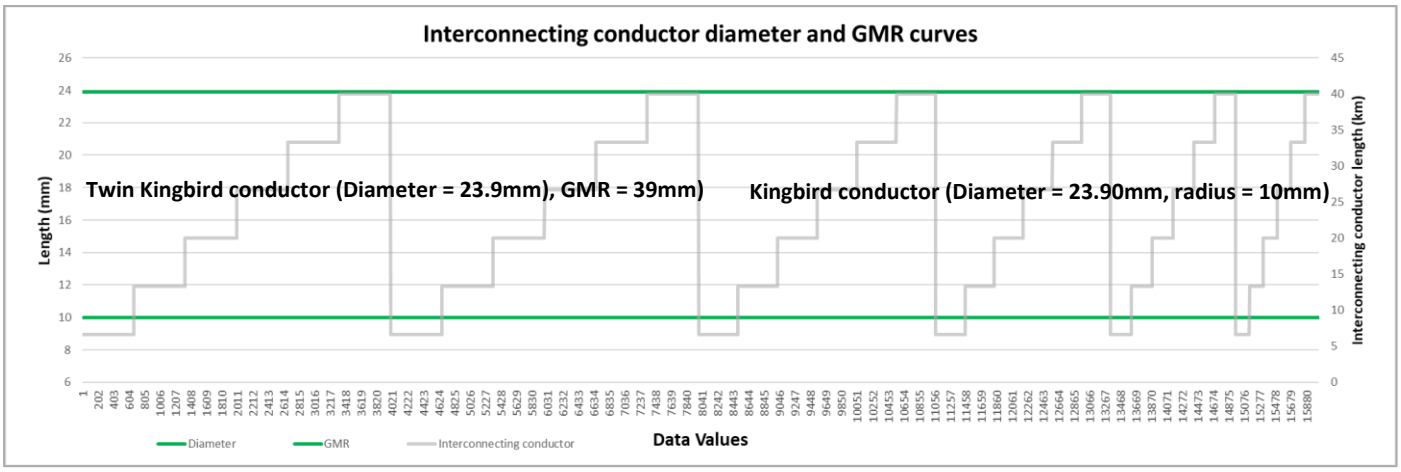

Figure A-36: 66kV Interconnecting conductor Diameter and GMR comparison (green), Interconnecting conductor length (grey).

G. Interconnecting conductor nominal current graph.

The interconnecting conductor nominal current values are superimposed onto the Segment A an interconnecting conductor length graph as shown in Figure A-37.

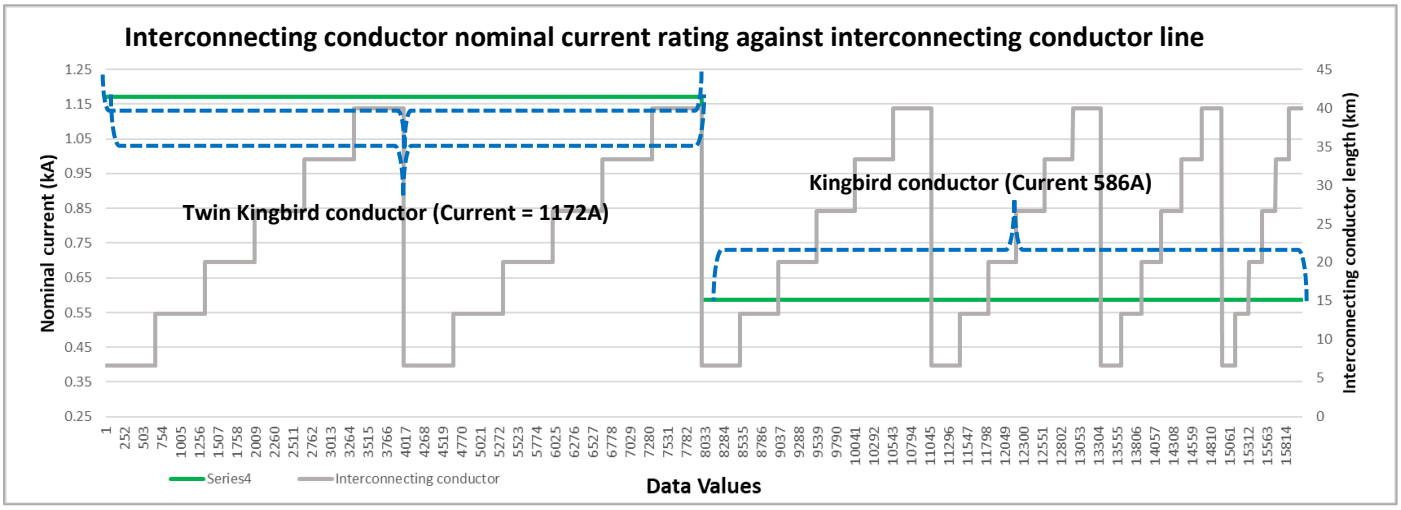

Figure A-37, showing 66kV interconnecting conductor nominal current rating (green).Interconnecting conductor length (grey).

H. Interconnecting conductor rated power versus IPP power graph.

Figure A-38 compares the interconnecting conductor rated power capacitiy againstst the IPP size. As seen, for all changes in IPP sizes, there is an adequate change in interconnecting conductor rating, to safely transfer the required IPP power.

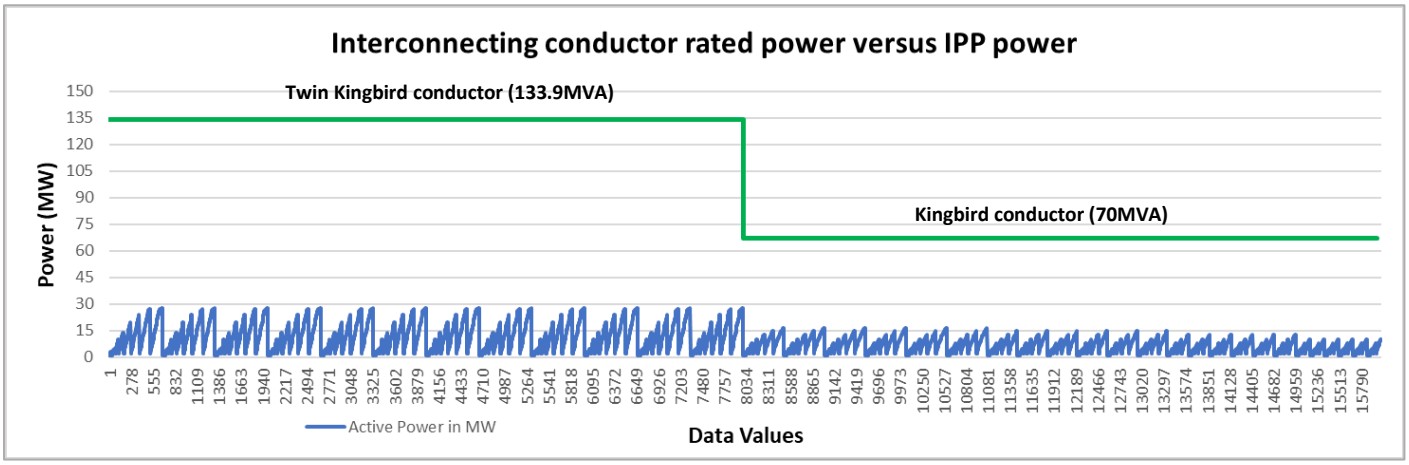

Figure A-38, showing 66kV interconnecting conductor maximum power rating at 66kV versus IPP export power.

I. IPP power factor variation graphs for unity, leading and lagging setpoints applicable to Category B (0.975) and Category C (0.95).

Figure A-39 shows the IPP power factor setpoints for all data values. The graph is further zoomed in to focus on the inductive setpoint values, which are the same in magnitude but negative in sign as the capacitive setpoint. As seen for IPP sizes less than 20MW, the power factor is set to 0.975, while for sizes greater than or equal to 20MW, the setpoint is changed to 0.95.

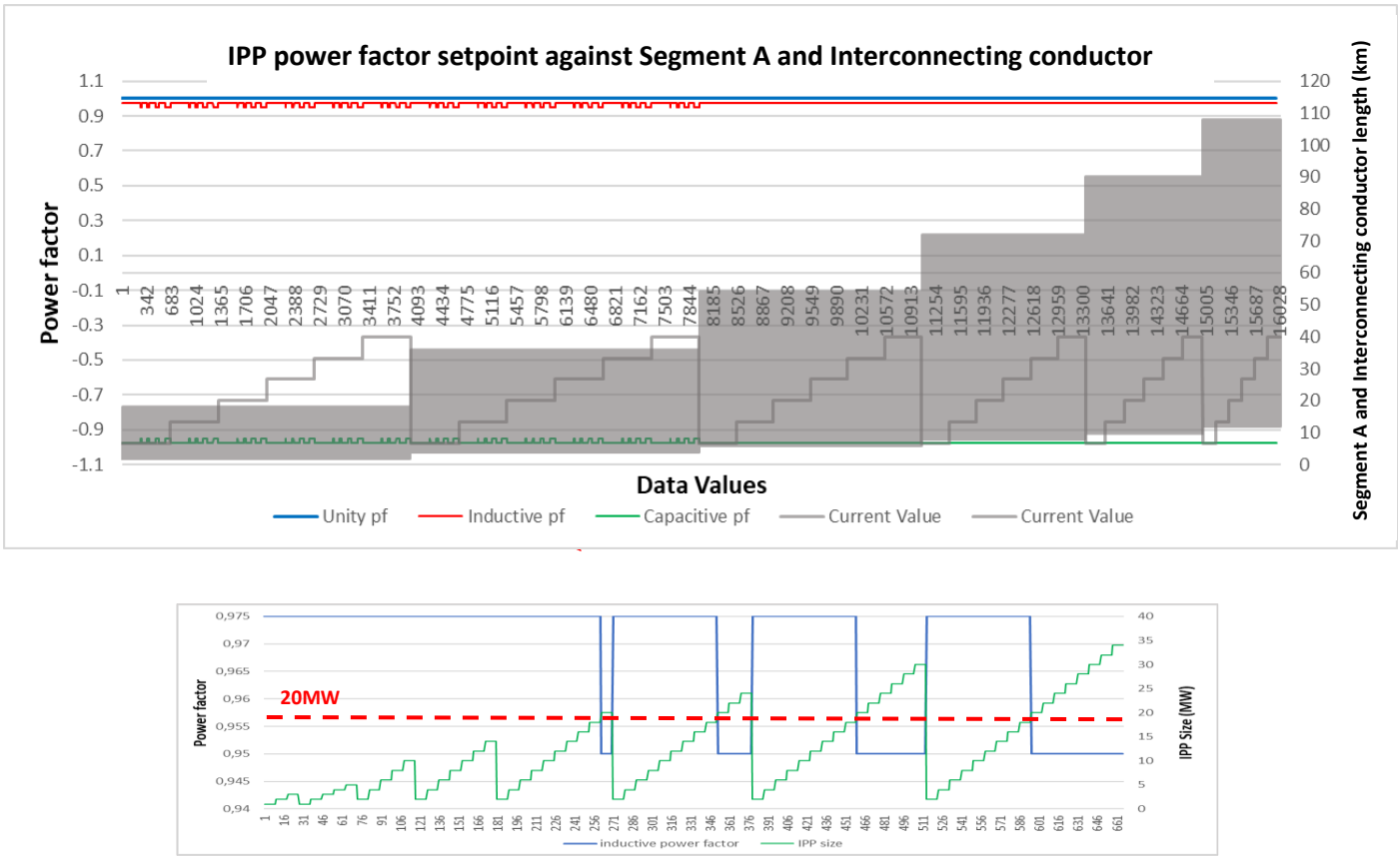

Figure A-39: 66kV IPP power factor variation graph

J. Power line loss graphs corresponding to IPP power factor variation graphs.

The corresponding power line losses curves are shown in Figures A-40 to A-42.

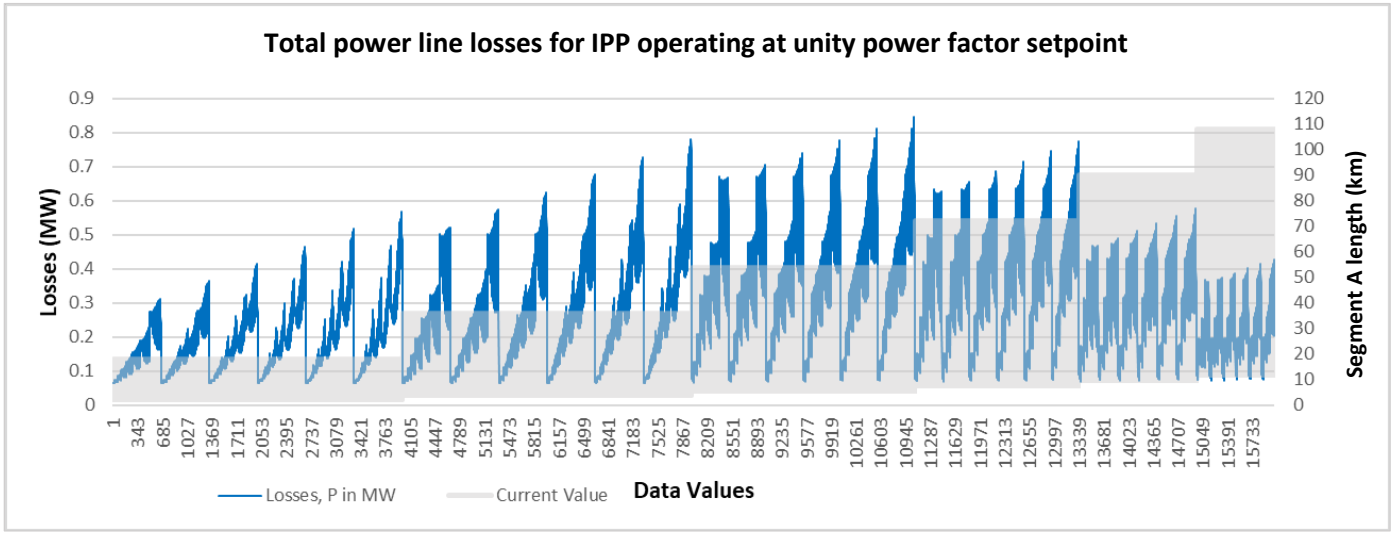

Figure A-40: 66kV total line losses while IPP operates at unity power factor setpoint.

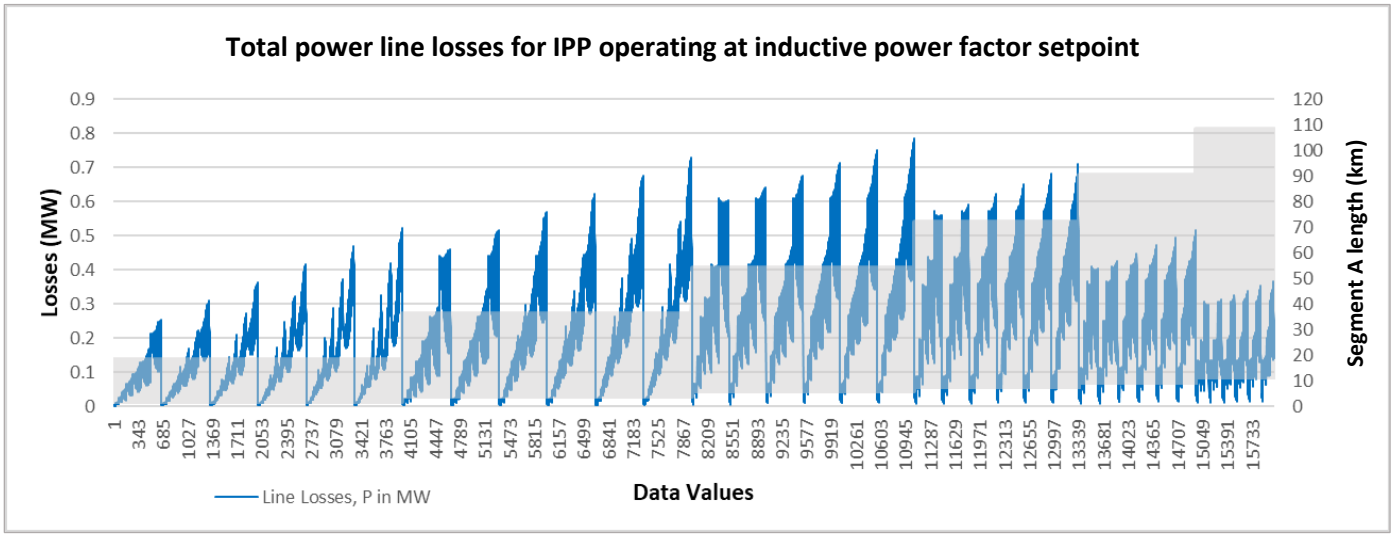

Figure A-41: showing 66kV total line losses while IPP at inductive power factor setpoint

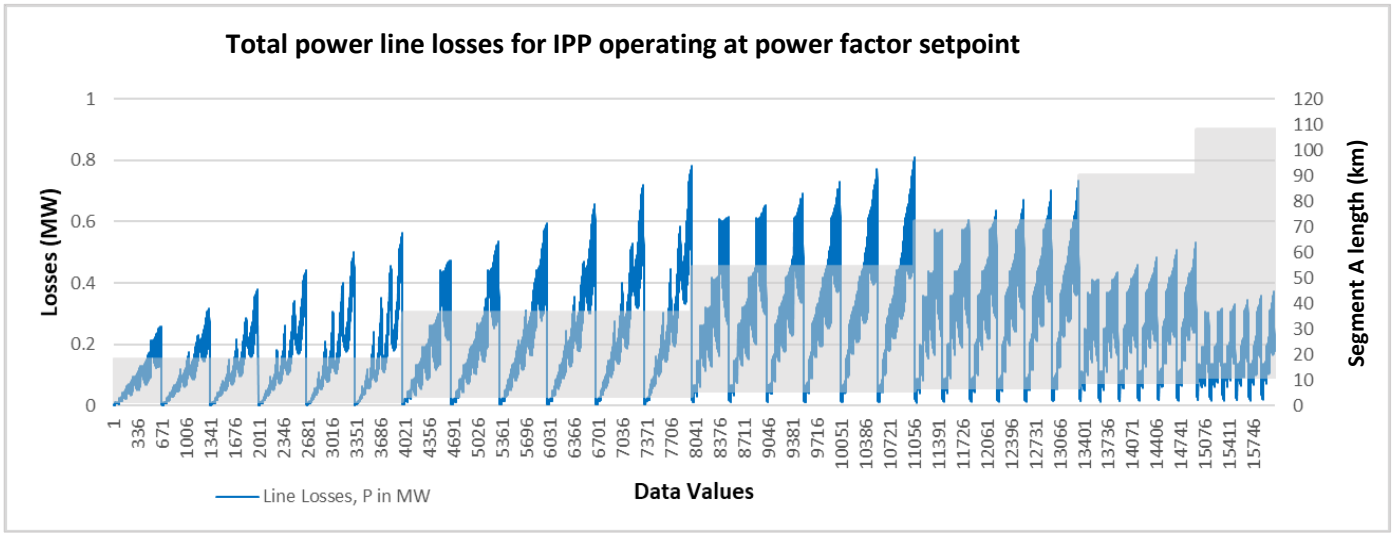

Figure A-42: 66kV total line losses while IPP at Capacitive power factor setpoint

For the 66kV technology, data shown from Sections (A)–(J) above is saved into three 16038x8 input data matrices, one representing the unity power factor IPP setpoint, another representing the lagging IPP setpoint, and another representing the leading power factor setpoint. When combined, a 48114 x 8 input data matrix (16038x3) is saved along with a 48114x1 target data matrix, and these are used in the ANN design and modelling section to follow in Section 3.3. In order to

capture losses for the scenarios in which the load is non-unity, the above simulations are redone in the same fashion as before, but for a receiving end (load) power factor setpoint of 0.975 (inductive) as well as 0.975 (capacitive). This means that the combined input data matrix to be used in the ANN design and modelling section expands in size from 48114x8 to 144342x8 and a target data size of 144342x1.

132kV Data

As was done for the 66kV network, the 132kV network integrates IPPs of Category B (±0.975 for IPP Size < 20 MW) and C (±0.95 for IPP Size >= 20 MW) with the same three power factor operating modes of unity, (0.975/0.95) capacitive and (0.975/0.95) inductive, with the value of 0.975 or 0.95 assigned depending on the IPP size in the 132kV network. The interconnecting feeder length is adjusted four times (15km, 30km, 40km and 50km) with the maximum backbone feeder length extending from 120km (for the 66kV network) to 140km. Loading at the receiving end is also increased to 176MW, with a corresponding maximum IPP export capacity of 82.5MW for backbone lengths up to 40km. For backbone lengths of 60km, 160MW is applied to the receiving end with a corresponding maximum IPP export capacity of 75MW. Backbone lengths of 80km and 100km are loaded to 110MW, with a maximum IPP export power of 36MW. 120km and 140km backbones are loaded to 90MW with maximum IPP power of 32MW.

For all cases, both Segments A and B use ACSR Triple-Berfort conductors per phase, having individual current ratings of 965A (1.93 kA per phase). Sub conductor bundle separation distances are set to 200mm, with a maximum phase-to-phase separation of 3.5m. A horizontal geometry is used in the DIgSILENT Powerfactory simulation model, included with transposition (Figure A-43). Interconnecting conductors are ACSR type Twin-Zebra and Kingbird, having individual current ratings of 710A and 586A respectively. Twin-Zebra conductors are used for the integration of IPPs up to 82MW – which only apply to backbone lengths up to 60km, while Kingbird conductors are used for the integration of IPPs of capacity 36MW – which apply to backbone lengths greater than 60km. For both receiving end and IPP substations, a single transformer substation topology is used.The IPP model transfers its power via a single 125MVA 132/66kV step up transformer in order to transfer the maximum export power of 82.5MW. This is used to ensure that the IPP sending end voltage is controlled within required pu limit. The receiving end makes use of a single 250MVA transformer (Figure A-44) .

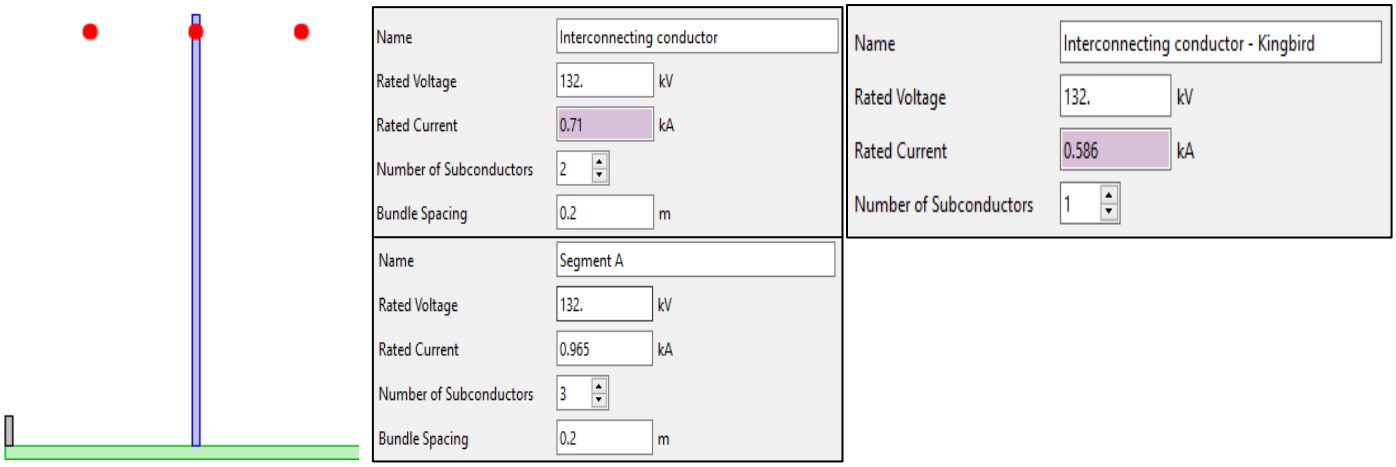

Figure A-43: 132 kV Interconnecting conductor current rating and Segment A, Segment B current rating, with horizontal intermediate structure used for the 132kV network simulation.

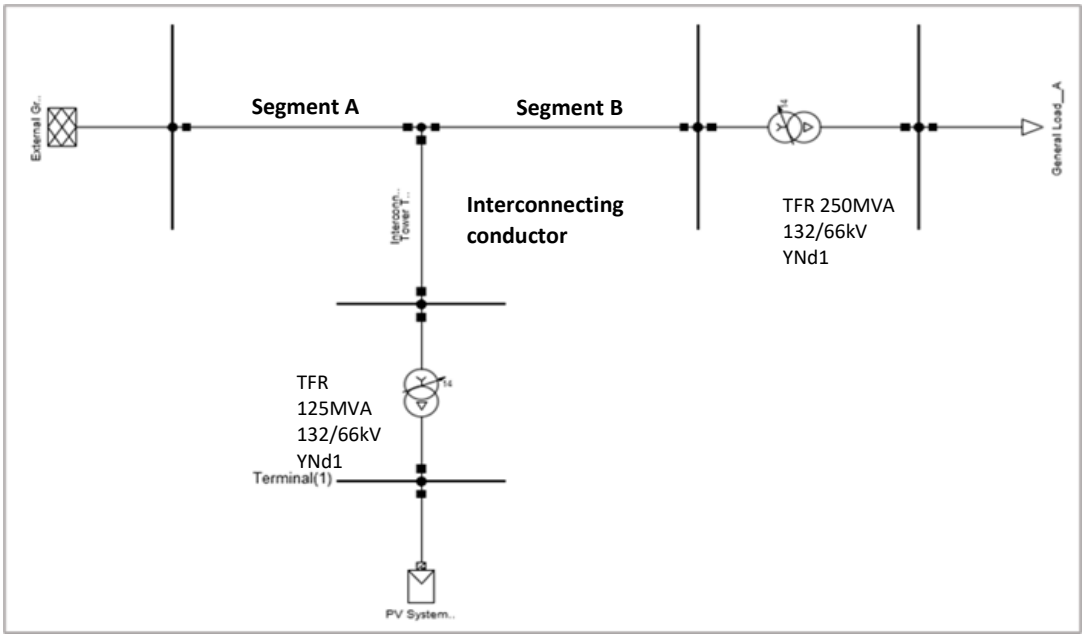

Figure 3-44: 132 kV DIgSILENT simulation network diagram

A. Interconnecting conductor location on backbone graph

Figure A-45 shows how the length of Segment A is changed in simulation time, allowing for 7 different backbone lengths, namely: 20 km (Data values 1 – 2952), 40 km (Data values 2953 – 5904), 60 km (Data values 5905 – 8424), 80 km (8425 - 10548), 100 km (10549 - 12672) and 120 km (12673 - 14112) and 140km (14413 – 1552) respectively. As seen, four different interconnecting conductor lengths in total divide all backbones into 4 sets of data, one set for every interconnecting conductor length. Within each set, different receiving end loads are again applied accordingly (Figure A-46). As seen, for all backbone lengths, all four sets of interconnecting conductor lengths from 15km to 50km have associated loads ranging from 8 MW to 176 MW.

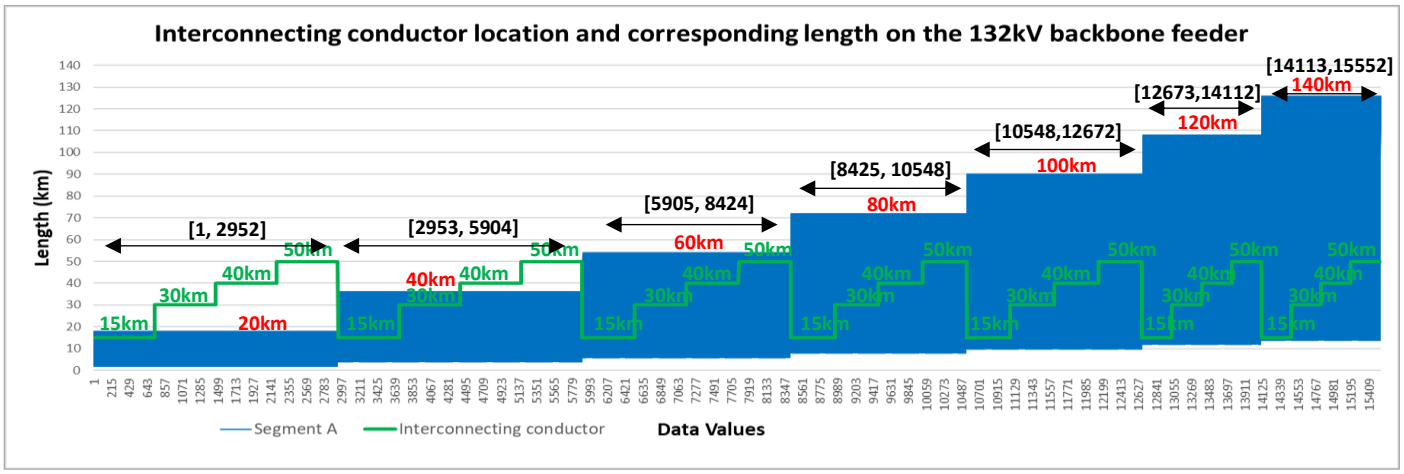

Figure 3-45: 132kV interconnecting conductor length and backbone length data.

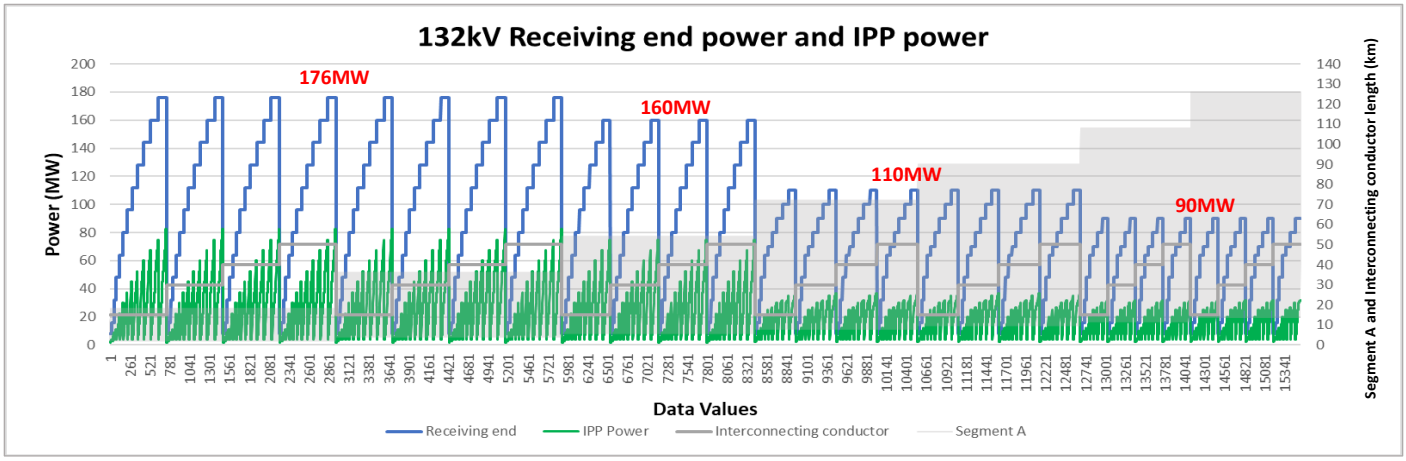

Figure A-46: 132kV MVA loading data

B. Maximum MVA loading graph for the interconnecting conductor, Segment A and Segment B of the backbone, for loads operating at unity power factor.

Figure A-47 shows the sending end power required (red curve) for the 132kV network. As seen again, this is the difference between load receiving end power and the power supplied by the IPP.

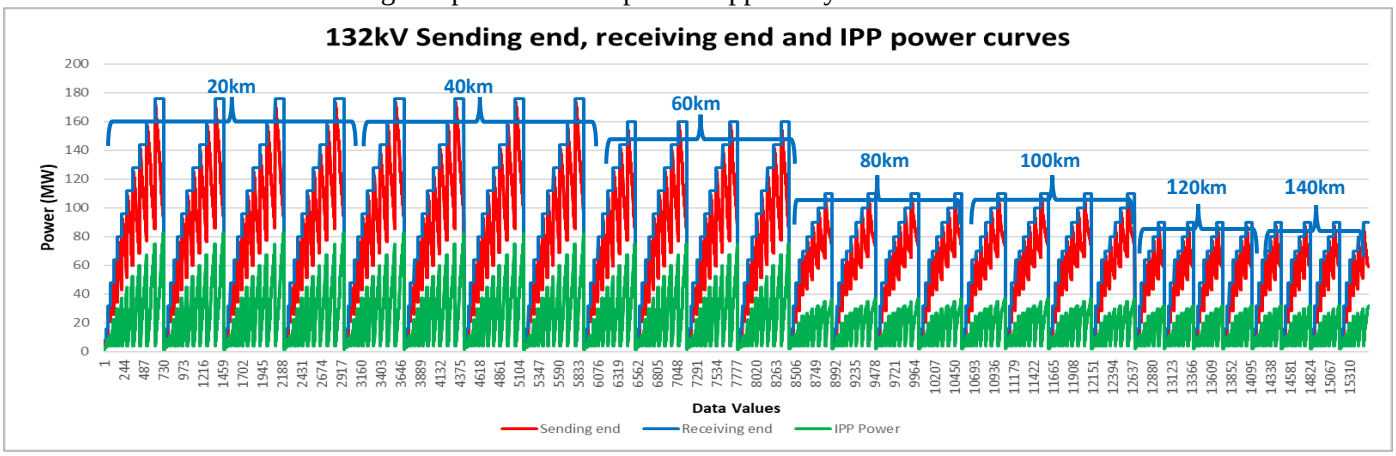

Figure A-47:132 kV Receiving end, sending end and IPP power curves

C. Maximum and minimum voltage graphs at the load end of the network as well as POC.

Figure A-48 to Figure A-50 show the receiving end, POC and IPP 132kV sending voltage graphs for changes in Segment A length and interconnecting conductor (for the IPP operating at unity, capacitive and inductive power factor setpoints). The inductive power factor setpoint corresponding to all IPPs (regardless of size), achieves the greatest increase in voltage, but as seen in Figures A-51 to A-52, for an increased load, there is a decreased trend of voltage at both the receiving end and POC, regardless of backbone length, as was the case for the previous networks.

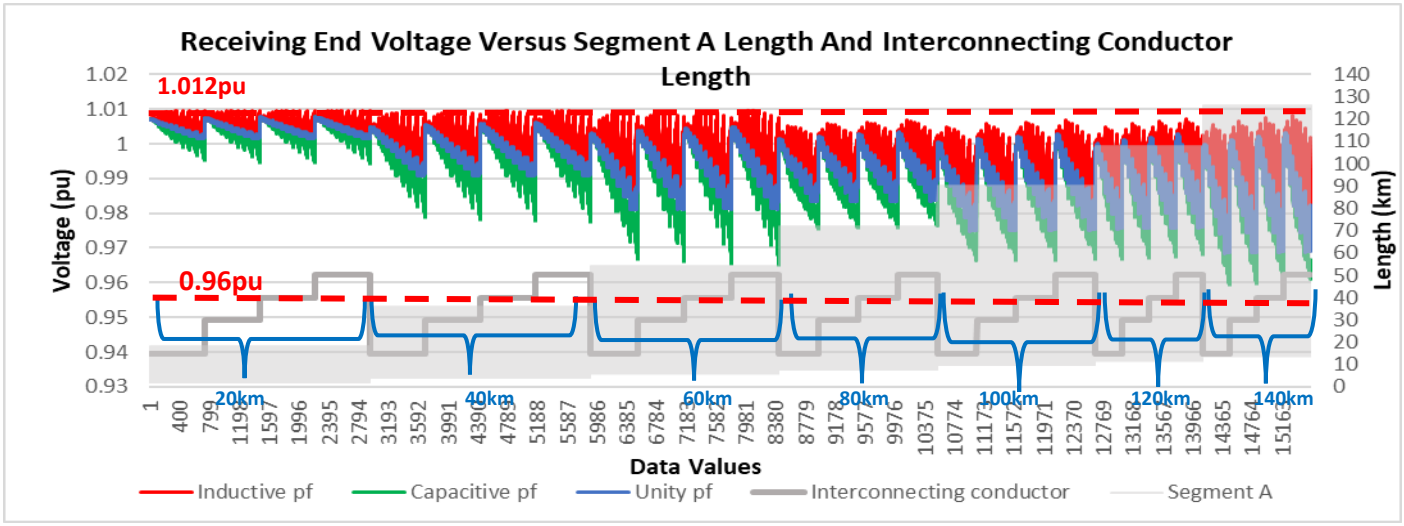

Figure A – 48: 132 kV Receiving end voltage as a response to changes in IPP Sizes with varying power factor setpoints

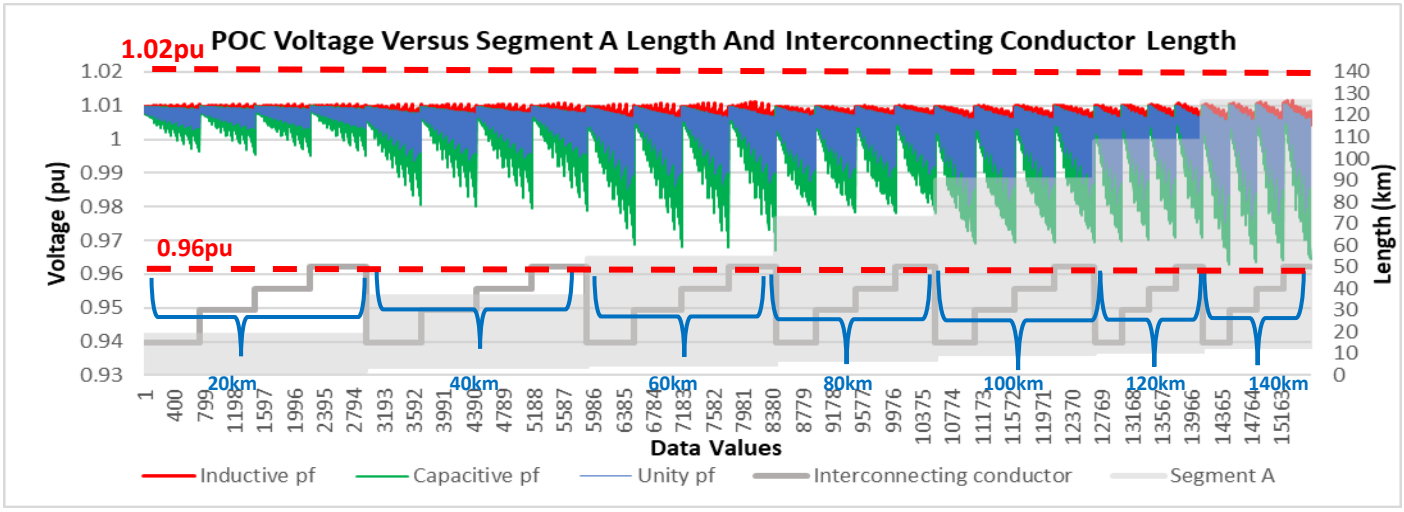

Figure A-49: 132 kV POC voltage as a response to changes in IPP Sizes with varying power factor setpoints.

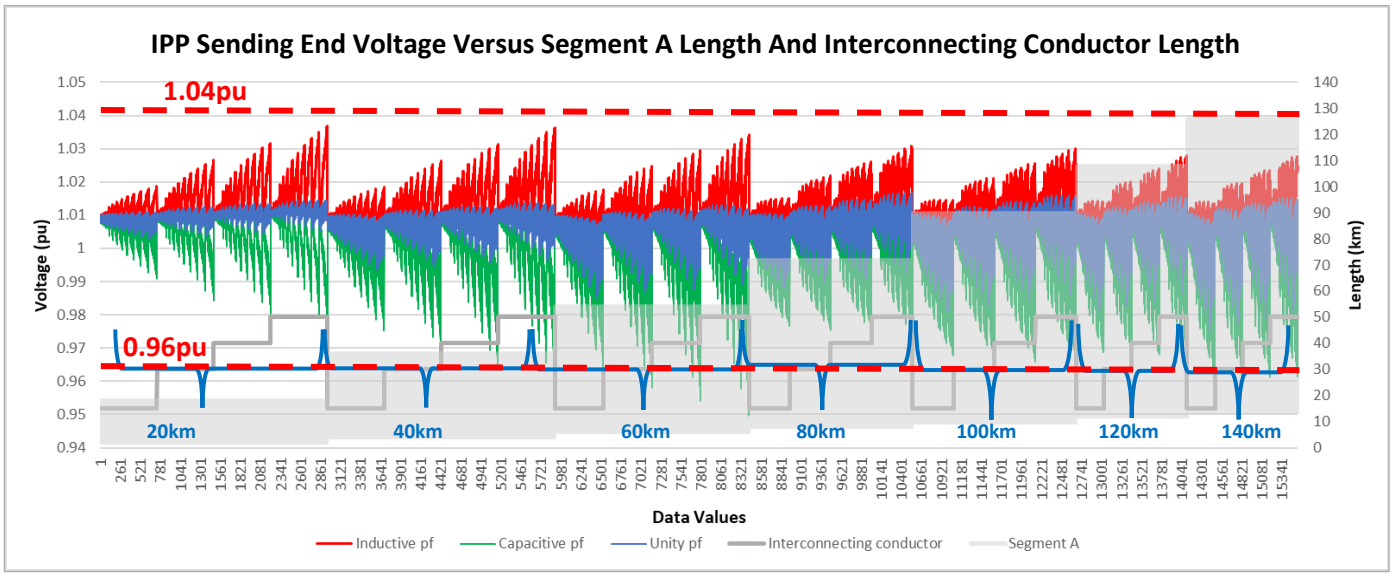

Figure A-50: 132 kV Receiving end voltage response to changes in IPP size.

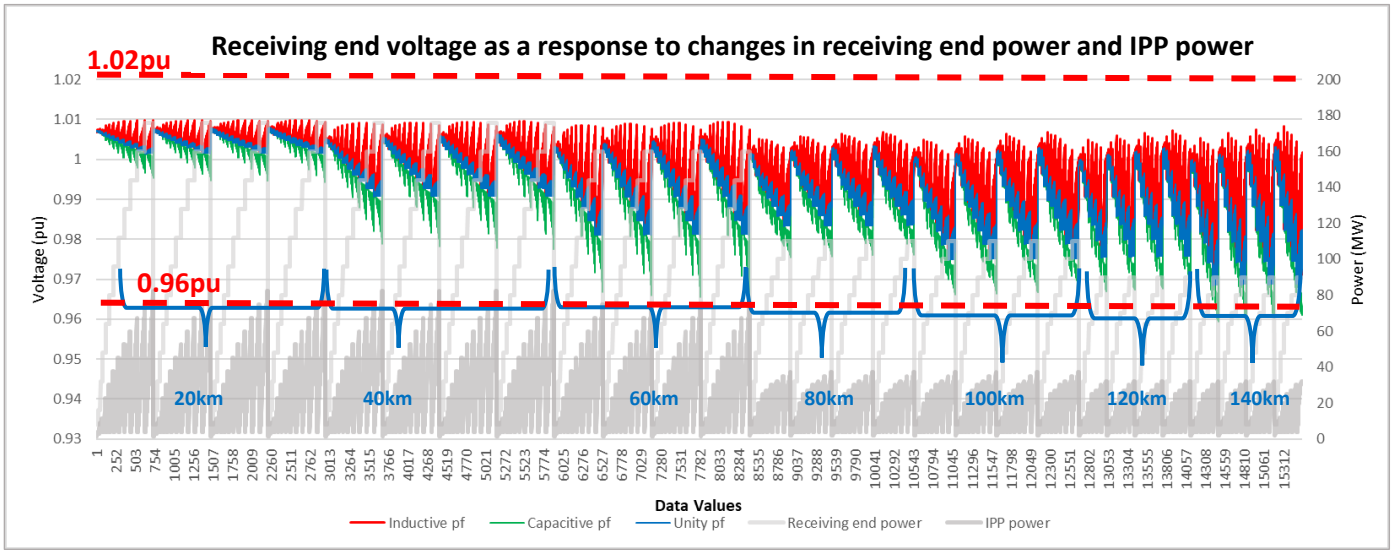

Figure A-51: 132 kV Receiving end voltage response to changes in IPP size and receiving end power.

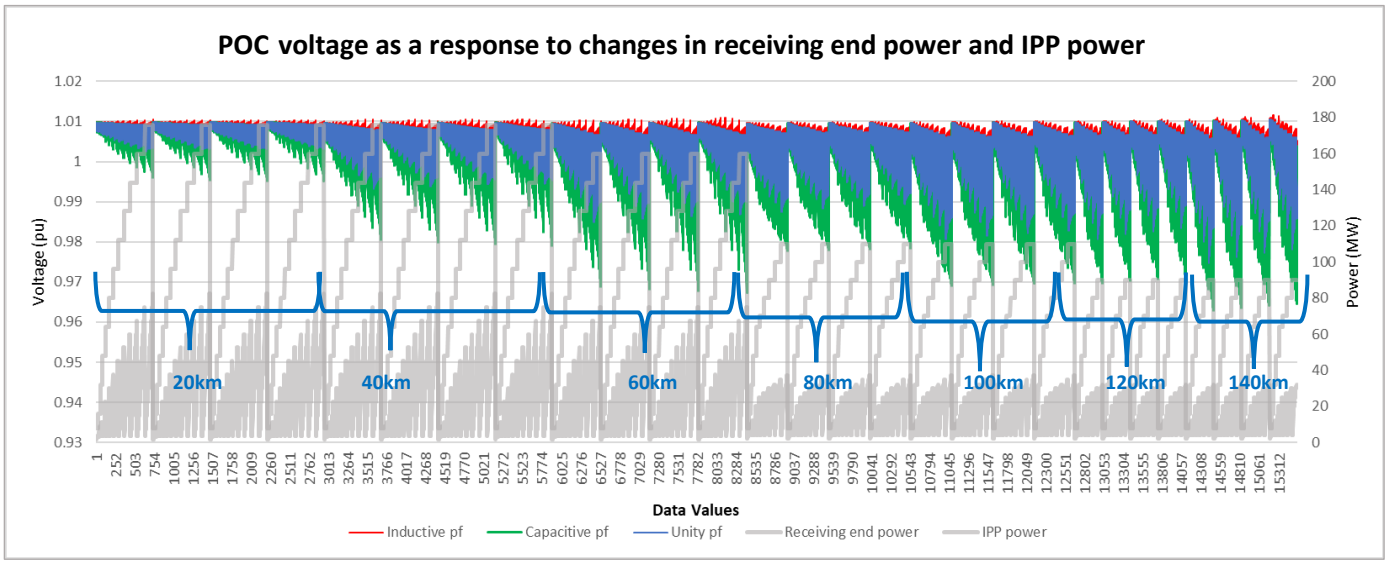

Figure A-52: 132 kV POC voltage response to changes in IPP power.

D. Thermal loading graphs for interconnecting conductor, and backbone conductors (Segment A and B).

The thermal loading of the backbone (Segment A and Segment B), and the interconnecting conductor are shown by Figures A-53 to A-55. As seen, for all simulations, there is again no excessive thermal stress on all conductors in the network, with the maximum loading value not exceeding 90%. Thermal loading graphs are produced for IPP setpoints of unity, capacitive and inductive power factors.

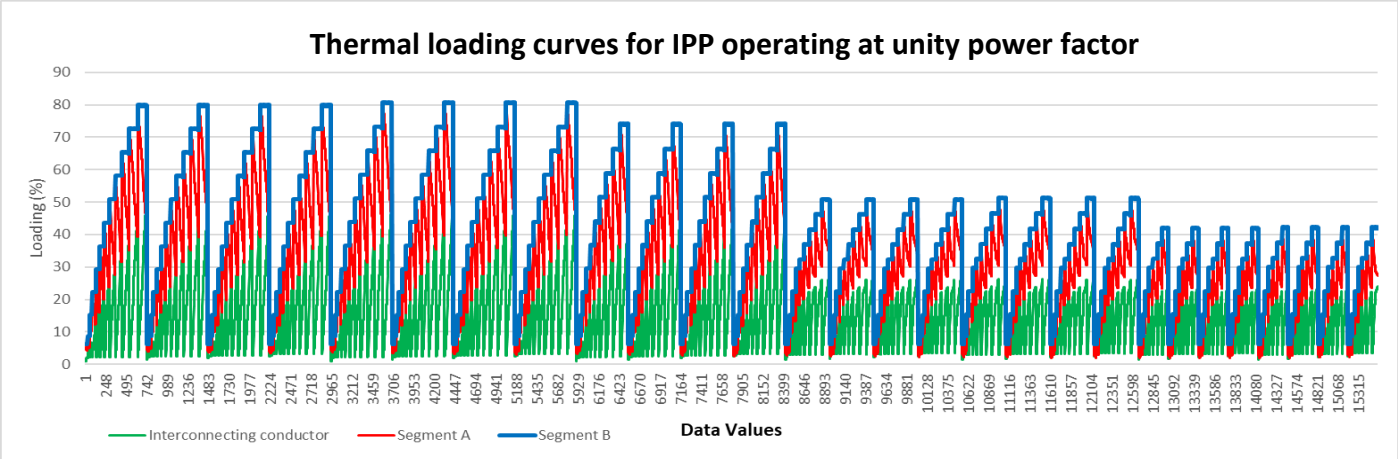

Figure A-53: 132 kV thermal loading for Segment A, Segment B and interconnecting conductor while IPP operates at unity pf

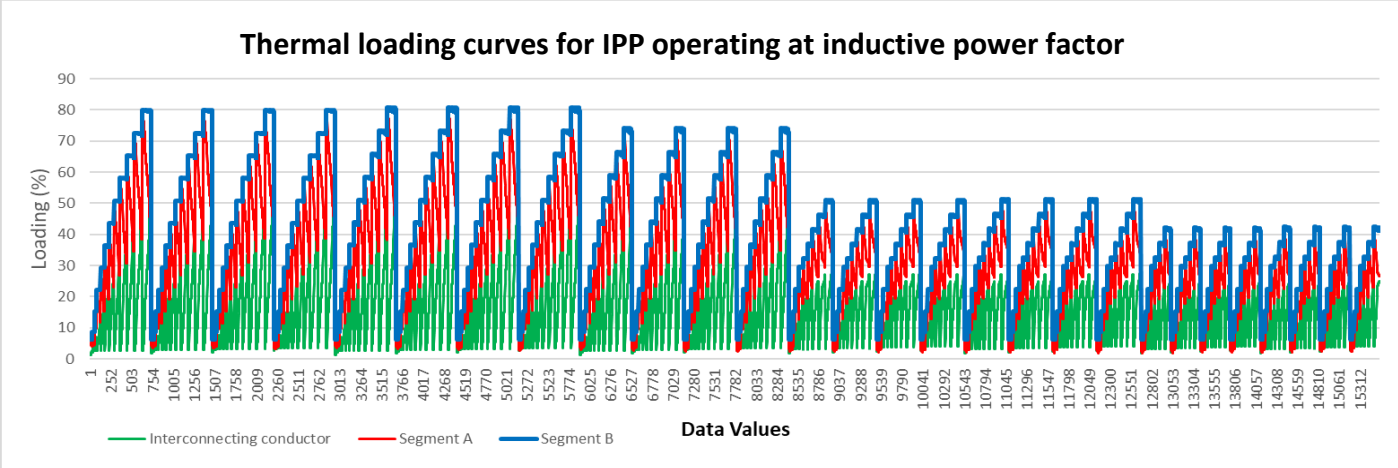

Figure A-54: 132 kV thermal loading for Segment A, Segment B and interconnecting conductor while IPP operates at 0.975 capacitive pf

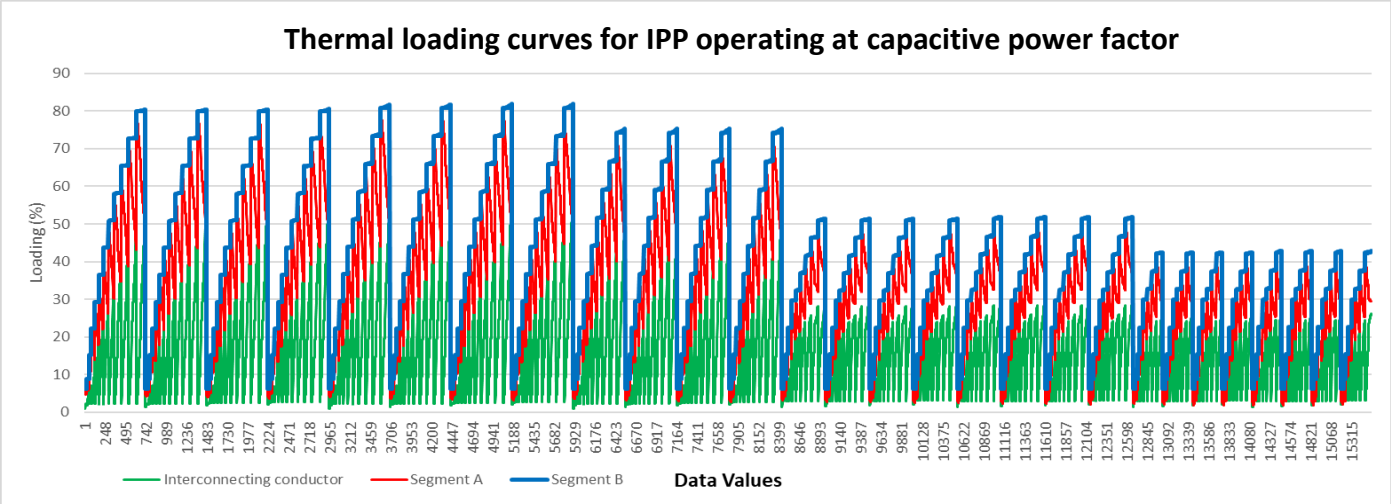

Figure A-55: 132 kV thermal loading for Segment A, Segment B and interconnecting conductor while IPP operates at 0.975 inductive pf

E. Interconnecting conductor DC resistance at 20 Deg C

Figure A-56 shows the interconnecting conductor DC resistance at 20 deg C. As seen, the standard Zebra (twin) and Kingbird conductors are used for the interconnecting feeder at 132kV.

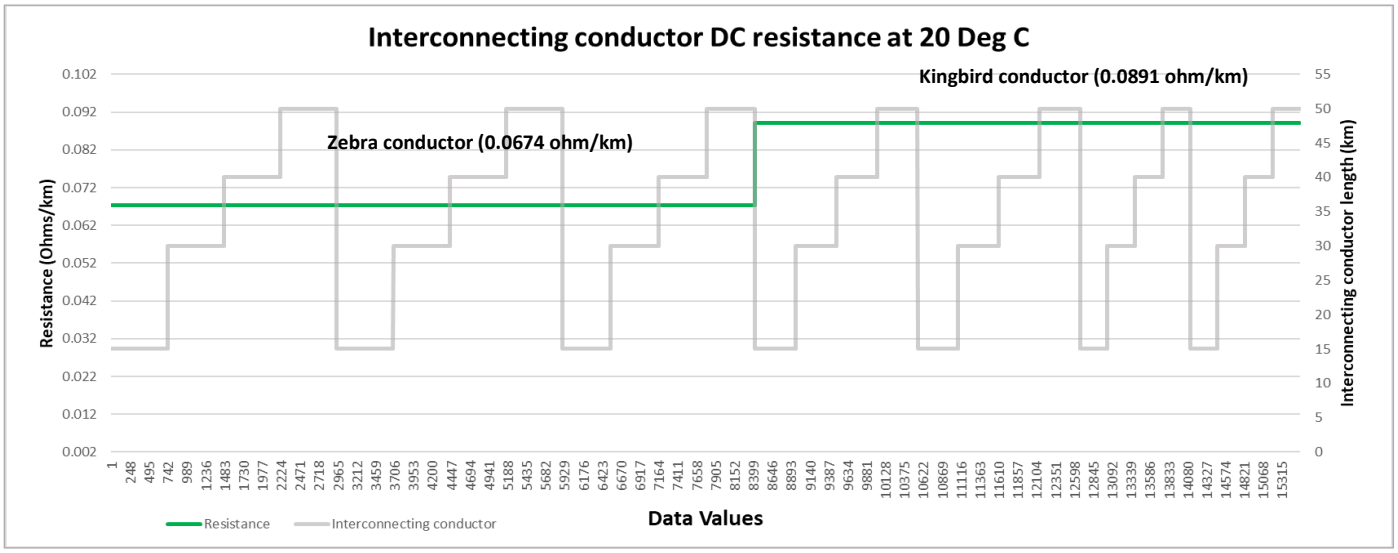

Figure A-56: 132 kV Interconnecting conductor DC resistance at 20 deg C (green), Interconnecting conductor length (grey).

F. Interconnecting conductor diameter and Geometric mean radius graph.

For the 132kV interconnecting conductor, the diameter and GMR are plotted as shown in Figure A-57.

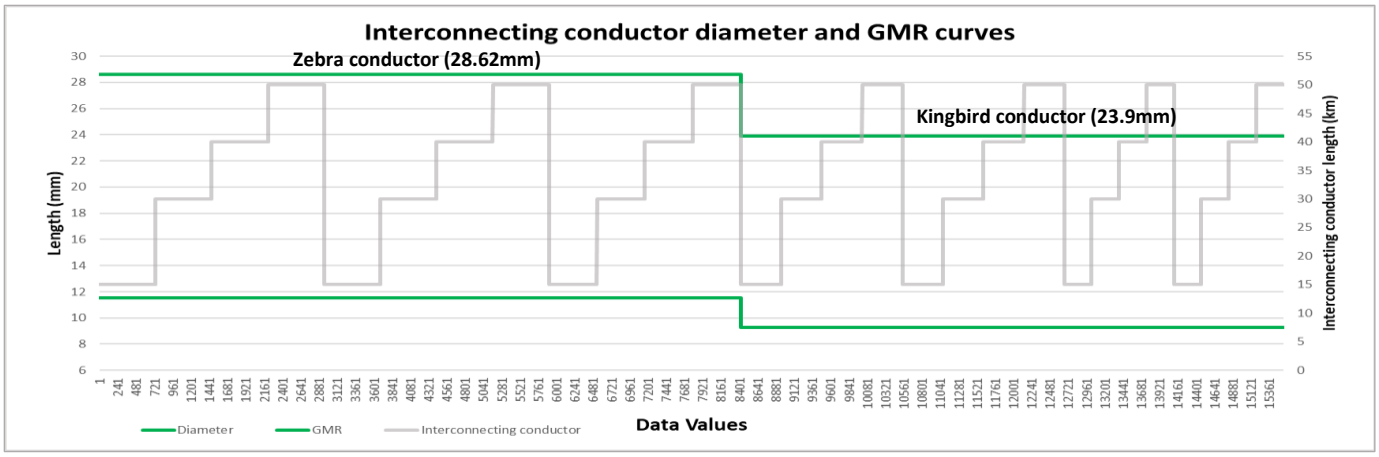

Figure A-57: 132 kV Interconnecting Conductor diameter versus GMR values (green). Interconnecting conductor length (grey).

G. Interconnecting conductor nominal current graph.

The interconnecting conductor nominal current values are superimposed onto the Segment A an interconnecting conductor length graph as shown in Figure A-58.

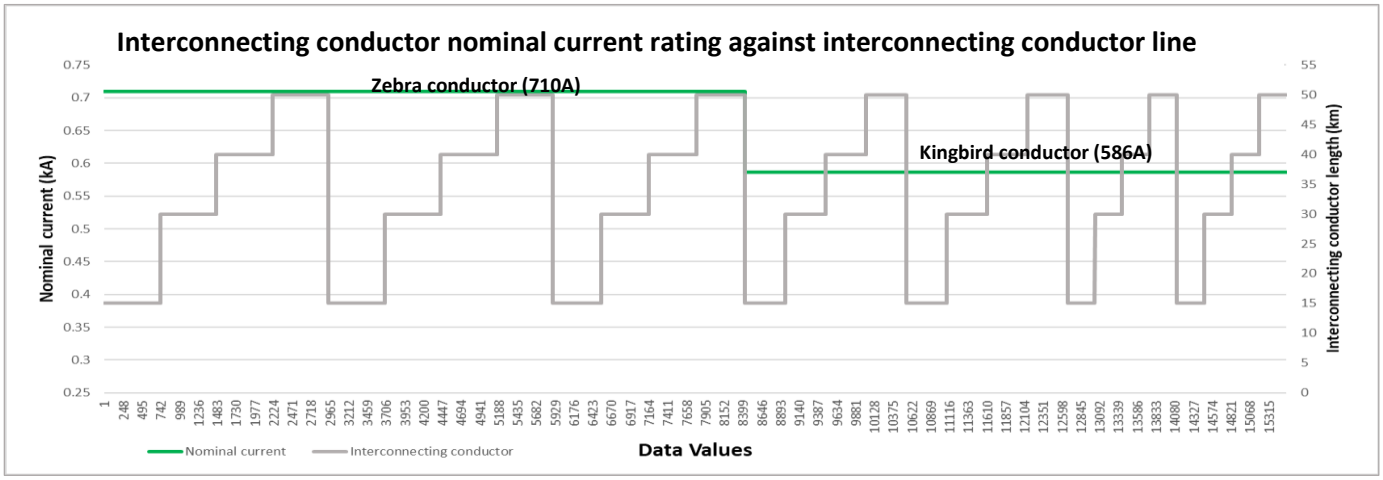

Figure A-58: 132 kV interconnecting conductor nominal current (green) applicable to Zebra and Kingbird conductors. Interconnecting conductor length (grey).

H. Interconnecting conductor rated power versus IPP power graph.

Figure A-59 compares the interconnecting conductor rated power capacitiy againstst the IPP size. As seen, for all changes in IPP sizes, there is an adequate change in interconnecting conductor rating, to safely transfer the required IPP power.

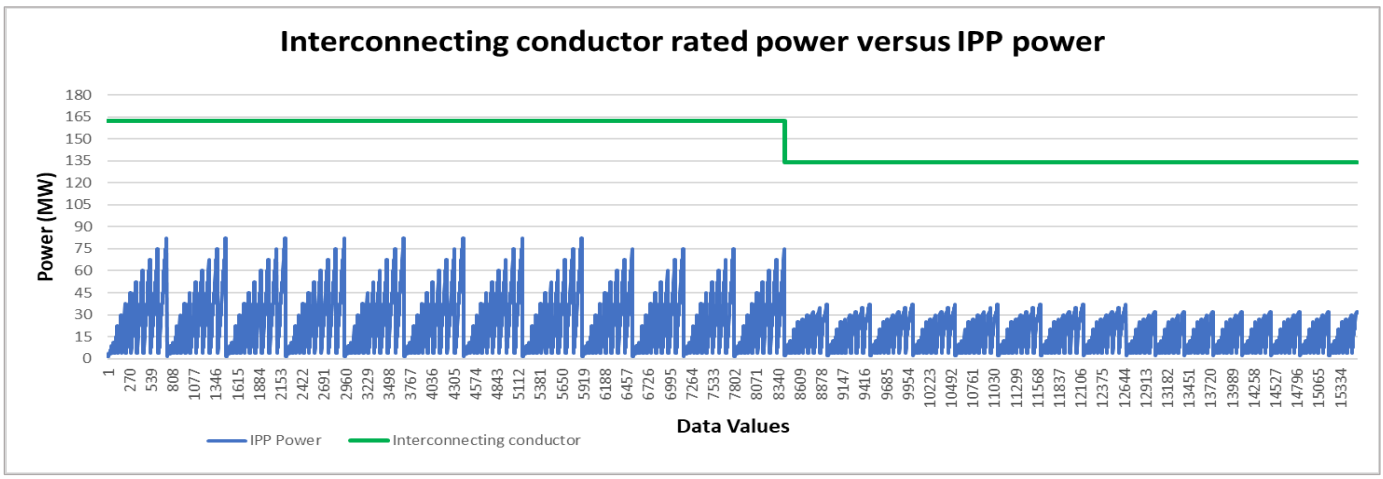

Figure A-59: 132 kV Interconnecting conductor is adequately rated to handle IPP export power

I. IPP power factor variation graphs for unity, leading and lagging setpoints applicable to Category B (0.975) and Category C (0.95).

The IPP power factor graph shown in Figure A-60 below shows the variation in IPP power factor the 132 kV network.

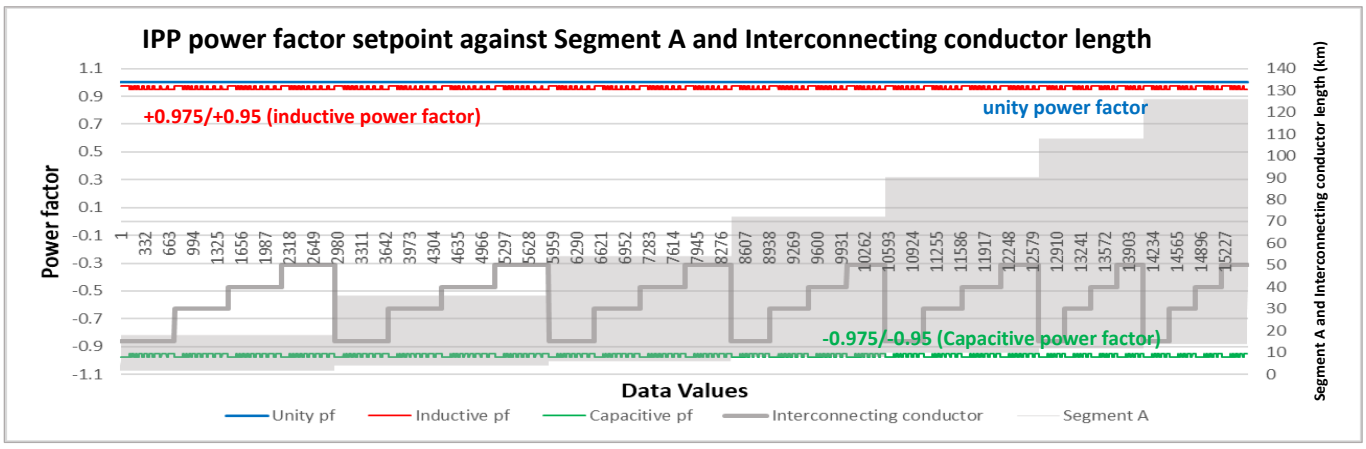

Figure A-60: 132 kV IPP variations in power factor (unity – blue; inductive – red; capacitive – green). Interconnecting conductor length (grey).

J. Power line loss graphs corresponding to IPP power factor variation graphs.

The corresponding power line losses curves are shown in Figures A-61 to Figures A-63.

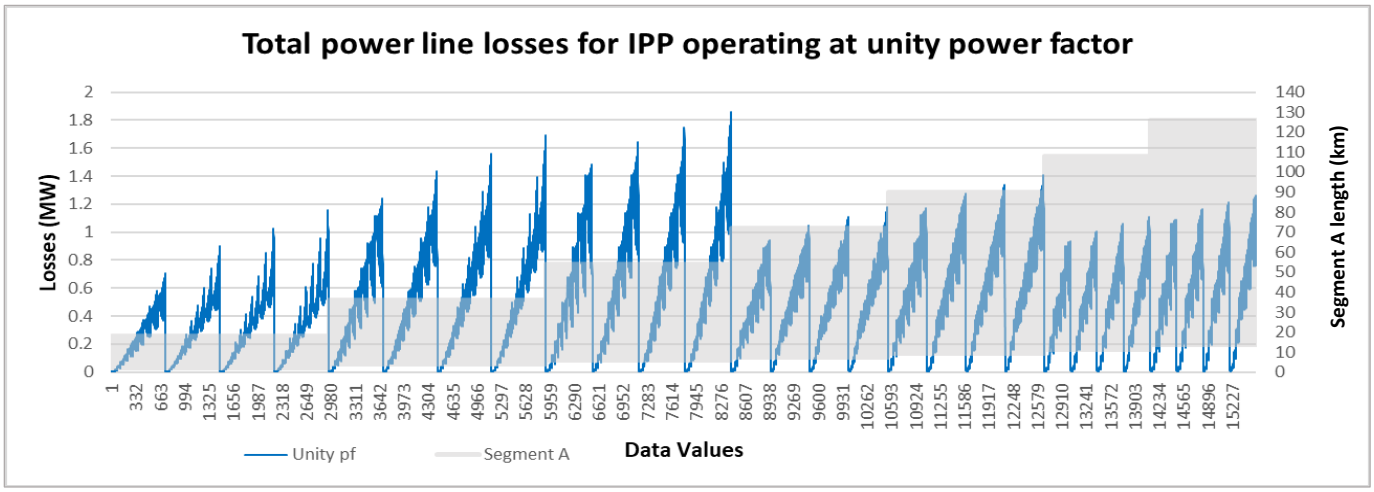

Figure A-61: 132 kV Total power line losses for unity power factor

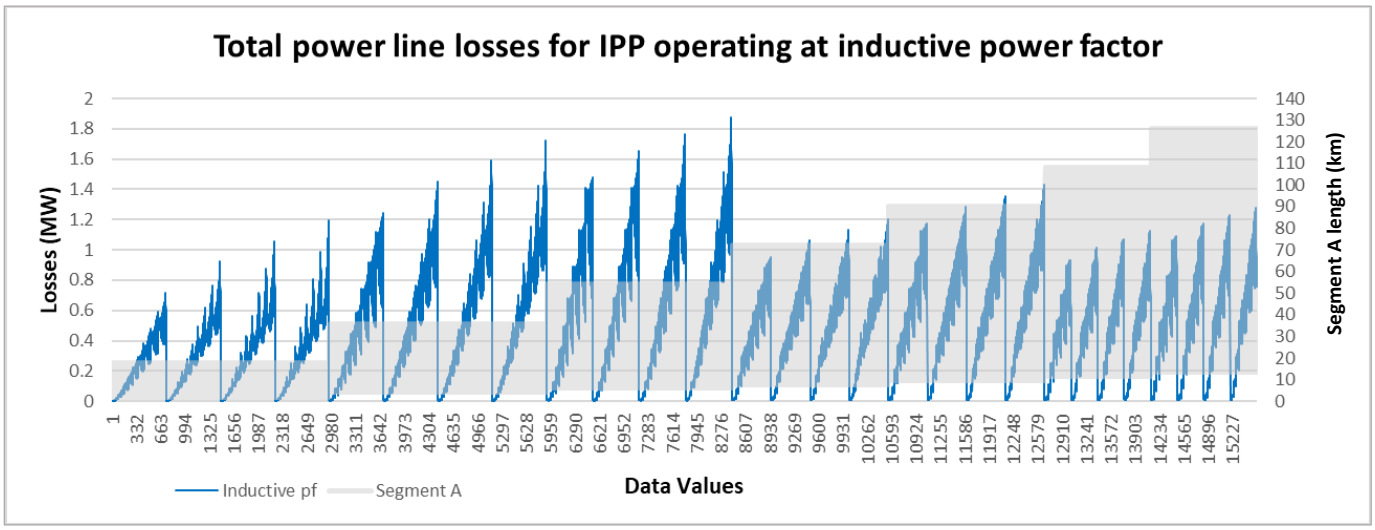

Figure A-62: 132 kV Total power line losses for an (-0.975/-0.95) inductive power factor

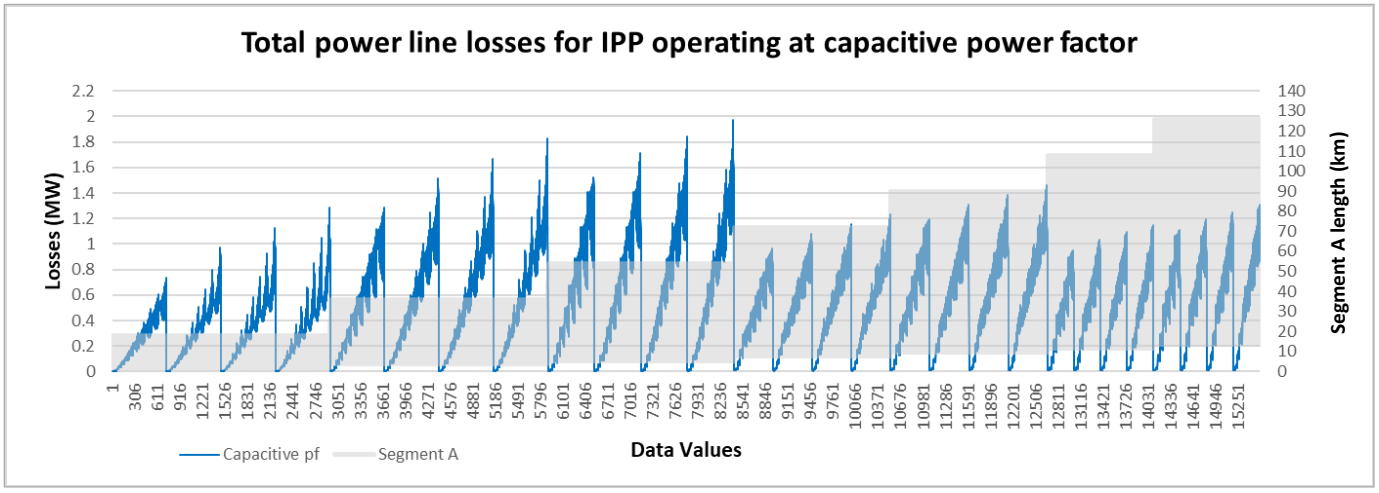

Figure A-63: 132 kV Total power line losses for a (+0.975/+0.95) capacitive power factor

For the 132kV technology, data shown from Sections (A) – (J) above, is saved into three 15554x8 input data matrices, one representing the unity power factor IPP setpoint, another representing the lagging IPP setpoint, and another representing the leading power factor setpoint. When combined, a 46662 x 8 input data matrix (15554x3) is saved, along with a 46662x1 target data matrix, and these are used in the ANN design and modelling section to follow in Section 3.3.

In order to capture losses for the scenarios in which the load is non-unity, the above simulations are redone in the same fashion as before, but for a receiving end (load) power factor setpoint of 0.95 (inductive) as well as 0.95 (capacitive). This means that the combined input data matrix to be used in the ANN design and modelling section expands in size from 46662x8 to 139968x8 and a target data size of 139968x1.

3.2.4.5 220kV, 275kV and 400kV Data

Since the number of Category B IPPs connecting to the EHV network is limited within South Africa, only Category C (> 20MW) IPPs are considered for the integration onto 220kV, 275kV and 400kV networks. For all remaining cases, both Segment A and Segment B use ACSR Quad-Berfort conductors per phase, having individual current ratings of 965A (1.93 kA per phase). Sub conductor bundle separation distances are set to 450mm, with a maximum phase-to-phase separation of 7m. A horizontal geometry is used in the DIgSILENT Powerfactory simulation model, included with transposition. This is to eliminate voltage balance concerns. The interconnecting conductor used for 220kV, 275kV and 400kV are ACSR Twin Zebra per phase, having individual current ratings of 710A (1.41kA per phase). Sub conductor seperation distances are also set to 450mm, with a maximum phase-to-phase separation of 7m (Figure A -64). For both receiving end and IPP substations, two transformers are required in order to achieve N-1 complience; this is standard practice for all EHV networks within South Africa.

3.2.4.5.1 220kV Data

For the 220kV network, the interconnecting feeder length is adjusted four times for backbone lengths up to 240km (25km, 50km, 75km and 80km). For backbone lengths greater than this, the interconnecting conductor is limited to 50km ensuring system voltages remain within the 1.05pu limit. From a loading perspective, at the receiving end, backbone lengths up to 80km are simulated for loads up to 300MW, while for 100km to 160km backbones, the receiving end load is limited to 230MW. For backbone lengths greater than this, a maximum power of 200MW is applied to the receiving end in order to ensure receiving end voltages are above the lower voltage limit threshold of 0.95pu. The IPP model transfers its power via two 125MVA 220/132kV step up transformers (Figure A-65) in order to transfer the maximum export power of 110MW. This is used to ensure that the IPP sending end voltage is controlled within required pu limit. The receiving end makes use of two 250MVA transformers.

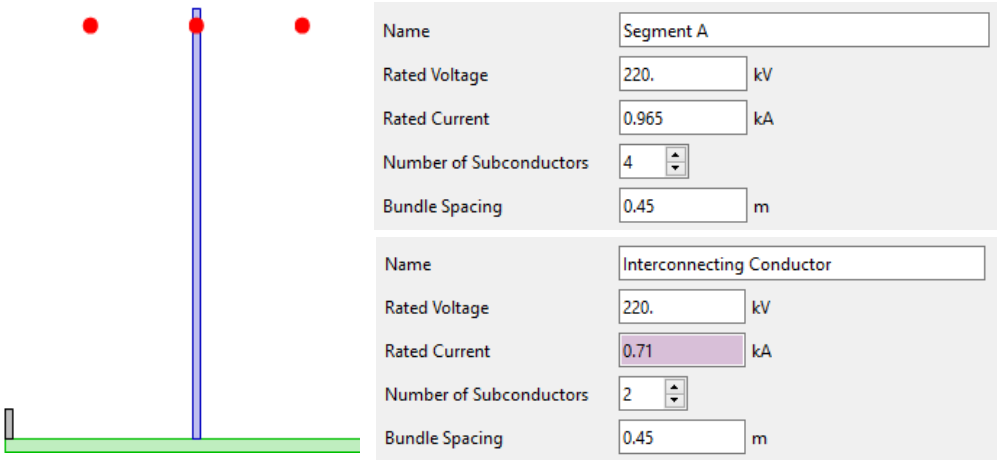

Figure A-64: 220 kV Interconnecting conductor current rating and Segment A, Segment B current rating, with horizontal intermediate structure used for the 220kV network simulation.

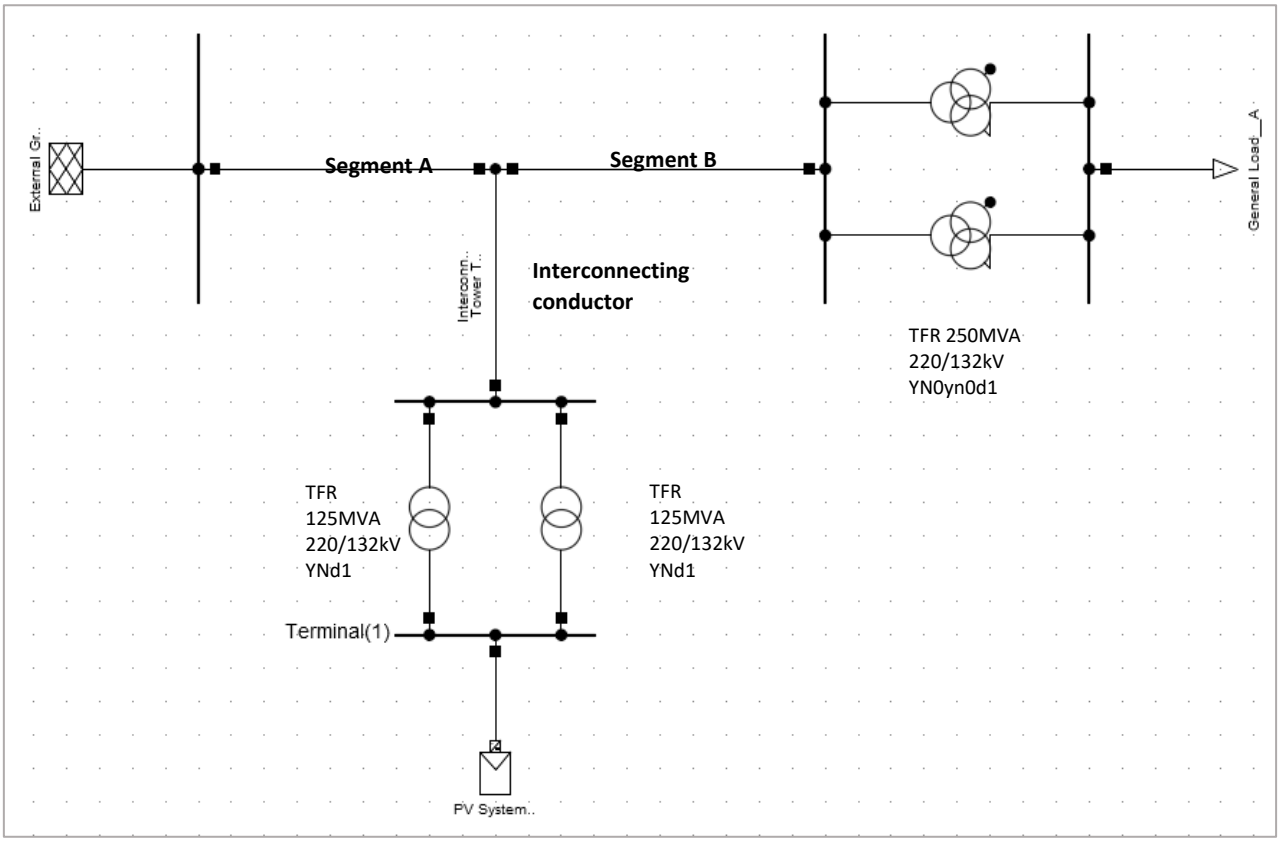

Figure A-65: 220 kV DIgSILENT simulation network diagram

A. Interconnecting conductor location on backbone graph

Figure A-66 shows how the length of Segment A is changed in simulation time, allowing for 12 different backbone lengths, namely: 20 km (Data values 1 – 1840), 40 km (Data values 1841 – 3680), 60 km (Data values 3681 – 5520), 80 km (5521 - 7360), 100 km (7361 - 8800) and 120 km (8801 - 10240),140km (10241 – 11680), 160km (11681 – 13120), 180km (13121 – 14560) and 200km (14561 – 15600), 220km(15601 - 16640) and 240km (16641 – 17680) respectively.

As seen, four different interconnecting conductor lengths in total divide all backbones into 4 sets of data, one set for every interconnecting conductor length (as was for the 132kV case). Within each set, different receiving end loads are again applied accordingly (Figure A-67). As seen, for all backbone lengths, all four sets of interconnecting conductor lengths from 25km to 100km have associated loads ranging from 20 MW to 300 MW.

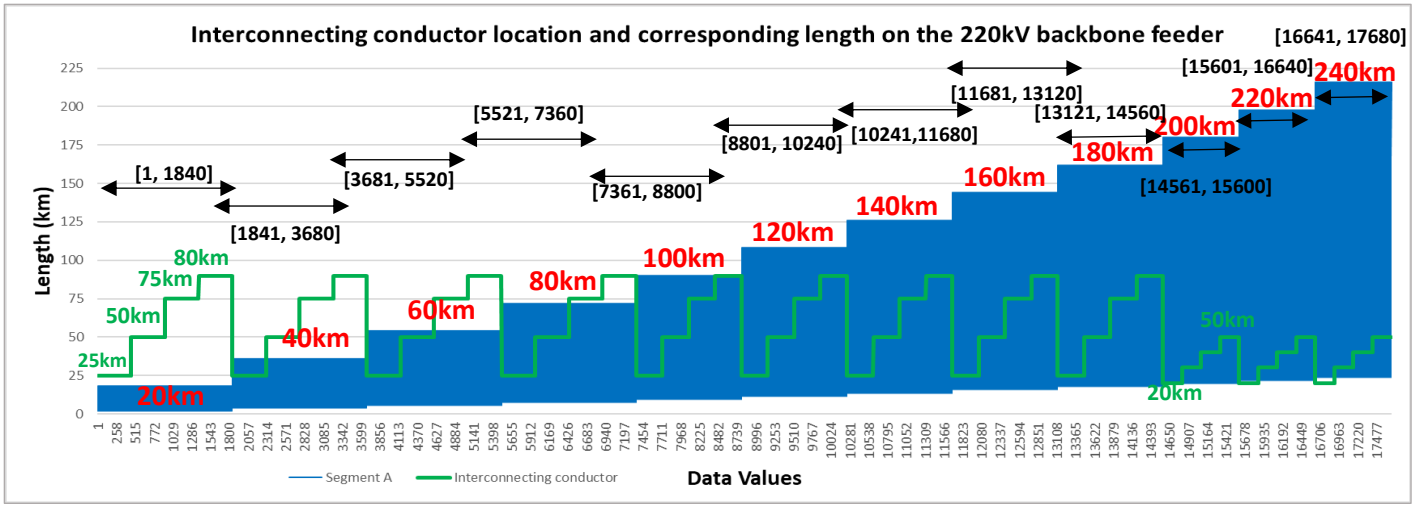

Figure A-66: 220 kV Interconnecting conductor length and location on backbone graph

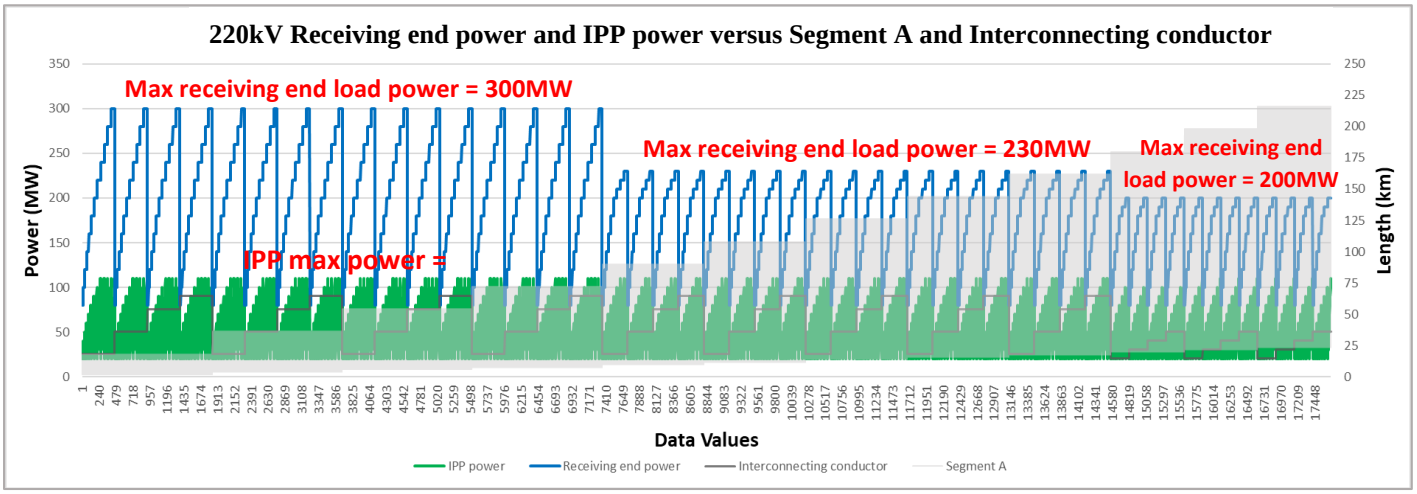

Figure A-67: 220 kV Interconnecting conductor length and its location on backbone graph, with receiving end power and IPP power curves

B. Maximum MVA loading graph for the interconnecting conductor, Segment A and Segment B of the backbone, for loads operating at unity power factor.

Figure A-68 shows the sending end power required (red curve) for the 220kV network. As seen again, this is the difference between load receiving end power and the power supplied by the IPP.

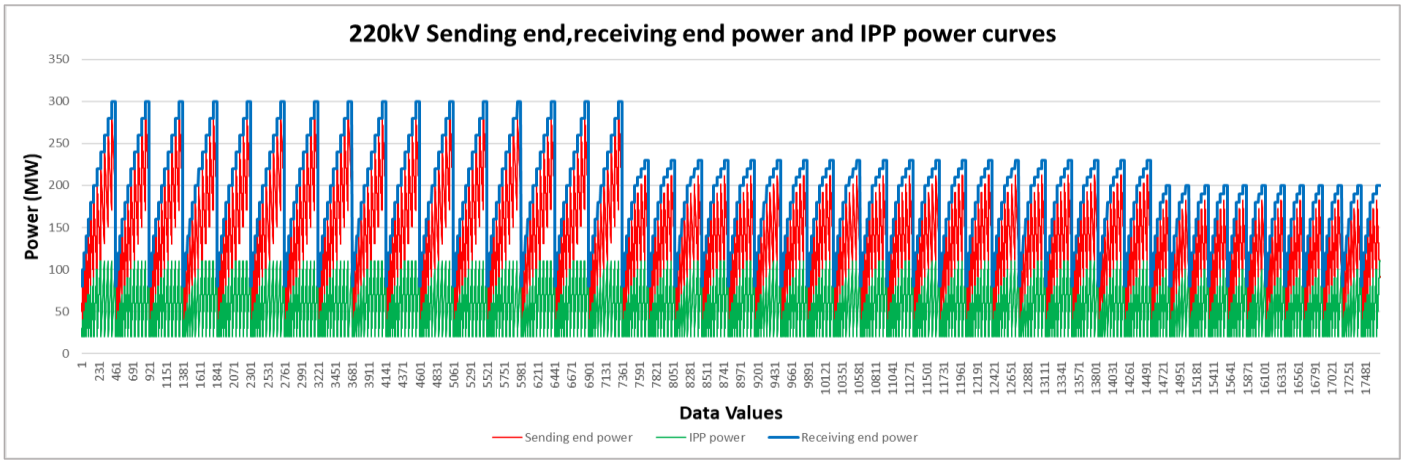

Figure A-68: 220 kV Receiving end, sending end and IPP power curves

C. Maximum and minimum voltage graphs at the load end of the network as well as POC.

Figure A-69 to Figure A-71 show the receiving end, POC and IPP 220kV sending voltage graphs for changes in Segment A length and interconnecting conductor (for the IPP operating at unity, capacitive and inductive power factor setpoints). The inductive power factor setpoint corresponding to all IPPs (regardless of size), achieves the greatest increase in voltage, but as seen in Figures A-72 to A-73, for an increased load, there is a decreased trend of voltage at both the receiving end and POC, regardless of backbone length, as was the case for the previous networks.

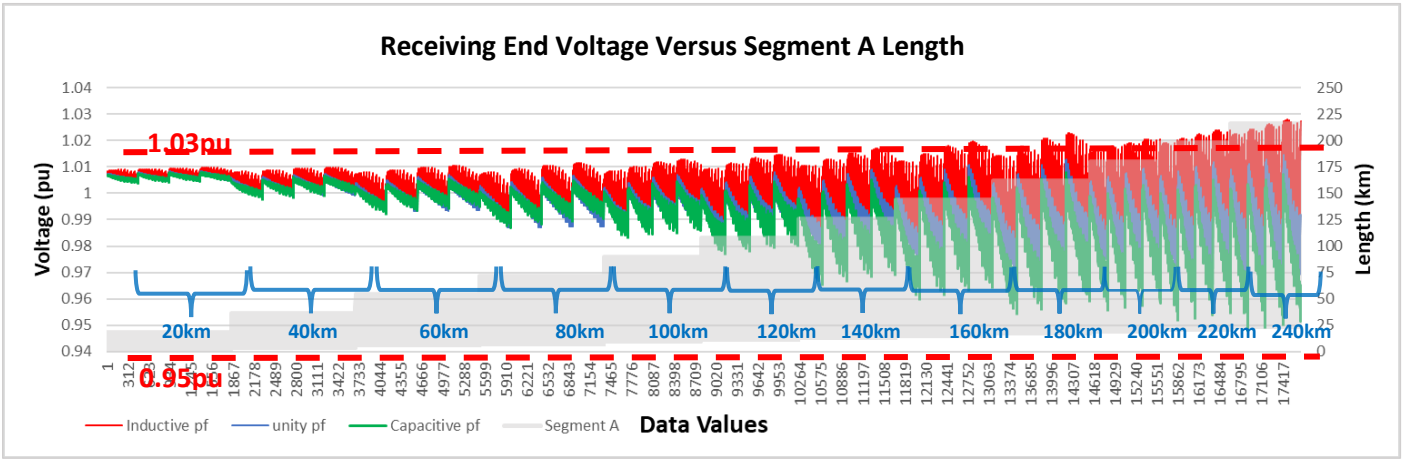

Figure A–69: 220 kV Receiving end voltage shown against Segment A length

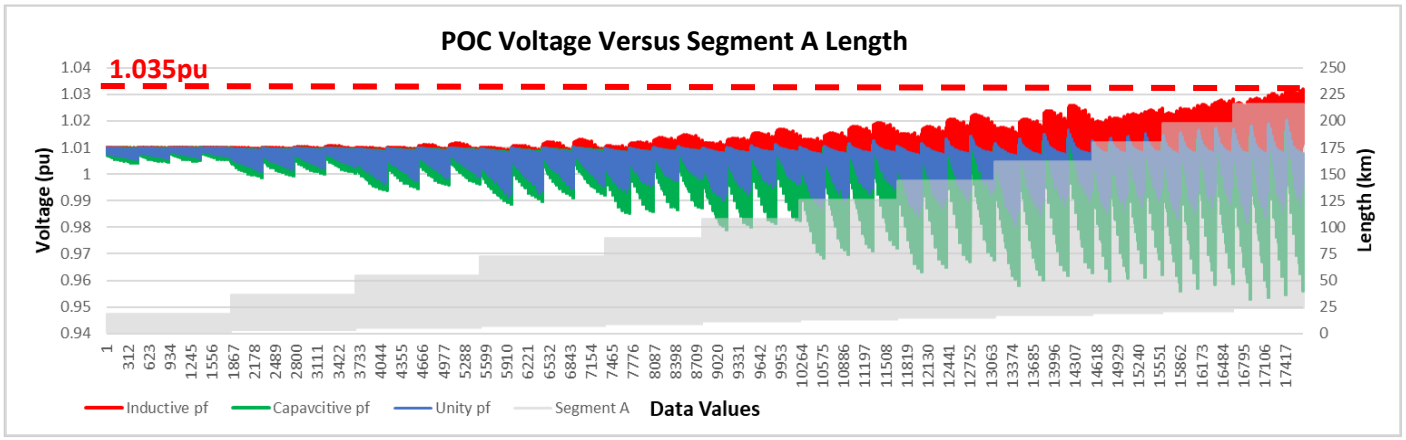

Figure A-70: 220kV POC voltage shown against Segment A length

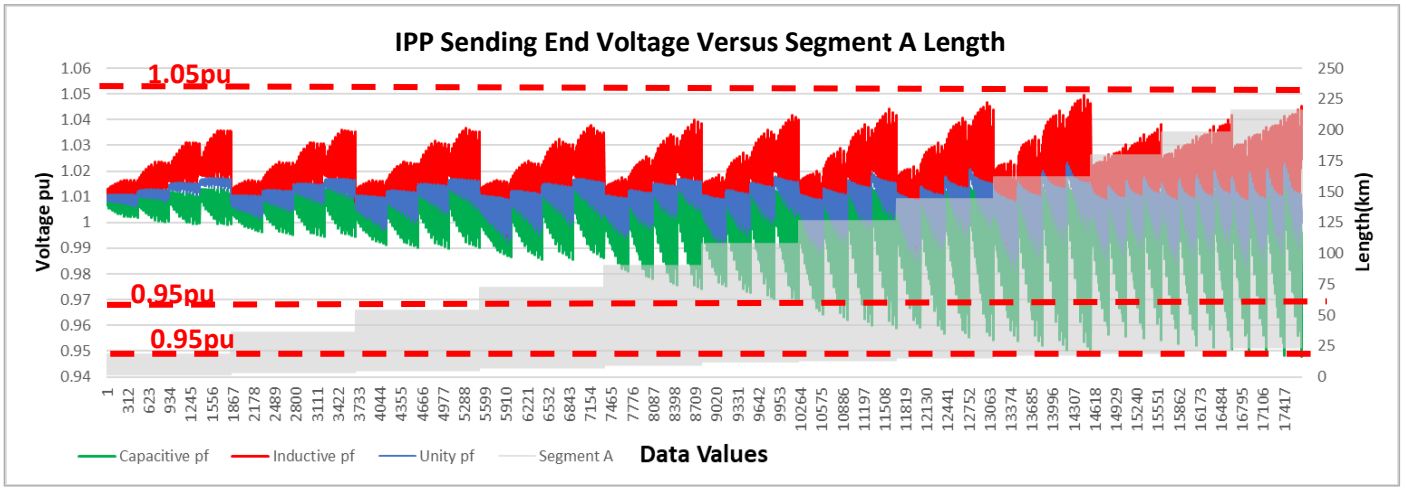

Figure A-71: 220 kV IPP sending end voltage response to changes in segment A length

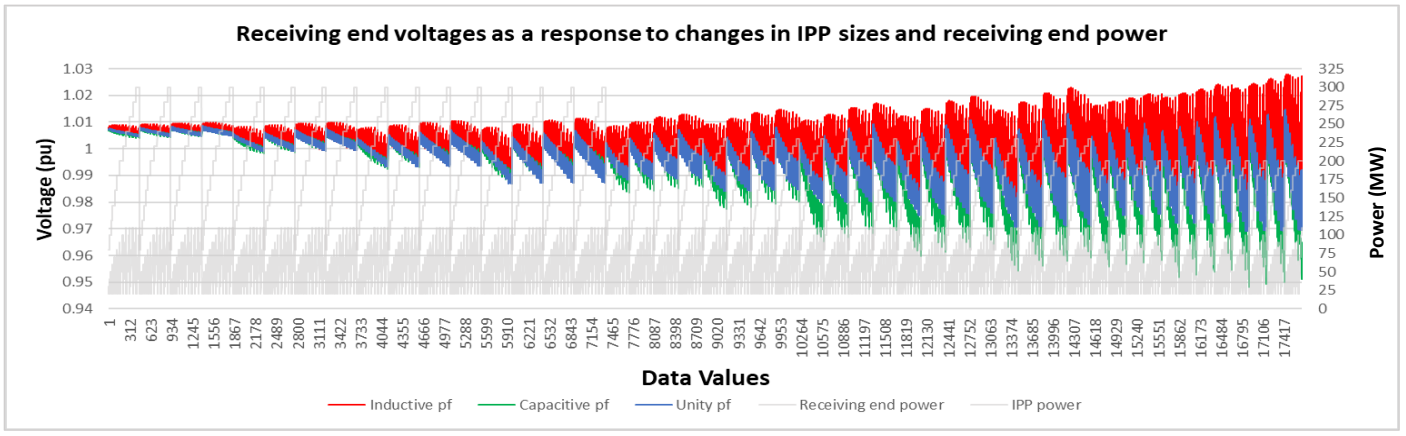

Figure A-72: 220 kV Receiving end voltage as a response to changes in IPP Sizes and receiving end load power

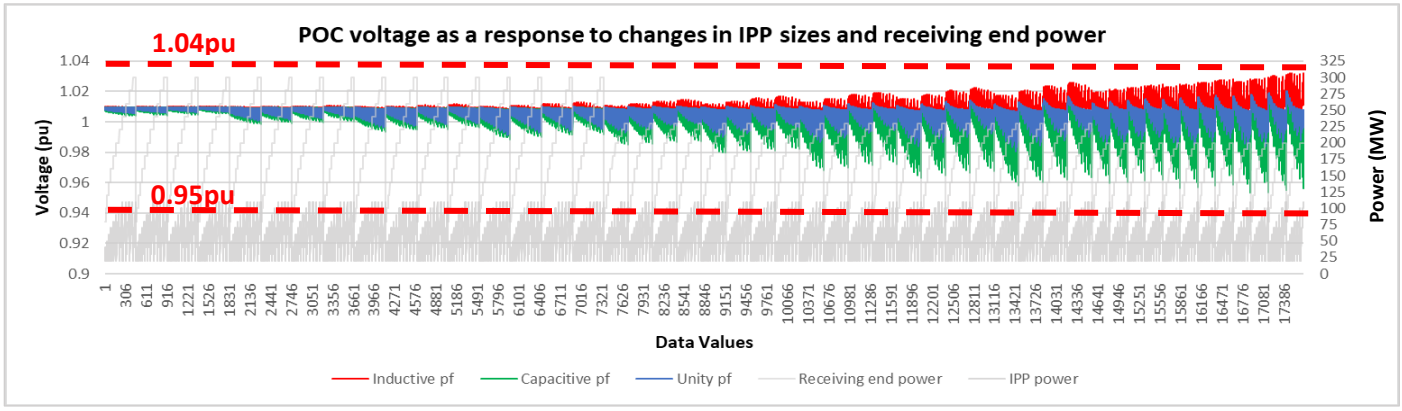

Figure A – 73: 220 kV POC voltage as a response to changes in IPP Sizes and receiving end load power

D. Thermal loading graphs for interconnecting conductor, and backbone conductors (Segment A and B).

The thermal loading of the backbone (Segment A and Segment B) and the interconnecting conductor are shown in Figures A-74 to A-76. As seen, for all simulations, there is again no excessive thermal stress on all conductors in the network, with the maximum loading value not exceeding 90%. Thermal loading graphs are produced for IPP setpoints of unity, 0.95 capacitive and 0.95 inductive power factors.

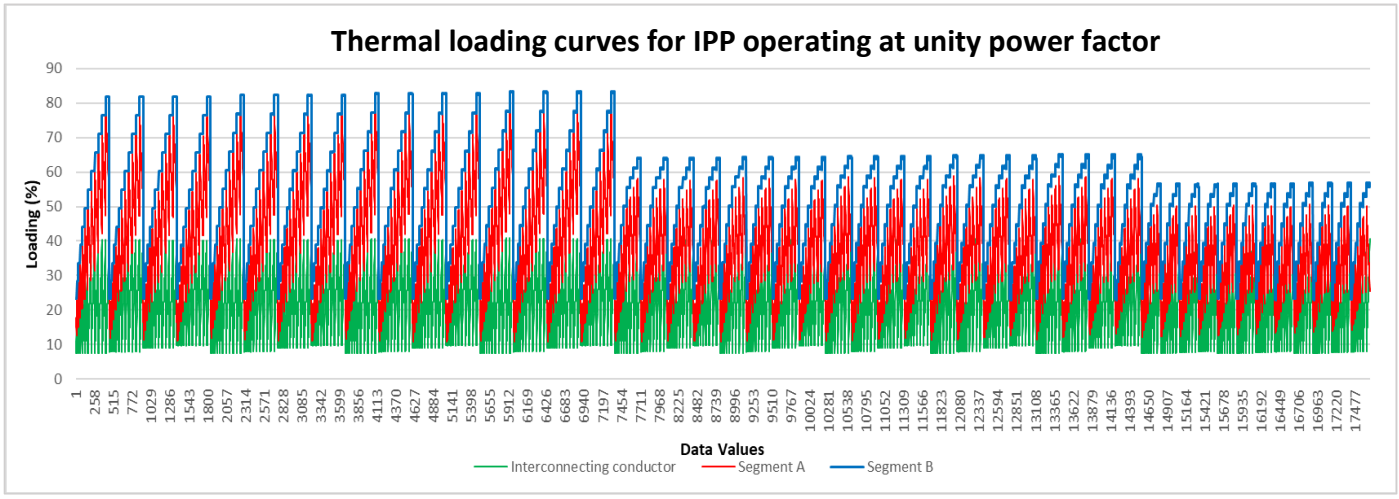

Figure A-74: 220 kV thermal loading for Segment A, Segment B and interconnecting conductor while IPP operates at unity pf (pf = 1).

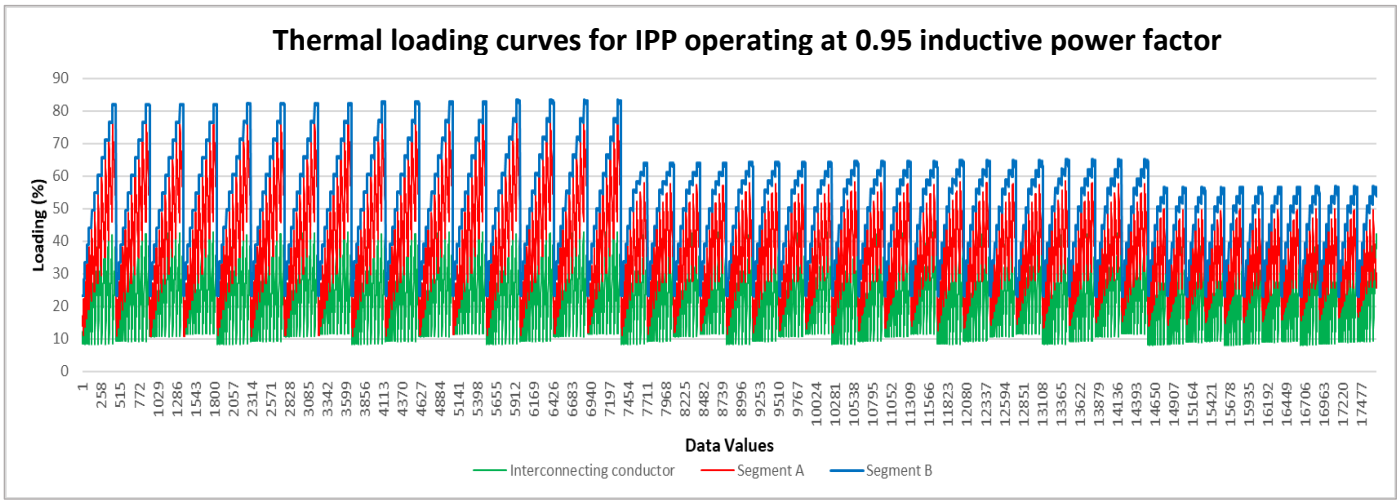

Figure A-75: 220 kV thermal loading for Segment A, Segment B and interconnecting conductor while IPP operates at 0.95 inductive pf (positive 0.95).

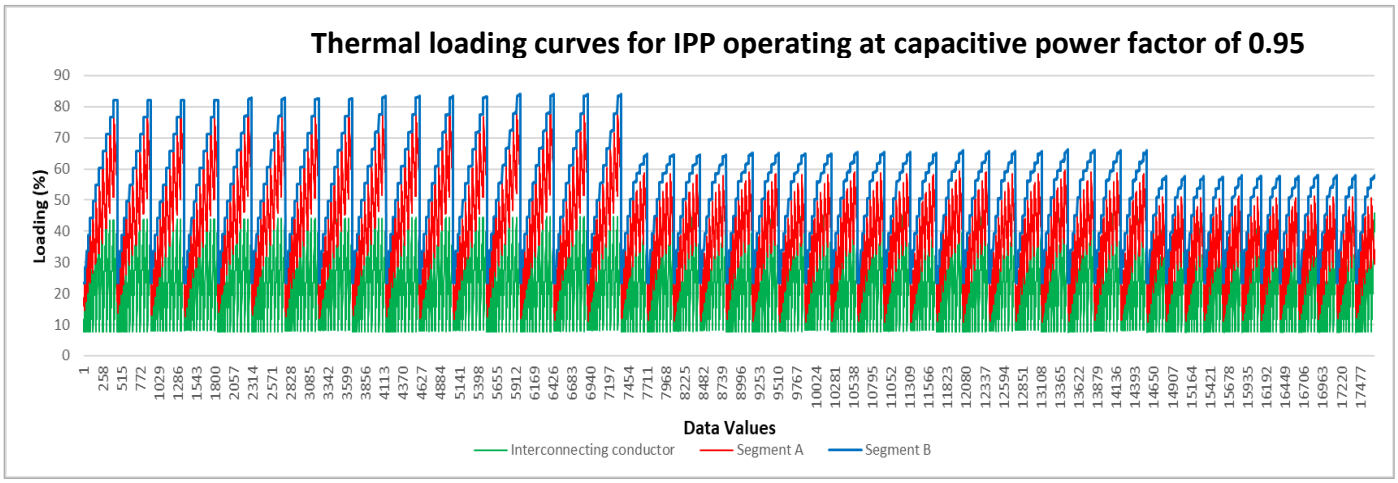

Figure A-76: 220 kV thermal loading for Segment A, Segment B and interconnecting conductor while IPP operates at 0.95 capacitive pf (negative 0.95).

E. Interconnecting conductor DC resistance at 20 deg C

Figure A-77 shows the interconnecting conductor DC resistance at 20 deg C. As seen, the standard twin Zebra conductor is used for the interconnecting feeder.

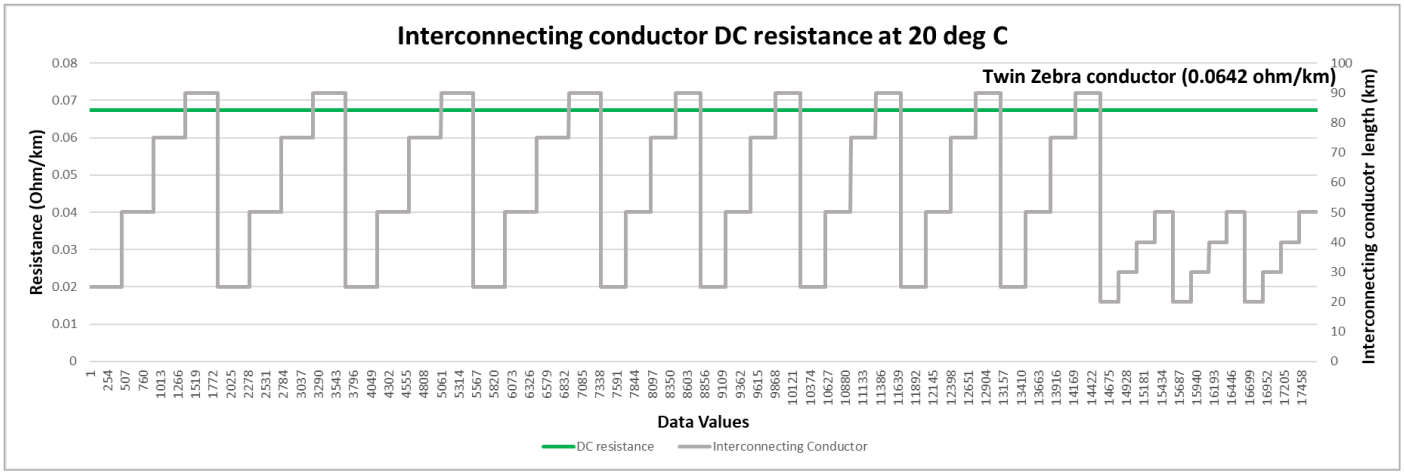

Figure A-77: 220 kV Interconnecting conductor DC resistance at 20 deg C

F. Interconnecting conductor diameter and Geometric mean radius graph.

For the 220 kV interconnecting conductor, the diameter and GMR are plotted as shown in Figure A-78.

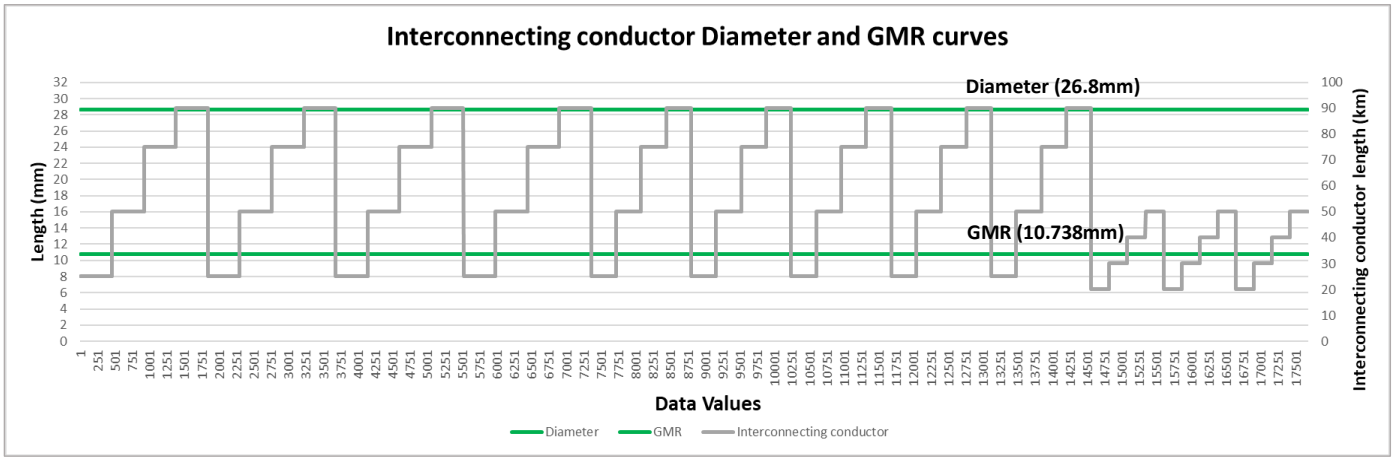

Figure A-78: 220 kV Interconnecting Conductor diameter versus GMR values

G. Interconnecting conductor nominal current graph.

The interconnecting conductor nominal current values are superimposed onto the Segment A an interconnecting conductor length graph as shown in Figure A-79.

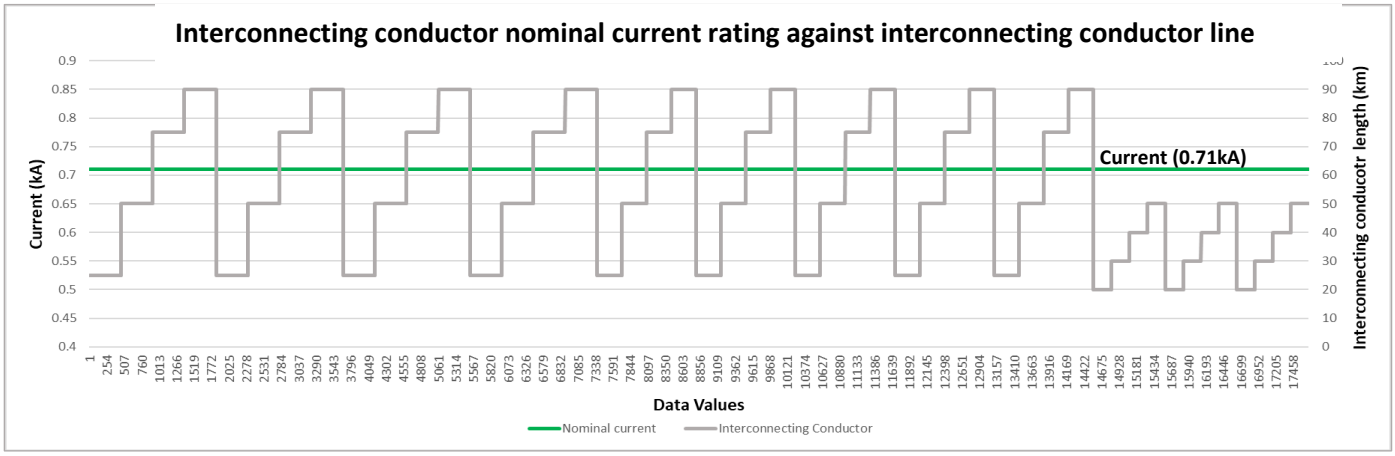

Figure A-79: 220 kV interconnecting conductor nominal current

H. Interconnecting conductor rated power versus IPP power graph.

Figure A-80 compares the interconnecting conductor rated power capacitiy againstst the IPP size. As seen, for all changes in IPP sizes, there is an adequate change in interconnecting conductor rating, to safely transfer the required IPP power.

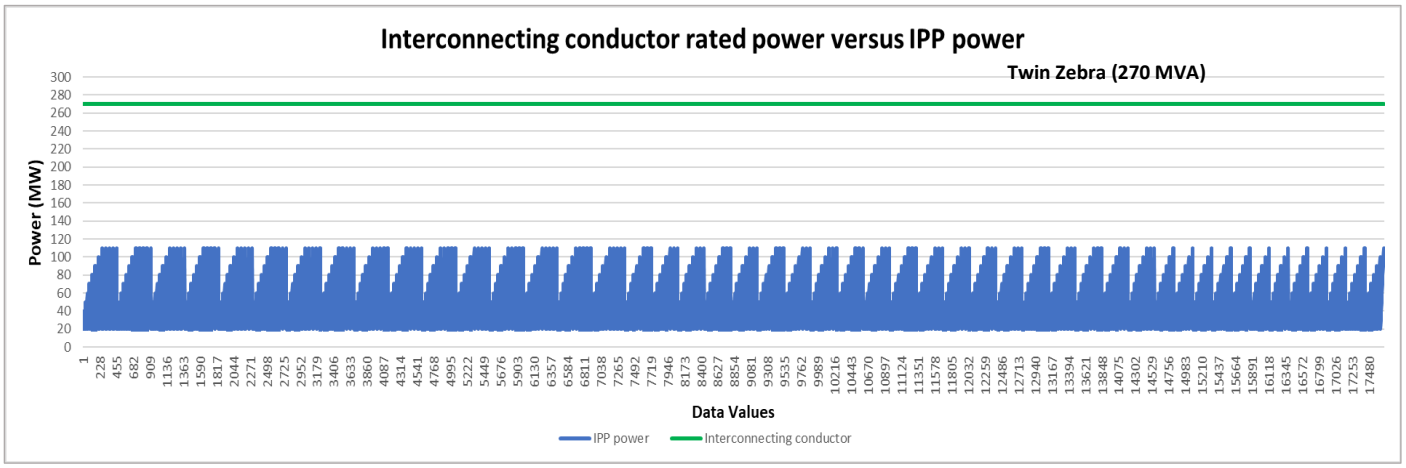

Figure A-80: 220 kV Interconnecting conductor is adequately rated to handle IPP export power

I. IPP power factor variation graphs for unity, leading and lagging setpoints applicable to Category C (0.95).

The IPP power factor graph shown in Figure A-81 below shows the variation in IPP power factor the 220 kV network.

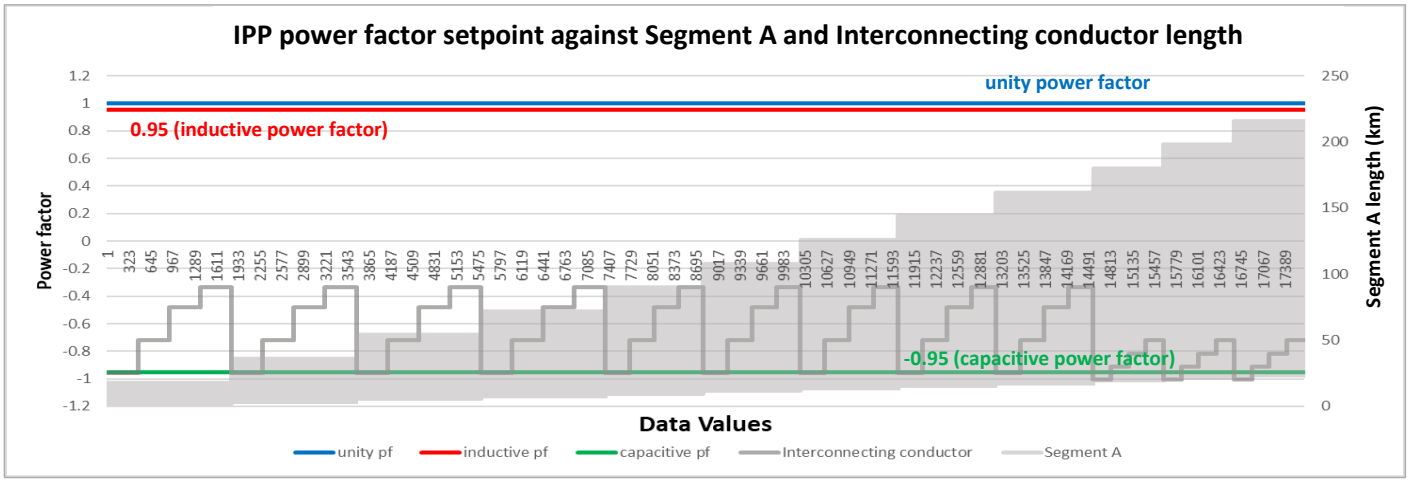

Figure A-81: 220kV IPP variations in power factor

J. Power line loss graphs corresponding to IPP power factor variation graphs.

The corresponding power line loss curves are shown in Figures A – 82 to 84 below.

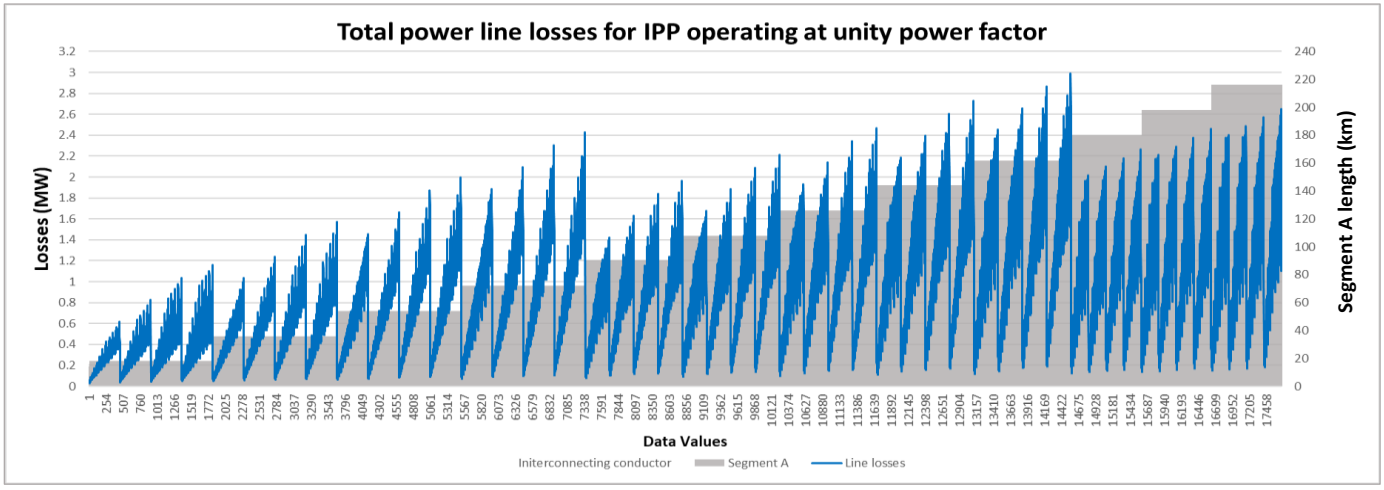

Figure A-82: 220 kV Total power line losses for a unity power factor setpoint

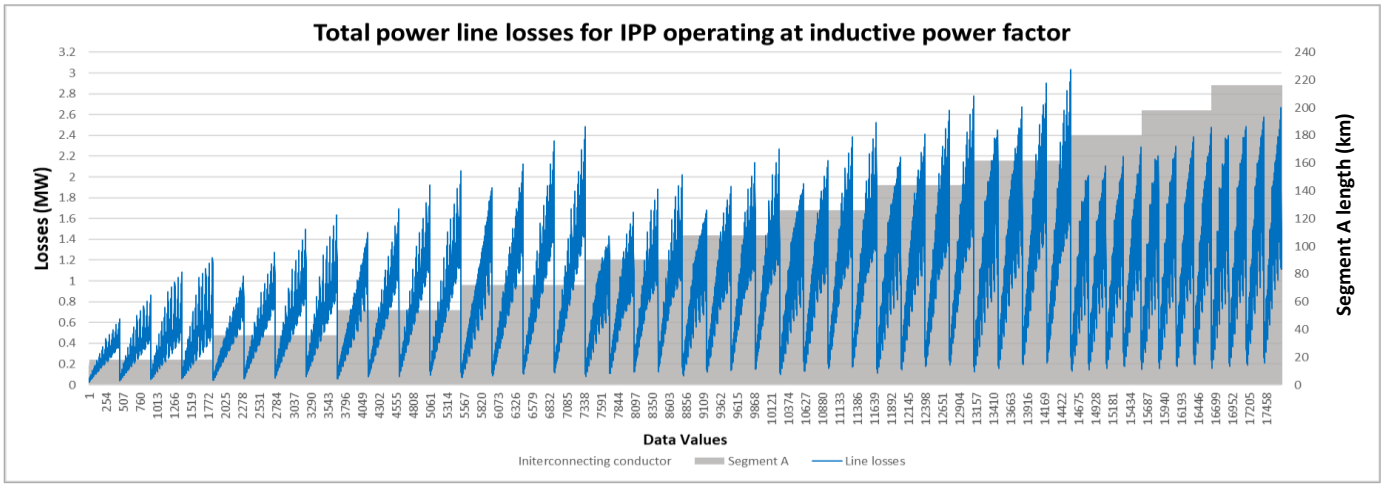

Figure A-83: 220 kV Total power line losses for an inductive power factor setpoint

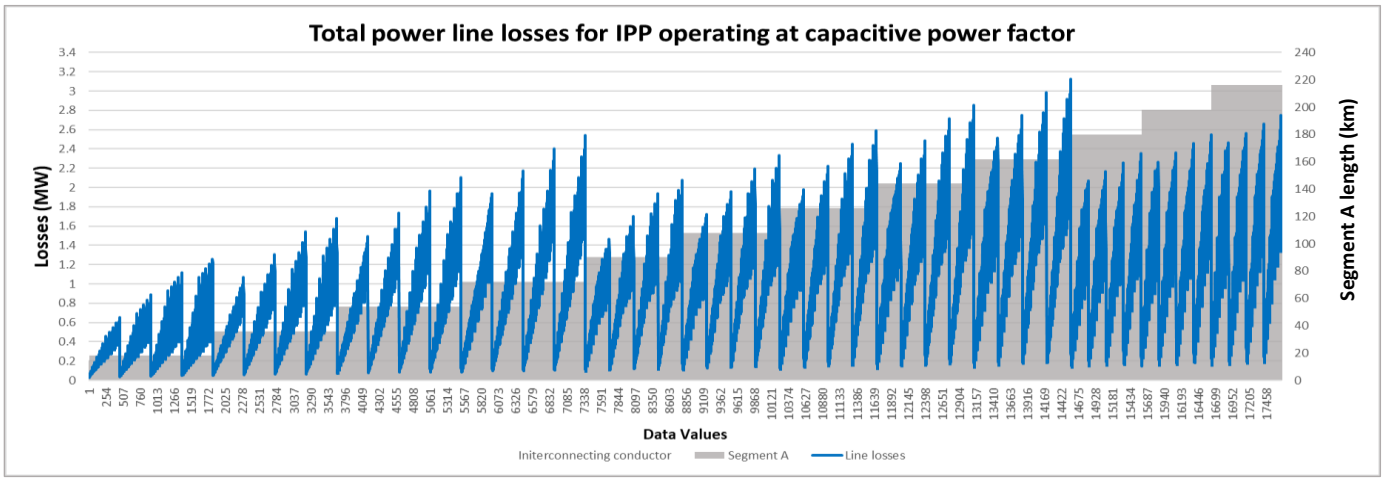

Figure A-84: 220kV Total power line losses for a capacitive power factor setpoint

For the 220kV technology, data shown from Sections (A) – (J) above is saved into three 17682x8 input data matrices, one representing the unity power factor IPP setpoint, another representing the lagging IPP setpoint, and another representing the leading power factor setpoint. When combined, a 53046 x 8 input data matrix (17682x3) is saved along with a 53046x1 target data matrix, and these are used in the ANN design and modelling section to follow in Section 3.3. In order to capture losses for the scenarios in which the load is non-unity, the above simulations are redone in the same fashion as before, but for a receiving end (load) power factor setpoint of 0.95 (inductive) as well as 0.95 (capacitive). This means that the combined input data matrix to be used in the ANN design and modelling section expands in size from 53046x8 to 159120x8 and a target data size of 159120x1.

3.2.4.6 275kV Data

For the 275kV network, the interconnecting feeder length is adjusted four times for backbone lengths up to 220km (25km, 50km, 75km and 80km). For all backbone lengths, the interconnecting conductor is limited to 80km ensuring system voltages remain within the 1.05pu limit. From a loading perspective - at the receiving end, backbone lengths are all simulated for loads varying from 80MW to 300MW. The receiving end makes use of two 250MVA transformers. The IPP model transfers its power via two 125MVA 275/132kV step up transformers (Figure A-85 and Figure A-86) in order to transfer the maximum export power of 110MW. This is used to ensure that the IPP sending end voltage is controlled within required pu limit. The receiving end makes use of two 250MVA transformers.

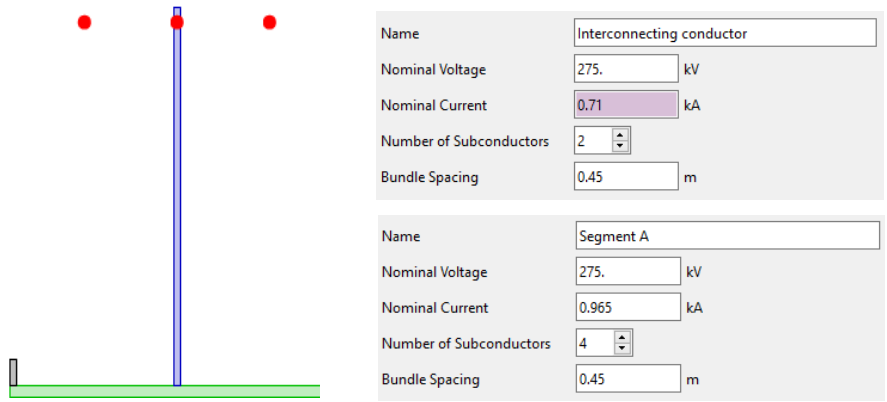

Figure A-85: 275 kV Interconnecting conductor length and location on backbone graph

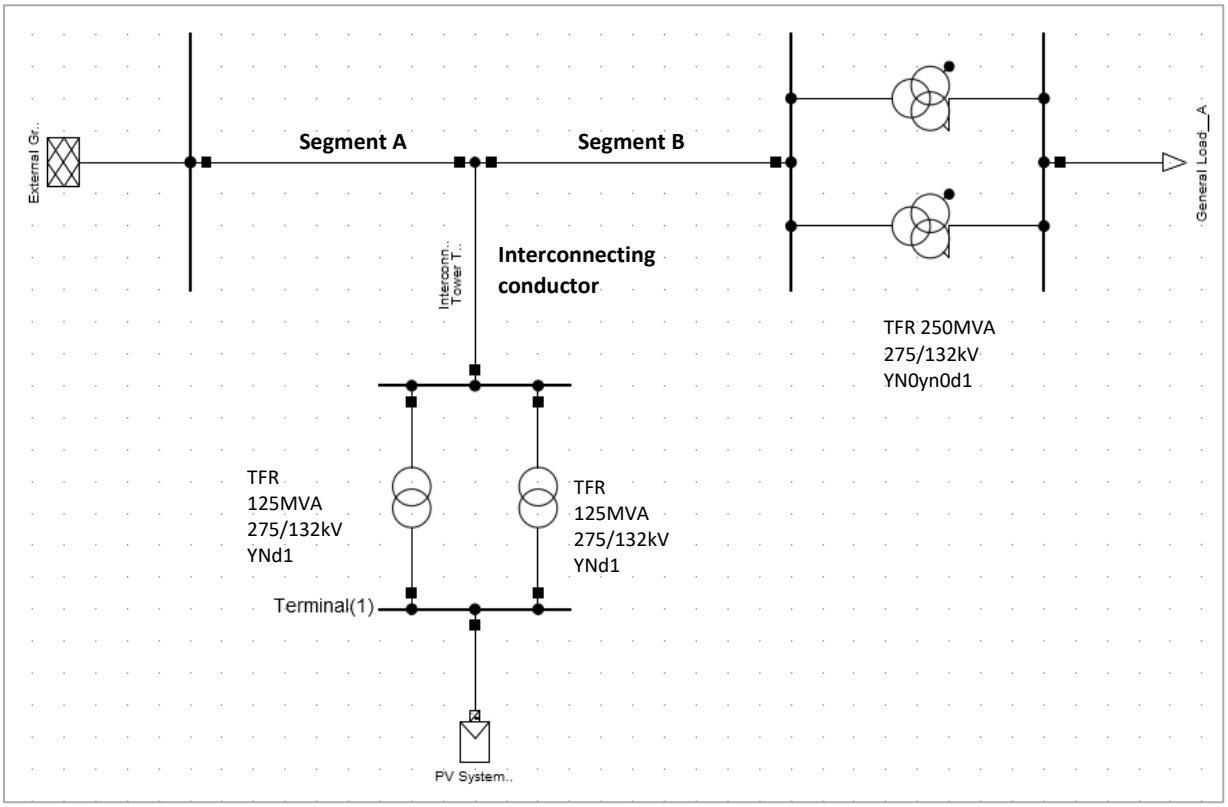

Figure A-86: 275 kV Interconnecting conductor length and location on backbone graph

A. Interconnecting conductor location on backbone graph

Figure A-87 shows how the length of Segment A is change which at 275kV, allows for 12 backbone lengths of 20 km (Data values 1 – 1840), 40 km (Data values 1841 – 3680), 60 km (Data values 3681 – 5520), 80 km (5521 - 7360), 100 km (7361 - 9200) and 120 km (9201 - 11040),140km (11041 – 12880), 160km (12881 – 14720), 180km (14721 – 16560) and 200km (16561 – 18401), 220km (18401 – 20240) respectively.

As seen, four different interconnecting conductor lengths in total divide all backbones into 4 sets of data, one set for every interconnecting conductor length (as was for the 220kV case). Within each set, different receiving end loads are again applied accordingly (Figure A-88). As seen, for all backbone lengths, all four sets of interconnecting conductor lengths from 25km to 90km have associated loads ranging from 20 MW to 300 MW.

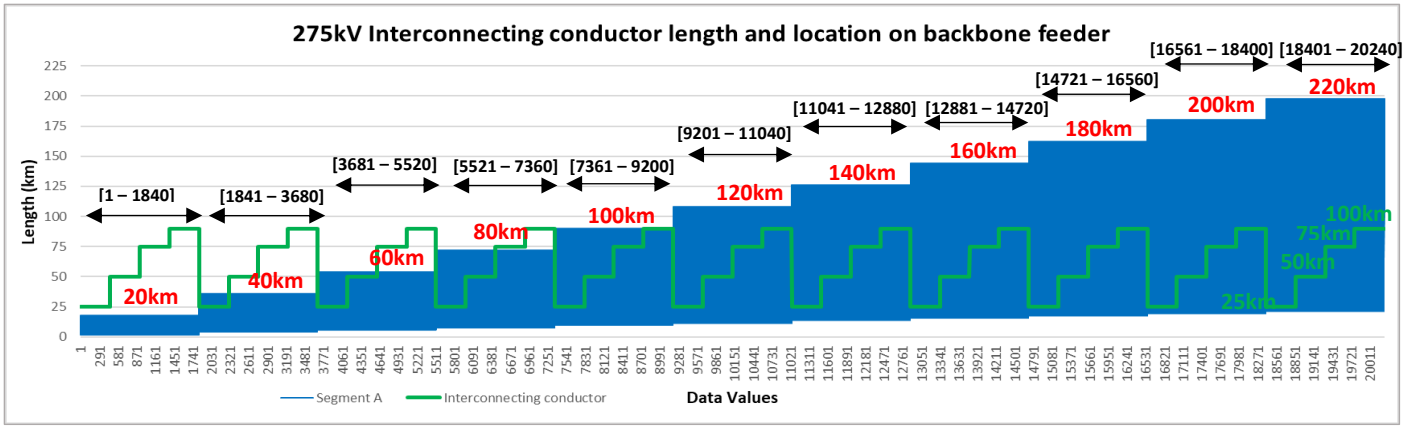

Figure A-87: 275 kV Interconnecting conductor length and location on backbone graph

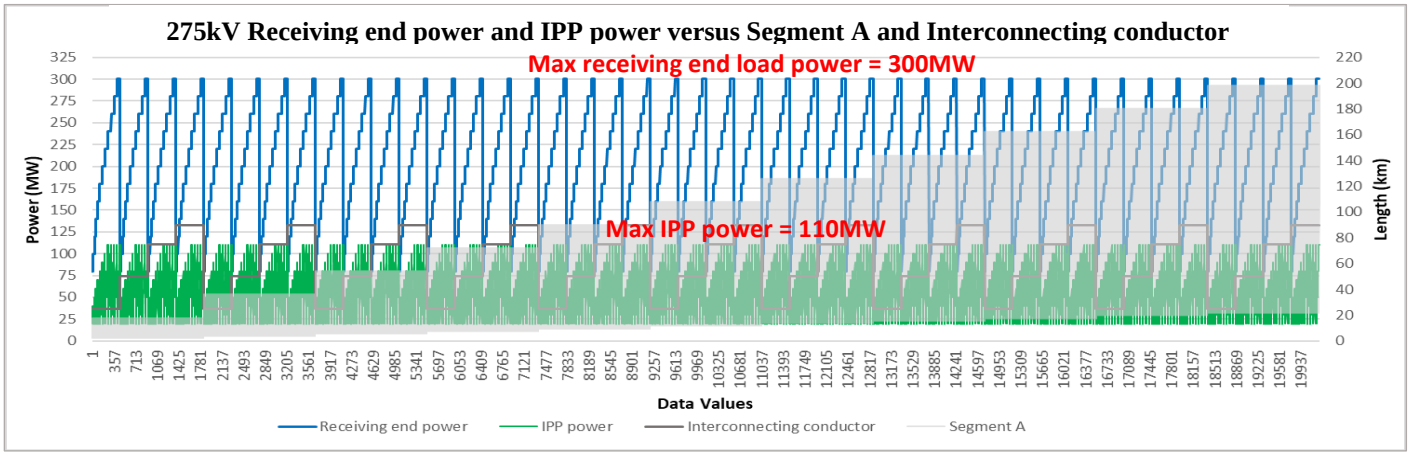

Figure A-88: 275 kV Interconnecting conductor length and its location on backbone graph, with receiving end power and IPP power curves

B. Maximum MVA loading graph for the interconnecting conductor, Segment A and Segment B of the backbone, for loads operating at unity power factor.

Figure A-89 shows the sending end power required (red curve) for the 275kV network. As seen again, this is the difference between load receiving end power and the power supplied by the IPP.

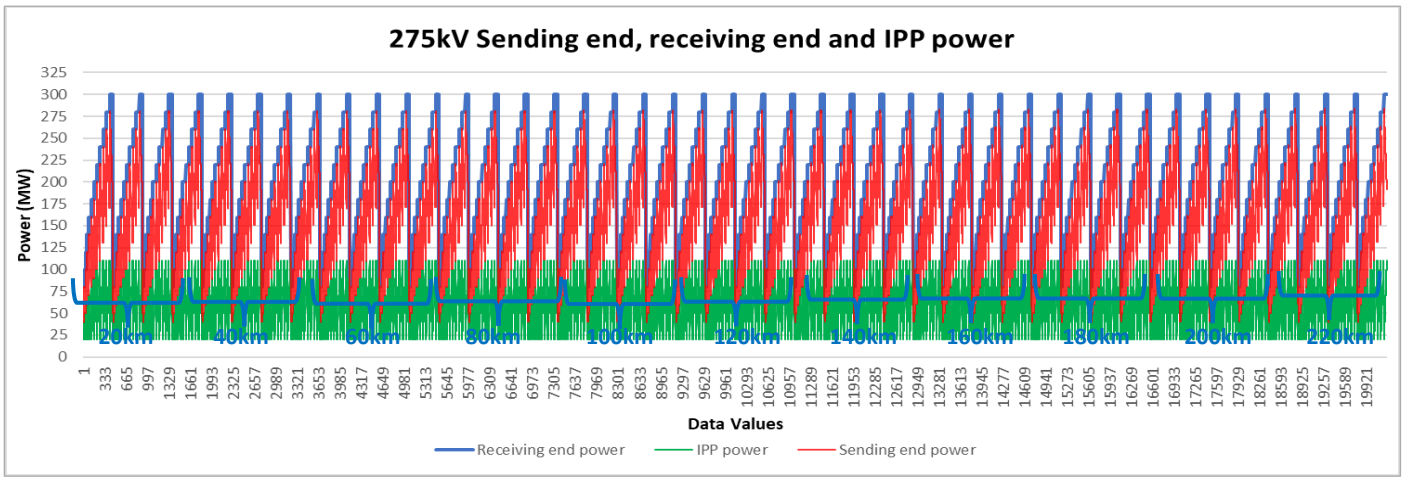

Figure A-89: 275 kV Receiving end, sending end and IPP power curves

C. Maximum and minimum voltage graphs at the receiving (load end), IPP 275kV busbar of the network as well as POC.

Figure A-90 to Figure A-92 respectively show the receiving end and POC voltage graphs against Segment A lengths and the interconnecting feeder lengths for the IPP operating at unity, capacitive and inductive power factor setpoints for the 275 kV network. Again, the inductive power factor setpoint corresponding to all IPPs (regardless of size) achieves the greatest increase in voltage at the receiving end and POC. But as seen in Figures A-93 to A-94, for an increased load there is a decreased trend of voltage at both the receiving end and POC, regardless of backbone length, as was the case for the previous networks.

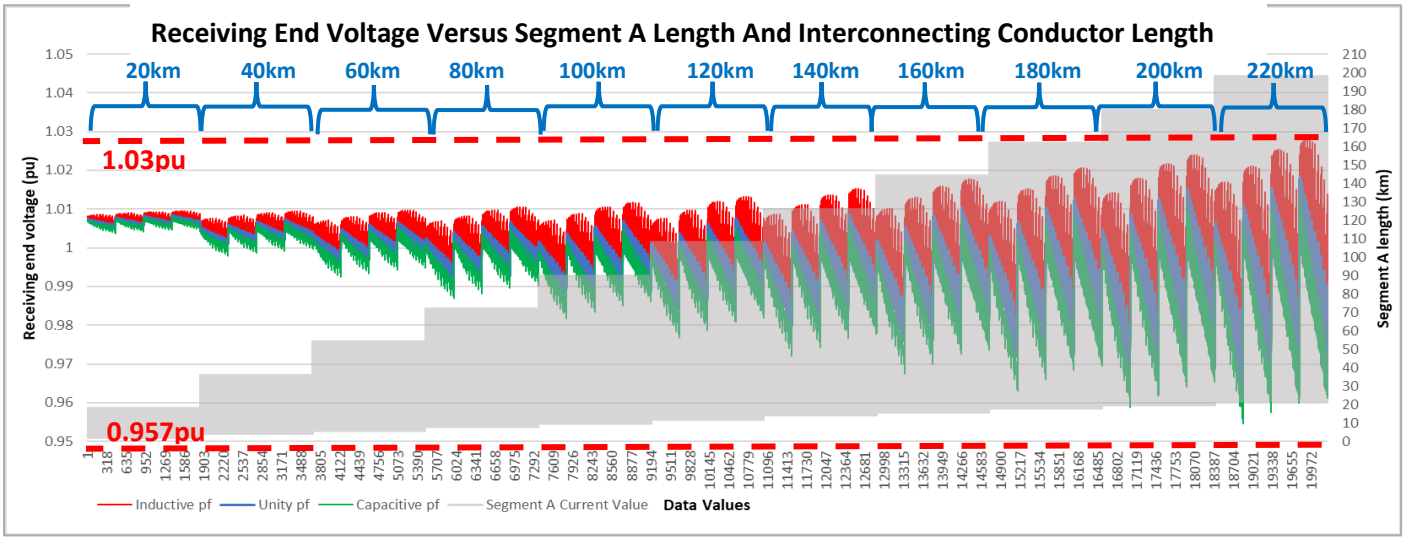

Figure A-90: 275 kV Receiving end versus segment A length and interconnecting conductor length

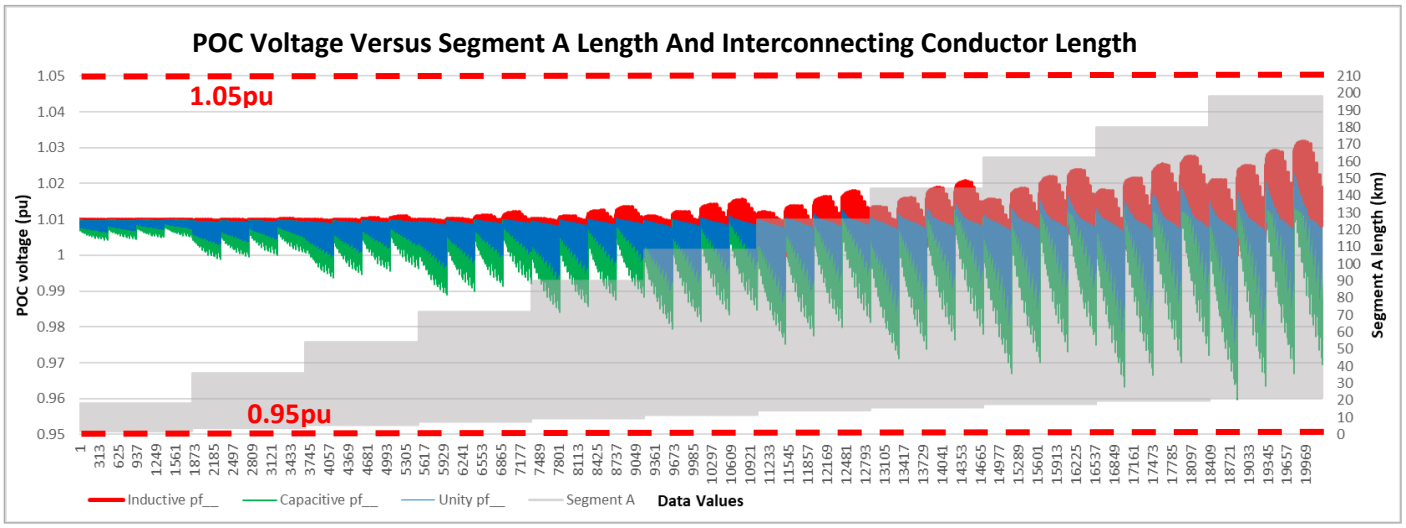

Figure A-91: 275 kV POC Voltage Versus Segment A Length And Interconnecting Conductor Length

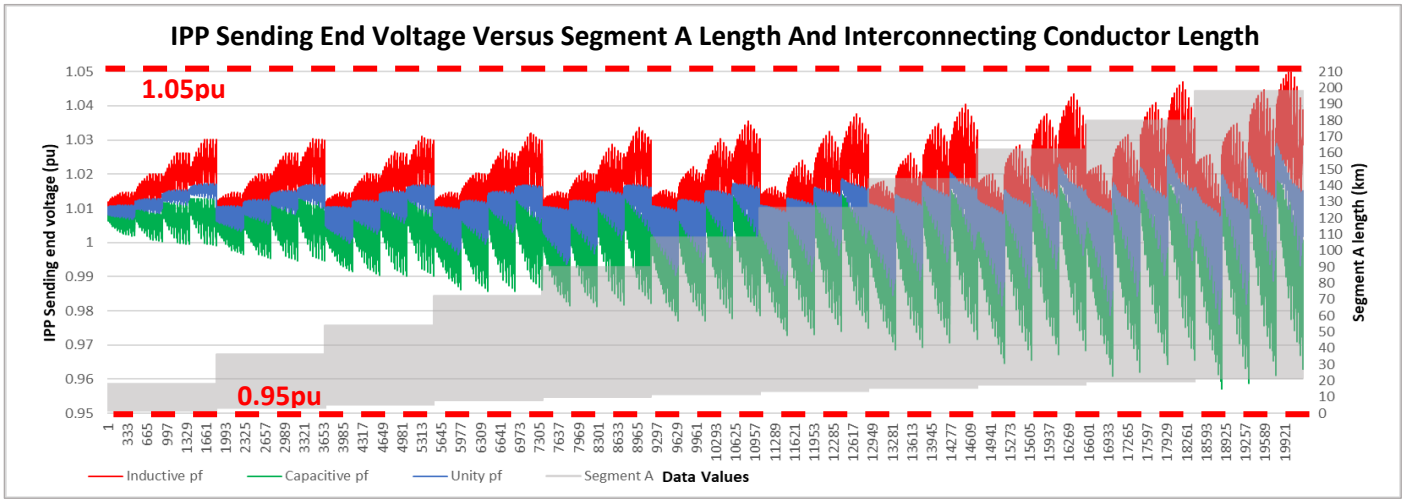

Figure A-92: 275 kV IPP sending end voltage as a response to changes in Segment A length and interconnecting conductor length

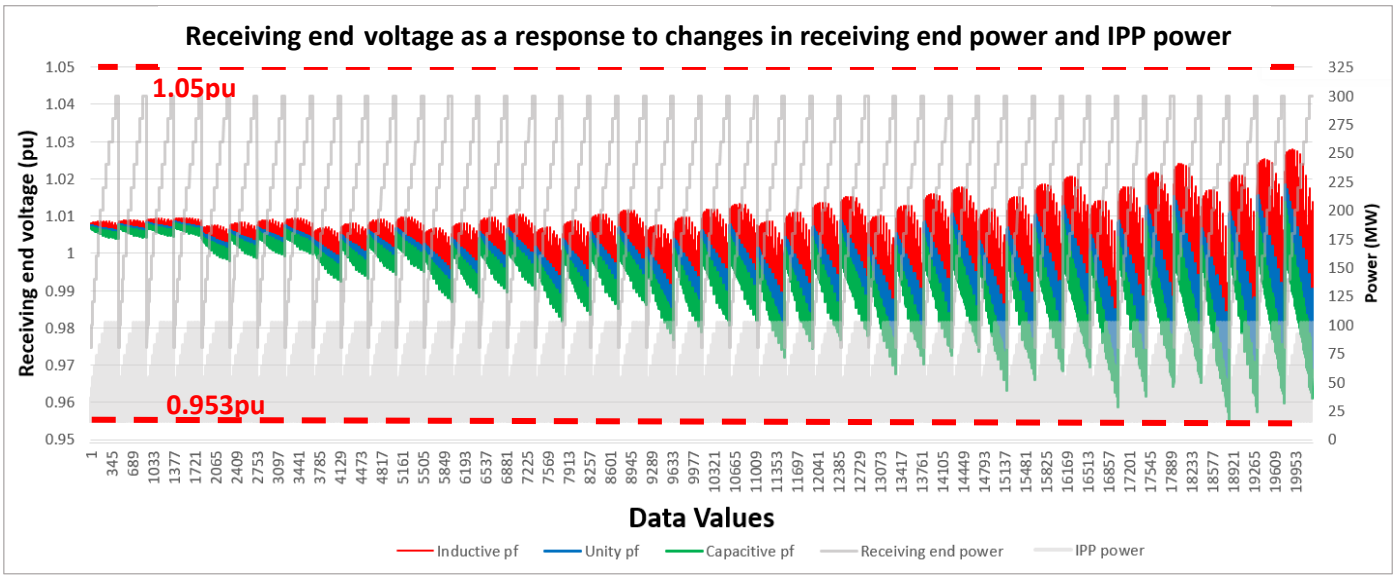

Figure A-93: 275 kV Receiving end voltage as a response to changes in IPP Sizes and receiving end load power

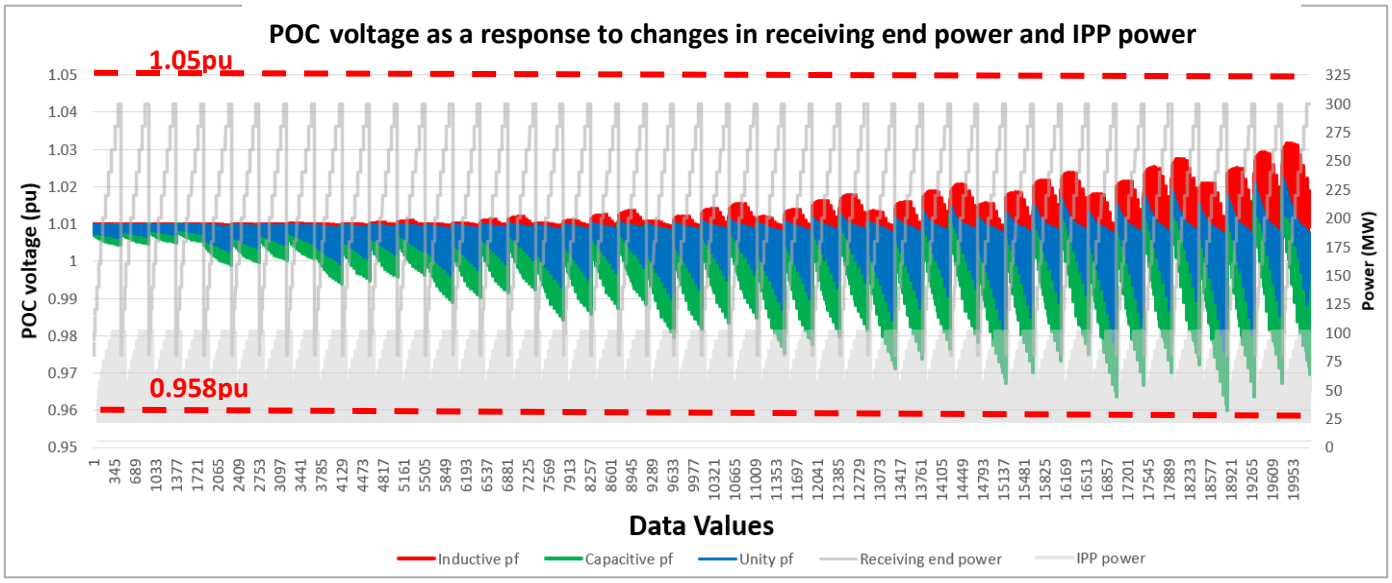

Figure A-94: 275 kV POC voltage as a response to changes in IPP Sizes and receiving end load power

D. Thermal loading graphs for interconnecting conductor, and backbone conductors (Segment A and B).

The thermal loading of the backbone (Segment A and Segment B), and the interconnecting conductor are shown by Figures A-95 to A-97. As seen, for all simulations, there is again no excessive thermal stress on all conductors in the network, with the maximum loading value not exceeding 90%. Thermal loading graphs are produced for IPP setpoints of unity, 0.95 capacitive and 0.95 inductive power factors.

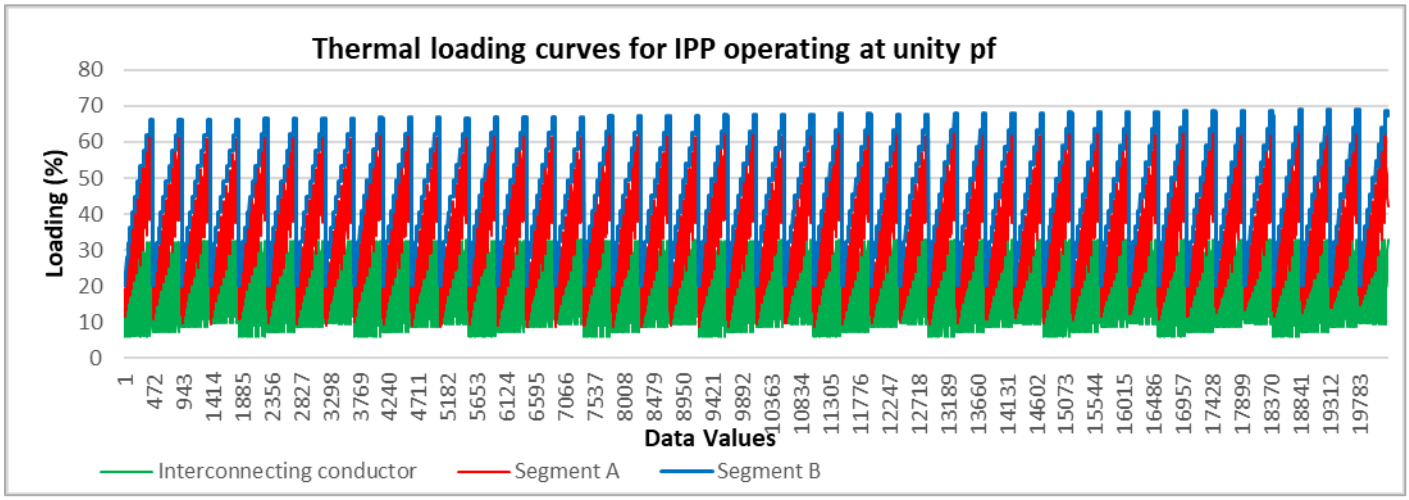

Figure A-95:275 kV thermal loading for segment A, segment B and interconnecting conductor while IPP operates at unity pf

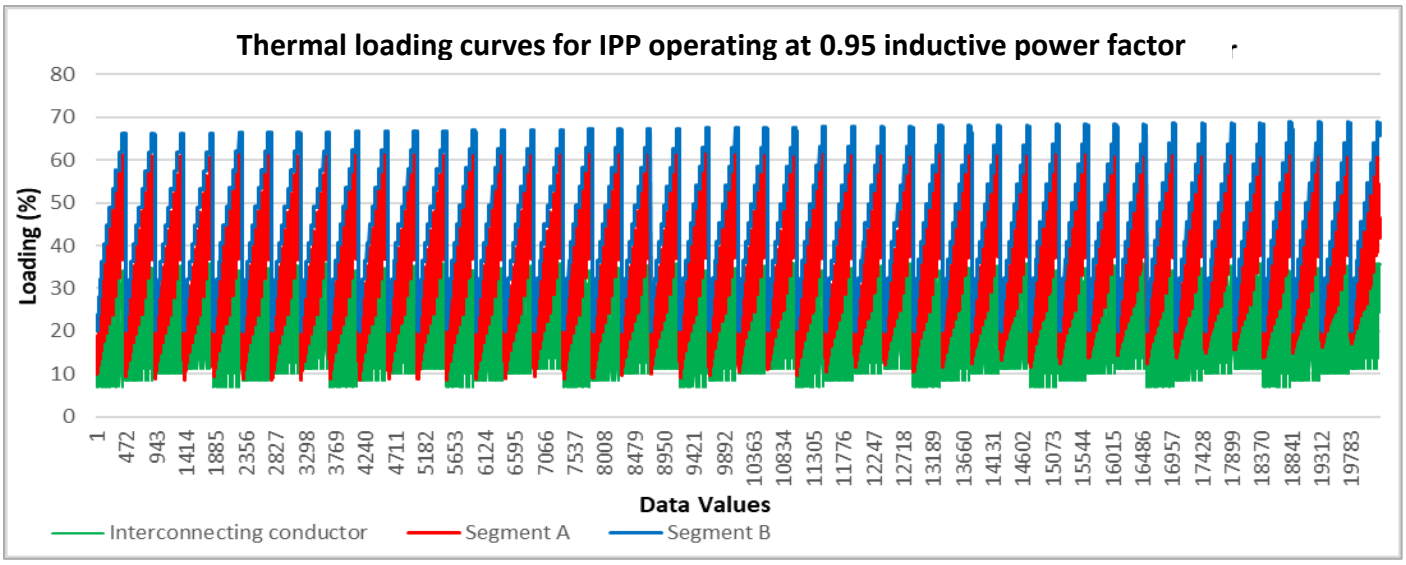

Figure A-96:275 kV thermal loading for segment A, segment B and interconnecting conductor while IPP operates at 0.95 inductive pf

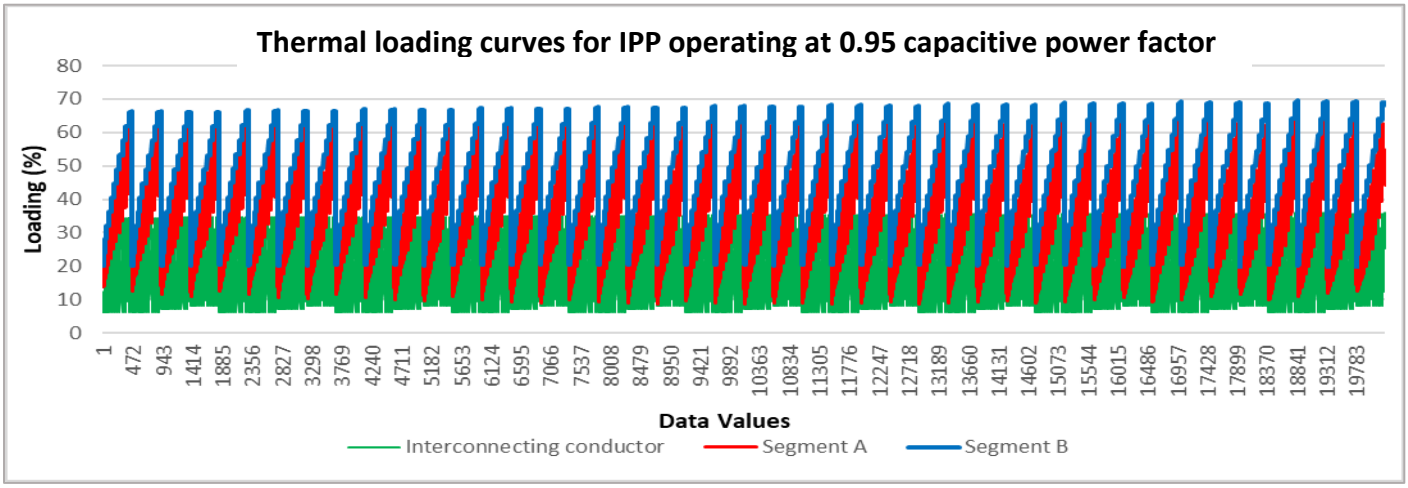

Figure A-97:275 kV thermal loading for Segment A, Segment B and interconnecting conductor while IPP operates at 0.95 capacitive pf`

E. Interconnecting conductor DC resistance at 20˚C

Figure A-98 shows the interconnecting conductor DC resistance at 20 deg. As seen, the standard Twin Zebra conductor is used for the interconnecting feeder at 275kV.

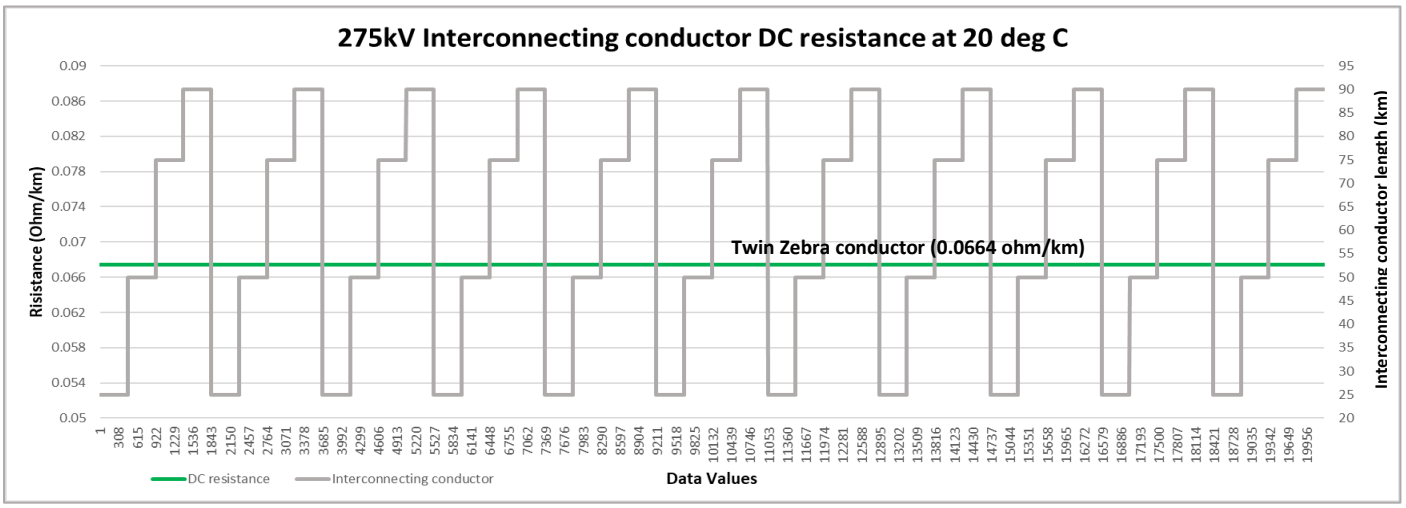

Figure A-98: 275 kV Interconnecting conductor DC resistance at 20 deg C

F. Interconnecting conductor diameter and Geometric mean radius graph.

Figure A-99 shows the interconnecting conductor diameter and GMR graph, for the interconnecting feeder at 275kV.

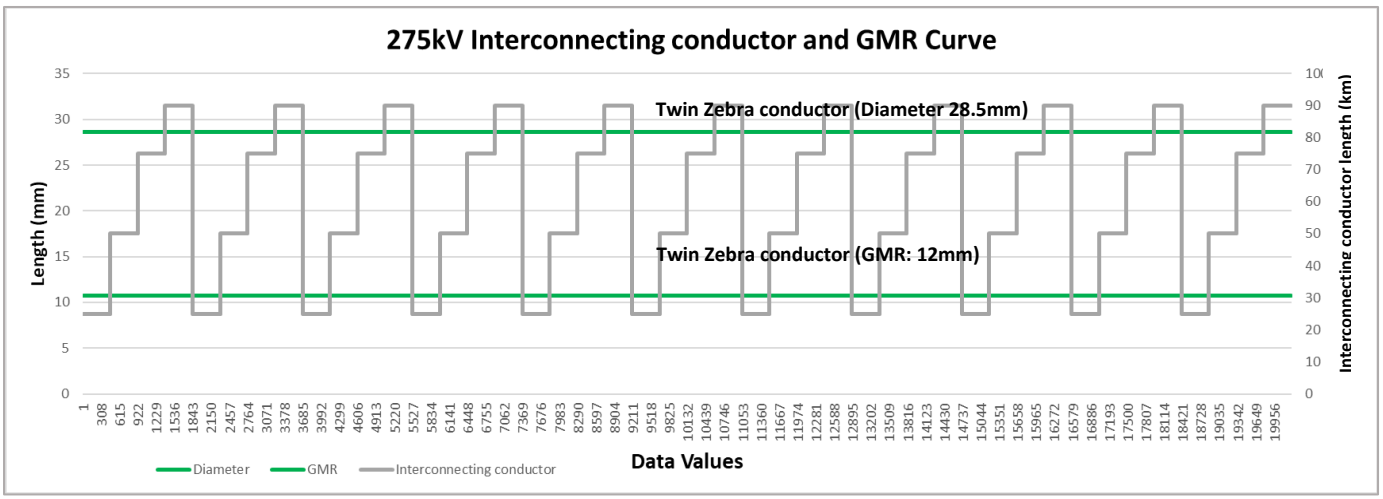

Figure A-99: 275 kV Interconnecting Conductor diameter versus GMR values

G. Interconnecting conductor nominal current graph.

The interconnecting conductor nominal current values are superimposed onto the Segment A an interconnecting conductor length graph as shown in Figure A-100.

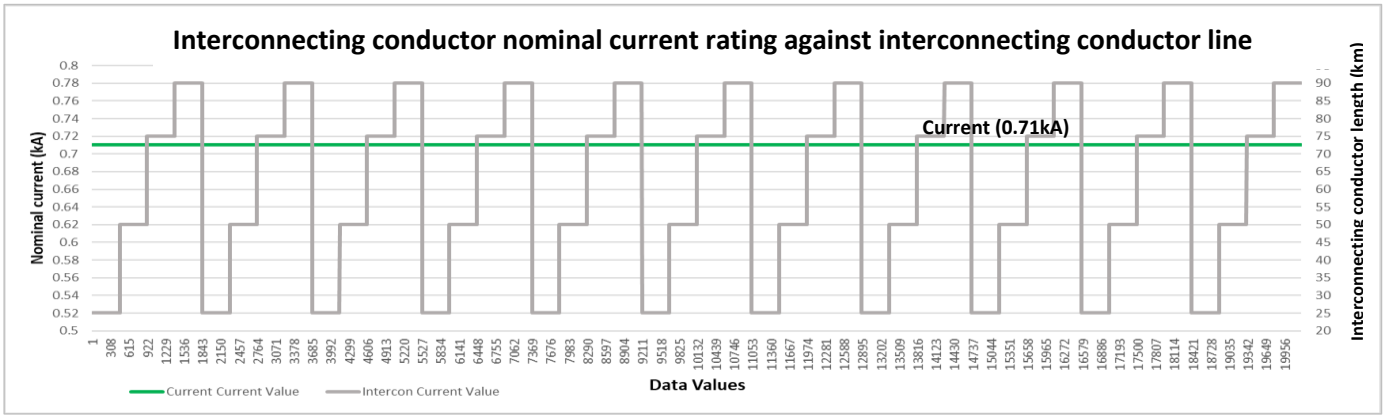

Figure A-100: 275 kV interconnecting conductor nominal current

H. Interconnecting conductor rated power versus IPP power graph.

Figure A -101 compares the interconnecting conductor rated power capacity against the IPP size. As seen, for all changes in IPP sizes, there is an adequate change in interconnecting conductor rating, to safely transfer the required IPP power.

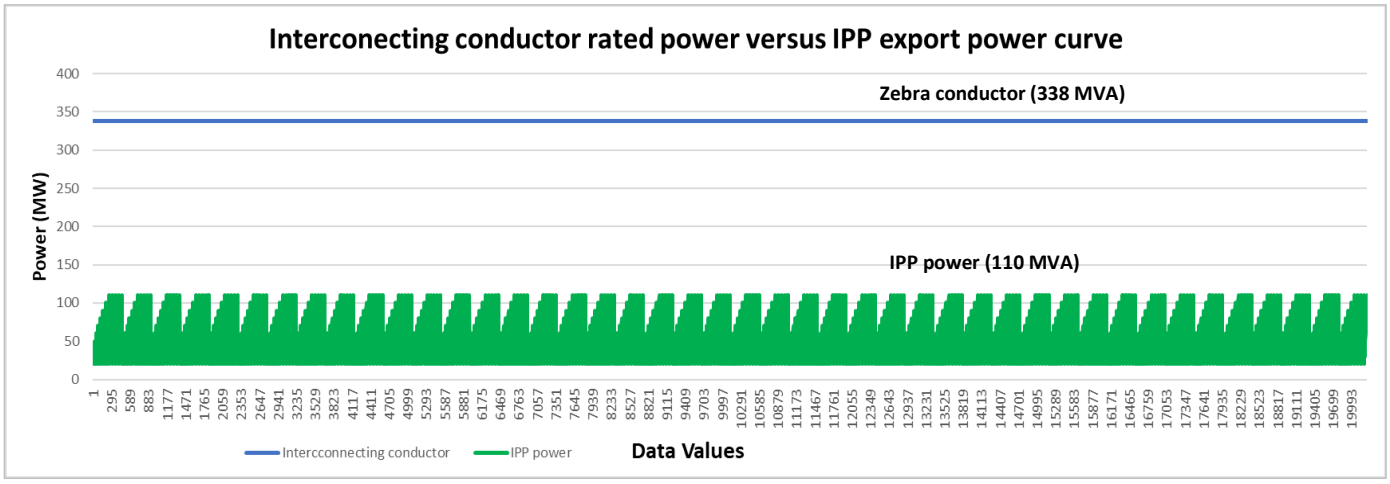

Figure A-101: 275 kV Interconnecting conductor is adequately rated to handle IPP export power

I. IPP power factor variation graphs for unity, leading and lagging setpoints applicable to Category C (0.95 pf).

The IPP power factor graph shown in Figure A-102 below shows the variation in IPP power factor the 275 kV network.

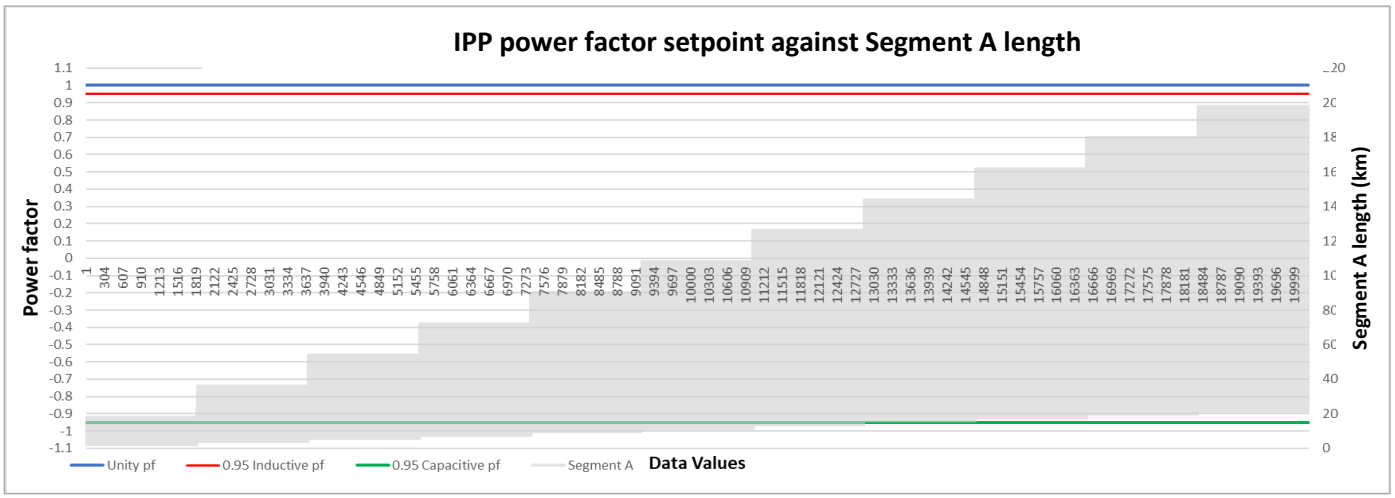

Figure A-102: 275 kV IPP variations in power factor

J. Power line loss graphs corresponding to IPP power factor variation graphs.

The corresponding power line losses curves are shown in Figures A-103 to A-105.

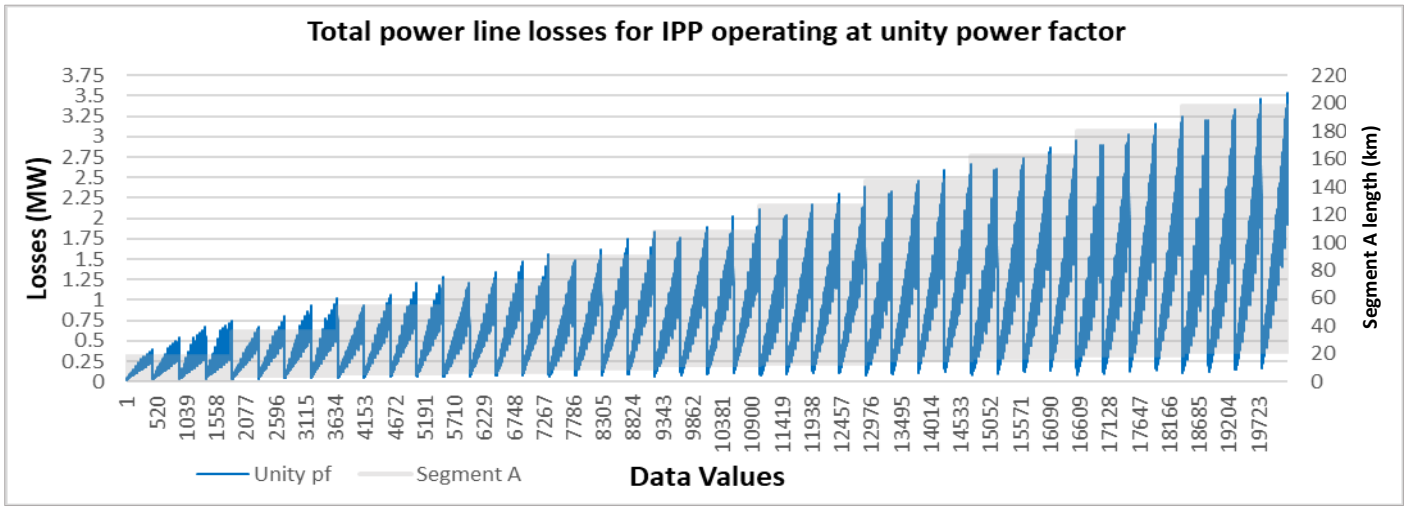

Figure A-103: 275 kV Total power line losses for the IPP at unity power factor

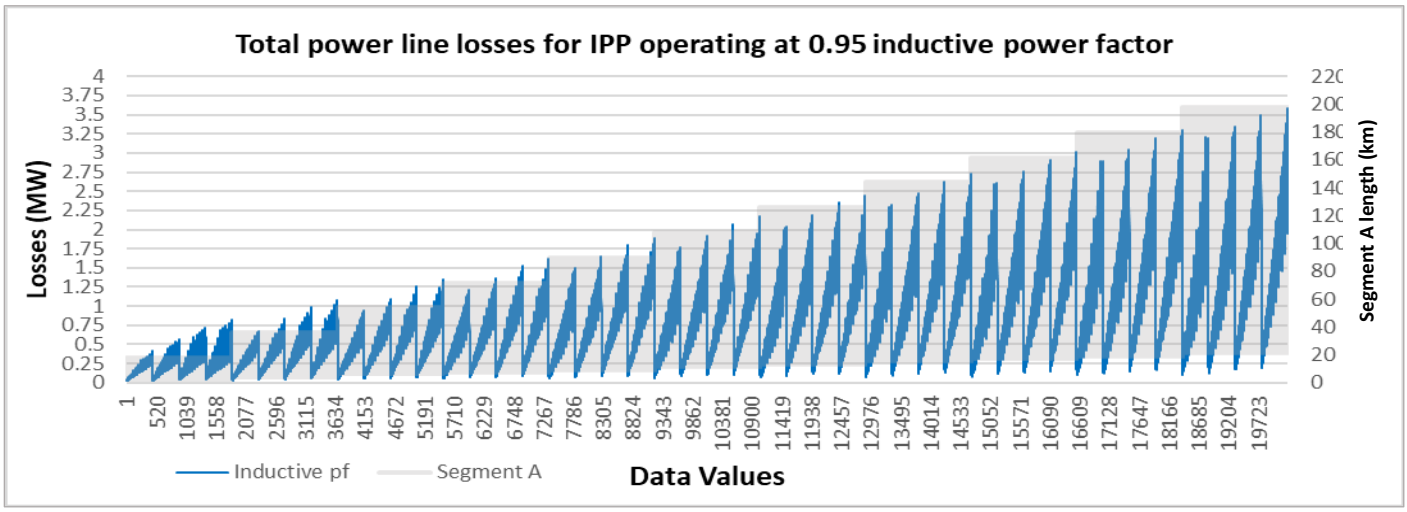

Figure A-104: 275 kV Total power line losses the IPP at inductive power factor

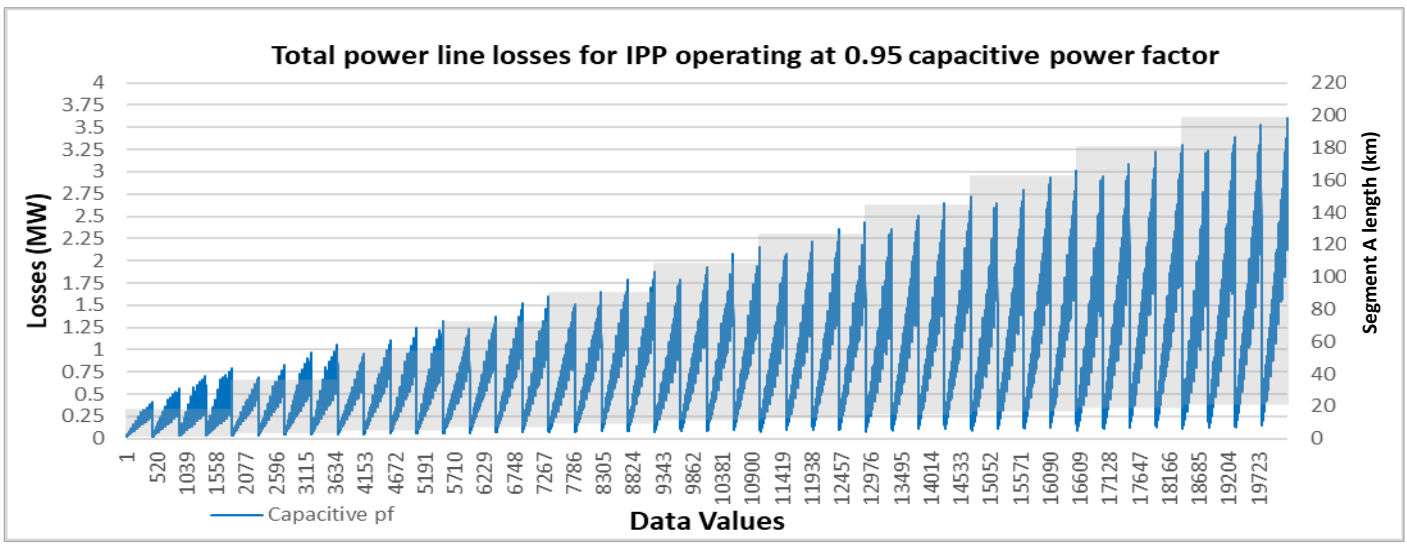

Figure A-105: 275 kV Total power line losses for the IPP at capacitive power factor

For the 275 kV technology, data shown from Sections (A) – (J) above is saved into three 27840x8 input data matrices, one representing the unity power factor IPP setpoint, another representing the lagging IPP setpoint, and another representing the leading power factor setpoint. When combined, a 83520 x 8 input data matrix (27840x3) is saved, along with a 83520x1 target data matrix, and these will be used in the ANN design and modelling section to follow in Section 3.3. In order to capture losses for the scenarios in which the load is non-unity, the above simulations are redone in the same fashion as before, but for a receiving end (load) power factor setpoint of 0.975 (inductive) as well as 0.975 (capacitive). This means that the combined input data matrix to be used in the ANN design and modelling section expands in size from 83520x8 to 182160x8 and a target data size of 182160x1.

400kV Data

For the 400kV network, the interconnecting feeder length is adjusted four times (25km, 50km, 75km and 100km), with the maximum backbone feeder length extending to 260km (Figure A-106 to Figure A-107). For 400kV backbones, loading is typically greater than 150 MW as indicated in [6]. For this reason, the receiving end is loaded from a minimum of 150 MW to a maximum of 560 MW. The load end uses two 500MVA transformers. The IPP model transfers its power via two 125MVA 400/132kV step up transformers in order to transfer the maximum export power of 110MW. This is used to ensure that the IPP sending end voltage is controlled within required pu limit.

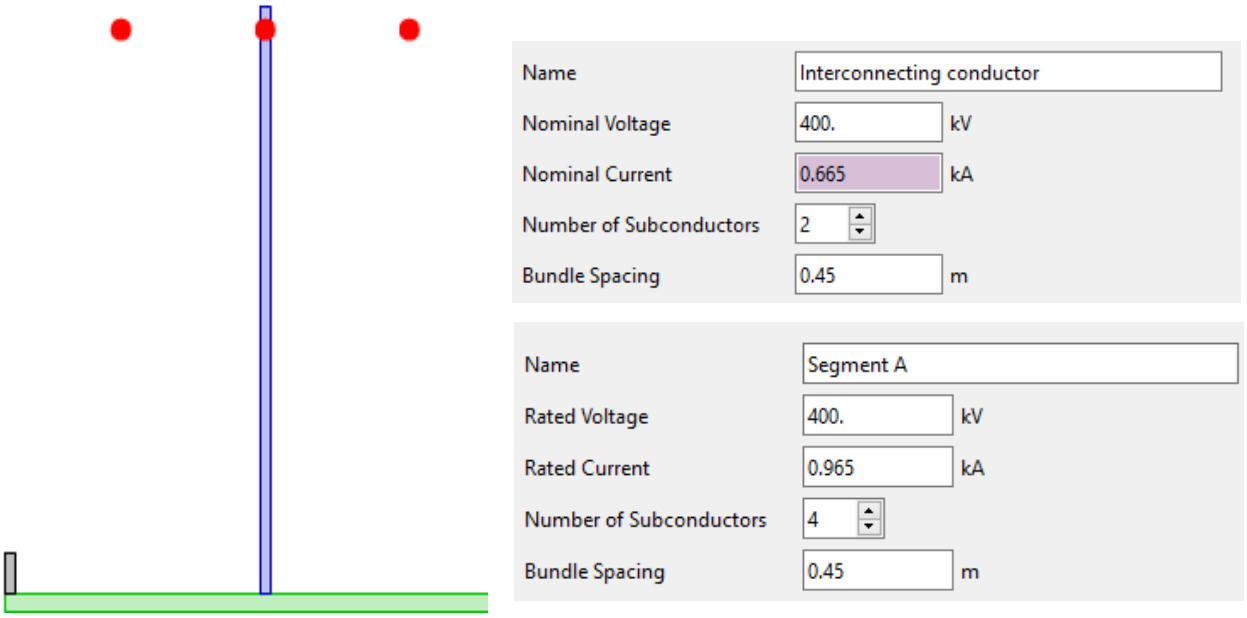

Figure A-106: 400 kV Interconnecting conductor length and location on backbone graph

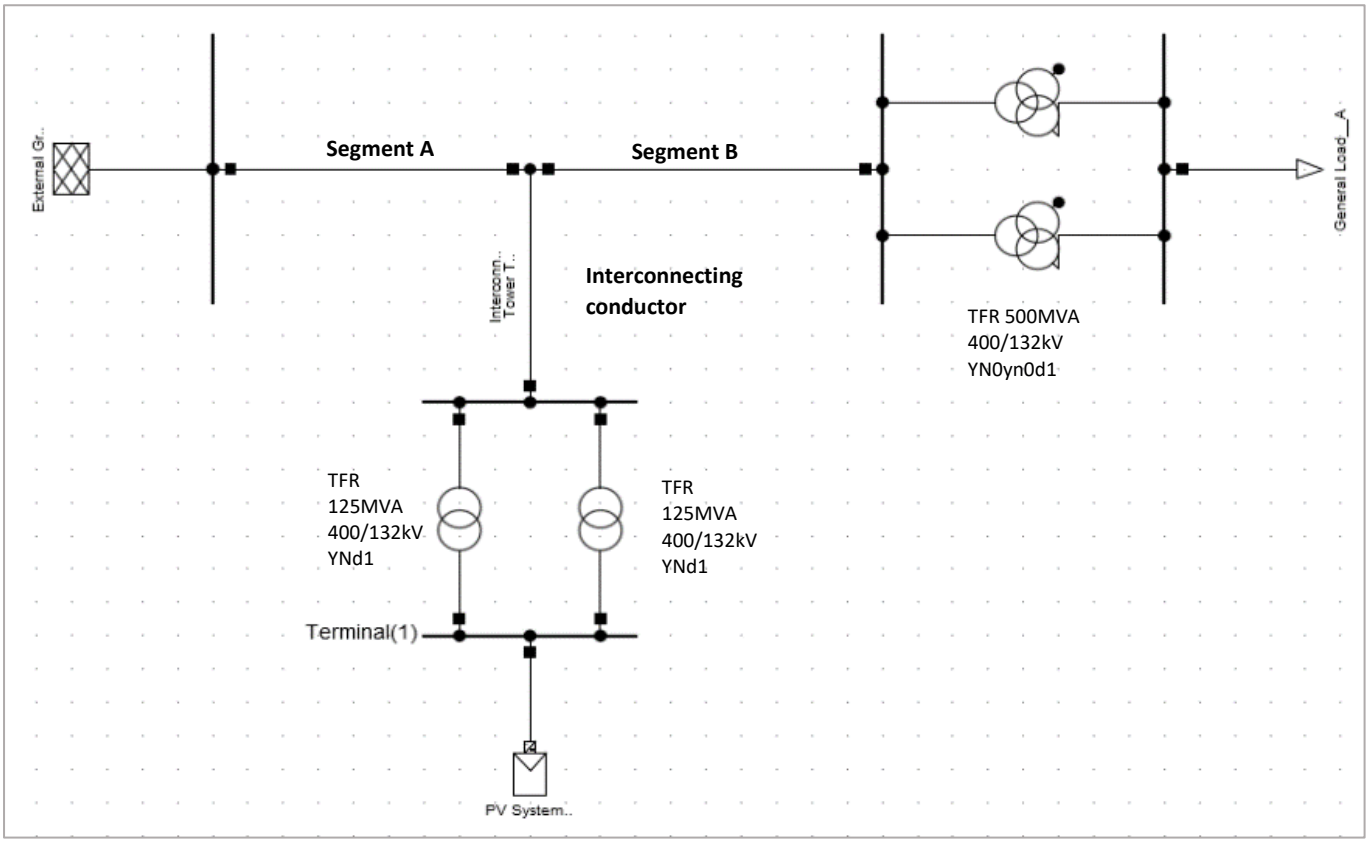

Figure A-107: 400 kV Interconnecting conductor length and location on backbone graph

A. Interconnecting conductor location on backbone graph

Figure A-108 shows how the length of Segment A is changed which at 400 kV, allows for 11 backbone lengths of 20 km (Data values 1 – 1840), 40 km (Data values 1841 – 3680), 60 km (Data values 3681 – 5520), 80 km (5521 – 7360), 100 km (7361 – 9200) and 120 km (9201 – 11040),140km (11041 – 12880), 160km (12881 – 14720), 180km (14721 – 16560) and 200km (16561 – 18400), 220km (18401 – 20240) and 240km 220km (20241 – 22082) respectively. Seen again, four different interconnecting conductor lengths in total now divide all backbones into 4 sets of data, one set for every interconnecting conductor length. Within each set, different receiving end loads are again applied accordingly (Figure A-109).

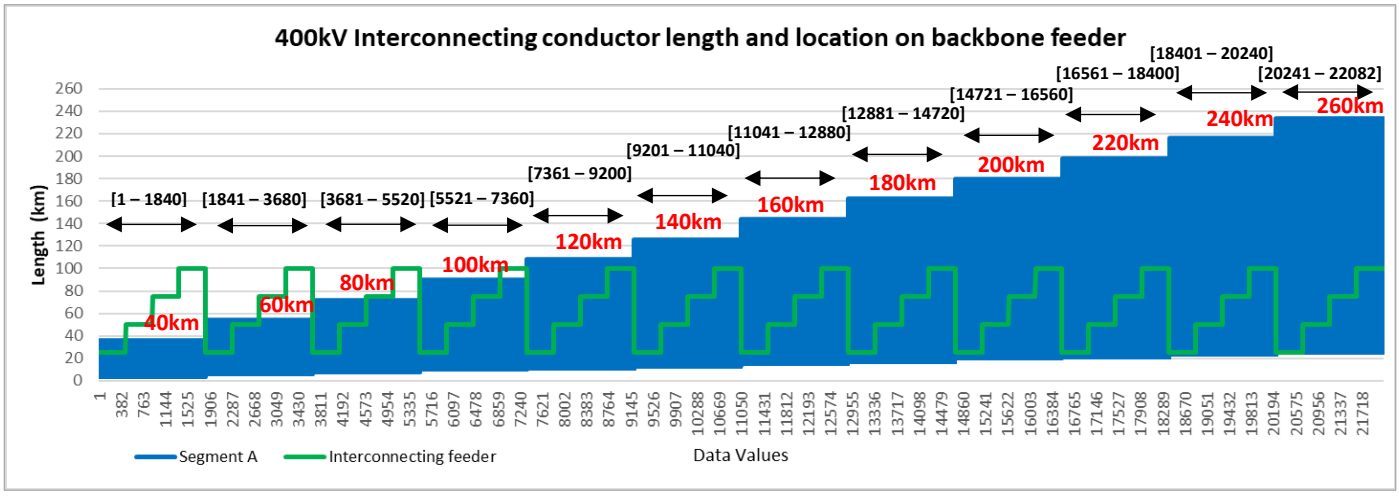

Figure A-108: 400 kV Interconnecting conductor length and location on backbone graph

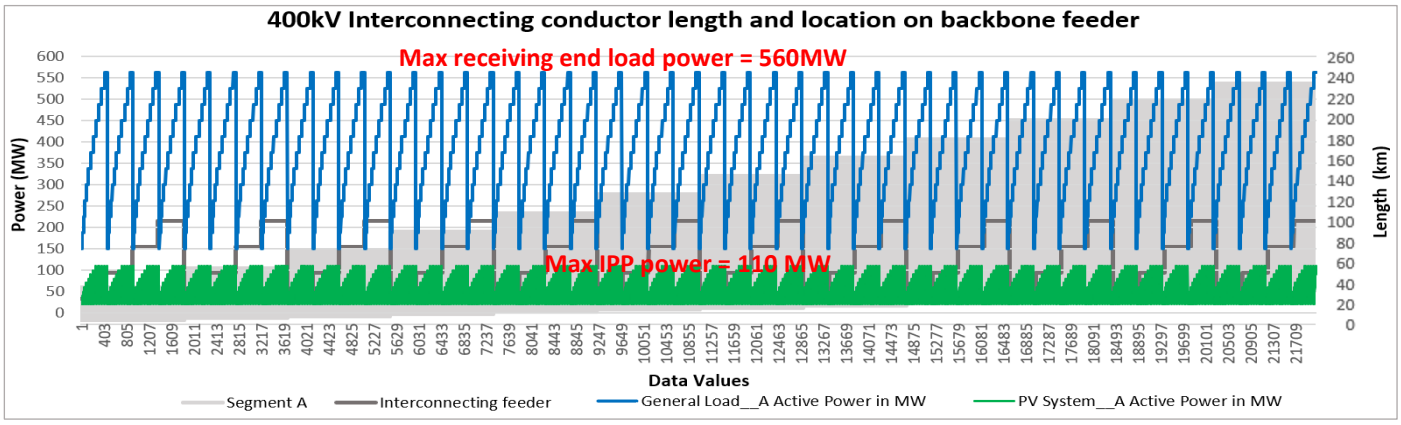

Figure A-109: 400 kV Interconnecting conductor length and its location on backbone graph, with receiving end power and IPP power curves

B. Maximum MVA loading graph for the interconnecting conductor, Segment A and Segment B of the backbone, for loads operating at unity power factor.

Figure A-110 shows the sending end power required (red curve) for the 400kV network. As seen again, this is the difference between load receiving end power and the power supplied by the IPP.

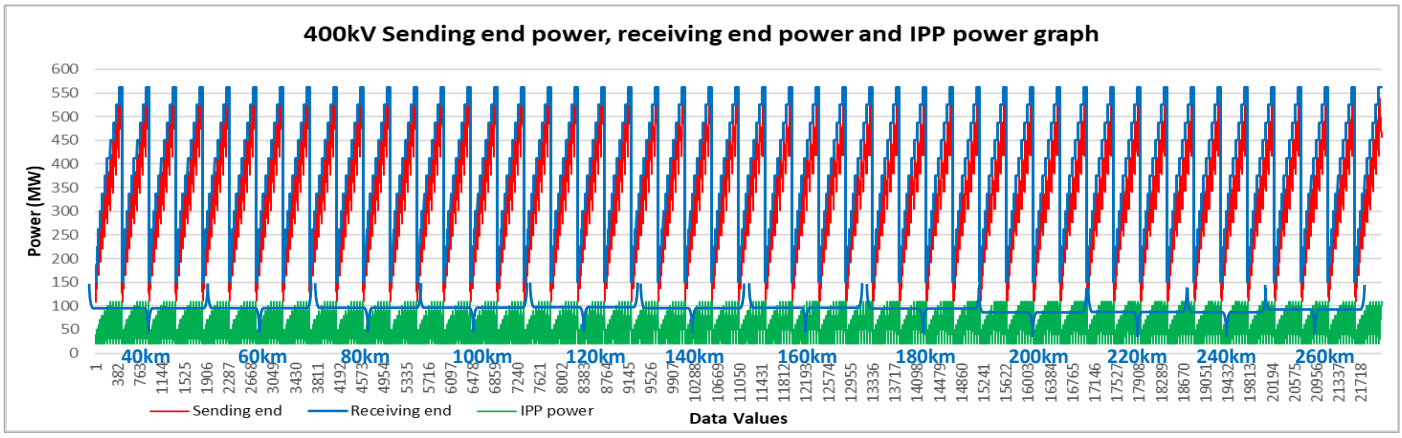

Figure A-110: 400 kV Receiving end, sending end and IPP power curves

C. Maximum and minimum voltage graphs at the receiving (load end, IPP 400kV busbar of the network as well as POC.

Figure A-111 and Figure A-113 respectively show the receiving end, IPP and POC voltage graphs against Segment A lengths and the interconnecting feeder lengths for the IPP operating at unity, capacitive and inductive power factor setpoints. Again, the inductive power factor setpoint corresponding to all IPPs (regardless of size) achieves the greatest increase in voltage at the receiving end and POC, but also as seen in Figures A-114 to A-115, for an increased load there is a decreasing trend of voltage at both the receiving end and POC, regardless of backbone length, as was the case for the previous networks.

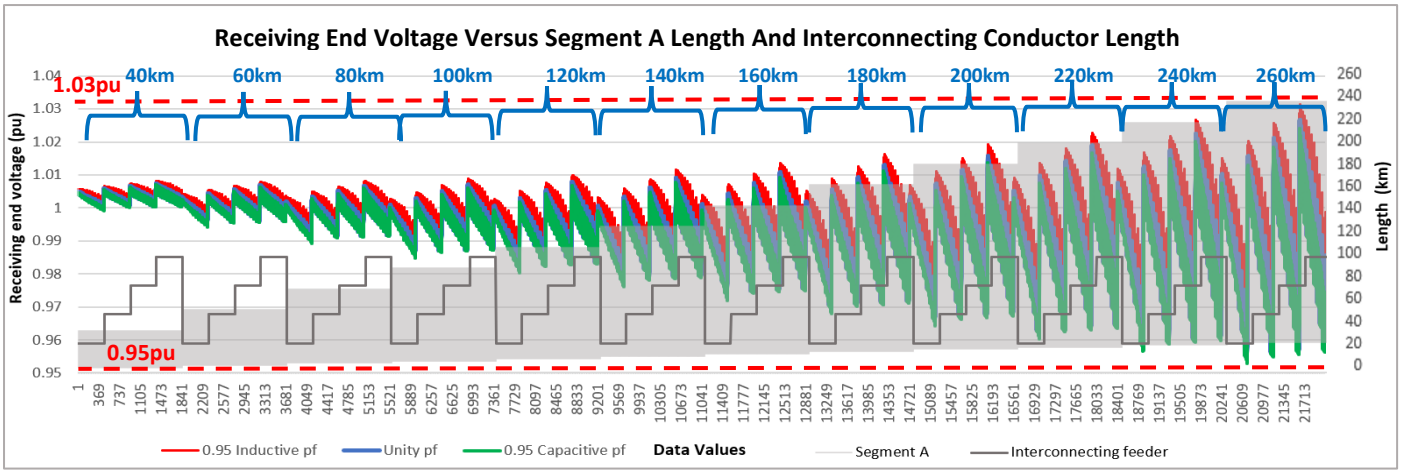

Figure A-111: 400 kV Receiving end voltage as a response to changes in Segment A and interconnecting conductor length

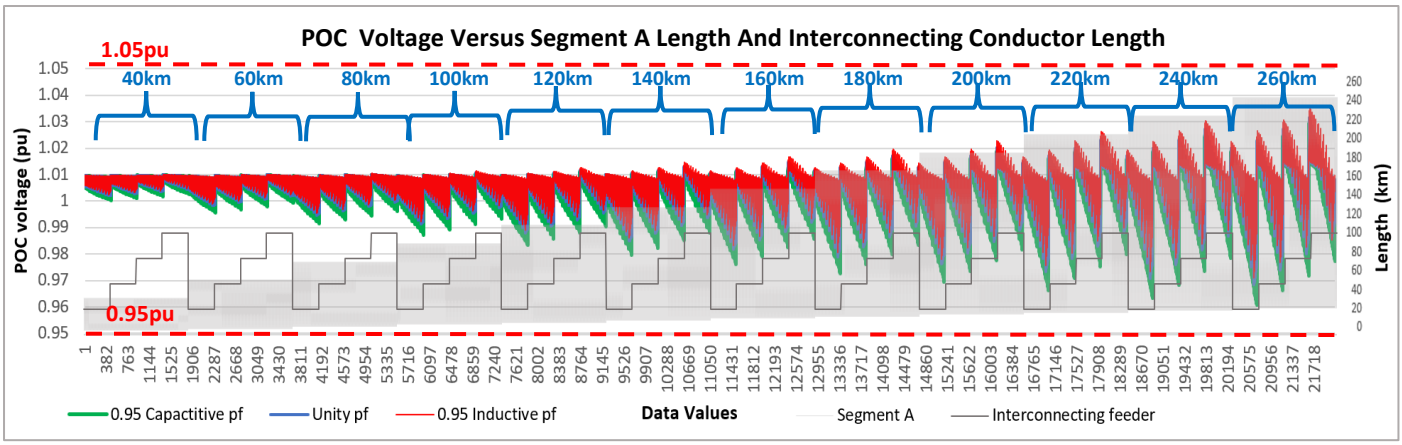

Figure A-112: 400 kV POC voltage as a response to changes in Segment A and interconnecting conductor length

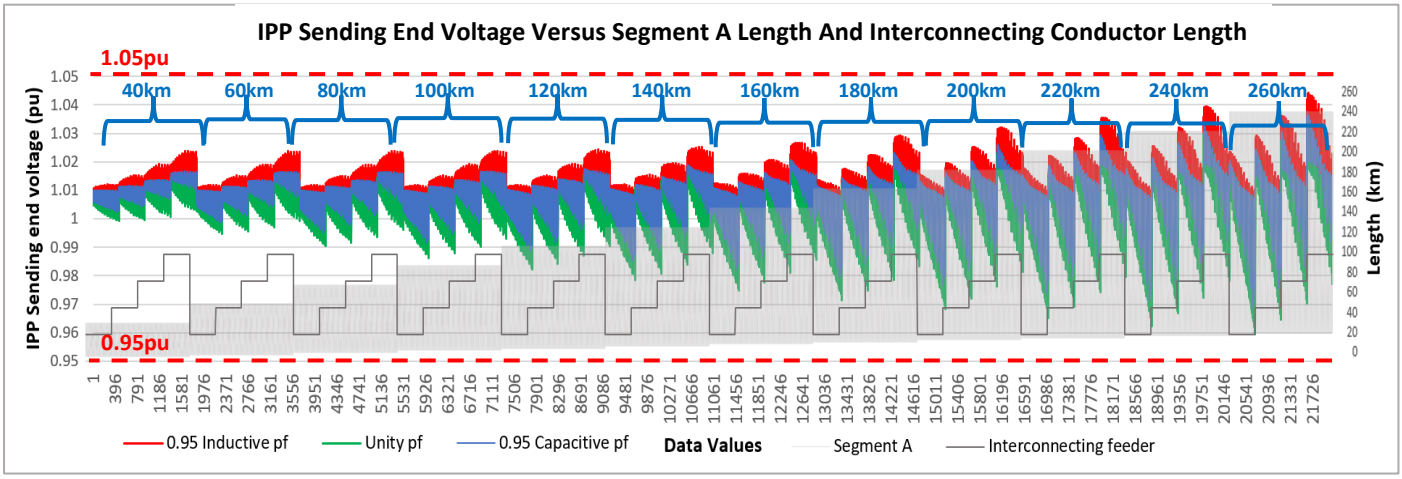

Figure A-113: 400 kV IPP sending end voltage as a response to changes in Segment A and interconnecting conductor length

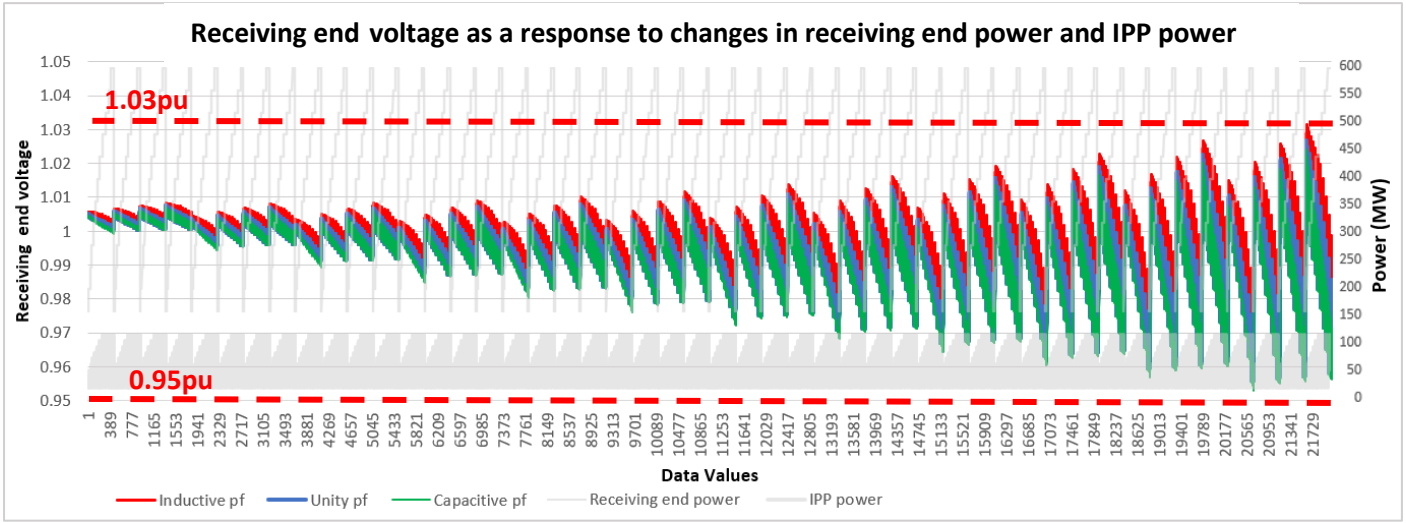

Figure A-114: 400 kV Receiving end voltage as a response to changes in receiving end power and IPP power.

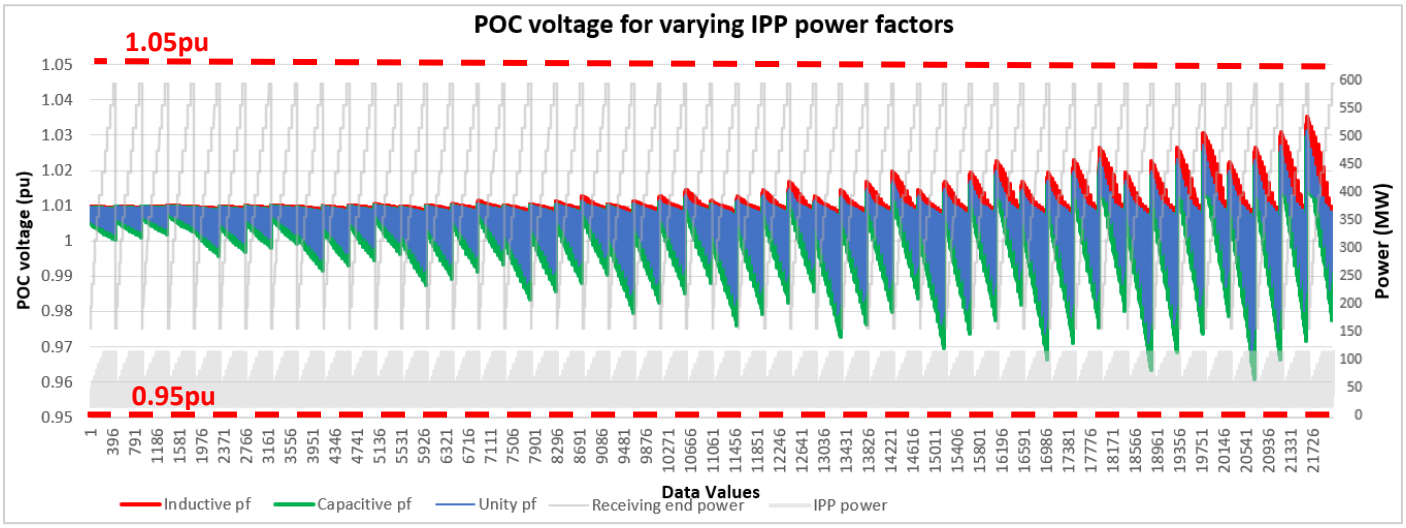

Figure A-115: 400 kV POC voltage as a response to changes in receiving end power and IPP power.

D. Thermal loading graphs for interconnecting conductor, and backbone conductors (Segment A and B).

The thermal loading of the backbone (Segment A and Segment B), and the interconnecting conductor are shown in Figures A-116 to A-118. As seen, for all simulations, there is again no excessive thermal stress on all conductors in the network, and the maximum loading value does not exceed 90%.

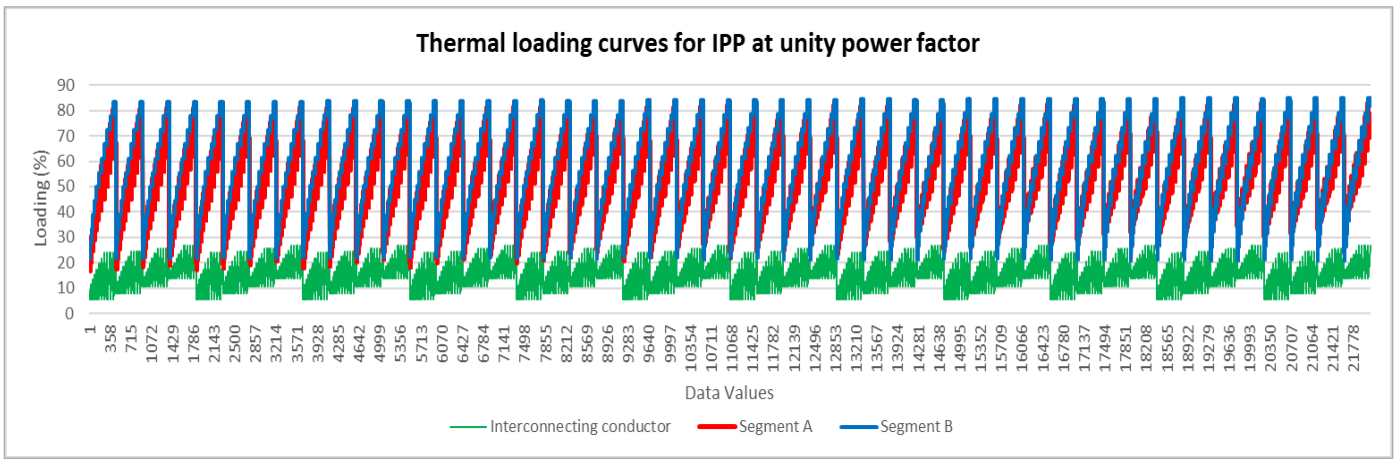

Figure A-116:400 kV thermal loading for Segment A, Segment B and interconnecting conductor while IPP operates at unity pf

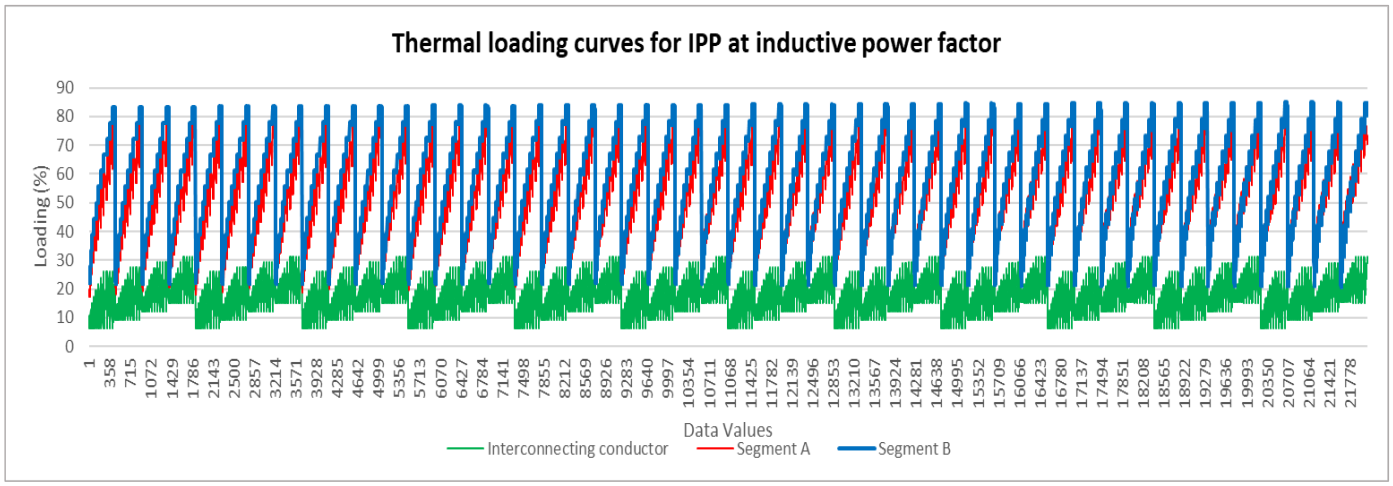

Figure A-117:400 kV thermal loading for Segment A, Segment B and interconnecting conductor while IPP operates at 0.95 inductive pf

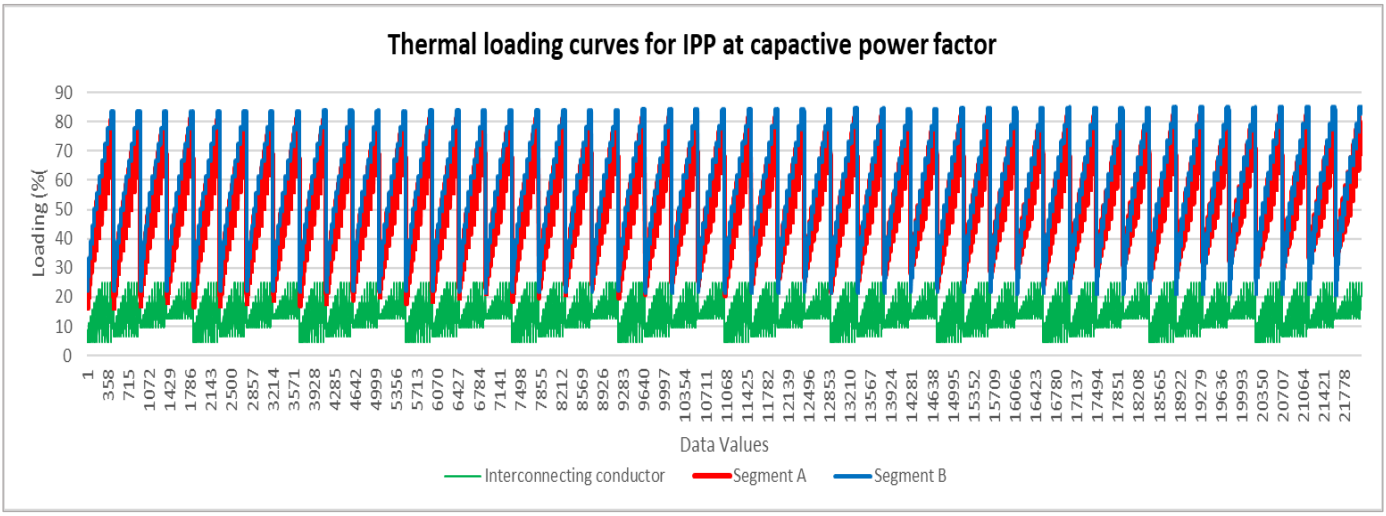

Figure A-118:400 kV thermal loading for Segment A, Segment B and interconnecting conductor while IPP operates at 0.95 capacitive pf

E. Interconnecting conductor DC resistance at 20℃

Figure 3-161 shows the interconnecting conductor DC resistance at 20 deg. As seen, the standard Twin Tern conductor is used for the interconnecting feeder.

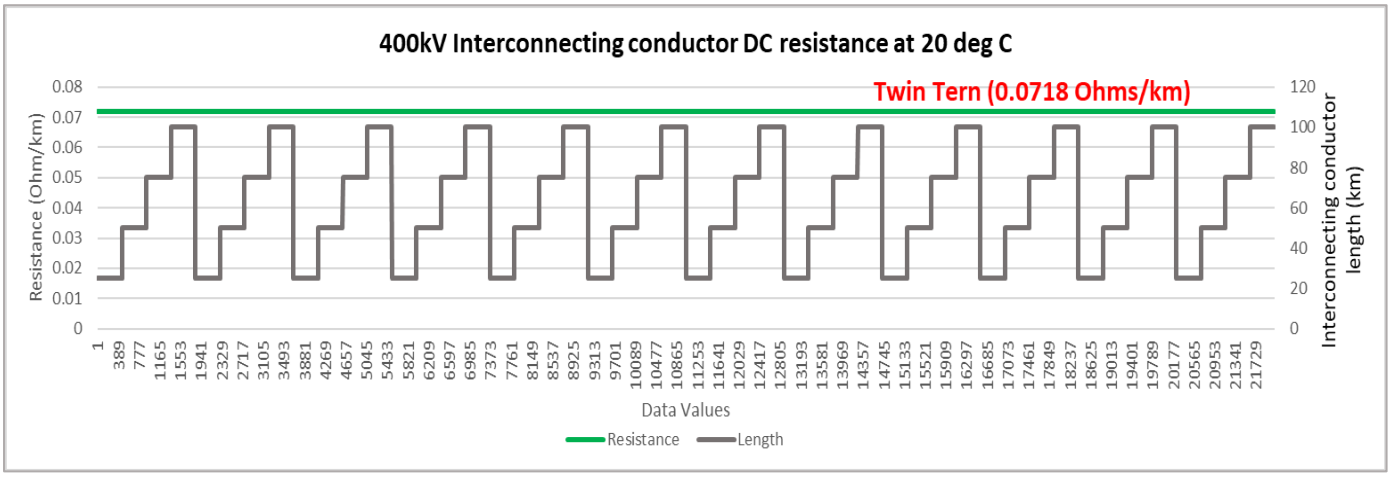

Figure A-119 shows the interconnecting conductor diameter and GMR graph, for the interconnecting feeder at 400kV.

F. Interconnecting conductor diameter and Geometric mean radius graph.

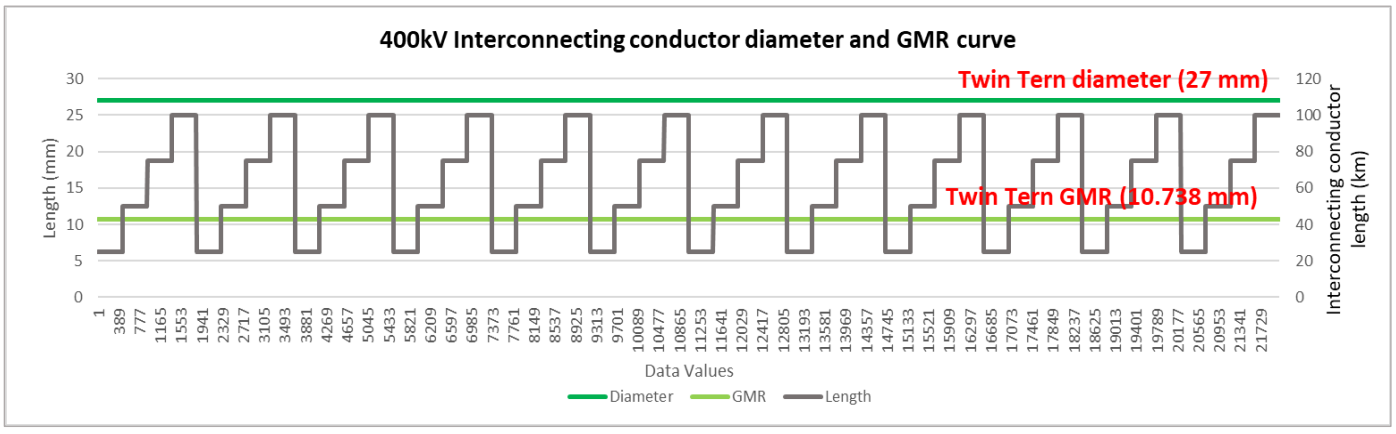

Figure A-120: 400 kV Interconnecting Conductor diameter versus GMR values

G. Interconnecting conductor nominal current graph.

The interconnecting conductor nominal current values are superimposed onto the Segment A an interconnecting conductor length graph as shown in Figure A-121.

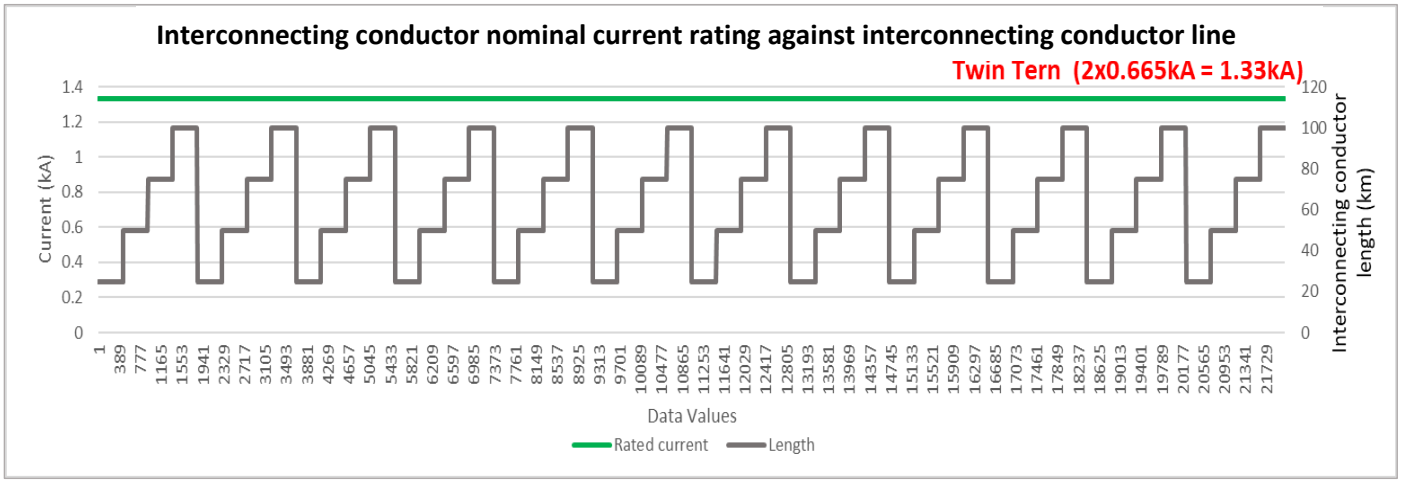

Figure A-121: 400 kV interconnecting conductor nominal current

H. Interconnecting conductor rated power versus IPP power graph.

Figure A-122 compares the interconnecting conductor rated power capacity against the IPP size. As seen, for all changes in IPP sizes, there is an adequate change in interconnecting conductor rating, to safely transfer the required IPP power.

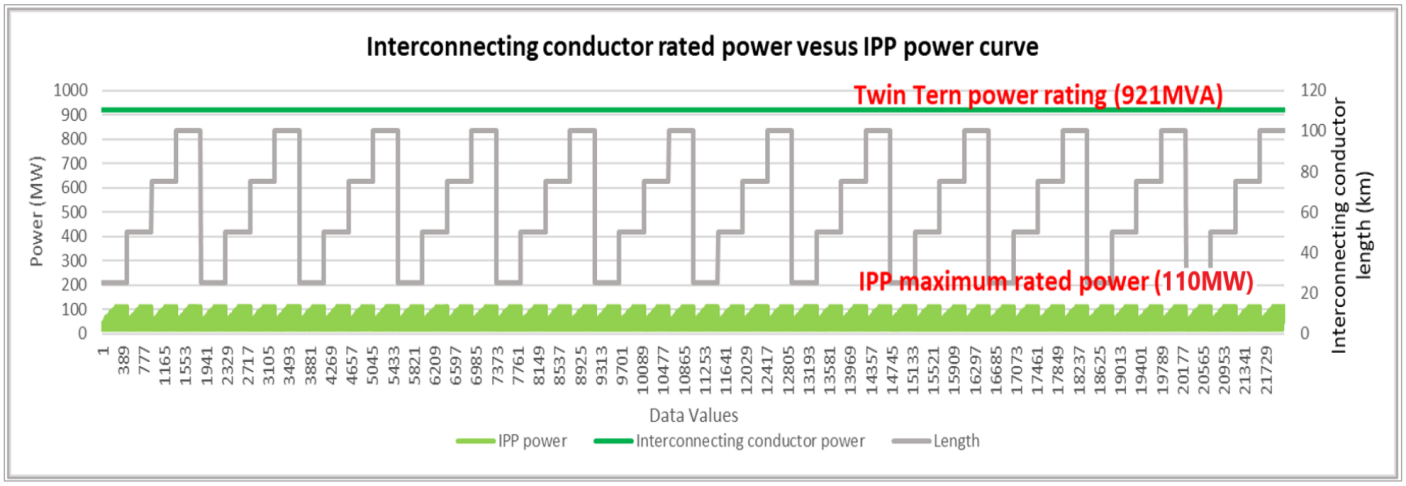

Figure A-122: 400 kV Interconnecting conductor is adequately rated to handle IPP export power

I. IPP power factor variation graphs for unity, leading and lagging setpoints applicable to Category C (0.95).

The IPP power factor graph shown in Figure A-123 below shows the variation in IPP power factor the 400 kV network. Since the number of Category B IPPs connecting to the 400 kV network is limited within South Africa, only Category C IPPs operating at 0.95 inductive, 0.95 capacitive and unity power factor are considered for the 400kV network.

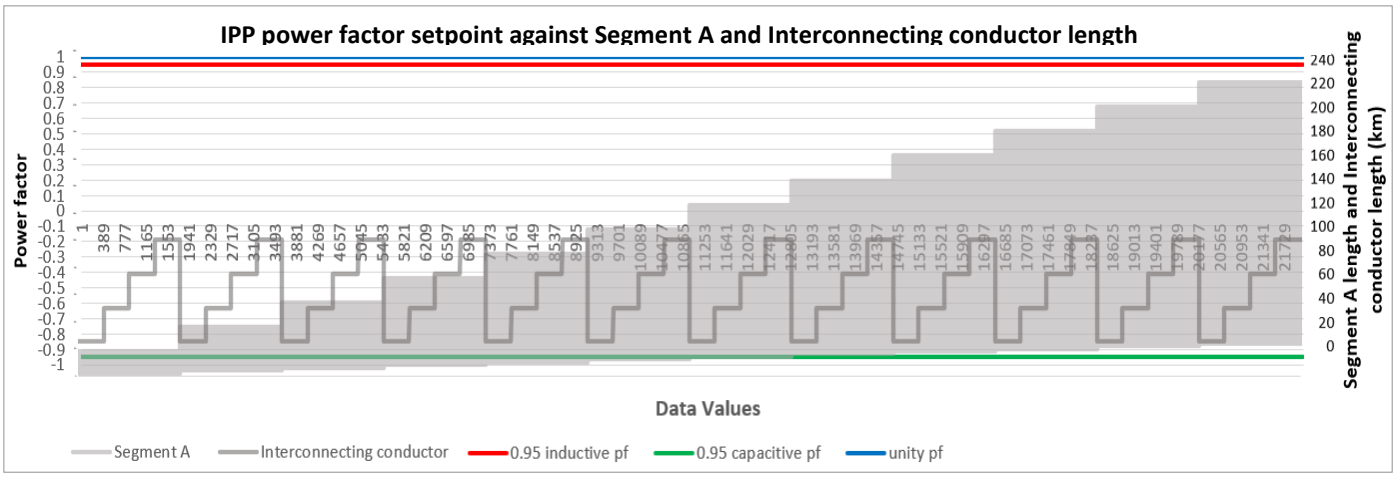

Figure A-123: 400 kV IPP variations in power factor

J. Power line loss graphs corresponding to IPP power factor variation graphs.

The corresponding power line losses curves are shown in Figures A-124 to A-126.

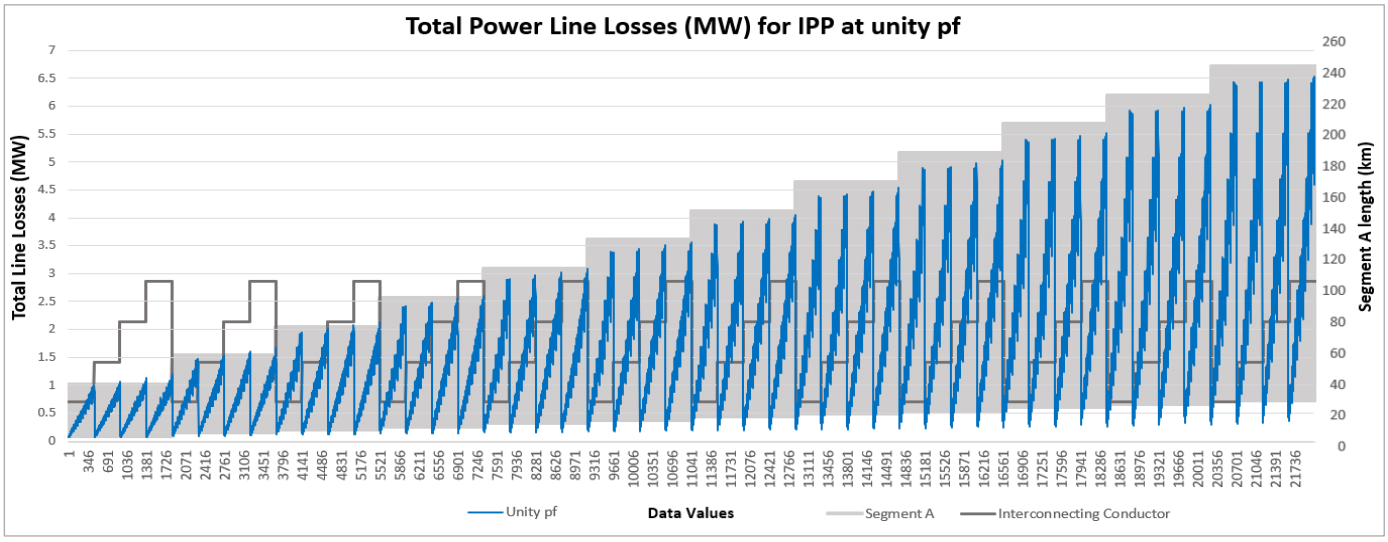

Figure A-124: 400 kV Total power line losses for the IPP operating at unity power factor.

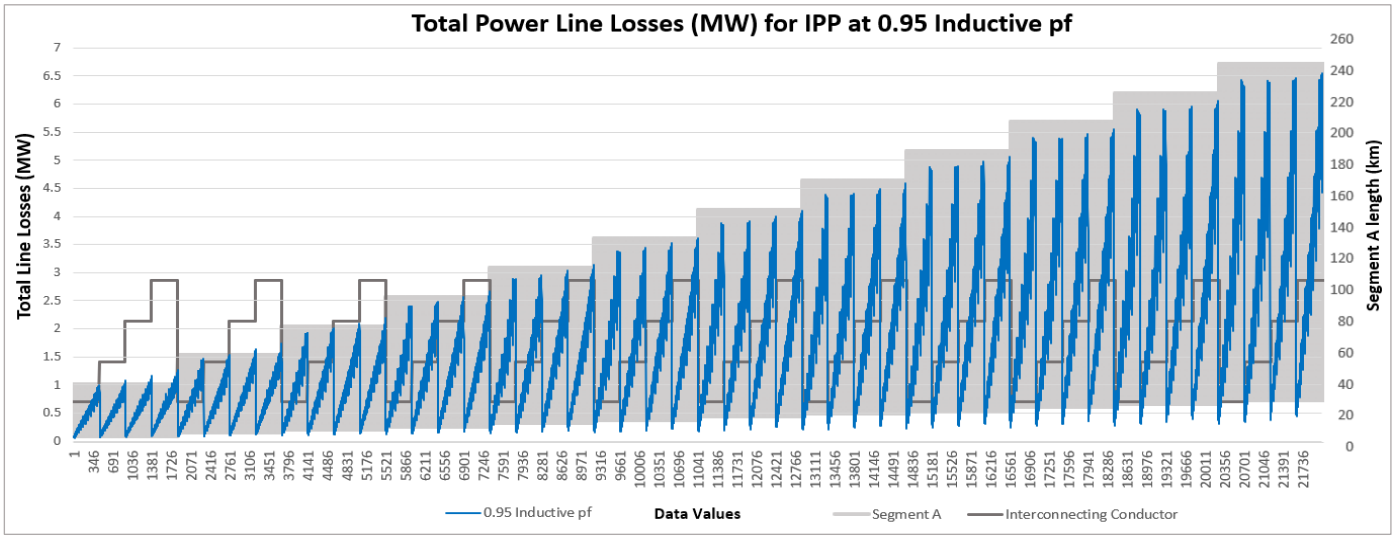

Figure A-125: 400 kV Total power line losses for the IPP operating at 0.95 inductive power factor.

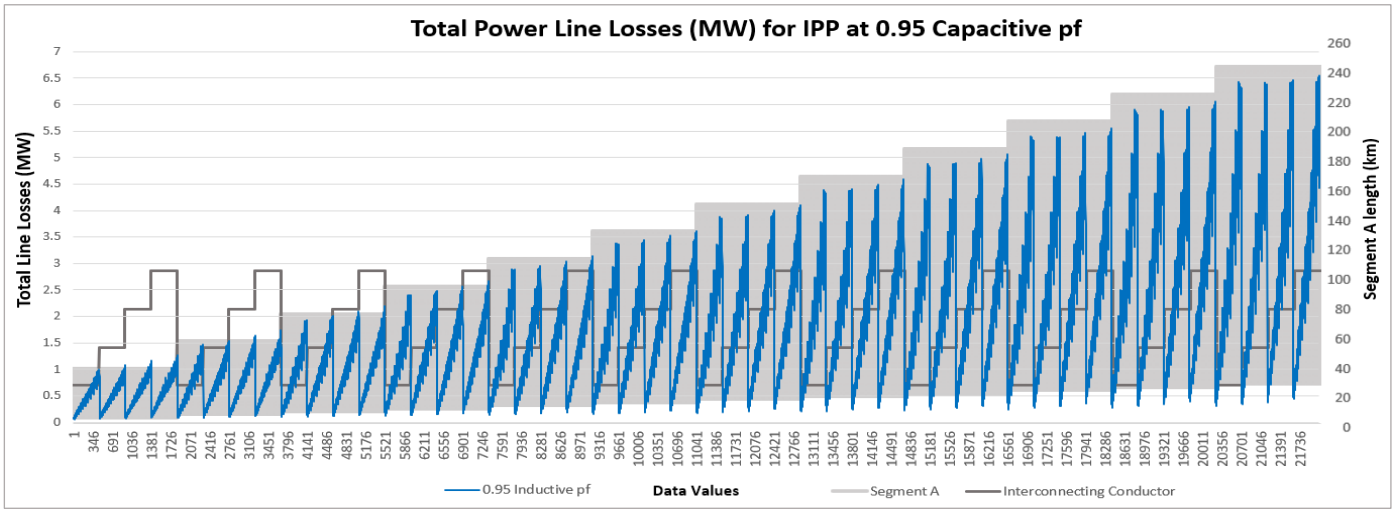

Figure A-126: 400 kV Total power line losses for the IPP operating at 0.95 capacitive power factor.

For the 400 kV technology, data shown from Sections (A) – (J) above is saved into three 22082x8 input data matrices, one representing the unity power factor IPP setpoint, another representing the lagging power factor IPP setpoint and the third representing the leading power factor IPP setpoint. When combined, a 66246 x 8 input data matrix (22082x3) is saved, along with a 66246x1 target data matrix, and these will be used in the ANN design and modelling section to follow in Section 3.3. The matrix combination is performed as shown in figure Figure 3-170. Each set of power factor data values obtained from DIgSILENT Powerfactory are copied from the individual unity, inductive and capacitive power factor data excel file, and combined to form a single 66246x8 matrix. In order to capture losses for the scenarios in which the load is non-unity, the above simulations are redone in the same fashion as before, but for a receiving end (load) power factor setpoint of 0.95 (inductive) as well as 0.95 (capacitive). This means that the combined input data matrix to be used in the ANN design and modelling section expands in size from 66246x8 to 198738x8 and a target data size of 198738x1.

APPENDIX B: Hidden layer performance curves

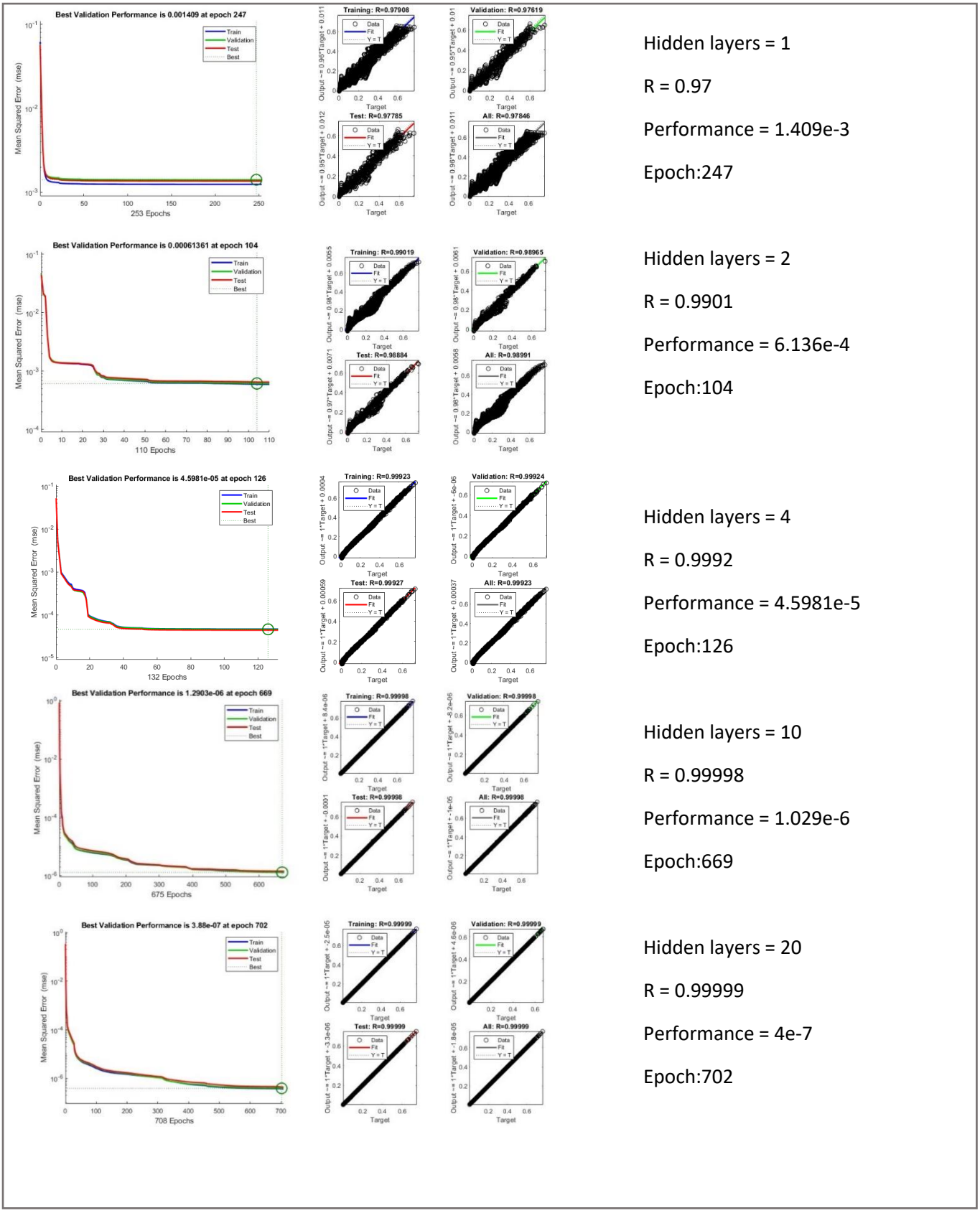

Figure B-1: Performance curves representing the 22kV ANN for varying hidden layer

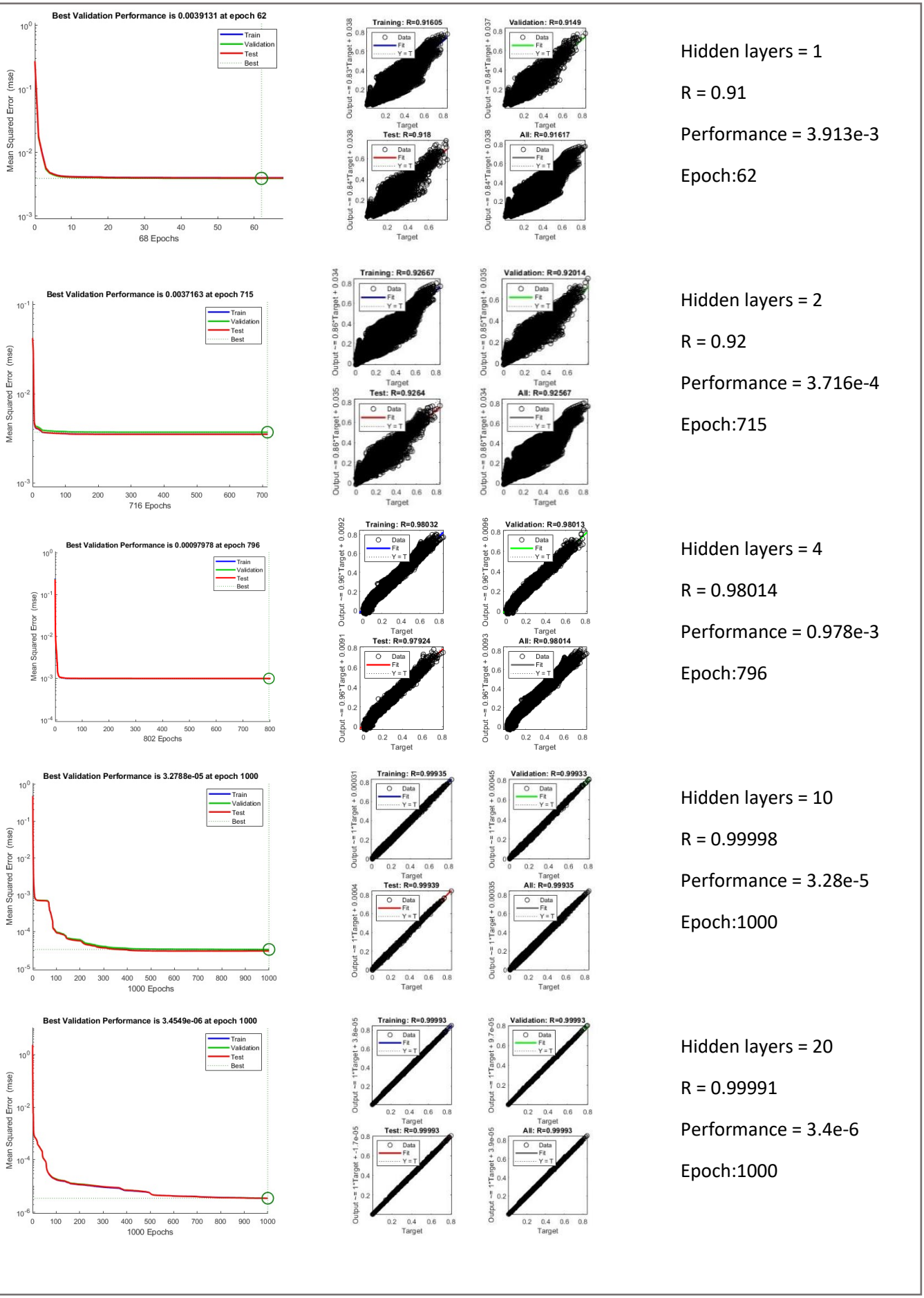

Figure B-2: Performance curves representing the 66kV ANN for varying hidden layer

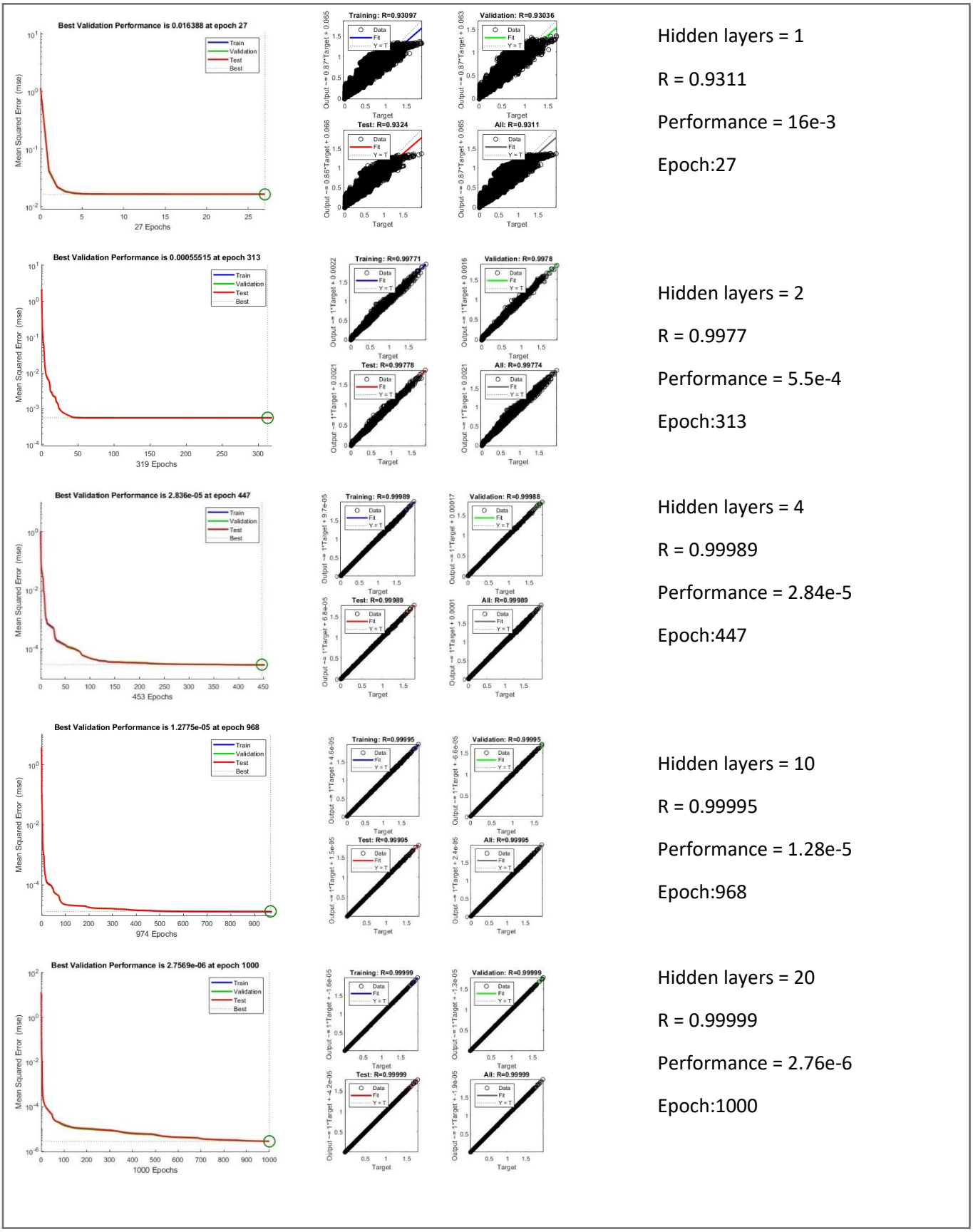

Figure B-3: Performance curves representing the 132kV ANN for varying hidden layer

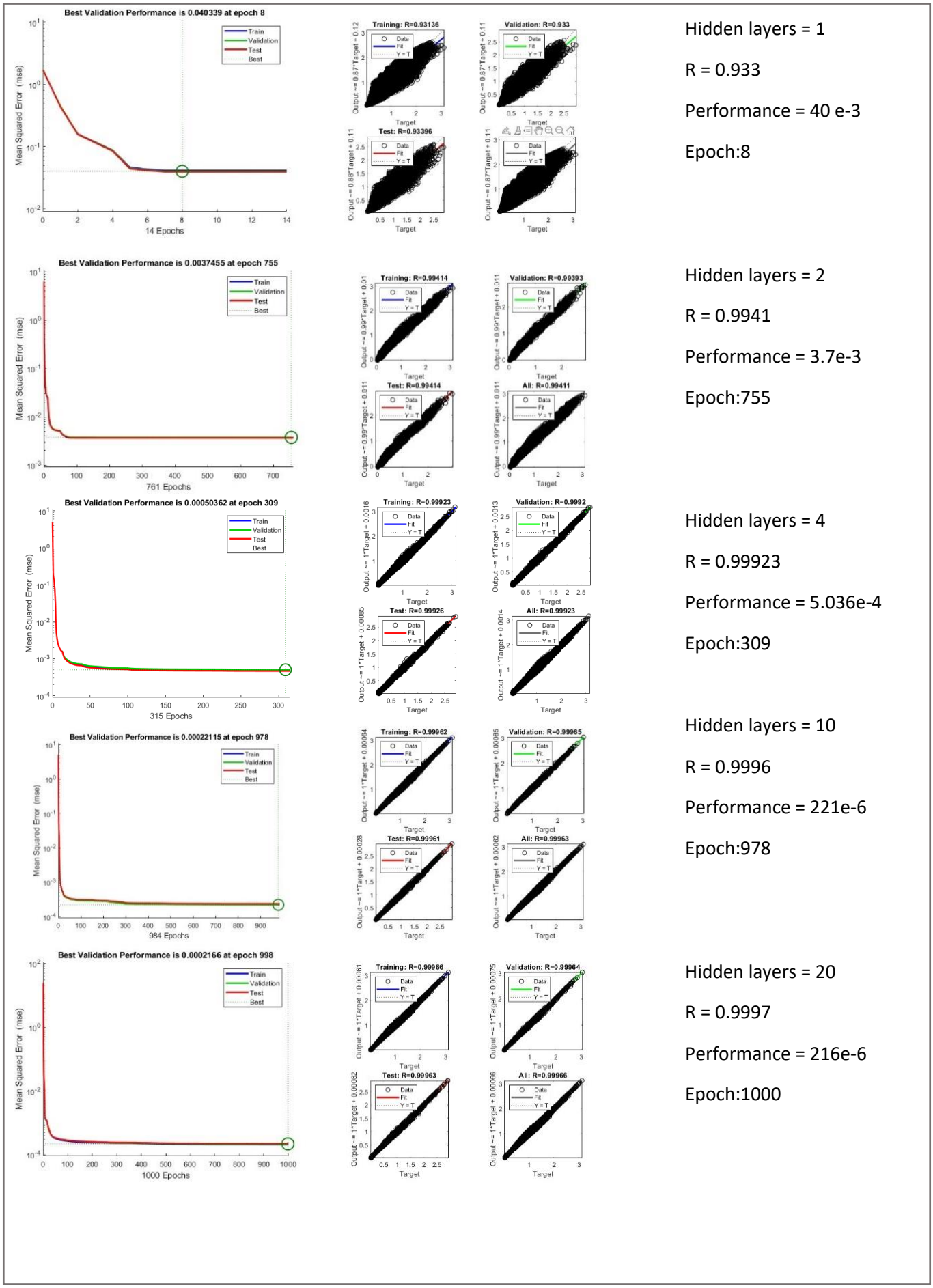

Figure B-4: Performance curves representing the 220kV ANN for varying hidden layer

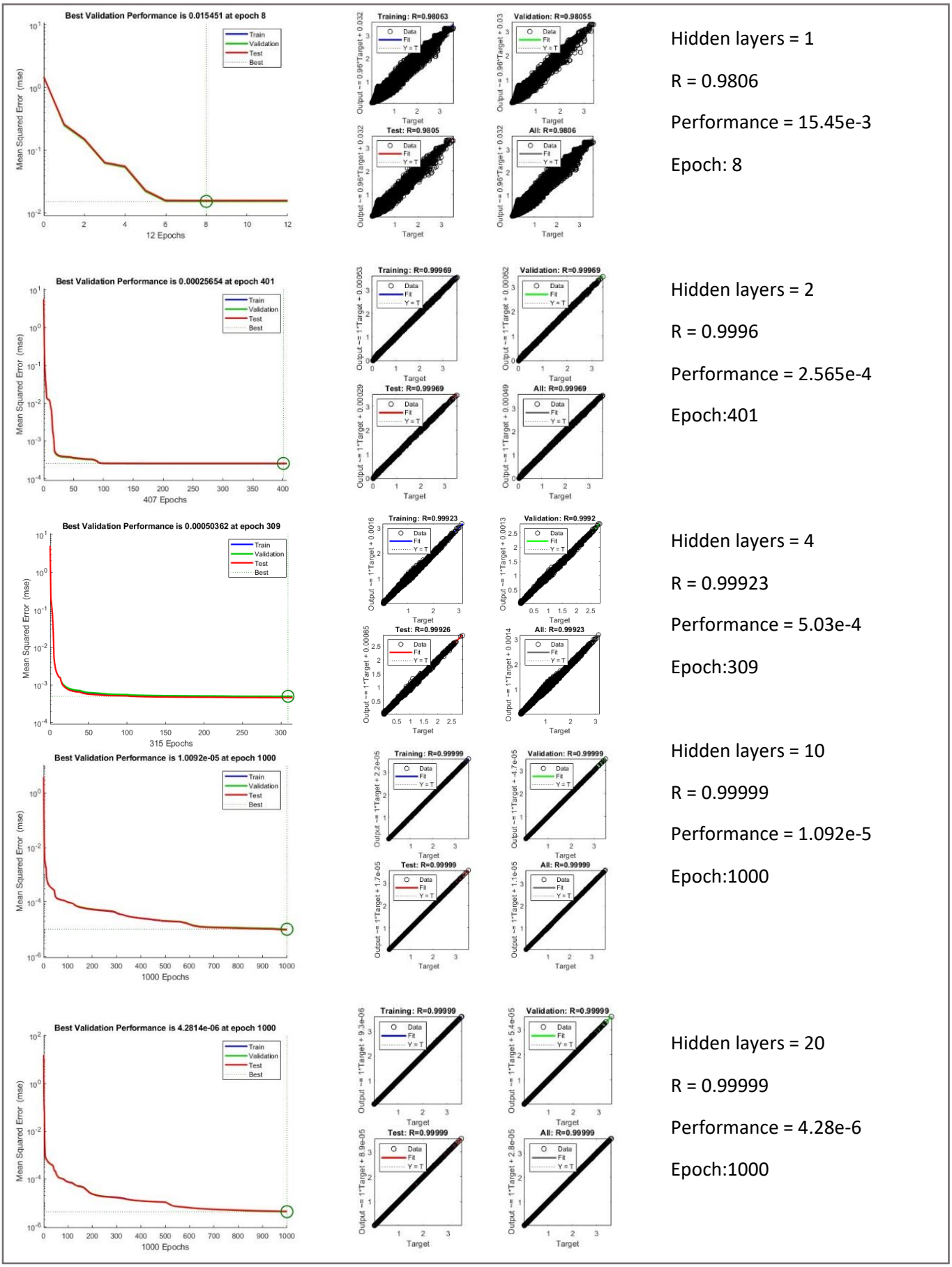

Figure B-5: Performance curves representing the 275kV ANN for varying hidden layer

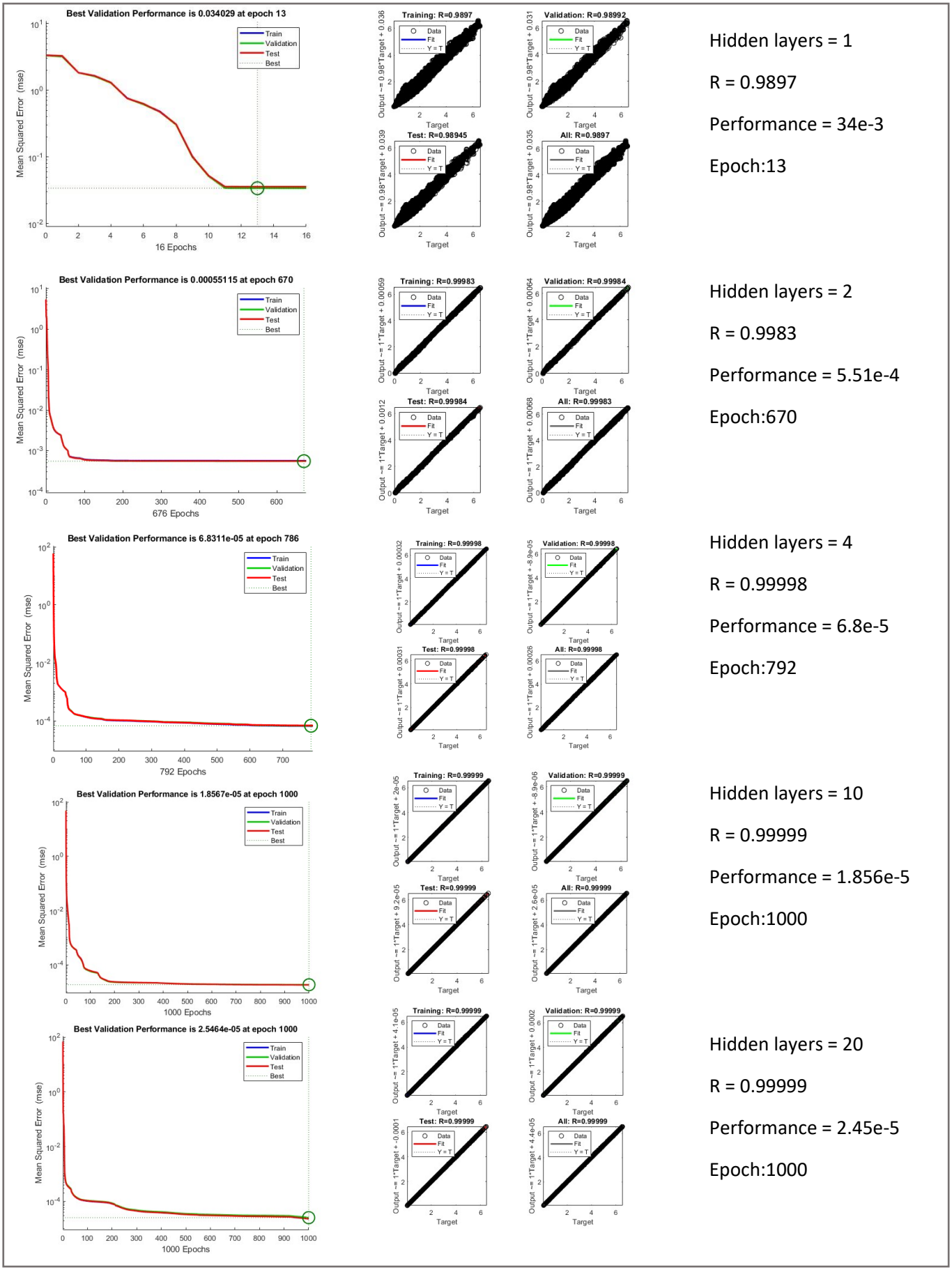

Figure B-6: Performance curves representing the 400kV ANN for varying hidden layer